THE MECHANISM ON DEVELOPMENT AND REGENERATION OF INNER EAR HAIR CELLS

EDITED BY: Dongdong Ren, Hongzhe Li and Yu Sun
PUBLISHED IN: Frontiers in Molecular Neuroscience

frontiers Research Topics

frontiers

ISSN 1664-8714
ISBN 978-2-83250-003-3
DOI 10.3389/978-2-83250-003-3

About Frontiers

Frontiers is more than just an open-access publisher of scholarly articles: it is a pioneering approach to the world of academia, radically improving the way scholarly research is managed. The grand vision of Frontiers is a world where all people have an equal opportunity to seek, share and generate knowledge. Frontiers provides immediate and permanent online open access to all its publications, but this alone is not enough to realize our grand goals.

Frontiers Journal Series

The Frontiers Journal Series is a multi-tier and interdisciplinary set of open-access, online journals, promising a paradigm shift from the current review, selection and dissemination processes in academic publishing. All Frontiers journals are driven by researchers for researchers; therefore, they constitute a service to the scholarly community. At the same time, the Frontiers Journal Series operates on a revolutionary invention, the tiered publishing system, initially addressing specific communities of scholars, and gradually climbing up to broader public understanding, thus serving the interests of the lay society, too.

Dedication to Quality

Each Frontiers article is a landmark of the highest quality, thanks to genuinely collaborative interactions between authors and review editors, who include some of the world's best academicians. Research must be certified by peers before entering a stream of knowledge that may eventually reach the public - and shape society; therefore, Frontiers only applies the most rigorous and unbiased reviews.
Frontiers revolutionizes research publishing by freely delivering the most outstanding research, evaluated with no bias from both the academic and social point of view. By applying the most advanced information technologies, Frontiers is catapulting scholarly publishing into a new generation.

What are Frontiers Research Topics?

Frontiers Research Topics are very popular trademarks of the Frontiers Journals Series: they are collections of at least ten articles, all centered on a particular subject. With their unique mix of varied contributions from Original Research to Review Articles, Frontiers Research Topics unify the most influential researchers, the latest key findings and historical advances in a hot research area! Find out more on how to host your own Frontiers Research Topic or contribute to one as an author by contacting the Frontiers Editorial Office: frontiersin.org/about/contact

THE MECHANISM ON DEVELOPMENT AND REGENERATION OF INNER EAR HAIR CELLS

Topic Editors:
Dongdong Ren, Fudan University, China
Hongzhe Li, VA Loma Linda Healthcare System, Veterans Health Administration, United States Department of Veterans Affairs, United States
Yu Sun, Huazhong University of Science and Technology, China

Citation: Ren, D., Li, H., Sun, Y., eds. (2022). The Mechanism on Development and Regeneration of Inner Ear Hair Cells. Lausanne: Frontiers Media SA.
doi: 10.3389/978-2-83250-003-3

Table of Contents

frontiers | Frontiers in Molecular Neuroscience

TYPE Editorial
PUBLISHED 09 August 2022
DOI 10.3389/fnmol.2022.974270

OPEN ACCESS

EDITED AND REVIEWED BY
Jean-Marc Taymans,
Institut National de la Santé et de la Recherche Médicale (INSERM), France

*CORRESPONDENCE
Yu Sun
sunyu@hust.edu.cn
Hongzhe Li
hongzhe@gmail.com
Dongdong Ren
dongdongren@fudan.edu.cn

SPECIALTY SECTION
This article was submitted to Molecular Signalling and Pathways, a section of the journal Frontiers in Molecular Neuroscience

RECEIVED 21 June 2022
ACCEPTED 24 June 2022
PUBLISHED 09 August 2022

CITATION
Sun H, Chen B, Sun Y, Li H and Ren D (2022) Editorial: The mechanism on development and regeneration of inner ear hair cells.
Front. Mol. Neurosci. 15:974270.
doi: 10.3389/fnmol.2022.974270

Editorial: The mechanism on development and regeneration of inner ear hair cells

Haojie Sun[1], Binjun Chen[1], Yu Sun[2]*, Hongzhe Li[3]* and Dongdong Ren[1]*

[1]Department of Otorhinolaryngology, Eye and ENT Hospital, Fudan University, Shanghai, China, [2]Department of Otorhinolaryngology, Tongji Medical College, Union Hospital, Huazhong University of Science and Technology, Wuhan, China, [3]VA Loma Linda Healthcare System, Veterans Health Administration, United States Department of Veterans Affairs, Loma Linda, CA, United States

KEYWORDS

inner ear, development, regeneration, vestibule, cochlea

Editorial on the Research Topic
The mechanism on development and regeneration of inner ear hair cells

The inner ear, which consists of the cochlea and vestibular systems, is a morphologically complex sensory organ. Hair cells (HC), which serve as inner ear sensory cells, are critical for the transduction of mechanical stimulus into auditory and balance signals in the inner ear. After inner ear injury, auditory abnormalities and balance disorders are major consequences. Promoting hair cell regeneration is one of the most promising strategies to address hearing loss and vestibular dysfunction. Exploring the mechanism of inner ear development provides a practical venue to understand the regeneration process of functional hair cells.

Six articles were included in this topic regarding inner ear development. With regard to cochlear development, a pseudo-temporal analysis of single-cell RNA sequencing done by Chen J. et al. focused on the greater epithelial ridge (GER) cells that solely present during cochlear development, and profiled the gene expression landscape of the rat's cochlear basal membrane (P1, P7, P14) to categorize major subtypes of GER cells. The authors documented the trans-differentiation of different GER subtypes to inner (IHC) and outer hair cells (OHC) by trajectory analysis. They also elucidated the key regulatory genes and signaling pathways during trans-differentiation, which is instrumental for future research on HC regeneration. Another study about the organ of Corti (OoC) in the present special topic conducted by Liu et al. dug into the connexin26 (Cx26) protein, which is encoded by the GJB2 gene. The study demonstrated that Cx26 is involved in the maturation of the cytoskeleton during the earlier postnatal development of the OoC. In addition, the polymerization of G-actin into F-actin is prevented in Cx26 knock-down (KD) mice. This study elucidated an underlying mechanism of the OoC deformity caused by Cx26 downregulation. Given that GJB2 mutation is one of the most common etiologies of hereditary deafness, the work is particularly noteworthy.

As to vestibular development, three articles were included in this topic focusing on the development of vestibular HCs and the formation of the vestibular flat epithelium. Chen B.-J. et al. described the role of Rab11a, a small G protein, in the formation of the polarity of cilia, thus revealing that Rab11a is essential to the normal development of cilia, as well as the intraflagellar transport. Another investigation conducted by Yan et al. explored the role of BAIAP2L2, a component of the row 2 complex in stereocilia, which was found to cause degeneration of the mechanotransducing stereocilia in cochlear hair cells when inactivated. Surprisingly, such degeneration was not found in the vestibular HC stereocilia, considering the unaffected morphology, the intact development and function of the vestibule, which might be explained by the differential dependency of CAPZB2 localization on BAIAI2L2 in cochlear and vestibular HCs. Thus, the comparative approach focusing on the phenotypic difference between vestibular and cochlear HC development could provide insights into their development, as well as regeneration.

Degeneration of the vestibular sensory epithelium leads to the formation of flat epithelium (FE) with unclear pathogenesis. He et al. uncovered the role of epithelial-mesenchymal transition (EMT) in this process. Upregulated mesenchymal cell markers in the vestibular FE compared to the normal utricle and robust cell proliferation were observed, which was consistent with GO and DEG analyses following a microarray analysis. The transcriptome features provided by this research provide the foundation for future studies in novel intervention strategies for FE.

Except for HC development, as the first and extremely important synaptic structures formed between IHCs and spiral ganglion neurons (SGN), ribbon synaptic maturity was also included in the topic. The study by Guo et al. found that in the earlier stages of auditory development, under the regulation of autophagy, ribbon synaptic refinement and the pruning of SGN fiber occur and are closely associated with the morphological and functional maturation of ribbon synapses. Further evidence pertaining to IHC functionalities is required to validate the conclusion on inner ear development.

Vestibular and cochlear HCs and SGNs are the major objectives of inner ear regeneration. Based on the past inner ear developmental research, three reviews and original articles were also included in our topic.

To expand the knowledge relating to HC regeneration in adult cochlear explant culture, which is complementary to inner ear organoids to study the inner ear *in vitro*, Li et al. hypothesized that the integral cochlear structure helps maintain the overall inner ear architecture and improve the sensory epithelium survival in culture. To test the hypothesis, they induced trans-differentiation of adult supporting cells to HC-like cells (HCLCs) after HC degeneration by overexpression of Atoh1 in adult mouse cochlear culture with the (surrounding) bone intact. Furthermore, HCLC-neuron connections were observed, proving the feasibility of culturing adult inner ear tissues for future research in regeneration, HC-neuron pathways, and inner ear drug screening.

Regeneration of vestibular HC is critical due to its vulnerability to ototoxic drugs and virus infection and limited restorative capacity after damage. Huang et al. summarized the development of human vestibular hair cells during the entire embryonic stage and the latest research on human vestibular hair cell regeneration. The regenerative potential of human vestibular HC and the application of gene therapy in this field were discussed. The author also pointed out the limitations of current studies and future directions, including some important problems such as how to regenerate and maintain mature and functional HCs, which are imminent issues to resolve in order to propel the field of regeneration of inner ear sensory epithelium, whether in vestibular or cochlear.

Another review about regeneration in our topic is about the SGN, which is a vital component in sensorineural hearing loss. SGNs are the primary neurons that relay sound signals from the inner ear to the brainstem, however, it is vulnerable to noise and ototoxic drugs. Degeneration of SGNs causes irreversible sensorineural hearing loss (SNHL) and cannot be rescued effectively because of their lack of regenerative potential. Wang et al. reviewed the recent advances in research of SGN regeneration including exogenous stem cell transplantation and endogenous glial cell reprogramming. In sum, SGN regeneration is facing a similar challenge to HC regeneration. Considering the progress of synaptic junction formation and the regeneration of hair cells and spiral ganglion neurons, inner ear regeneration is becoming a promising field in otology.

In addition to the development and regeneration of the inner ear, this topic also included a study about the protective effect of shikonin, a pigment isolated from traditional Chinese herbal medicine, on spiral ganglion cells. Du et al. found that shikonin reduced the ouabain-induced auditory nerve damage and increase the expression of Nrf2 and its downstream molecules HO-1 and NQO1. Shikonin treatment enhanced the antioxidant capacity of SGNs and spiral ganglion Schwann cells, promoted cell proliferation, and inhibited apoptosis by activating the Nrf2/antioxidant response elements signal pathway, thereby testifying it as a candidate therapeutic drug for neurological deafness.

Overall, this topic, with ten papers encompassing various subjects in the area of inner ear development, revealed the promising potential of this research interest and promoted the progress of this lesser-known research direction.

Author contributions

DR, HS, and HL designed the literature. HS and BC co-authored the manuscript and reviewed previous research.

All authors contributed to the article and approved the submitted version.

Conflict of interest

The authors declare that the research was conducted in the absence of any commercial or financial relationships that could be construed as a potential conflict of interest.

Publisher's note

frontiers in Molecular Neuroscience

ORIGINAL RESEARCH
published: 19 November 2021
doi: 10.3389/fnmol.2021.762916

Rab11a Regulates the Development of Cilia and Establishment of Planar Cell Polarity in Mammalian Vestibular Hair Cells

Bin-Jun Chen[1,2,3†], Xiao-qing Qian[1,2,3†], Xiao-yu Yang[1,2,3], Tao Jiang[1,2,3], Yan-mei Wang[1,2,3], Ji-han Lyu[1,2,3], Fang-lu Chi[1,2,3], Ping Chen[4,5*] and Dong-dong Ren[1,2,3*]*

[1] Department of Otorhinolaryngology, ENT Institute, Eye and ENT Hospital, Fudan University, Shanghai, China, [2] NHC Key Laboratory of Hearing Medicine, Fudan University, Shanghai, China, [3] Shanghai Auditory Medical Center, Shanghai, China, [4] Department of Cell Biology, Emory University, Atlanta, GA, United States, [5] Department of Otolaryngology, Emory University, Atlanta, GA, United States

OPEN ACCESS

Edited by:
Hiroshi Hibino,
Osaka University, Japan

Reviewed by:
Takahisa Furukawa,
Osaka University, Japan
Kazusaku Kamiya,
Juntendo University, Japan

***Correspondence:**
Fang-lu Chi
chifanglu@126.com
Ping Chen
ping.chen@emory.edu
Dong-dong Ren
dongdongren@fudan.edu.cn

[†] These authors have contributed equally to this work

Specialty section:
This article was submitted to Molecular Signaling and Pathways, a section of the journal Frontiers in Molecular Neuroscience

Received: 23 August 2021
Accepted: 25 October 2021
Published: 19 November 2021

Citation:
Chen B-J, Qian X-q, Yang X-y, Jiang T, Wang Y-m, Lyu J-h, Chi F-l, Chen P and Ren D-d (2021) Rab11a Regulates the Development of Cilia and Establishment of Planar Cell Polarity in Mammalian Vestibular Hair Cells.
Front. Mol. Neurosci. 14:762916.
doi: 10.3389/fnmol.2021.762916

Vestibular organs have unique planar cell polarity (**Figure 1A**), and their normal development and function are dependent on the regular polarity of cilia (**Figure 1B**) requires. Rab11a is a small G protein that participates in the transportation of intracellular and extracellular materials required for polarity formation; however, our understanding of the mechanisms of the actions of Rab11a in vestibular organs is limited. Here, we showed that the general shape of the utricle was abnormal in *Rab11a*$^{CKO/CKO}$ mice. These mice also showed abnormal morphology of the stereocilia bundles, which were reduced in both length and number, as well as disturbed tissue-level polarity. Rab11a affected the distribution of polarity proteins in the vestibular organs, indicating that the normal development of cilia requires Rab11a and intraflagellar transportation. Furthermore, small G protein migration works together with intraflagellar transportation in the normal development of cilia.

Keywords: Rab11a, cilia, planar cell polarity, vestibular, development

INTRODUCTION

The morphology and polarization of hair cells in the vestibular organs are essential for maintaining balance and sensing head movement. In mammals, the vestibular system is composed of five sensory organs within the inner ear: the utricle, the saccule, and three ampullae (Cullen, 2019). The utricle and saccule sense linear acceleration, while the ampullae located at the end of the semicircular canal are responsible for detecting rotational acceleration (Lempert et al., 1998; Wang and Nathans, 2007). Detecting and transducing mechanical signals from the environment to electrical signals in neurons are dependent on the well-aligned cilia bundles on the hair cells (Fettiplace and Kim, 2014). The hair bundle is composed of a kinocilium with a microtubule core, and stereocilia that develop from microvilli. The kinocilium becomes asymmetrically aligned during development, leading to the formation of staircase-aligned stereocilia from behind. This asymmetrical location of hair bundles on the planar plane of the hair cells is defined as hair

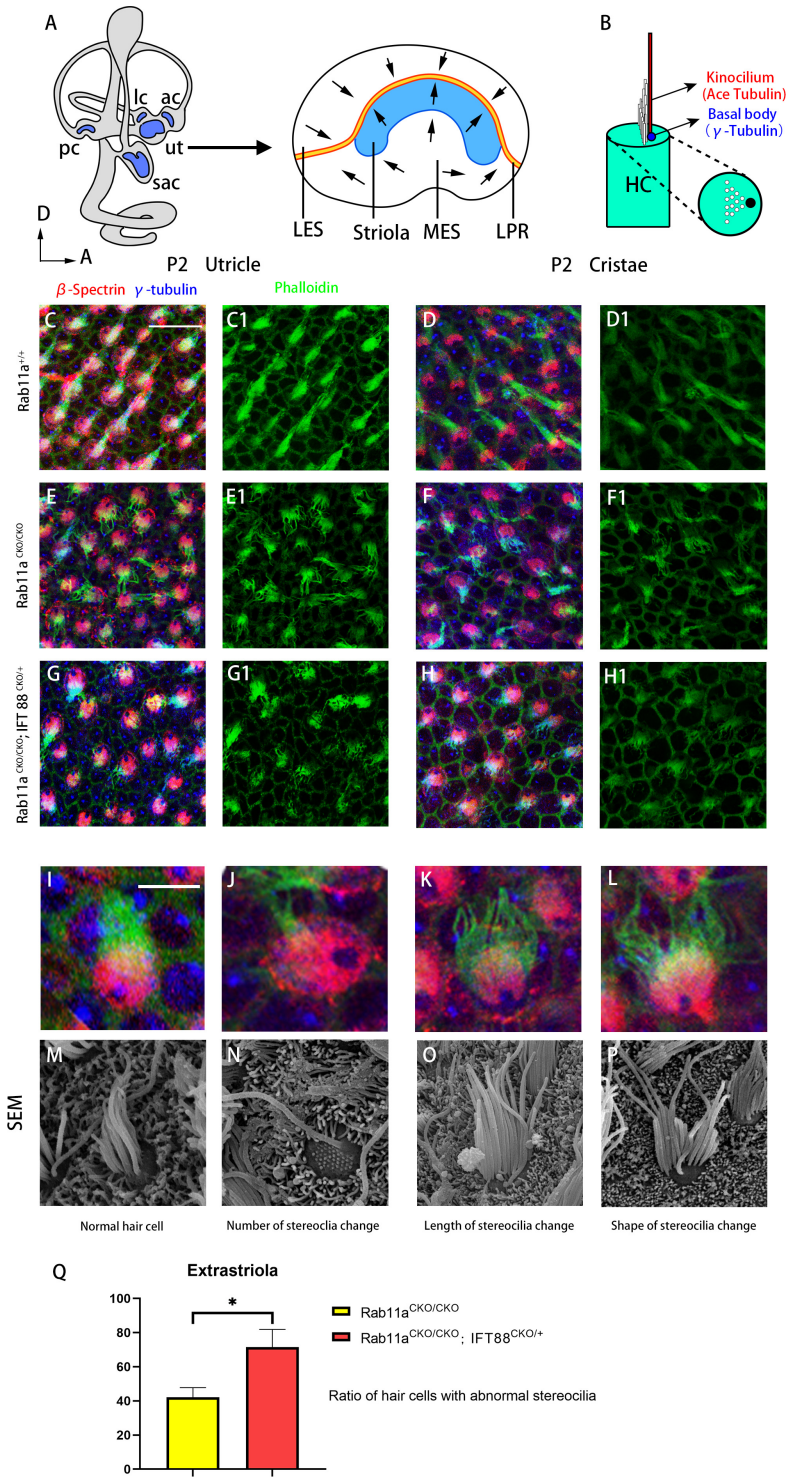

FIGURE 1 | Morphological changes of stereocilia in the extrastriolar hair cells from *Rab11a* single or *Rab11a/IFT88* double-mutant utricles. **(A)** Medial view of a mouse left inner ear with its five vestibular sensory organs (gray). Enlarged are the utricle showing their subdivisions, LPR (yellow line), and striola (blue). LES, lateral extrastriola; MES, medial extrastriola; LPR, line of polarity reversal. **(B)** Schematic view of vestibular hair cell. Kinocilium is marked with ace-tubulin. Basal body is marked with γ-tubulin. **(C,C1,D,D1)** Normal appearance of the stereocilia of extrastriolar hair cells of wild-type controls. **(E,E1,F,F1)** Altered morphology in *Rab11a*$^{CKO/CKO}$ animals. **(G,G1,H,H1)** The changes in the stereocilia morphology were more severe in *Rab11a*$^{CKO/CKO}$/*IFT 88*$^{CKO/+}$ mice. **(I–L)** Higher magnification of confocal images of hair cells. **(M–P)** Scanning electron microscopy images of hair cells from wild-type controls and *Rab11a* mutants. **(I,M)** Morphology of normal. hair cells of wild-type controls. **(J,N)** The number of stereocilia on a single hair cell was deceased in the *Rab11a* mutant. **(K,O)** Stereocilia were shorter in mutants

(Continued)

FIGURE 1 | compared to the wild-type controls. **(L,P)** The staircase-like hair bundle architecture of hair cells was lost in *Rab11a* mutant mice. **(Q)** The percentage of hair cells with abnormal development of static cilia bundles in the extrastriola region was counted as a percentage of the total ($n = 5$). The percentage of abnormal hair cells was higher in Rab11a$^{CKO/CKO}$, IFT88$^{CKO/+}$ mice compared to Rab11a$^{CKO/CKO}$. The abnormal ratios of single and double knockout hair cells were 42.1 ± 5.7 and 71.5 ± 10.4, respectively. In **(A–J)**, for all primary panels, hair cell stereociliary bundles were marked with phalloidin (green), the actin-rich cuticular plate of hair cells was labeled with β-spectrin (red), while the basal body of the hair cell was labeled with γ-tubulin (blue). Scale bars: 10 μm **(C–H1)**, 5 μm **(J–N)**. $^*P < 0.05$.

cell polarity (Furness and Hackney, 2006; Fettiplace and Kim, 2014). Intact hair cell polarity is indispensable for hearing (Jacobson et al., 2008) and maintaining balance in three-dimensional space (Ren et al., 2013). Furthermore, hair cells in each sensory organ of the inner ear are arranged in a coordinated manner that manifests as a specific pattern of planar cell polarity (PCP) (Rida and Chen, 2009). The hair cells in the vestibular organ are highly organized, with a precise microstructure that is important for balance function. Vestibular hair bundles contain 50–100 actin-filled stereocilia, arranged in 10–15 ranks of successively increasing height, giving the bundle a staircase-like appearance. During embryonic development, the PCP signaling pathway can lead cells to convergent extension and oriented cell division, leading to organ morphogenesis. Mutation of the PCP gene can cause serious developmental defects, including neural tube defects, cystic kidney disease (Karner et al., 2009), bone disease (Randall et al., 2012), and congenital heart malformations (Gibbs et al., 2016).

The asymmetric distribution of planar cell polar proteins is a characteristic of polarity. Gαi3 plays an important role in the asymmetric distribution of stereocilia. The Insc/Gαi/LGN complex is formed in the bare zone near the outer side that lacks microvilli, and the aPKC/Par3/Par6 complex is found in the opposite direction near the middle (Ezan et al., 2013; Tarchini et al., 2013). Gαi3 and LGN are also distributed at the top of the stereocilia bundles adjacent to the bare area (Tarchini et al., 2016).

The Rab GTPases are key regulators of intracellular membrane trafficking and endocytic recycling. Rab11 is a small G protein belonging to the Ras superfamily, which plays an important role in regulating the expression of cell surface receptors and adhesion proteins. It has been reported that members of the Rab protein family are related to ciliary transportation, and Rab11 is involved in the formation of protein complexes and in endocytosis and exocytosis (D'Souza-Schorey and Chavrier, 2006; Bos et al., 2007; Stenmark, 2009). In retinoblasts *in vitro*, Rab11a interacted with Rab GTPases in intracellular transportation during the formation of cilia (Knödler et al., 2010). Rab11 was also reported to interact with the core PCP protein, Vangl2. The expression of Rab11 was affected by Vangl2 expression and affected the distribution of Vangl2 during gastrula formation in *Xenopus laevis* (Ossipova et al., 2015).

However, whether Rab protein has a regulatory effect on mammalian inner ear cilia development remains unknown. The mammalian genome encodes three Rab11 proteins, designated as Rab11a, Rab11b, and Rab11c. We found that Rab11a is expressed in the basal body (**Supplementary Figure 1**) of the vestibular organs and plays an important role in cilia formation via the interaction of intraflagellar transport (IFT), the PCP, and tissue polarity.

MATERIALS AND METHODS

Mouse Strains and Animal Care

Animal care and use were performed in accordance with the National Institutes of Health Guide for the Care and Use of Laboratory Animals and the experiments received approval from the Emory University Institutional Animal Care and Use Committee. *Rab11a* conditional knockout mice and *IFT88* conditional knockout mice were described previously (Kibar et al., 2001; Haycraft et al., 2007; Yu et al., 2014). The Looptail mouse strain with a missense mutation in *Vangl2* was obtained from The Jackson Laboratory (Jax stock #000220; Bar Harbor, ME, United States). *Rab11a* and *IFT88* conditional alleles were inactivated via Cre recombinase in the *Foxg1*$^{Cre+}$ mouse line as described previously (Hébert and McConnell, 2000; Pirvola et al., 2002). In this article, *Rab11a*$^{CKO/CKO}$ indicates that Rab11a has been knocked out via *Foxg1*$^{Cre+}$. Similarly, *Ift88*$^{CKO/CKO}$ indicates that Ift88 has been knocked out via *Foxg1*$^{Cre+}$. All Rab11a$^{+/+}$ mice in this research are littermates of mutants such as Rab11a$^{CKO/CKO}$ mice.

Whole-Mount Immunostaining

Neonatal (P0) or postnatal day 2 (P2) *C57Bl/6* mice were anesthetized on ice and disinfected with 75% alcohol and AnEr iodine. The heads of mice were removed and placed in a glass petri dish with sterile 1 × phosphate-buffered saline (PBS). The skull and brain were removed to expose the otic vesicles before fixing with 4% paraformaldehyde in PBS for 1 h at room temperature. The otic vesicles were washed with 1 × PBS three times and then stored at 4°C.

The freshly dissected otic vesicles were placed into sterile 1 × PBS. Microdissecting forceps were used to enter from the cochlea and the inner wall of the vestibule. The bone outside was removed to expose the utricle and saccule, and then the upper cap membrane was peeled off and the otoliths were cleaned carefully to obtain only the vestibular sensory epithelia.

The vestibular epithelia were incubated in blocking solution consisting of 10% donkey serum and in PBS-T (0.1% Triton X-100 in 1 × PBS) at room temperature for 1 h, followed by incubation with primary antibody in PBS-T supplemented with 5% donkey serum overnight at 4°C. After washing three times in PBS-T for 1 h each time, tissues were incubated in a solution containing secondary antibody with or without phalloidin in PBS-T supplemented with 5% donkey serum for 2 h at room temperature. Tissues were again washed

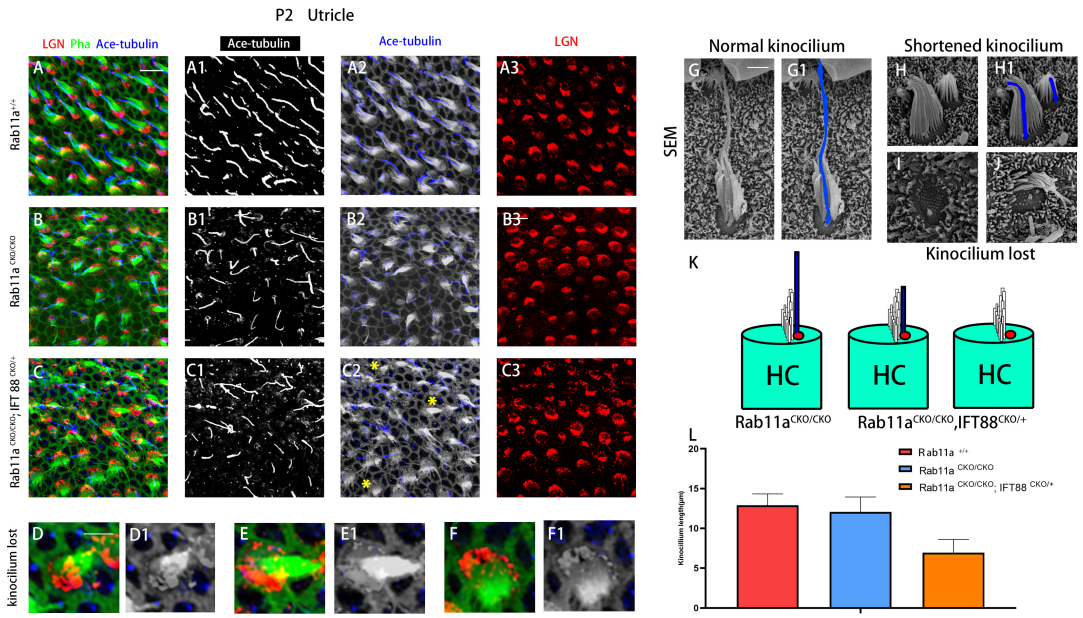

FIGURE 2 | Kinocilia were shortened or lost in *Rab11a* IFT mutant mice. **(A–A3)** In P2 wild-type mice, kinocilia were located on one side of the hair cells, marking the planar cell polarity of single hair cells. **(B–B3)** The length and number of kinocilia were generally normal in *Rab11a* mutant utricles. **(C–C3)** Kinocilia were lost or shortened in *Rab11a*$^{CKO/CKO}$; *IFT88*$^{CKO/+}$ utricle (yellow asterisks). **(D–F1)** Enlarged images of hair cell marked with yellow arrowheads in **(C2)**. **(G,G1)** Scanning electron microscopy image of a normal hair cell. The kinocilia are outlined (blue). **(H,H1)** Shortened kinocilia were found in the hair cells of *Rab11a* mutant utricular macules. **(I,J)** The whole kinocilia were lost in the hair cells of *Rab11a* mutant utricular macules. **(K)** The schematic view of kinocilium shortened or lost in *Rab11a*$^{CKO/CKO}$; *IFT88*$^{CKO/+}$ utricle. **(L)** The average kinocilium length of control, *Rab11a*$^{CKO/CKO}$, *Rab11a*$^{CKO/CKO}$; *IFT88*$^{CKO/+}$ utricle. The kinocilium length of control, single and double knockout hair cells were 12.90 ± 1.43, 12.07 ± 1.87, and 6.95 ± 1.67 μm, respectively. In **(A–F)**, for all primary panels, hair cell stereociliary bundles were marked with phalloidin (green), kinocilium were labeled with acetylated tubulin (blue), and intrinsic cell polarity was labeled with LGN (red). Scale bars: 10 μm **(A–C3)**, 5 μm **(D–F1)**, 1 μm **(G–J)**.

three times in PBS-T, mounted in Fluoromount-G (#0100-01; SouthernBiotech, Birmingham, AL, United States) covered with 1.5-cm coverslips, and sealed.

The following primary antibodies were used: Rab11a (#2413, 1:200; Cell Signaling Technology, Danvers, MA, United States), LGN (1:200, a gift from Fumio Matsuzaki, RIKEN, Kobe, Japan) (Konno et al., 2008), β-spectrin (#612562, 1:200; BD Transduction Laboratories, Franklin Lakes, NJ, United States), acetylated tubulin (#23950, 1:400; Santa Cruz Biotechnology, Dallas, TX, United States), Prickle2 (1:500; a gift from Doris K Wu, NIDCD Laboratory of Molecular Biology, Bethesda, MD, United States), g-tubulin (#T6657, 1:200; Sigma Aldrich, St. Louis, MO, United States), and Vangl2 (#AF4815, 1:200; R&D Systems, Minneapolis, MN, United States).

The following secondary antibodies were used: donkey anti-rabbit-647 (#2492288, 1:1,000; The Jackson Laboratory), donkey anti-rabbit-555 (#2307443, 1:1,000; The Jackson Laboratory), donkey anti-mouse-647 (#2340862, 1:1,000; The Jackson Laboratory), donkey anti-mouse-555 (#2340813, 1:1,000; The Jackson Laboratory), donkey anti-sheep-488 (#2340750, 1:1,000; The Jackson Laboratory), FITC-conjugated phalloidin (#A12379, 1:1,000, Alexa Fluor; Thermo Fisher Scientific, Waltham, MA, United States), and Rho-conjugated phalloidin (#R415, 1:200, Alexa Fluor; Thermo Fisher Scientific).

The specimens were first pre-screened with an Olympus IX71 inverted fluorescence microscope. Confocal images were obtained with either a Leica TCS SP8 or Zeiss LSM510 with excitation wavelengths of 488, 543, and 633 nm.

Scanning Electron Microscopy

Epithelia were washed three times in PBS for 10 min each time, and then fixed in 2.5% glutaraldehyde in 0.1 M PBS at room temperature for 30 min. Samples were then rinsed with 0.1 M cacodylate buffer followed by post-fixation with 1% osmium tetroxide in 0.1 M cacodylate for 1 h. Next, the samples were sequentially fixed in 30 and 50% ethanol for 15 min each, and 70% ethanol overnight at 4°C. The next day, the samples were fixed in 80, 90, and 100% ethanol for 15 min each. The specimens were placed into labeled microporous capsules and loaded into the sample boat of a chilled Polaron E3000 critical point drying unit (Quorum Tech, Laughton, United Kingdom). Samples were sputtered with gold for 3.5 min and scanned at 10 kV using a field emission scanning electron microscope (DS-130F; Topcon, Tokyo, Japan).

Phenotypic and Statistical Analysis

Pictures were processed using Adobe Photoshop CC2017 (San Jose, CA, United States). Statistical analyses of relevant angle data were performed using SPSS ver. 22 (IBM Corp., Armonk, NY, United States). Differences in the means between groups were analyzed using the *t*-test. In all analyses, $P < 0.05$ was taken to indicate statistical significance. GraphPad Prism6 (San

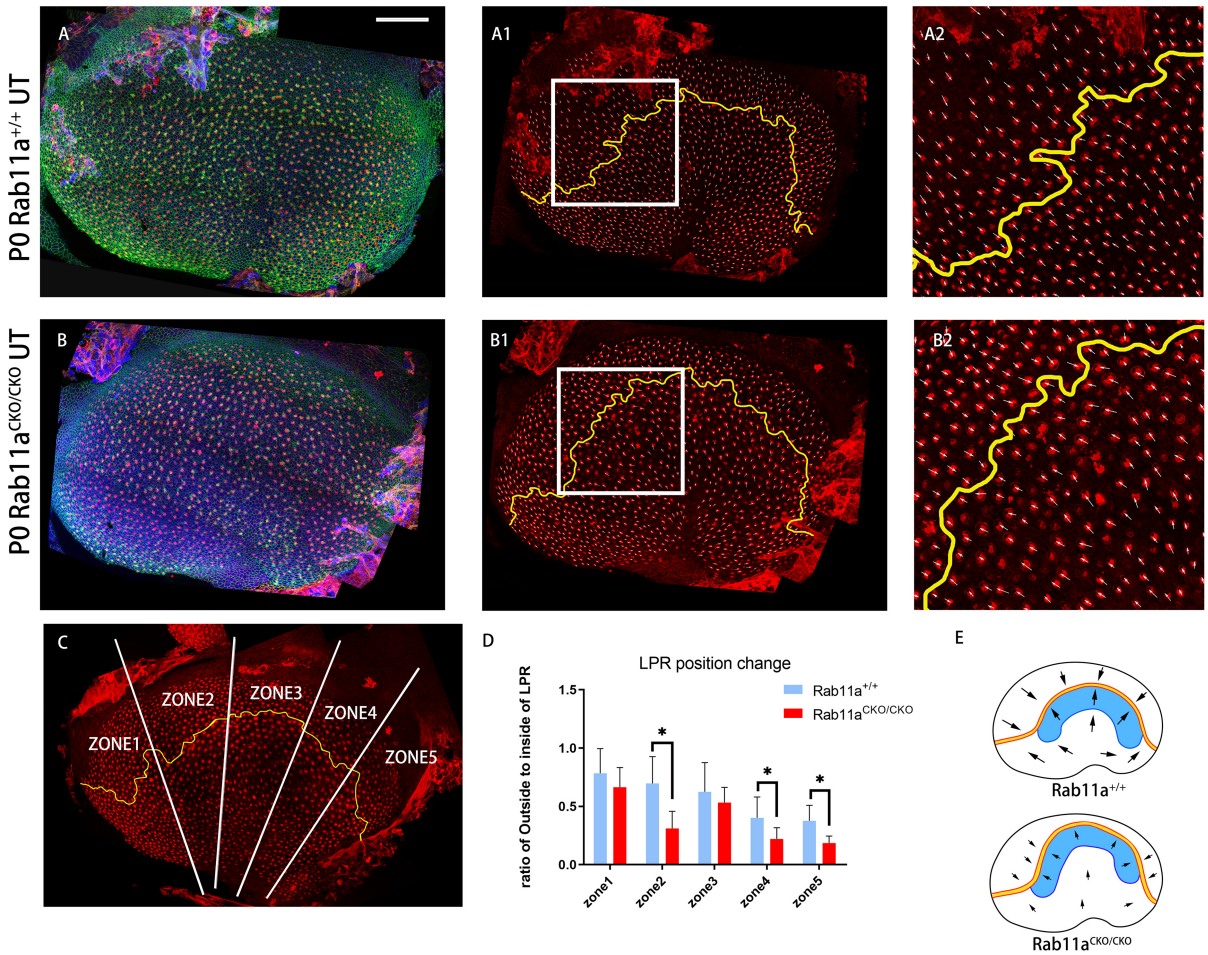

FIGURE 3 | Changes in shape and position of the line of polarity reversal (LPR) in *Rab11a*$^{CKO/CKO}$ utricles. **(A–A2)** In utricular macules of wild-type controls, the planar cell polarity of hair cells was labeled with the cell intrinsic planar cell polarity protein β-spectrin (red). White arrowhead shows the orientation of hair cells. Utricular hair cells were oriented with their bundles pointed toward each other along the LPR (yellow line). **(A2)** Zoomed image of white square in **(A1)**. **(B–B2)** In the *Rab11a* mutant utricle, the utricle was flattened compared to the wild-type utricle. **(B2)** Zoomed image of white square in **(B1)**. **(C)** The utricle was separated into five segments (white line) of similar size according to the length of the LPR (yellow line). The numbers of hair cells located inside and outside the LPR were counted. **(D)** The ratio of the number of hair cells located outside to inside of the LPR was calculated in each of the five segments for each genotype. Five mice were assayed at P0 for each of the wild-type and *Rab11a* knockout groups. Statistical analyses were performed using Student's *t*-test with unequal variance, $^{*}P < 0.01$. The lower ratios in regions 2, 4, and 5 of the *Rab11a*$^{CKO/CKO}$ group indicated that there were fewer hair cells located outside the LPR compared to the wild-type controls, while the total number of hair cells in the utricle was not significantly different between the two groups, and we concluded that the LPR moved toward the outside. **(E)** Schematic view of control and Rab11a$^{CKO/CKO}$ utricle the LPR moved toward the outside in mutant utricle (black arrow). Scale bars: 100 μm.

Diego, CA, United States) was used to draw histograms. The rose function in MatLab software (MathWorks, Natick, MA, United States) was used to draw rose diagrams to show the polar distribution of utricle hair cells.

RESULTS

Rab11a$^{CKO/CKO}$ Leads to Morphological Changes in Cilia in the Mouse Vestibule

Morphological Changes of Stereocilia in the *Rab11a* Mutant Utricle

The morphology of the stereocilia bundles was disrupted in the *Rab11a*$^{CKO/CKO}$ utricle and cristae, while the kinocilium was morphologically normal. Immunofluorescence staining revealed disordered arrangement and dispersion of stereocilia in the utricle and cristae (**Figures 1C–F1**). In the extrastriolar area, stereocilia of wild-type mice were arranged in clusters behind the kinocilium. In contrast, the stereocilia bundles showed morphological alterations in their length, number, and stepped arrangement in the *Rab11a*$^{CKO/CKO}$ utricle. The percentage of hair cells with abnormal development of stereocilia tracts in the extrastriolar area was determined (in five areas in each sample). The proportion of abnormal hair cells was higher in *Rab11a*$^{CKO/CKO}$ mice than in wild-type controls with a ratio of 42.1 ± 5.7 (**Figure 1Q**).

Given that the intraflagellar transporter IFT88 was reported to affect the development of the cochlear PCP, we speculated

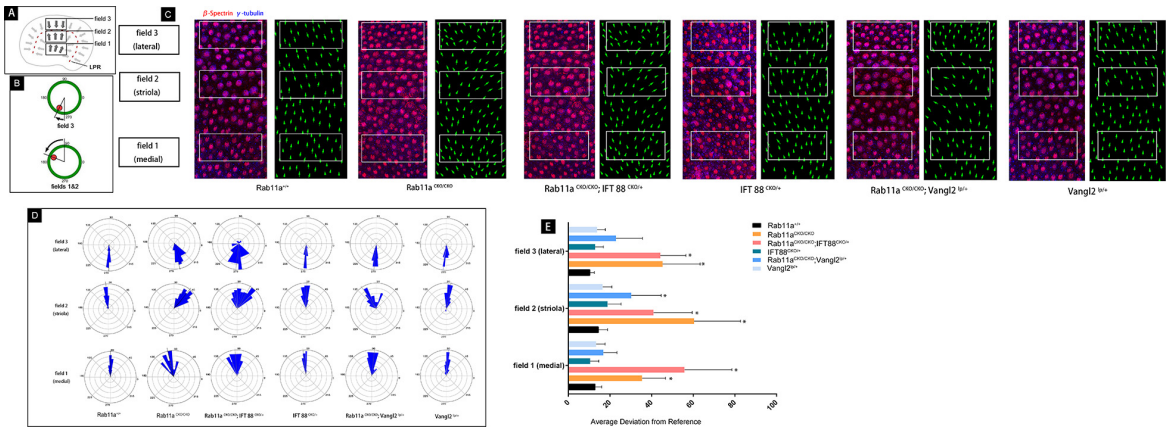

FIGURE 4 | Quantification of vestibular hair cell orientation in control and *Rab11a* mutant utricles. **(A)** Schematic illustrating the positions of the three analysis fields relative to the position of the line of polarity reversal (LPR; red dashed line). Hair cells in the maculae are patterned about the LPR, and as a result cells in the lateral extrastriolar region (LES) have stereociliary bundle orientations that are opposite of those in the striola and medial extrastriolar region (MES). **(B)** Individual stereociliary bundle orientations for vestibular hair cells of the utricular maculae graphed as circular histograms indicated stereociliary bundle misorientation in the striolar region of the *Rab11a* mutant mice. A 90° is directed toward the lateral and 180° toward the medial edge of the utricular maculae, and each bin is 12°. The total numbers of hair cells represented by each histogram (*n*) are shown, and black bars mark the mean stereociliary bundle orientation. The dimensions of the analysis fields are all 100 mm × 50 mm. **(C)** Wild-type utricle hair cells labeled for planar polarity analysis with antibodies to γ-tubulin (blue) and β-spectrin (red). The region close to the LPR was selected from each sample. Individual hair cell orientations have been annotated based on the labeling. Utricles from $Rab11a^{CKO/CKO}$ and $Rab11a^{CKO/CKO}$; $IFT\ 88^{CKO/+}$ mice had misoriented hair cells throughout fields 1–3, while misoriented hair cells in utricles from $Rab11a^{CKO/CKO}$; $Vangl2^{Lp/+}$ mice were restricted to field 2. **(D)** The average mean deviation of stereocilia bundle orientations was determined by measuring the absolute value of the angle formed by the bundle axis and a reference line drawn perpendicular to the striola. In this schematic, red indicates the position of the kinocilium and green is the cell periphery. **(E)** The average deviation from 0° for hair cells located in fields 1, 2, and 3 for each experimental and control genotype. Error bars indicate standard deviation. Statistical significance was calculated using Student's *t*-test with unequal variance, $^*P < 0.01$.

that Rab11a, as a component of the transportation system, may affect cilia formation via the interaction with IFT88. We used *IFT88* and *Rab11a* double mutants to examine the mechanism underlying the role of Rab11a in vestibular development. As conditional double knockout of *Rab11a* and *IFT88* is lethal, we used $Foxg1^{Cre+}$; $IFT88^{fl/+}$; $Rab11a^{fl/fl}$ mice to screen for polarity phenotypes. In the utricle and cristae, the changes in the stereocilia were more severe and more stereocilia bundles were lost in these mutants compared to *Rab11a* single mutants (**Figures 1G-H1**). The abnormalities of the stereocilia, including the number, length, and shape of the stereocilia, could be seen by scanning electron microscopy (**Figures 1I–P**). The proportion of abnormal hair cells in $Rab11a^{CKO/CKO}$; $IFT88^{CKO/+}$ mice was higher compared to $Rab11a^{CKO/CKO}$ mice. The abnormal ratios of single- and double-knockout hair cells were 42.1 ± 5.7 and 71.5 ± 10.4, respectively (**Figure 1Q**).

Kinocilium Shortening or Loss in *Rab11a* and Intraflagellar Transport Double-Mutant Mice

The PCP of vestibular organs consists of three levels: subcellular, intercellular, and tissue-level polarity (Deans, 2013). The kinocilium is tethered to the tallest rod of the hair bundle. The stereocilia staircase is built next to the kinocilium after acquiring its final position (Lu and Sipe, 2016). Within a hair cell, cellular structures, such as the stereocilia, are positioned asymmetrically on the apical plane along the tissue axis, which is defined as subcellular polarity. Therefore, we used phalloidin staining to label the actin-enriched stereocilia, and acetylated tubulin to mark the kinocilia.

In the $Rab11a^{CKO/CKO}$ mouse utricle, the length and number of kinocilia were generally normal compared to those of wild-type controls (**Figures 2A–B3**). The length and number of kinocilia were also reported previously to be unaffected in the utricles of $IFT88^{CKO/CKO}$ mice (Jones et al., 2008). Furthermore, to characterize the hair bundle morphology of $Foxg1^{Cre+}$;$Rab11a^{fl/fl}$; $IFT88^{fl/+}$ mice, we applied both scanning electron microscopy and immunostaining (**Figures 2C–J**). The kinocilium lengths of wild-type, single-gene, and double-gene knockout hair cells were 12.9 ± 1.43, 12.1 ± 1.87, and 6.95 ± 1.67 nm, respectively. The kinocilium developed abnormally, and they became shorter or even disappeared (**Figures 2K,L**).

$Rab11a^{CKO/CKO}$ Leads to Morphological and Line of Polarity Reversal Position Changes in the $Rab11a^{CKO/CKO}$ Utricle

The Insc/Gαi/LGN complex guides the asymmetrical distribution of hair bundles. Therefore, we stained LGN to track the subcellular polarity of hair cells.

In mouse vestibular organs, the subcellular polarity of hair cells is reflected by the direction and pattern of three-dimensional cilia bundles and the position of kinocilium. There was a lack of β-spectrin staining indicating the position of the basal body. The $Rab11a^{CKO/CKO}$ mouse utricle had a flatter morphology compared to the controls. Furthermore, in the development of stereocilia bundles in the hair cells of $Rab11a^{CKO/CKO}$; $IFT88^{CKO//+}$ mice, the proportion of abnormally developed

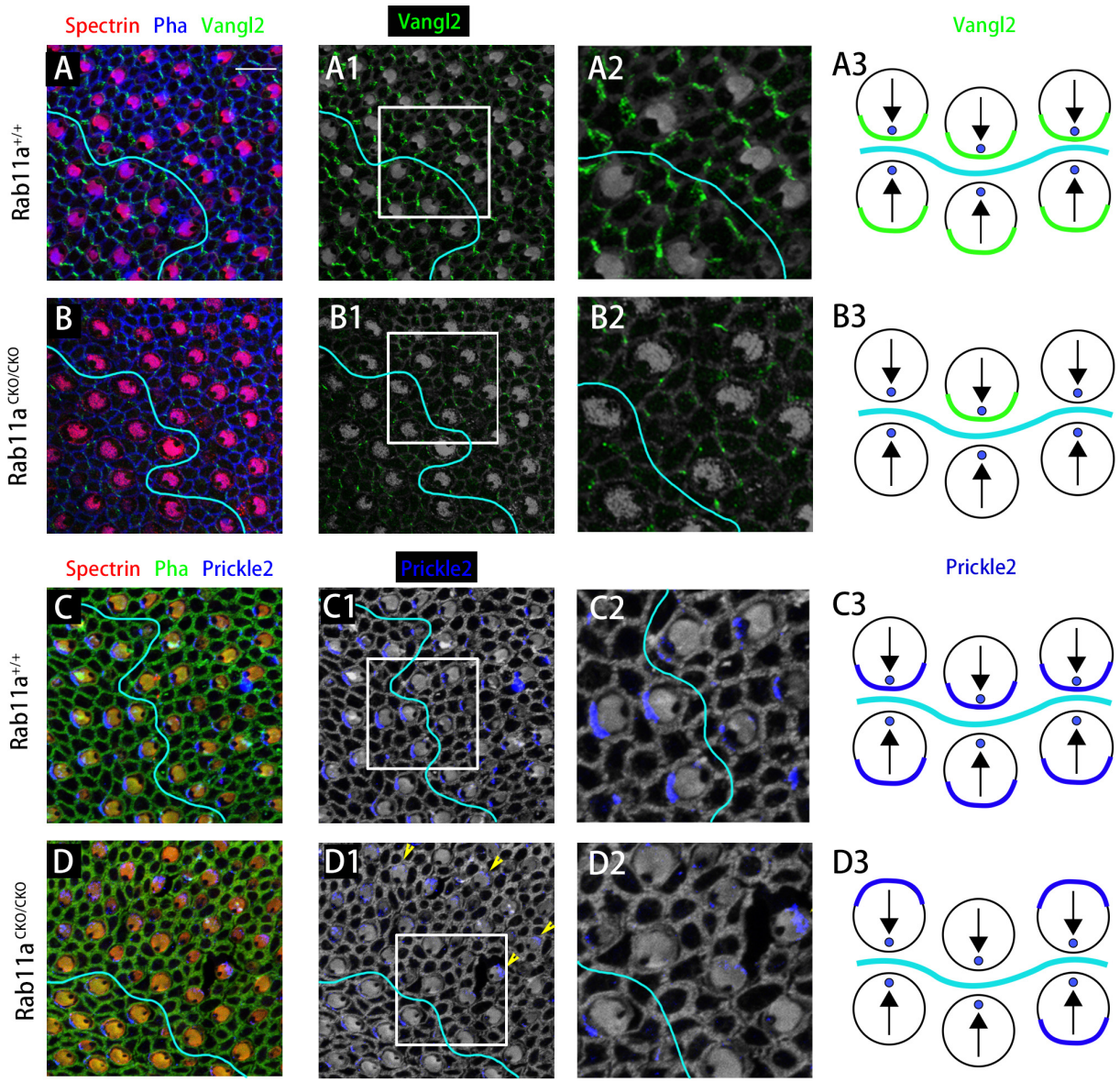

FIGURE 5 | The subcellular distributions of core planar cell polarity (PCP) proteins are affected in *Rab11a* mutant utricles. **(A,A1,A2)** Vangl2 immunolabeling was enriched at cell boundaries in the wild-type utricular maculae. Asymmetrical protein localization was evident at many cell boundaries. **(B,B1,B2)** Vangl2 protein was significantly reduced from apical cell boundaries in *Rab11a*$^{CKO/CKO}$ utricles. **(C,C1,C2)** Prickle2 was enriched at hair cell/support cell boundaries throughout the wild-type utricle. For cells located reversely across in different side of LPR, Prickle2 located in the same side of hair cells. **(D,D1,D2)** In *Rab11a*$^{CKO/CKO}$ mice, the distribution of Pk2 changed in a region-specific manner. Prickle2 moved to the opposite side of hair cells located in two regions across the LPR (yellow arrowheads). **(A3,B3,C3,D3)** Schematic view of Vangl2 and Prickle2 expression in control and Rab11a$^{CKO/CKO}$ utricle. For primary panels in **(A–B2)**, hair cell stereociliary bundles were marked with phalloidin (blue), the actin-rich cuticular plate of hair cells was labeled with an antibody to β-spectrin (red), and with an antibody to the core PCP protein Vangl2 is shown in green. In **(C–D2)**, phalloidin is shown in green, β-spectrin in red, and core PCP protein Prickle2 in blue. Scale bars: 10 μm.

hair cells in the extrastriolar area was higher than that in *Rab11a*$^{CKO/CKO}$ mice (**Figure 1Q**). Staining for the intrinsic polar protein LGN showed the direction of the hair cells (**Figures 3A–B2**), allowing us to draw the line of polarity reversal (LPR). To calculate the shift of LPR, we further counted the number of hair cells adjacent to the LPR (**Figure 3C**), which indicated that the LPR moved to the outside in *Rab11a*$^{CKO/CKO}$ mice (**Figures 3D,E**).

Quantification of Vestibular Hair Cell Orientation in Control and *Rab11a* Mutant Utricles

The direction of hair cells in *Rab11a*$^{CKO/CKO}$; *IFT88*$^{CKO//+}$ utricles was disordered, while the stereocilia appeared to point neatly in the same direction in the normal utricle.

These results indicated that the *Rab11a* and *IFT88* gene was specifically knocked out in vestibular hair cells, the development of stereocilia was affected, and the polarity was also changed.

To study the mechanism underlying the role of *Rab11a* in the core PCP pathway, we used *Rab11a*$^{CKO/CKO}$; *Vangl2*$^{lp/+}$ mice and *Rab11a*$^{CKO/CKO}$; *IFT88*$^{CKO//+}$ double-knockout mice. First, we examined the direction of the hair cells to evaluate the changes in polarity of the tissues (**Figures 4D,E**). The direction of a single hair cell in the utricle could be determined by immunofluorescence analysis of the epidermal plate marker β-spectrin (**Figure 4C**). Studies have shown that Looptail mice with knockout of the *Vangl2* gene do not show effects on the direction of the hair cells in the plaques, while the hair cells of the semicircular canals are whorled (Qian et al., 2007). The hair cell orientation differed significantly in *Rab11a*$^{CKO/CKO}$; *Vangl2*$^{lp/+}$ mice compared to wild-type mice. However, simply knocking out *IFT88* did not affect the hair cells in the vestibule. In *Rab11a*$^{CKO/CKO}$; *IFT88*$^{CKO//+}$ mice, the direction of hair cells was disordered (**Figure 4E**).

Subcellular Distributions of Core Planar Cell Polarity Proteins Are Affected in *Rab11a* Mutant Utricles

To study the PCP of adjacent cells, we performed immunostaining analysis for the core PCP proteins Vangl2 and Prickle2. In the wild-type utricle, Prickle2 and Vangl2 were distributed on the same side of the hair cell regardless of the side of the LPR. In the *Rab11a*$^{CKO/CKO}$ utricle, the level of Vangl2 protein expression was significantly reduced compared to the wild-type controls (**Figures 5A–B3**). As no specific changes were observed in Vangl2 other than its expression level, we examined the expression of Prickle2 in the *Rab11a*$^{CKO/CKO}$ utricle. Some hair cells in the utricles of *Rab11a*$^{CKO/CKO}$ mice showed disordered distribution of Prickle2 compared with the controls (**Figures 5C–D3**), while the direction of the hair cells was still opposite to the two sides of the LPR. These observations confirmed that Rab11a, as an important transport tool, plays an important role in transporting polar proteins to the surface of hair cells, and its knockout affects the expression and distribution of polar proteins.

DISCUSSION

In the vestibular system, unlike the V-shaped arrangement of the cochlea, the stereocilia bundles of hair cells are clustered around the kinocilium. The appropriate arrangement of cilia is essential for hair cells to respond to stimuli and maintain balance function (Fettiplace and Kim, 2014).

The critical role of PCP core proteins in regulating planar polarization in various organs is well conserved across species. However, our understanding of the mechanisms underlying the actions of Rab11a in vestibular organs and how it regulates PCP core proteins is limited.

Cilia Development

The kinocilium plays an important role in the development of hair cell cilia bundles. The extension and maintenance of the length of cilia relies on IFT to transport the required materials along the axons (Eatock and Songer, 2011). Specific knockout of IFT-related genes in the inner ear, including *IFT88*, *Kif3a*, and *IFT20*, leads to dysplasia or loss of kinocilia, and the stereocilia bundles become flattened (Jones et al., 2008; Sipe and Lu, 2011; May-Simera et al., 2015). Besides, deficiency of Ick/Cilk1, which encodes a ciliary kinase regulating IFT, results in kinocilia elongation and PCP defects including misshaping of stereocilia in the cochlea (Okamoto et al., 2017).

Knockout of *Rab11* in the retinoblast cells *in vitro* resulted in damage to the cilia without affecting the vestibular utricle hair cells, but the number, length, and shape of the stereocilia were altered.

Cilia are rich in actin, and the protein synthesis process does not occur in ciliated axons, but kinocilia are aggregated and maintained through IFT (Bisgrove and Yost, 2006; Davis et al., 2006). In the process of cilia transport, the cell transfers various substances to the anchor point through the IFT complex, of which IFT88 is a subunit. Studies of the inner ear of IFT88/Polaris mutants have shown that after conditionally knocking out the *IFT88* gene in cochlear hair cells, the position of the basal body changes. It is no longer polarized to the side of the cell but rather is present in the center of the hair cell. In some cells, kinocilia did not develop, the stereocilia were arranged in a circle, and the internal polarity of the cells was disrupted, while no morphological changes were observed in the vestibular hair cells (Jones et al., 2008).

The kinocilia of the utricle were missing or reduced in length in *Foxg1*$^{Cre+}$; *Rab11a*$^{fl/fl}$; *IFT88*$^{fl/+}$ mice. In addition, the phenotype of *Rab11a* and *IFT* mutant utricles included a higher proportion of abnormal cilia than the utricles of single *Rab11a* mutants. We concluded that the roles of Rab11a and IFT88 in the development of kinocilia are redundant, and their in stereocilia development partially overlap.

Influence on Planar Cell Polarity

Disruption of the arrangement and polarity distribution of inner ear cilia bundles can cause hearing and balance disorders in mice and humans (Lempert et al., 1998; Littlewood Evans and Müller, 2000; Alagramam et al., 2001; Adato et al., 2005; Corey, 2009). In the inner ear sensory organs, the hair cells are arranged in a

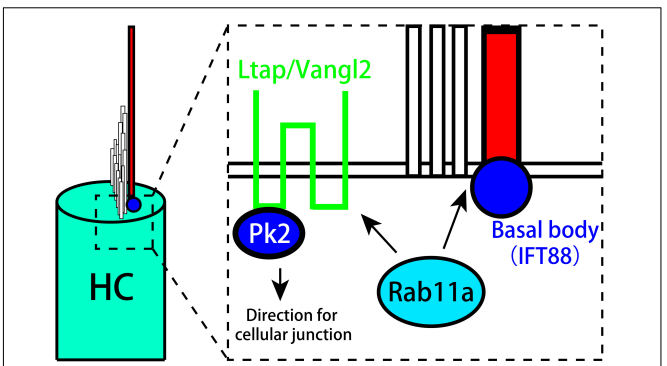

FIGURE 6 | Model showing the role of Rab11a in the formation of planar cell polarity in utricle. Rab11a intracts with Ift88 expressed in kinocilium basal body to affect the development of vestibular cilia. Besides, Rab11a affects the polarization of PCP core proteins including Vangl2 and Prickle2.

coordinated and regular manner, showing a unique PCP (Rida and Chen, 2009). The polar arrangement of hair cells plays an important role in the complete functioning of sensory organs (Jacobson et al., 2008). For the five vestibular organs, the relative arrangement of hair cells is indispensable for maintaining balance in three-dimensional space.

The PCP is reflected at three different anatomical levels in the vestibular organs. First, there is PCP at the intracellular level, the so-called intrinsic polarity of the cell. In mice, at about embryonic day 12.5, the hair cells begin to develop characteristics different from the precursor cells. A fibril appears in the center of the hair cell, and it is surrounded by micropili that develop into stereocilia. The original cilia gradually elongate into kinocilia, which is mediated by the core PCP protein. For example, core PCP protein migrates to the side of the hair cell, marking the establishment of the internal polarity of the cell (Deans, 2013). Second, there is intercellular polarity, marked by the localization of Dvl2/3, Fzd3, Pk, and Vangl2 that coordinate the arrangement of stereocilia between adjacent cells (Denman-Johnson and Forge, 1999). Our results showed that in the *Rab11a*$^{CKO/CKO}$ utricle, the direction of the hair cells was disordered compared to the controls (**Figure 4**). In addition, immunofluorescence staining demonstrated changes in the expression of Vangl2 and Prickle-2 in the *Rab11a*$^{CKO/CKO}$ utricle. Thus, Rab11a appears to affect the intercellular polarity by affecting Vangl2 and Prickle-2.

Finally, there is tissue polarity. In both the utricle and saccule, the LPR divides the sensory epithelial cells into two groups with opposite stereociliary bundle polarities that are able to detect movements in opposite directions (Deans, 2013). One hypothesis is that hair cells located on opposite sides of the LPR have unique transcriptional profiles and can respond to the PCP-based tissue polarity information in opposite manners. Emx2 is a candidate regulator for transcriptional patterning because the LPR did not form in Emx2 mutants (Holley et al., 2010). The mechanisms regulating tissue polarity and patterning of the LPR have not been elucidated. However, we observed abnormal LPR formation in the *Rab11a*$^{CKO/CKO}$ utricle in the present study but did not investigate the underlying mechanisms.

CONCLUSION

Rab11a affects the development of cilia and the PCP of vestibular organs. In addition, it works together with IFT in the development of kinocilia and stereocilia. Rab11a also affects cell polarity by controlling the distribution of Vangl2 and Prickle-2, and can cause the LPR to move toward the outside to affect tissue polarity (**Figure 6**).

AUTHOR'S NOTE

Planar cell polarity refers to the asymmetric distribution of cell morphology and polar proteins. The regular formation of planar cell polarity in vestibular organs is the basis for balance function. We found that small G protein knockout during development led to the disordered distribution of polarity proteins and immature phenotypes of sensory hair cells, suggesting its important role in vestibular organ development.

DATA AVAILABILITY STATEMENT

The original contributions presented in the study are included in the article/**Supplementary Material**, further inquiries can be directed to the corresponding authors.

ETHICS STATEMENT

The animal study was reviewed and approved by the Institutional Animal Care and Use Committee Emory University.

AUTHOR CONTRIBUTIONS

D-dR, F-lC, and PC conceptualized and designed the study and reviewed the data. B-JC and X-qQ analyzed the data. B-JC, X-qQ, X-yY, and TJ wrote and edited the manuscript. Y-mW and J-hL retrieved and validated the data. D-dR and F-lC provided funding support, administered the project, and edited the manuscript. D-dR, F-lC, B-JC, X-qQ, and X-qQ provided data resources. All authors have reviewed, discussed and approved the manuscript.

FUNDING

This study was supported by the National Natural Science Foundation of China (NSFC; Grant Nos. 81420108010 and 81970889 to F-lC and 81771017 and 81970880 to D-dR); the "Zhuo-Xue Plan" of Fudan University to D-dR; The Original Research Personalized Support Project of Fudan University to D-dR; The Medical and industrial integration project of Fudan University to D-dR.

SUPPLEMENTARY MATERIAL

The Supplementary Material for this article can be found online at: https://www.frontiersin.org/articles/10.3389/fnmol.2021.762916/full#supplementary-material

Supplementary Figure 1 | (A) Rab11a gene conditional knockout mice were constructed by inserting two Loxp sites between exons 2 and 5, and excising specific sheared exons 3,4 by binding to Cre recombinase. **(B)** Identification of genotype of Rab11a: the genotype of *Rab11*$^{fl/fl}$ we need to obtain. Three cases can be seen in the figure. Pure type *Rab11*$^{fl/fl}$ has a flox band with a product size of 564 bp. wild type *Rab11*$^{+/+}$ has a WT band with a product size of 400 bp. heterozygous Rab11a has both flox and WT bands. **(C)** Identification of genotype of Foxg1Cre: To specifically knock out Rab11a in the inner ear, *Foxg1*$^{Cre+}$ was selected for specific expression. Cre-positive had a band and the product size was 500 bp.

Supplementary Figure 2 | Rab11a expression in hair cells of the wild-type mouse vestibular system. In the P0 utricle **(A–A3)** and saccule **(B–B3)** of wild-type controls, Rab11a was located in the basal body of hair cells overlapping with the expression of γ-tubulin. The basal body was labeled with an antibody to γ-tubulin (red). The cytoskeleton was labeled with phalloidin (green), and staining for Rab11a is shown in blue. Scale bars: 10 μm.

Supplementary Figure 3 | (A,A1) Normal appearance of anterior cristae in wild-type controls. The utricle is labeled with an anti-β-spectrin, the hair cell basal body is labeled with anti-γ-tubulin (blue), while stereocilia bundles are labeled with phalloidin (green). In the anterior and superior cristae of the mouse vestibular system, the well-organized planar cell coordination can be observed. **(B,B1)** In *Rab11a* mutants, the alignment of neighboring hair cells was not disrupted in P2 hair cells of the anterior cristae. **(C,C1)** Tissue planar cell polarity could be seen in hair cells from the lateral cristae of wild-type controls. **(D,D1)** In *Rab11a* mutants, all neighboring hair cells retained the same orientation. Scale bars: 50 μm.

Supplementary Figure 4 | The *Rab11a*$^{CKO/CKO}$ utricle **(A)** was labeled with anti-β-spectrin **(A1)**, the hair cell basal body **(A2)** like IFT88 was labeled with anti-γ-tubulin (blue), and stereocilia bundles **(A3)** were labeled with phalloidin (green).

REFERENCES

Adato, A., Lefèvre, G., Delprat, B., Michel, V., Michalski, N., Chardenoux, S., et al. (2005). Usherin, the defective protein in Usher syndrome type IIA, is likely to be a component of interstereocilia ankle links in the inner ear sensory cells. *Hum. Mol. Genet.* 14, 3921–3932. doi: 10.1093/hmg/ddi416

Alagramam, K. N., Murcia, C. L., Kwon, H. Y., Pawlowski, K. S., Wright, C. G., and Woychik, R. P. (2001). The mouse Ames waltzer hearing-loss mutant is caused by mutation of Pcdh15, a novel protocadherin gene. *Nat. Genet.* 27, 99–102. doi: 10.1038/83837

Bisgrove, B. W., and Yost, H. J. (2006). The roles of cilia in developmental disorders and disease. *Development* 133, 4131–4143.

Bos, J. L., Rehmann, H., and Wittinghofer, A. (2007). GEFs and GAPs: critical elements in the control of small G proteins. *Cell* 129, 865–877. doi: 10.1016/j.cell.2007.05.018

Corey, D. P. (2009). Cell biology of mechanotransduction in inner-ear hair cells. *F1000 Biol. Rep.* 1:58.

Cullen, K. E. (2019). Vestibular processing during natural self-motion: implications for perception and action. *Nat. Rev. Neurosci.* 20, 346–363.

Davis, E. E., Brueckner, M., and Katsanis, N. (2006). The emerging complexity of the vertebrate cilium: new functional roles for an ancient organelle. *Dev. Cell.* 11, 9–19. doi: 10.1016/j.devcel.2006.06.009

Deans, M. R. (2013). A balance of form and function: planar polarity and development of the vestibular maculae. *Semin. Cell. Dev. Biol.* 24, 490–498. doi: 10.1016/j.semcdb.2013.03.001

Denman-Johnson, K., and Forge, A. (1999). Establishment of hair bundle polarity and orientation in the developing vestibular system of the mouse. *J. Neurocytol.* 28, 821–835.

D'Souza-Schorey, C., and Chavrier, P. (2006). ARF proteins: roles in membrane traffic and beyond. *Nat. Rev. Mol. Cell. Biol.* 7, 347–358. doi: 10.1038/nrm1910

Eatock, R. A., and Songer, J. E. (2011). Vestibular hair cells and afferents: two channels for head motion signals. *Annu. Rev. Neurosci.* 34, 501–534.

Ezan, J., Lasvaux, L., Gezer, A., Novakovic, A., May-Simera, H., Belotti, E., et al. (2013). Primary cilium migration depends on G-protein signalling control of subapical cytoskeleton. *Nat. Cell. Biol.* 15, 1107–1115. doi: 10.1038/ncb2819

Fettiplace, R., and Kim, K. X. (2014). The physiology of mechanoelectrical transduction channels in hearing. *Physiol. Rev.* 94, 951–986. doi: 10.1152/physrev.00038.2013

Furness, D. N., and Hackney, C. M. (2006). "The structure and composition of the stereociliary bundle of vertebrate hair cells," in *Vertebrate Hair Cells*, eds R. A. Eatock, R. R. Fay, and A. N. Popper (New York: Springer), 20–94.

Gibbs, B. C., Damerla, R. R., Vladar, E. K., Chatterjee, B., Wan, Y., Liu, X., et al. (2016). Prickle1 mutation causes planar cell polarity and directional cell migration defects associated with cardiac outflow tract anomalies and other structural birth defects. *Biol. Open* 5, 323–335. doi: 10.1242/bio.015750

Haycraft, C. J., Zhang, Q., Song, B., Jackson, W. S., Detloff, P. J., Serra, R., et al. (2007). Intraflagellar transport is essential for endochondral bone formation. *Development* 134, 307–316. doi: 10.1242/dev.02732

Hébert, J. M., and McConnell, S. K. (2000). Targeting of cre to the Foxg1 (BF-1) locus mediates loxP recombination in the telencephalon and other developing head structures. *Dev. Biol.* 222, 296–306. doi: 10.1006/dbio.2000.9732

Holley, M., Rhodes, C., Kneebone, A., Herde, M. K., Fleming, M., and Steel, K. P. (2010). Emx2 and early hair cell development in the mouse inner ear. *Dev. Biol.* 340, 547–556. doi: 10.1016/j.ydbio.2010.02.004

Jacobson, S. G., Cideciyan, A. V., Aleman, T. S., Sumaroka, A., Roman, A. J., Gardner, L. M., et al. (2008). Usher syndromes due to MYO7A, PCDH15, USH2A or GPR98 mutations share retinal disease mechanism. *Hum. Mol. Genet.* 17, 2405–2415. doi: 10.1093/hmg/ddn140

Jones, C., Roper, V. C., Foucher, I., Qian, D., Banizs, B., Petit, C., et al. (2008). Ciliary proteins link basal body polarization to planar cell polarity regulation. *Nat. Genet.* 40, 69–77. doi: 10.1038/ng.2007.54

Karner, C. M., Chirumamilla, R., Aoki, S., Igarashi, P., Wallingford, J. B., and Carroll, T. J. (2009). Wnt9b signaling regulates planar cell polarity and kidney tubule morphogenesis. *Nat. Genet.* 41, 793–799. doi: 10.1038/ng.400

Kibar, Z., Vogan, K. J., Groulx, N., Justice, M. J., Underhill, D. A., and Gros, P. (2001). Ltap, a mammalian homolog of Drosophila Strabismus/Van Gogh, is altered in the mouse neural tube mutant Loop-tail. *Nat. Genet.* 28, 251–255. doi: 10.1038/90081

Knödler, A., Feng, S., Zhang, J., Zhang, X., Das, A., Peränen, J., et al. (2010). Coordination of Rab8 and Rab11 in primary ciliogenesis. *Proc. Natl. Acad. Sci. U. S. A.* 107, 6346–6351. doi: 10.1073/pnas.1002401107

Konno, D., Shioi, G., Shitamukai, A., Mori, A., Kiyonari, H., Miyata, T., et al. (2008). Neuroepithelial progenitors undergo LGN-dependent planar divisions to maintain self-renewability during mammalian neurogenesis. *Nat. Cell. Biol.* 10, 93–101. doi: 10.1038/ncb1673

Lempert, T., Gianna, C., Brookes, G., Bronstein, A., and Gresty, M. (1998). Horizontal otolith-ocular responses in humans after unilateral vestibular deafferentation. *Exp. Brain Res.* 118, 533–540. doi: 10.1007/s002210050309

Littlewood Evans, A., and Müller, U. (2000). Stereocilia defects in the sensory hair cells of the inner ear in mice deficient in integrin alpha8beta1. *Nat. Genet.* 24, 424–428. doi: 10.1038/74286

Lu, X., and Sipe, C. W. (2016). Developmental regulation of planar cell polarity and hair-bundle morphogenesis in auditory hair cells: lessons from human and mouse genetics. *Wiley Interdiscip. Rev. Dev. Biol.* 5, 85–101. doi: 10.1002/wdev.202

May-Simera, H. L., Petralia, R. S., Montcouquiol, M., Wang, Y. X., Szarama, K. B., Liu, Y., et al. (2015). Ciliary proteins Bbs8 and Ift20 promote planar cell polarity in the cochlea. *Development* 142, 555–566. doi: 10.1242/dev.113696

Okamoto, S., Chaya, T., Omori, Y., Kuwahara, R., Kubo, S., Sakaguchi, H., et al. (2017). Ick ciliary kinase is essential for planar cell polarity formation in inner ear hair cells and hearing function. *J. Neurosci.* 37, 2073–2085. doi: 10.1523/JNEUROSCI.3067-16.2017

Ossipova, O., Chuykin, I., Chu, C. W., and Sokol, S. Y. (2015). Vangl2 cooperates with Rab11 and Myosin V to regulate apical constriction during vertebrate gastrulation. *Development* 142, 99–107. doi: 10.1242/dev.111161

Pirvola, U., Ylikoski, J., Trokovic, R., Hébert, J. M., McConnell, S. K., and Partanen, J. (2002). FGFR1 is required for the development of the auditory sensory epithelium. *Neuron* 35, 671–680. doi: 10.1016/s0896-6273(02)00824-3

Qian, D., Jones, C., Rzadzinska, A., Mark, S., Zhang, X., Steel, K. P., et al. (2007). Wnt5a functions in planar cell polarity regulation in mice. *Dev. Biol.* 306, 121–133.

Randall, R. M., Shao, Y. Y., Wang, L., and Ballock, R. T. (2012). Activation of Wnt Planar Cell Polarity (PCP) signaling promotes growth plate column formation in vitro. *J. Orthop. Res.* 30, 1906–1914. doi: 10.1002/jor.22152

Ren, D. D., Kelly, M., Kim, S. M., Grimsley-Myers, C. M., Chi, F. L., and Chen, P. (2013). Testin interacts with vangl2 genetically to regulate inner ear sensory

cell orientation and the normal development of the female reproductive tract in mice. *Dev. Dyn.* 242, 1454–1465. doi: 10.1002/dvdy.24042

Rida, P. C., and Chen, P. (2009). Line up and listen: Planar cell polarity regulation in the mammalian inner ear. *Semin. Cell. Dev. Biol.* 20, 978–985. doi: 10.1016/j.semcdb.2009.02.007

Sipe, C. W., and Lu, X. (2011). Kif3a regulates planar polarization of auditory hair cells through both ciliary and non-ciliary mechanisms. *Development* 138, 3441–3449. doi: 10.1242/dev.065961

Stenmark, H. (2009). Rab GTPases as coordinators of vesicle traffic. *Nat. Rev. Mol. Cell. Biol.* 10, 513–525. doi: 10.1038/nrm2728

Tarchini, B., Jolicoeur, C., and Cayouette, M. (2013). A molecular blueprint at the apical surface establishes planar asymmetry in cochlear hair cells. *Dev. Cell.* 27, 88–102. doi: 10.1016/j.devcel.2013.09.011

Tarchini, B., Tadenev, A. L., Devanney, N., and Cayouette, M. (2016). A link between planar polarity and staircase-like bundle architecture in hair cells. *Development* 143, 3926–3932. doi: 10.1242/dev.139089

Wang, Y., and Nathans, J. (2007). Tissue/planar cell polarity in vertebrates: new insights and new questions. *Development* 134, 647–658. doi: 10.1242/dev.02772

Yu, S., Yehia, G., Wang, J., Stypulkowski, E., Sakamori, R., Jiang, P., et al. (2014). Global ablation of the mouse Rab11a gene impairs early embryogenesis and matrix metalloproteinase secretion. *J. Biol. Chem.* 289, 32030–32043. doi: 10.1074/jbc.M113.538223

Conflict of Interest: The authors declare that the research was conducted in the absence of any commercial or financial relationships that could be construed as a potential conflict of interest.

Publisher's Note: All claims expressed in this article are solely those of the authors and do not necessarily represent those of their affiliated organizations, or those of the publisher, the editors and the reviewers. Any product that may be evaluated in this article, or claim that may be made by its manufacturer, is not guaranteed or endorsed by the publisher.

frontiers in Molecular Neuroscience

ORIGINAL RESEARCH
published: 17 December 2021
doi: 10.3389/fnmol.2021.809878

Epithelial–Mesenchymal Transition Participates in the Formation of Vestibular Flat Epithelium

*Lu He†, Guo-Peng Wang†, Jing-Ying Guo, Zhong-Rui Chen, Ke Liu and Shu-Sheng Gong**

Department of Otolaryngology-Head and Neck Surgery, Beijing Friendship Hospital, Capital Medical University, Beijing, China

The vestibular sensory epithelium of humans and mice may degenerate into a layer of flat cells, known as flat epithelium (FE), after a severe lesion. However, the pathogenesis of vestibular FE remains unclear. To determine whether the epithelial–mesenchymal transition (EMT) participates in the formation of vestibular FE, we used a well-established mouse model in which FE was induced in the utricle by an injection of streptomycin into the inner ear. The mesenchymal and epithelial cell markers and cell proliferation were examined using immunofluorescence staining and quantitative reverse transcription polymerase chain reaction (qRT-PCR). The function of the EMT was assessed through transcriptome microarray analysis. The results demonstrated that mesenchymal cell markers (α-SMA, S100A4, vimentin, and Fn1) were upregulated in vestibular FE compared with the normal utricle. Robust cell proliferation, which was absent in the normal status, was observed in the formation of FE. Microarray analysis identified 1,227 upregulated and 962 downregulated genes in vestibular FE. Gene Ontology (GO) analysis revealed that differentially expressed genes (DEGs) were highly associated with several EMT-related GO terms, such as cell adhesion, cell migration, and extracellular matrix. Pathway enrichment analysis revealed that DEGs were enriched in the EMT-related signaling pathways, including extracellular matrix (ECM)-receptor interaction, focal adhesion, PI3K/Akt signaling pathway and cell adhesion molecule. Protein–protein interaction networks screened 20 hub genes, which were *Akt, Casp3, Col1a1, Col1a2, Fn1, Hgf, Igf1,Il1b, Irs1, Itga2, Itga5, Jun, Mapk1, Myc, Nras, Pdgfrb, Tgfb1, Thbs1*, *Trp53*, and *Col2a1*. Most of these genes are reportedly involved in the EMT process in various tissues. The mRNA expression level of hub genes was validated using qRT-PCR. In conclusion, the present study indicates that EMT plays a significant role in the formation of vestibular FE and provides an overview of transcriptome characteristics in vestibular FE.

Keywords: epithelial–mesenchymal transition, vestibular, microarray, cell proliferation, hair cell, supporting cell

OPEN ACCESS

Edited by:
Yu Sun,
Huazhong University of Science and Technology, China

Reviewed by:
Renjie Chai,
Southeast University, China
Yilai Shu,
Fudan University, China

****Correspondence:***
Shu-Sheng Gong
gongss1962@163.com

† These authors have contributed equally to this work

Specialty section:
This article was submitted to Molecular Signalling and Pathways, a section of the journal Frontiers in Molecular Neuroscience

Received: *05 November 2021*
Accepted: *02 December 2021*
Published: *17 December 2021*

Citation:
He L, Wang G-P, Guo J-Y, Chen Z-R, Liu K and Gong S-S (2021) Epithelial–Mesenchymal Transition Participates in the Formation of Vestibular Flat Epithelium. Front. Mol. Neurosci. 14:809878. doi: 10.3389/fnmol.2021.809878

INTRODUCTION

Vestibular end organs, including the utricle, saccule, and cristae ampullae, are responsible for the perception of linear acceleration and head rotation. Sensory epithelia of vestibular end-organs consist of two kinds of highly differentiated cells: hair cells (HCs) and supporting cells (SCs). HCs and SCs are alternatively arranged in a special mosaic structure required for normal vestibular

function. Various insults to the vestibular sensory epithelium could lead to vestibular dysfunction (McCall et al., 2009; Wang et al., 2015; Brosel et al., 2016; Isgrig et al., 2017; You et al., 2018; Zhang et al., 2020; Fu et al., 2021). Severe lesions damage both vestibular HCs and SCs and induce the sensory epithelium to be replaced by a layer of flat cells, referred to as flat epithelium (FE) (Wang et al., 2017). FE has been found in the inner ear of patients with severe deafness and/or vestibular dysfunction (Nadol and Eddington, 2006; Teufert et al., 2006; McCall et al., 2009), suggesting that FE is an important pathological change in patients with inner ear diseases. However, the pathogenesis of vestibular FE remains unknown, and there is no biological intervention for patients with FE in the inner ear. Elucidation of the molecular mechanism underlying FE formation is significant for designing therapeutic strategies for vestibular dysfunction.

The epithelial–mesenchymal transition (EMT) is a biological process (BP) that allows epithelial cells to acquire a mesenchymal cell phenotype, including migratory capacity, invasiveness, resistance to apoptosis, and increased production of extracellular matrix (ECM) components (Kalluri and Weinberg, 2009). The EMT is integral in development and wound healing, and contributes pathologically to fibrosis and cancer progression (Lamouille et al., 2014). In addition, the EMT participates in inner ear development and damage repair (Simonneau et al., 2003; Kobayashi et al., 2008; Johnen et al., 2012; Wu and Kelley, 2012). The EMT is involved in the formation of cochlear FE, which is characterized by a robust proliferative response, upregulation of mesenchymal cell markers, and cell migration (Kim and Raphael, 2007; Ladrech et al., 2017). Because the two components of the inner ear, cochlea and vestibular end-organs, share common embryonic origins and biological features, we hypothesize that the EMT also participates in the process of vestibular FE formation.

The EMT is characterized by a change in cell phenotype from epithelial to mesenchymal cells with upregulation of mesenchymal cell markers (vimentin, α-SMA, S100A4, fibronectin, N-cadherin, etc.) and downregulation of epithelial cell markers (E-cadherin, cytokeratin, and ZO-1, etc.). Thus, these factors are usually used as biomarkers to define the involvement of EMT (Kalluri and Weinberg, 2009). Recently, high-throughput screening, such as microarray and RNA-seq technologies, has enabled researchers to identify gene expression profiles in various diseases, rendering exploration of the underlying molecular mechanisms less difficult. The role of the EMT in diseases and the specific genes or signaling pathways involved have been explored using these techniques in the past decades (Puram et al., 2018). However, whether EMT participates in the inner flattening process of vestibular sensory epithelium has not been identified.

To determine the role of the EMT in the formation of vestibular FE, a high dose of streptomycin was inoculated into the mouse inner ear to induce FE in the utricle (Wang et al., 2017). Mesenchymal and epithelial cell markers and cell proliferation were assessed in normal utricle and vestibular FE using immunofluorescence staining. Then, the mRNA expression profile was examined using microarray analysis. Bioinformatics analysis was used to further analyze the biological functions of differentially expressed genes (DEGs). Finally, the representative DEGs were validated using quantitative reverse transcription polymerase chain reaction (qRT-PCR). In the present study, the role of EMT in vestibular FE formation was investigated, and the potential mechanisms underlying this process were explored.

RESULTS

Expression of Mesenchymal and Epithelial Cell Markers in Utricular Flat Epithelium

To determine the potential mechanisms underlying FE formation after the loss of nearly all original epithelial cells, the expression of mesenchymal and epithelial cell markers was examined using immunofluorescence staining and qRT-PCR in the normal utricle and utricular FE samples. As shown in **Figures 1A–D″**, mesenchymal cell markers α-SMA and S100A4 were poorly expressed in normal utricle but highly expressed in FE. In contrast, epithelial cell marker ZO-1 was significantly expressed in the normal samples but weakly expressed in FE (**Figures 1E–F″**). Furthermore, the mRNA expression levels of mesenchymal cell markers, *S100A4*, *α-SMA*, *vimentin*, and *fibronectin 1* (*Fn1*) were significantly higher in FE than in the normal utricle (**Figure 1G**). The expression of epithelial cell markers (*E-cadherin, ZO-1, keratin 5*, and *keratin 8*) was not significantly different between the normal utricle and FE (**Figure 1H**).

Robust Mitosis in Adult Mouse Utricle After Severe Damage

To evaluate if the utricular sensory epithelium possesses proliferation capacity during FE formation, the normal utricle and FE were stained with EdU to observe mitosis in the cells and with the epithelial cell marker E-cadherin to label the actin cytoskeleton. At 3 days after streptomycin injection, a few EdU-positive cells were observed (**Figures 2A–A′**). At 7 days after the lesion, the number of EdU-positive cells was increased (**Figures 2B–B′**). At 11 days after the lesion, most of the original sensory epithelium areas expressed E-cadherin, and EdU-positive cells were extensively distributed throughout the FE, indicating robust cell proliferation in the utricular FE during the early period of FE formation (**Figures 2C–C′,E–E‴**). At 22 days after the lesion, the epithelial cytoskeleton was completely formed, and the number of EdU-positive cells was dramatically decreased in the epithelial layer (**Figures 2D–D′**).

The expression levels of proliferation markers Ki-67 and MCM2 (Chow et al., 2016; Yousef et al., 2017), as well as the cell cycle inhibitor $p27^{kip1}$ (Kim and Raphael, 2007), were evaluated and compared between the normal utricle and the utricular FE at 14 days after streptomycin injection. As shown in **Figure 2F**, the mRNA level of Ki-67 was significantly increased and that of $p27^{kip1}$ decreased in FE compared with the control groups (**Figure 2F**).

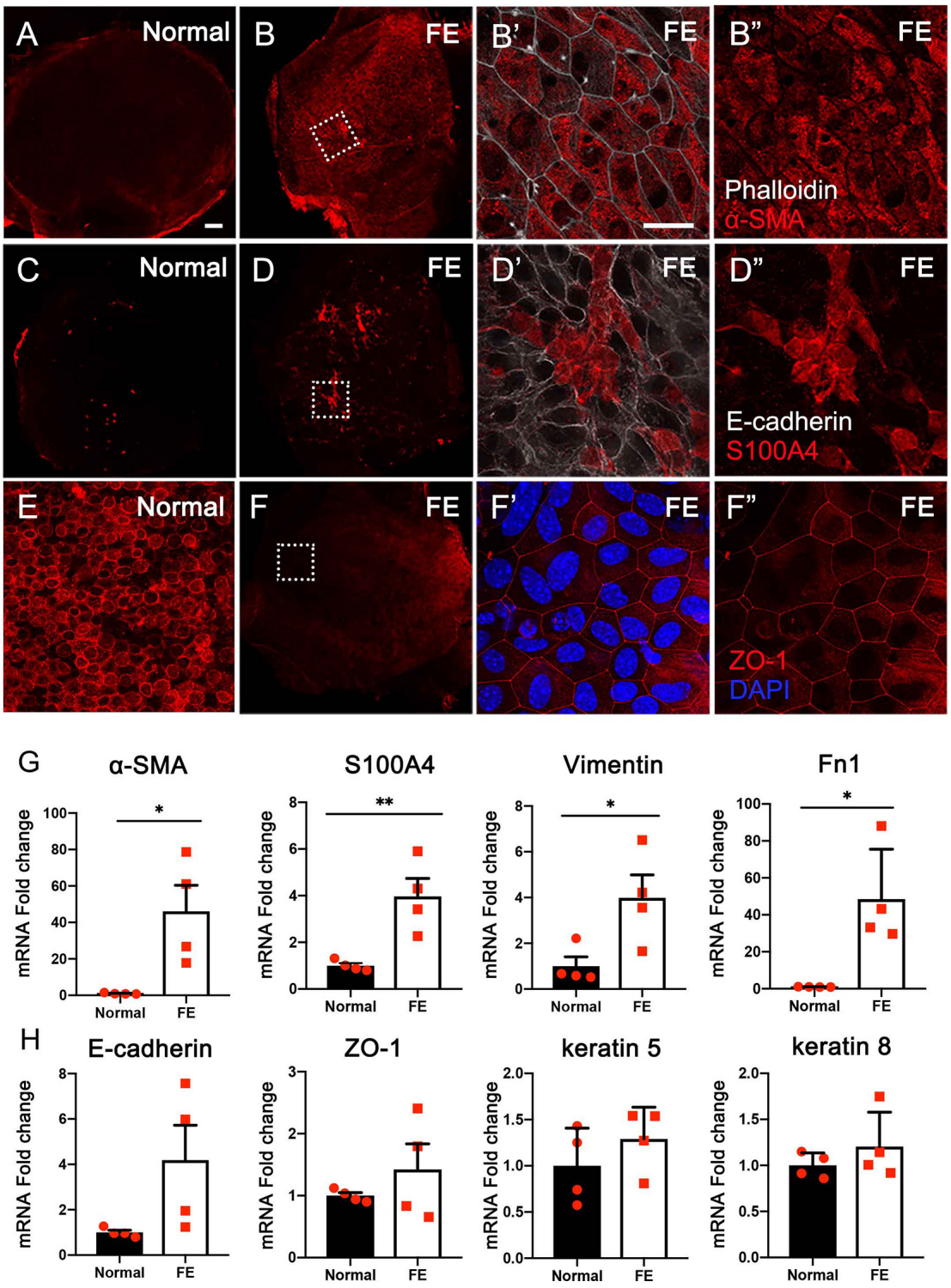

FIGURE 1 | Expression of epithelial and mesenchymal cell markers in the normal utricle and flat epithelium (FE). Immunofluorescence staining of α-SMA **(A–B″)**, S100A4 **(C–D″)**, and ZO-1 **(E–F″)** showing the expression of α-SMA and S100A4 is upregulated and ZO-1 expression is downregulated in FE. High magnification images of square areas in **(B,D,F)** are shown in **(B′–B″,D′–D″,F′–F″)**, respectively. Scale bars: **(A)** (applies to **B–D**,**F**), 50 μm; **(B′)** (applies to **B″,D′,D″,E,F′, F″**), 20 μm. **(G)** qRT-PCR results revealing that the mRNA expression levels of mesenchymal cell markers (α-*SMA*, *S100A4*, *vimentin*, and *Fn1*) are significantly increased in FE compared with the normal utricle. **(H)** mRNA expression levels of epithelial cell markers (*E-cadherin*, *ZO-1*, *keratin 5*, and *keratin 8*) are not significantly different between FE and normal utricle. $^{*}P < 0.05$ and $^{**}P < 0.01$ according to Student's *t*-test.

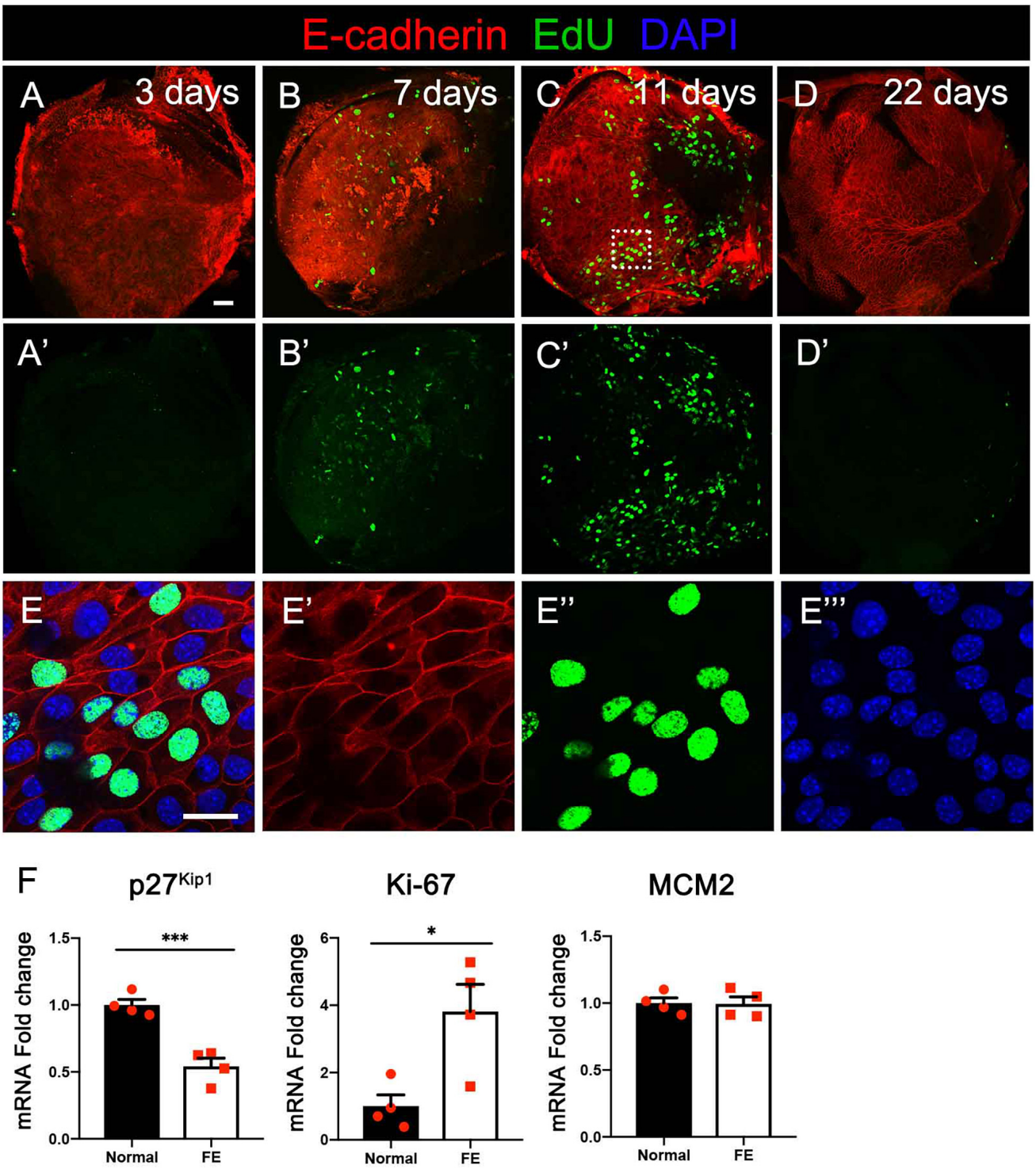

FIGURE 2 | Cell division at different timepoints after severe damage to the utricular sensory epithelium. **(A–A′)** At 3 days after the lesion, the actin cytoskeleton disappeared in most areas of the epithelial layer, with a few cells labeled by EdU. **(B–B′)** The number of EdU-positive cells increased at 7 days. **(C–C′)** Robust proliferation of EdU-positive cells was detected in flat epithelium (FE) at 11 days. **(D–D′)** EdU-positive cells were not observed in the epithelial layer at 22 days. **(E–E‴)** High-magnification view of the square area in **(C)** showing EdU labeling of the nuclei of FE cells. Scale bars: **(A)** (applies to **A′–D′**), 50 μm; **(E)** (applies to **E′–E‴**), 20 μm. **(F)** qRT-PCR results revealing that the mRNA expression levels of the cell proliferation marker Ki-67 were significantly increased in FE compared with the normal utricle, and the $p27^{kip1}$ expression level was decreased at 14 days after damage. $^{*}P < 0.05$ and $^{***}P < 0.001$ according to Student's *t*-test.

Microarray Analysis

To further determine the characteristics of FE transcriptomes and how the EMT is involved in the repair process of utricular sensory epithelium after severe damage, microarray analysis was performed using the Affymetrix mouse Clariom S array to analyze the transcriptomic differences between the normal utricle and FE. A total of 22,206 genes were extracted from each sample. When comparing transcripts between the normal utricle and FE, 2,189 transcripts differentially expressed (fold change > 2, $P < 0.05$) in FE were identified. **Figures 3A,B** show a volcano plot and hierarchical cluster analysis of the DEGs between the two groups; 1,227 upregulated and 962 downregulated genes were detected in FE samples, and heatmap analysis showed distinct differences in the mRNA expression profiles of the normal utricle and FE.

To characterize the genes most significantly differentially expressed between FE and normal utricle, the top 100 upregulated and downregulated genes were selected and are listed in **Figures 3C,D**. Among the DEGs, those previously reported to be associated with EMT were labeled with the # symbol; *Ibsp*, *Fn1*, *Gdf10*, *Lcn2*, *Loxl2*, *Htra1*, *C3*, *Lox*, *Postn*, *Aspn*, *Ncf4*, *Bmp5*, *Slpi*, *Anxa3*, *Mir675*, *Nkd2*, *Cd36*, *Timp1*, *Sulf2*, *Acp5*, *Csf1r*, and *Tgfb1* were upregulated in FE, whereas *Bdnf* and *Wdr66* were downregulated in FE.

Gene Ontology Analysis

Gene Ontology (GO) enrichment analysis was performed based on the DEGs. Among the upregulated genes, 616 significant BP, 121 cellular component (CC), and 153 molecular function (MF) GO categories were detected ($P < 0.01$; **Supplementary Table 1**). According to the BP category results, the DEGs were significantly associated with cell adhesion and migration. In the CC category, DEGs were mainly associated with extracellular components. Among the downregulated genes, 129 significant BP, 59 CC, and 36 MF categories were detected ($P < 0.01$; **Supplementary Table 2**). In the BP category, DEGs were mostly associated with inner ear development and function. In the CC category, DEGs were associated with membrane, cilium, and synapse. The top 20 upregulated and the top 20 downregulated GO terms are shown in **Figure 4**. Among these GO terms, 34 were associated with EMT.

Pathway Enrichment Analysis and Pathway Interaction Network Analysis

Pathway enrichment analysis was performed based on the KEGG (Kyoto Encyclopedia of Genes and Genomes) database. Based on the upregulated and downregulated genes, 98 and 34 signaling pathways were detected, respectively ($P < 0.05$; **Supplementary Tables 3, 4**). Among the top 40 significantly enriched signaling pathways (**Figures 5A,B**), 4 were associated with the EMT, including ECM–receptor interaction (mmu04512) (Gonzalez and Medici, 2014), focal adhesion (mmu04510) (Ji et al., 2019), PI3K/Akt signaling pathway (mmu04151) (Xu et al., 2015), and cell adhesion molecules (mmu04514) (Keller et al., 2019).

Next, pathway interaction network analysis was performed to generate an interaction network encompassing 44 significantly altered pathways; each pathway in the network was measured by counting the upstream and downstream pathways (**Supplementary Table 5**). A group of EMT-related signaling pathways was found to be closely associated with other pathways, including the MAPK signaling pathway (degree = 54), PI3K/Akt signaling pathway (degree = 41), TGF-β signaling pathway (degree = 17), NF-κB signaling pathway (degree = 16), regulation of actin cytoskeleton (degree = 16), and focal adhesion (degree = 16) (**Figure 5C**).

Construction of the Protein–Protein Interaction Network and Screening of Hub Genes

The Search Tool for the Retrieval of Interacting Genes (STRING) database was used to construct a protein–protein interaction (PPI) network of selected genes. Genes involved in EMT-related signaling pathways (**Figure 5**) were selected to build a network using Cytoscape (v3.7.2). All the nodes and edges were mapped in the PPI network, as shown in **Figure 6A**. To screen hub genes from the entire PPI network, the Cytoscape plugin cytoHubba was used. A total of 20 hub genes were screened using the maximum neighborhood component (MNC) algorithm: *Akt, Casp3, Col1a1, Col1a2, Fn1, Hgf, Igf1, Il1b, Irs1, Itga2, Itga5, Jun, Mapk1, Myc, Nras, Pdgfrb, Tgfb1, Thbs1*, *Trp53*, and *Col2a1* (**Figure 6B**). Among those genes, 19 have been shown to participate in the EMT process in other tissues; however, an association of *Col2a1* with EMT has not been reported (**Table 1**).

Quantitative Reverse Transcription Polymerase Chain Reaction Validation

The gene expression levels of the 20 hub genes were examined between FE and normal utricle using qRT-PCR. Compared with normal utricle, mRNA expression levels of *Casp3, Col1a1, Col1a2, Col2a1, Fn1, Igf1, Irs1, Itga5, Mapk1, Myc, Pdgfrb, Tgfb1*, and *Thbs1* were significantly upregulated in FE (**Figure 7**). The expression levels of the rest genes showed no significant differences in FE compared with normal utricle.

DISCUSSION

The present study results revealed that mesenchymal cell markers (α-SMA, S100A4, vimentin, and Fn1) were upregulated, and robust cell proliferation was detected, during the formation of vestibular FE. Furthermore, microarray analysis further confirmed that multiple EMT-related pathways and genes were involved in this process. These findings demonstrated that EMT participated in the epithelial reorganization of vestibular sensory epithelium after severe damage induced by aminoglycoside antibiotics.

Epithelial–mesenchymal transition is a physiological process that enables epithelial cells to acquire a mesenchymal cell phenotype (Kalluri and Weinberg, 2009). The expression changes in specific markers are used to confirm EMT (Nieto et al., 2016). Vimentin is a type of intermediate filament and a commonly used marker of mesenchymal properties (Thiery et al., 2009).

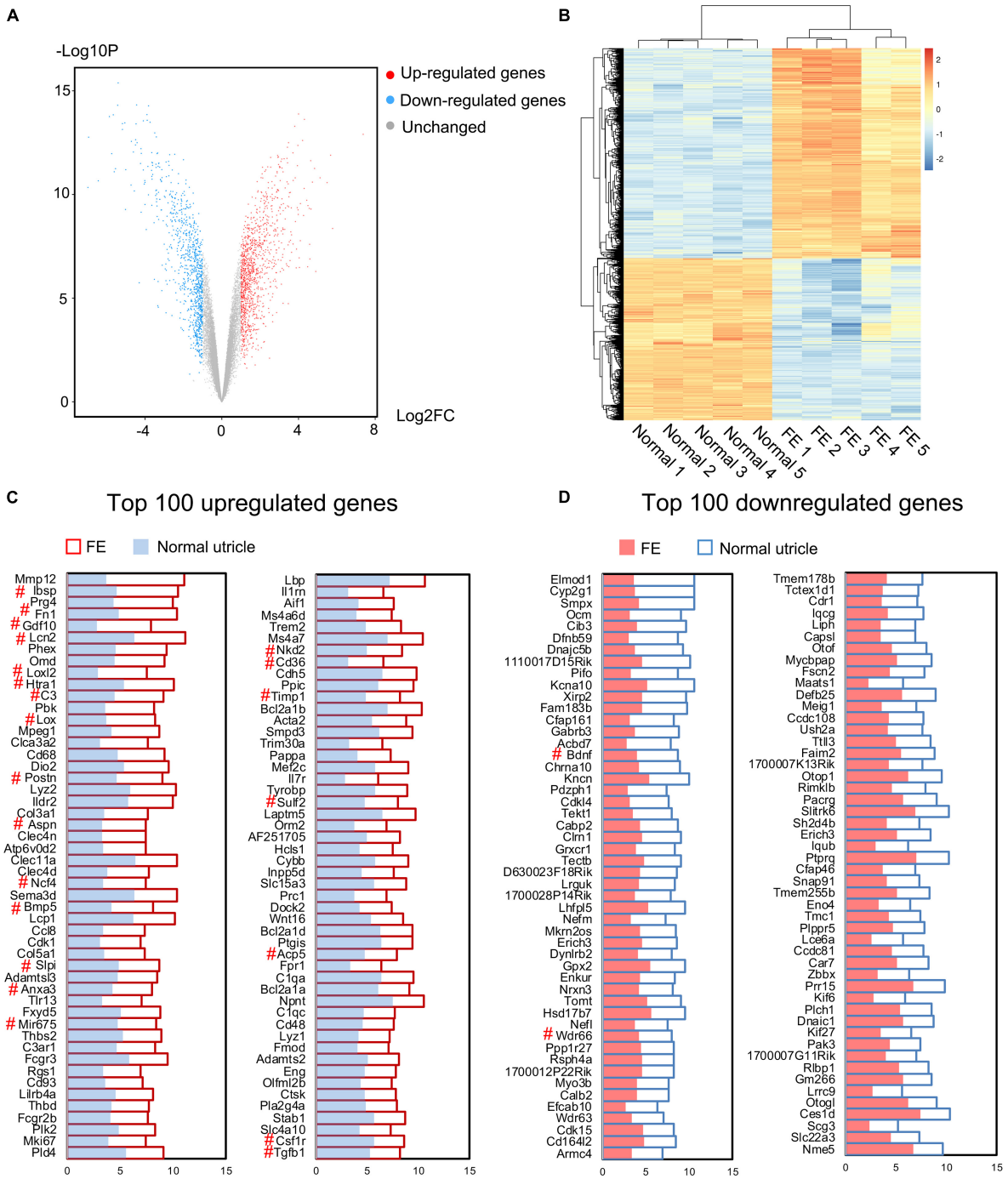

FIGURE 3 | Microarray analysis of the normal utricle and flat epithelium (FE). **(A)** Volcano plot representing the whole transcriptome changes in FE compared with the normal utricle. **(B)** Hierarchical clustering showing the differentially expressed genes (DEGs). Each group has five replicates. Yellow represents the upregulated genes and blue represents the downregulated genes. **(C)** Top 100 upregulated genes in FE compared with the normal utricle. **(D)** Top 100 downregulated genes in FE compared with the normal utricle. The horizontal axis represents the expression value. The # symbol indicates genes associated with epithelial–mesenchymal transition (EMT).

Vimentin is upregulated in several wound healing models (Cheng and Eriksson, 2017). In the inner ear, vimentin is expressed in the SCs of normal cochlea and might contribute to the process of scar formation after HC loss (Oesterle et al., 1990; Ladrech et al., 2017). Vimentin is also present in the cochlear FE (Ladrech et al., 2017). In the present study, vimentin expression was significantly upregulated in the vestibular FE compared with the normal utricle (**Figure 1G**). In addition, α-SMA, S100A4,

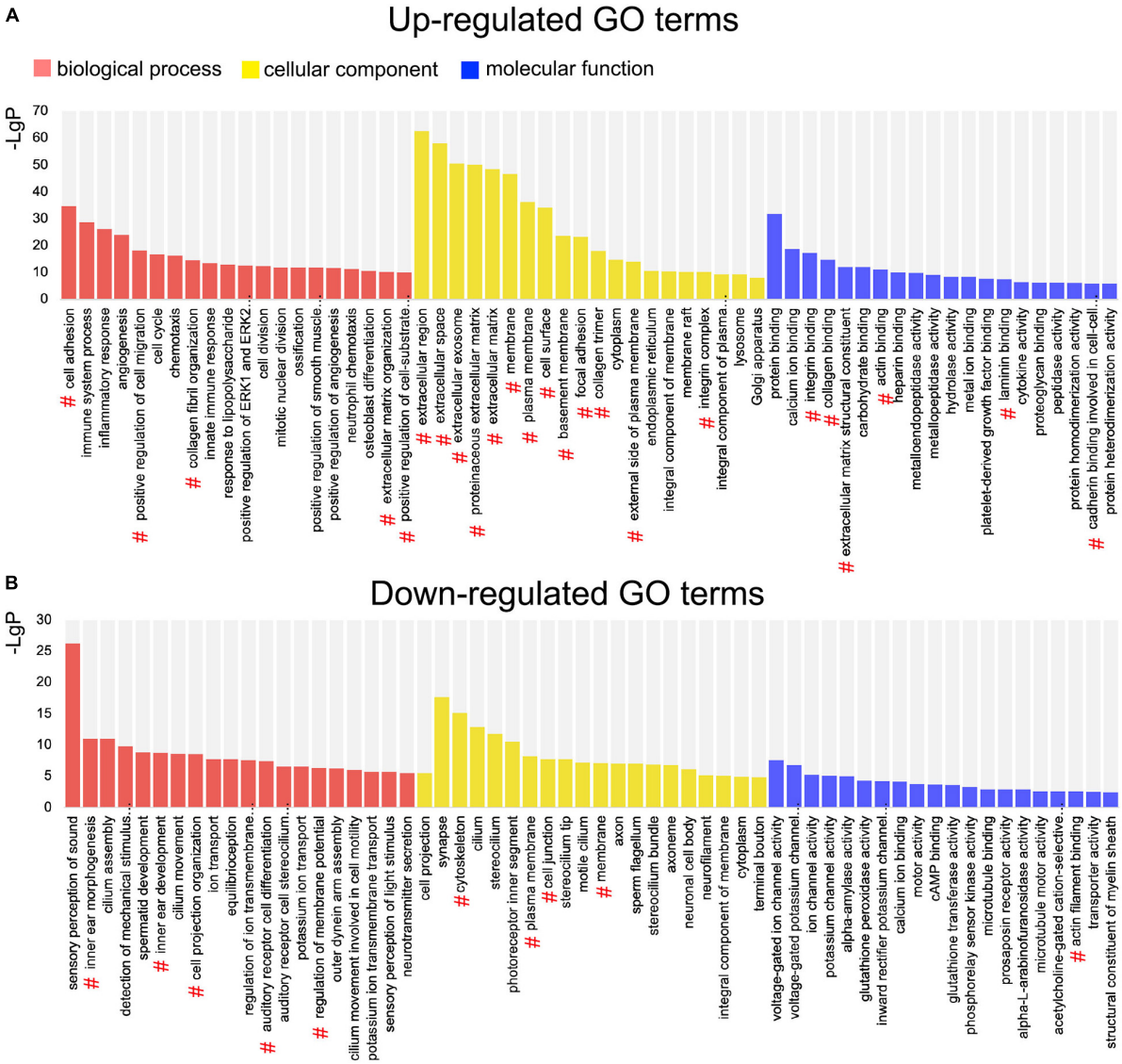

FIGURE 4 | Gene Ontology (GO) enrichment analysis of differentially expressed genes (DEGs) between the normal utricle and flat epithelium (FE). **(A)** Top 20 upregulated GO terms associated with the biological process (BP; red), cellular component (CC; yellow), and molecular function (MF; blue). **(B)** Top 20 downregulated GO terms. The # symbol indicates GO terms associated with the epithelial–mesenchymal transition (EMT).

and Fn1 are mesenchymal markers commonly used to evaluate EMT (Kalluri and Weinberg, 2009). In the present study, α-SMA and S100A4 were poorly expressed in the normal utricle, while they showed evident expression in FE (**Figures 1A–D″**). The mRNA expression levels of α-*SMA*, *S100A4*, and *Fn1* were significantly increased in FE compared with normal utricle (**Figure 1G**), indicating that expression of mesenchymal cell markers is increased in the vestibular FE.

E-cadherin and cytokeratin are two commonly used markers of epithelial properties (Nieto et al., 2016). In the present study, immunostaining results showed that the epithelial markers E-cadherin and ZO-1 were expressed in the vestibular FE (**Figures 1C–F″**). Furthermore, qRT-PCR revealed no significant difference in the expression of epithelial cell markers (E-cadherin, keratin 5, keratin 8, and ZO-1) between FE and normal utricle (**Figure 1H**). In the cochlea, E-cadherin was strongly expressed in both normal sensory epithelium and FE, although a drastic downregulation was found after aminoglycoside ototoxicity (Ladrech et al., 2017). These data indicate that the inner ear FE possesses both epithelial and mesenchymal phenotypes. The hybrid phenotype, which is involved in various pathophysiological processes and diseases, is considered to be resulted from partial EMT (Hahn et al., 2016; Nieto et al., 2016; Ladrech et al., 2017; Takahashi et al., 2019). The hybrid phenotype of FE cells may facilitate maintenance of the epithelial barrier in the inner ear.

In the present study, robust cell proliferation was found during the early stage of vestibular FE after the damage

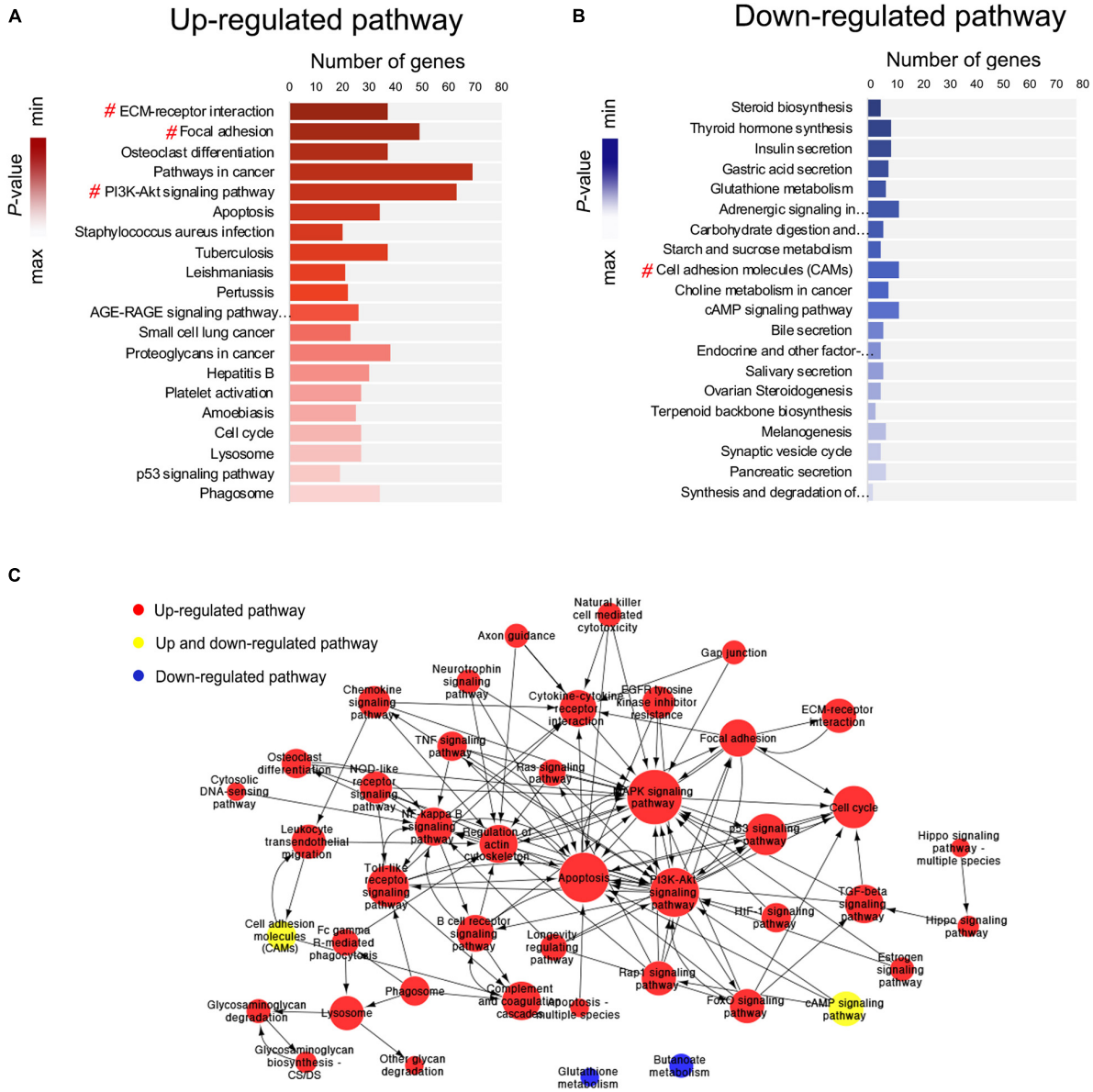

FIGURE 5 | Pathway enrichment analysis and pathway interaction network analysis. **(A,B)** Pathway enrichment analysis showing the top 20 upregulated and top 20 downregulated signaling pathways. The # symbol indicates pathways associated with the epithelial–mesenchymal transition (EMT). **(C)** Pathway interaction network analysis. Nodes represent pathways, and the arrows represent an interaction target between pathways.

(**Figure 2**), which was similar to cell proliferation in the formation of cochlear FE (Kim and Raphael, 2007). EMT has been reported to induce stem cell properties, including proliferation and self-renewal in various types of tissues (Jessen and Arthur-Farraj, 2019; Wang and Unternaehrer, 2019). During the cutaneous wound healing process, partial EMT induces epithelial cells undergoing proliferation and migration (Haensel and Dai, 2018). Complex mechanisms may underlie the activity of EMT and proliferation. The PI3K/Akt pathway and *Myc* gene are involved in this process (King et al., 2015; Yu and Cui, 2016). PI3K/Akt signaling plays a key role in the regulation of cell proliferation. Akt is the major downstream target of PI3K. Akt overexpression decreases the level of mitosis marker $p27^{kip1}$ and results in enhanced proliferation (Shen et al., 2020). In the present study, *Akt1* upregulation (**Figure 6B**) and $p27^{kip1}$ downregulation (**Figure 2F**) were detected at 14 days after the damage of the vestibular sensory epithelium. In addition, *Myc* was significantly upregulated and identified as one of the 20 hub genes (**Figure 7** and **Table 1**). A major role of *Myc* is control of cell proliferation (Bretones et al., 2015), and *Myc* could lead to the proliferation of mature SCs in adult mice (Shu et al., 2019). The role of such key genes in cell proliferation in vestibular FE needs further investigation.

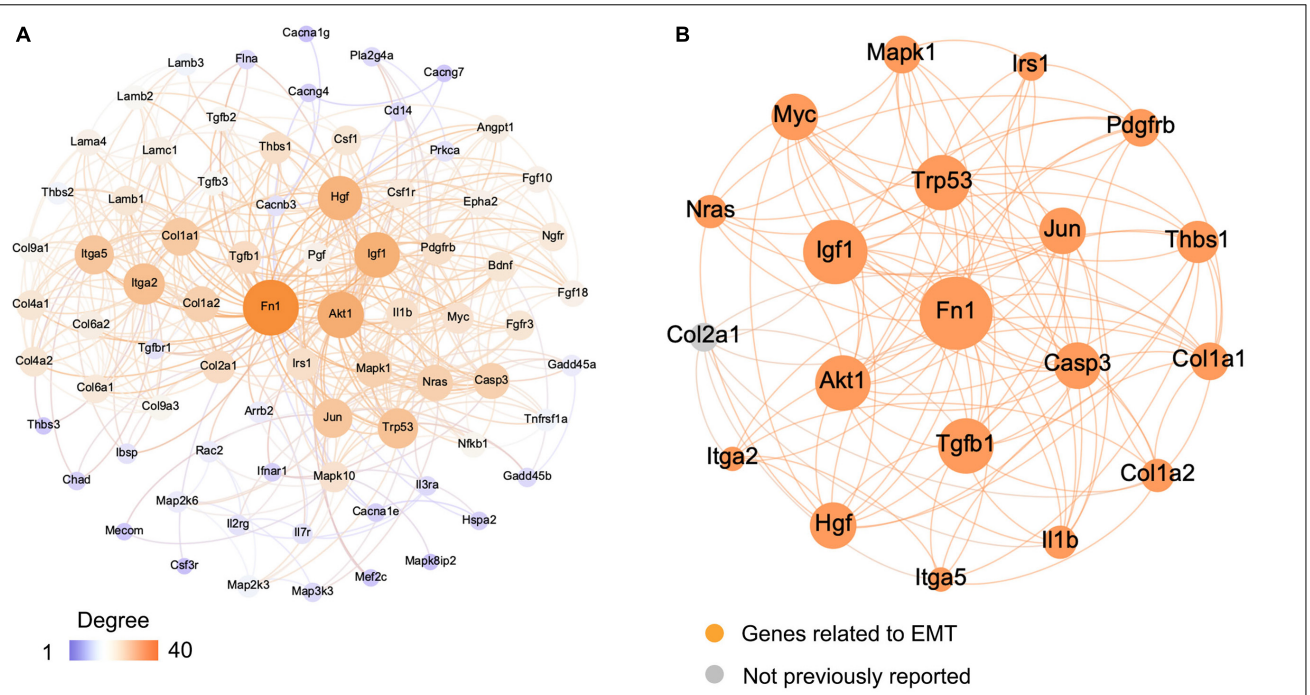

FIGURE 6 | Visualization of the protein–protein interaction (PPI) network and the candidate genes. **(A)** Entire PPI network. The edges indicate the PPIs in the Search Tool for the Retrieval of Interacting Genes (STRING) database. **(B)** Identification of the candidate genes from the entire PPI network using the maximum neighborhood component (MNC) algorithm. Edges represent the protein–protein associations. The orange nodes represent the genes that have been reported to be associated with the epithelial–mesenchymal transition (EMT), and gray nodes represent genes that have not been reported previously.

A multi-step integrative bioinformatics analysis was performed to explore the EMT function in vestibular FE. Based on GO analysis, DEGs were significantly enriched in GO terms associated with cell adhesion, cell migration, and extracellular components. Changes in cell adhesion molecules and acquisition of migratory ability are major characteristics of the EMT process (Nieto et al., 2016). Based on KEGG pathway enrichment analysis and pathway interaction network analysis, the PI3K/Akt signaling pathway was among the core positions in the pathway interaction network, indicating that this pathway plays an important role in the formation of vestibular FE. PI3K/Akt pathway, an important signaling pathway involved in the EMT process, may directly induce EMT by regulating transcription factors or other signaling pathways (Xu et al., 2015). PI3K/Akt signaling accelerates EMT and wound healing in epithelial tissue (Xiao et al., 2017).

In the present study, 19 of 20 hub genes selected using the MNC algorithm have been reportedly involved in EMT in various tissues (**Figure 6B** and **Table 1**). Among them, the expression of 13 hub genes changed significantly by qRT-PCR (**Figure 7**). Some of them are involved in the proliferation, development, nerve regeneration and protection of the inner ear. *Fn1* promotes cell invasion and migration by regulating cell adhesion and ECM proteins (Ritzenthaler et al., 2008; Sen et al., 2010). Fn1 may be involved in EMT process during cochlear fibrosis (Jia et al., 2016). The present study revealed that *Fn1* was in the core position in the PPI network (**Figure 6B**), indicating that *Fn1* might be a key regulator of the EMT process in vestibular FE. *Igf1* is an activator of EMT through several signaling pathways (Haisa, 2013). In the developing inner ear, *Igf1* is highly expressed during otic development, and it could protect HCs from ototoxic damage and increase the HC proliferation rate (Varela-Nieto et al., 2004). *Myc* and *Casp3* regulate cell proliferation and apoptosis in the inner ear respectively (Van De Water et al., 2004; Hu et al., 2021). *Thbs1* promotes EMT through activation of TGF-β and plays an important role in the development of cochlear afferent synapse (Jayachandran et al., 2014; Mendus et al., 2014). Altogether, these studies suggest that the hub genes relevant to the inner ear, such as *Fn1, Igf1, Myc, Casp3*, and *Thbs1*, may play a significant role during EMT process of vestibular FE. However, the exact pathophysiological mechanisms need to be further explored.

In conclusion, the present study results showed that upregulation of mesenchymal cell markers, downregulation of epithelial cell markers, and robust cell proliferation were detected in vestibular FE. Furthermore, this is the first study in which the transcriptome profile of vestibular FE was reported. Microarray analysis showed a significant difference in the transcriptome profiles between the normal utricle and FE, with many genes associated with EMT. In addition, a group of GO terms and pathways were associated with EMT. Altogether, these findings demonstrated that the EMT plays a significant role in the transition from normal vestibular sensory epithelium to FE induced by aminoglycoside antibiotics. Additional research is needed to determine the probable biological intervention strategies of FE based on the transcriptome features identified in the present study.

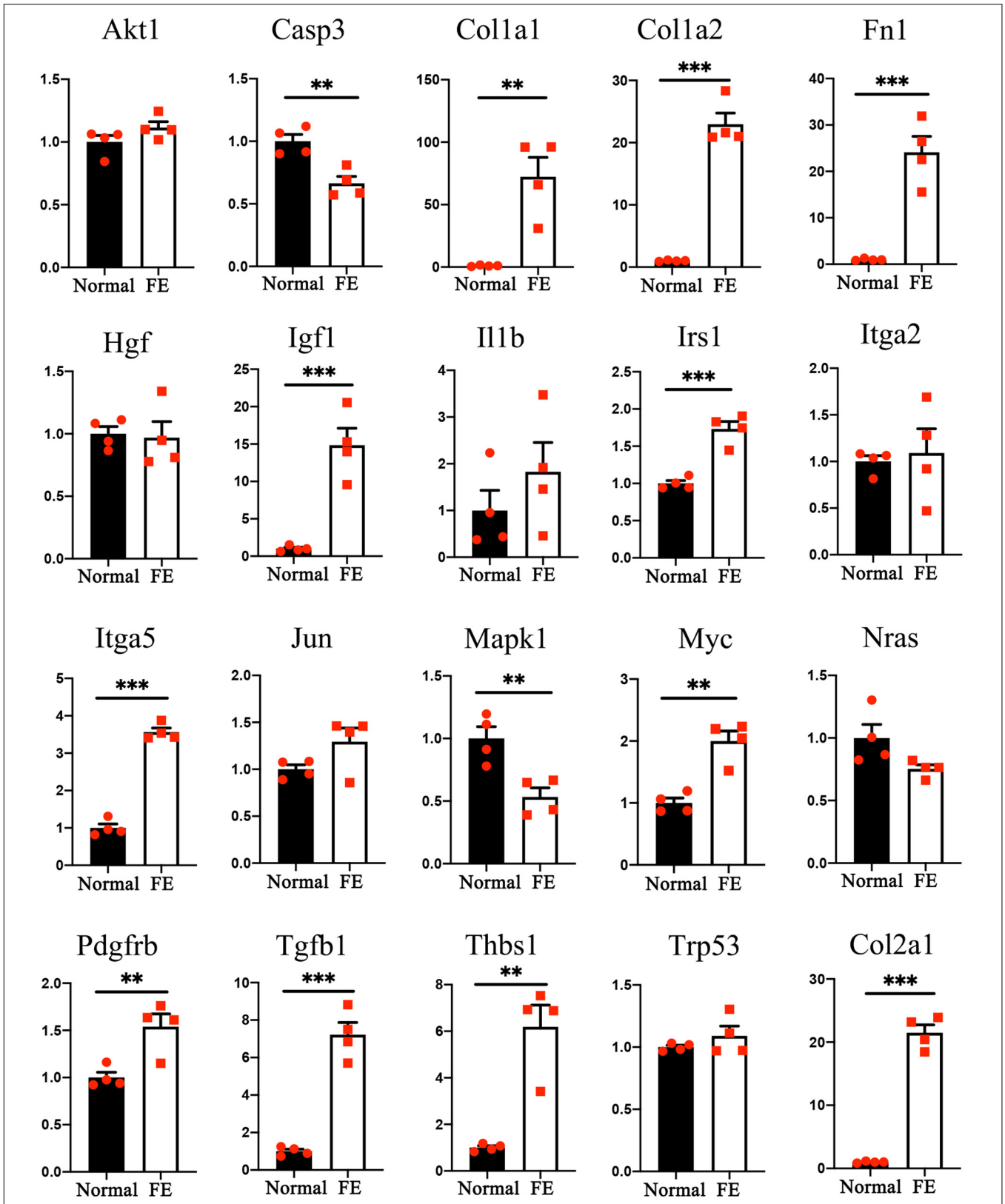

FIGURE 7 | Quantitative reverse transcription polymerase chain reaction analysis of the 20 hub genes. $^{**}P < 0.01$ and $^{***}P < 0.001$ according to Student's *t*-test.

TABLE 1 | mRNAs involved in epithelial–mesenchymal transition (EMT) and their associated diseases or potential mechanisms.

Gene symbol	Description (disease/mechanisms)	References
Akt1	Breast cancer	Li et al., 2016
Casp3	Colon cancer cells	Zhou et al., 2018
Col1a1	Colorectal cancer	Zhang et al., 2018
Col1a2	Colon cancer	Zhu et al., 2020
Fn1	ECM glycoprotein; enhances cell invasion and migration	Ritzenthaler et al., 2008; Sen et al., 2010
Hgf	Activates downstream pathways including MAPK and PI3K	Liu et al., 2017
Igf1	Activator of EMT in several types of cancer through signaling pathways including JNK, MAPK, and PI3K/Akt	Haisa, 2013
Il1b	Epithelial and cancer cells	Wang et al., 2018
Irs1	Regulates the expression of E-cadherin; promotes Wnt-mediated EMT	Geng et al., 2014
Itga2	Prostate cancer	Gaballa et al., 2020
Itga5	Oral squamous carcinoma	Deng et al., 2019
Jun	Human nasopharyngeal carcinoma cells	Lin et al., 2018
Mapk1	Inhibits invasion and metastasis	Li et al., 2015
Myc	Breast cancer	Yin et al., 2017
Nras	Drives a switch in EMT transcriptional factor expression	Caramel et al., 2013
Pdgfrb	Tongue squamous carcinoma	Zhang et al., 2016
Tgfb1	Regulates genes associated with ECM, cellular motility, and tight junctions	Zarzynska, 2014
Thbs1	Major activator of TGF-β	Murphy-Ullrich and Poczatek, 2000
Trp53	Regulates specific miRNAs	Chang et al., 2011
Col2a1	Not previously reported	

MATERIALS AND METHODS

Animals and Surgery

FVB/N mice (4–5-week-old) were purchased from SPF Biotechnology (Beijing, China) and housed in the Laboratory Animal Department of Capital Medical University. All animal experiments were approved by the Animal Care and Use Committee of Capital Medical University of China.

When mice were 6 weeks old, 400 μg of streptomycin (Sigma, St. Louis, MO, United States) dissolved in normal saline (400 g/L, 1 μL), was inoculated into the inner ear through the posterior semicircular canal to induce a severe lesion in the mouse utricle. The surgery was performed as described previously (Guo et al., 2018).

Immunofluorescence Staining

Mice were euthanized 2 weeks after the surgery. The temporal bones were fixed in 4% paraformaldehyde in phosphate-buffered saline (PBS) for 2 h. The utricles were dissected out and treated with 0.3% Triton X-100 (Sigma) and 5% normal goat serum (ZSGB-BIO, Beijing, China) in PBS for 2 h at room temperature. Samples were incubated with primary antibody at 4°C overnight. We used the following primary antibodies: mouse anti-α-SMA (diluted 1:300, Sigma), rabbit anti-S100A4 (diluted 1:300, Sigma), E-cadherin (diluted 1:200, BD Biosciences, San Jose, CA, United States), and ZO-1 (diluted 1:200, Invitrogen, Carlsbad, CA, United States). After rinsing in PBS for three times, samples were incubated in fluorescence-labeled secondary antibodies tagged with Alexa Fluor 568 or 647 (diluted 1:300, Invitrogen) for 2 h at room temperature. Alexa Fluor 647-conjugated phalloidin (diluted 1:300, Invitrogen) was used for F-actin labeling. Samples were incubated in the DNA-binding fluorescent stain 4′,6-diamidino-2-phenylindole (diluted 1:1000, AppliChem, Darmstadt, Germany) for 5 min to label nuclei.

To detect cells entering the cell cycle at different time points after streptomycin administration, EdU (20 mg/kg body weight, Invitrogen) was given once intraperitoneally at 3, 7, 11, or 22 days after surgery. Mice were euthanized 24 h after EdU administration. The Click-iT EdU Cell Proliferation Kit (Invitrogen) was used to perform the click reaction. Samples were then treated with primary and secondary antibodies as described above.

Samples were mounted on glass slides with Fluoromount-G (Southern Biotech, Birmingham, AL, United States) and examined with a scanning confocal microscope (Leica Camera AG, Solms, Hessen, Germany). Images were labeled and spaced using Photoshop (Adobe Systems, San Jose, CA, United States).

mRNA Microarray Analysis

The utricle tissues were collected for microarray analysis 2 weeks after surgery. Total RNA was isolated using the Qiagen RNeasy Mini Kit (Qiagen, Hilden, Germany). Each group contained five samples, and each sample had three utricles. Microarray analysis was performed by CapitalBio (Beijing, China). The Affymetrix mouse Clariom S Array (Affymetrix, Santa Clara, CA, United States) was used for hybridization. Student's *t*-test was applied for comparison of the two groups. Genes with a fold change > 2 and a P-value < 0.05 were considered significantly different. The dataset was submitted to Gene Expression Omnibus (GSE179063).

Bioinformatics Analysis

Gene Ontology analysis was performed for the DEGs. The distribution of genes in the three ontologies, including BP, CC, and MF, reflects the effects of the particular genes. GO statistical analysis was performed using Fisher's exact test. A P-value < 0.01 was used as cutoff to select significantly enriched GO terms.

Pathway analysis was used to find significantly enriched functional pathways according to the KEGG database. Fisher's exact test was used to identify the enriched pathways, and P-value < 0.05 was used as cutoff to select significantly enriched pathways.

A pathway interaction network was constructed based on the KEGG analysis to determine the relationships between enriched pathways. The degree represents the relationship between one pathway and the pathways around it. Cytoscape (v3.7.2) (Shannon et al., 2003) was used to draw the network diagram.

To better illustrate the interactions of the DEGs, the STRING[1] database was used to predict the associations of the selected genes. The parameter was set as interaction score ≥ 0.5. The PPI network

[1]https://string-db.org/

was constructed and visualized using Cytoscape (v3.7.2). The key DEGs were selected using the MNC. The MNC of each node was calculated using cytoHubba, a Cytoscape plugin, and the genes with the top 20 MNC values were considered hub genes.

Quantitative Reverse Transcription Polymerase Chain Reaction Analysis

Four independent RNA pools were prepared for each group, and three utricles were dissected in RNAlater (Qiagen, Hilden, Germany). TRIzol reagent (Life Technologies, Carlsbad, CA, United States) was used to isolate total RNA. cDNA was synthesized using FastQuant RT Super Mix reverse transcription (Tiangen Biotech Co., Ltd.). qRT-PCR was performed using FastStart Universal SYBR Green reagent (Bio-Rad Laboratories, Hercules, CA, United States) and primers. The mouse glyceraldehyde-3-phosphate dehydrogenase (*GAPDH*) gene was used as a reference. The $2^{-\Delta\Delta CT}$ method was applied to calculate changes in mRNA expression levels of the candidate genes.

Statistical Analysis

Statistical analysis was performed using GraphPad Prism 8 (GraphPad Software, Inc., La Jolla, CA, United States). The mRNA expression levels detected by qRT-PCR were expressed as means ± SE and analyzed using unpaired Student's *t*-test. Differences were considered statistically significant at $P < 0.05$.

DATA AVAILABILITY STATEMENT

The datasets presented in this study can be found in online repositories. The names of the repository/repositories and accession number(s) can be found below: https://www.ncbi.nlm.nih.gov/geo/, GSE179063.

ETHICS STATEMENT

The animal study was reviewed and approved by the Animal Care and Use Committee of Capital Medical University of China.

AUTHOR CONTRIBUTIONS

LH contributed to the conceptualization and methodology of the study and wrote the original draft. G-PW contributed to the conceptualization and methodology of the study, manuscript writing, reviewing, and editing. J-YG completed the formal analysis and data curation. Z-RC performed the investigation and formal analysis. KL was responsible for the software and validation. S-SG provided the conceptualization, writing, reviewing, and supervision. All authors contributed to the article and approved the submitted version.

FUNDING

This work was supported by the National Natural Science Foundation of China (grant numbers 81771016, 81830030, 81900929, and 82101210), Beijing Natural Science Foundation (grant numbers 7212022 and 7194256), and the Beijing Hospitals Authority Youth Program (grant number QML20180101).

SUPPLEMENTARY MATERIAL

The Supplementary Material for this article can be found online at: https://www.frontiersin.org/articles/10.3389/fnmol.2021.809878/full#supplementary-material

REFERENCES

Bretones, G., Delgado, M. D., and Leon, J. (2015). Myc and cell cycle control. *Biochim. Biophys. Acta* 1849, 506–516. doi: 10.1016/j.bbagrm.2014.03.013

Brosel, S., Laub, C., Averdam, A., Bender, A., and Elstner, M. (2016). Molecular aging of the mammalian vestibular system. *Ageing Res. Rev.* 26, 72–80. doi: 10.1016/j.arr.2015.12.007

Caramel, J., Papadogeorgakis, E., Hill, L., Browne, G. J., Richard, G., Wierinckx, A., et al. (2013). A switch in the expression of embryonic EMT-inducers drives the development of malignant melanoma. *Cancer Cell* 24, 466–480. doi: 10.1016/j.ccr.2013.08.018

Chang, C. J., Chao, C. H., Xia, W., Yang, J. Y., Xiong, Y., Li, C. W., et al. (2011). p53 regulates epithelial-mesenchymal transition and stem cell properties through modulating miRNAs. *Nat. Cell Biol.* 13, 317–323. doi: 10.1038/ncb2173

Cheng, F., and Eriksson, J. E. (2017). Intermediate Filaments and the Regulation of Cell Motility during Regeneration and Wound Healing. *Cold Spring Harb. Perspect. Biol.* 9:a022046. doi: 10.1101/cshperspect.a022046

Chow, C. L., Trivedi, P., Pyle, M. P., Matulle, J. T., Fettiplace, R., and Gubbels, S. P. (2016). Evaluation of Nestin Expression in the Developing and Adult Mouse Inner Ear. *Stem Cells Dev.* 25, 1419–1432. doi: 10.1089/scd.2016.0176

Deng, Y., Wan, Q., and Yan, W. (2019). Integrin alpha5/ITGA5 Promotes The Proliferation, Migration, Invasion And Progression Of Oral Squamous Carcinoma By Epithelial-Mesenchymal Transition. *Cancer Manag. Res.* 11, 9609–9620. doi: 10.2147/CMAR.S223201

Fu, X., Wan, P., Li, P., Wang, J., Guo, S., Zhang, Y., et al. (2021). Mechanism and Prevention of Ototoxicity Induced by Aminoglycosides. *Front. Cell Neurosci.* 15:692762. doi: 10.3389/fncel.2021.692762

Gaballa, R., Ali, H. E. A., Mahmoud, M. O., Rhim, J. S., Ali, H. I., Salem, H. F., et al. (2020). Exosomes-Mediated Transfer of Itga2 Promotes Migration and Invasion of Prostate Cancer Cells by Inducing Epithelial-Mesenchymal Transition. *Cancers* 12:2300. doi: 10.3390/cancers12082300

Geng, Y., Ju, Y., Ren, F., Qiu, Y., Tomita, Y., Tomoeda, M., et al. (2014). Insulin receptor substrate 1/2 (IRS1/2) regulates Wnt/beta-catenin signaling through blocking autophagic degradation of dishevelled2. *J. Biol. Chem.* 289, 11230–11241. doi: 10.1074/jbc.M113.544999

Gonzalez, D. M., and Medici, D. (2014). Signaling mechanisms of the epithelial-mesenchymal transition. *Sci. Signal.* 7:re8. doi: 10.1126/scisignal.2005189

Guo, J. Y., He, L., Qu, T. F., Liu, Y. Y., Liu, K., Wang, G. P., et al. (2018). Canalostomy As a Surgical Approach to Local Drug Delivery into the Inner Ears of Adult and Neonatal Mice. *J. Vis. Exp.* 135:e57351. doi: 10.3791/57351

Haensel, D., and Dai, X. (2018). Epithelial-to-mesenchymal transition in cutaneous wound healing: where we are and where we are heading. *Dev. Dyn.* 247, 473–480. doi: 10.1002/dvdy.24561

Hahn, J. M., McFarland, K. L., Combs, K. A., and Supp, D. M. (2016). Partial epithelial-mesenchymal transition in keloid scars: regulation of keloid keratinocyte gene expression by transforming growth factor-beta1. *Burn. Trauma* 4:30. doi: 10.1186/s41038-016-0055-7

Haisa, M. (2013). The type 1 insulin-like growth factor receptor signalling system and targeted tyrosine kinase inhibition in cancer. *J. Int. Med. Res.* 41, 253–264. doi: 10.1177/0300060513476585

Hu, Z., Singh, A., Bojrab, D. II, and Sim, N. (2021). Insights into the molecular mechanisms regulating mammalian hair cell regeneration. *Curr. Opin. Otolaryngol. Head Neck Surg.* 29, 400–406. doi: 10.1097/moo.0000000000000752

Isgrig, K., Shteamer, J. W., Belyantseva, I. A., Drummond, M. C., Fitzgerald, T. S., Vijayakumar, S., et al. (2017). Gene Therapy Restores Balance and Auditory Functions in a Mouse Model of Usher Syndrome. *Mol. Ther.* 25, 780–791. doi: 10.1016/j.ymthe.2017.01.007

Jayachandran, A., Anaka, M., Prithviraj, P., Hudson, C., McKeown, S. J., Lo, P. H., et al. (2014). Thrombospondin 1 promotes an aggressive phenotype through epithelial-to-mesenchymal transition in human melanoma. *Oncotarget* 5, 5782–5797. doi: 10.18632/oncotarget.2164

Jessen, K. R., and Arthur-Farraj, P. (2019). Repair Schwann cell update: adaptive reprogramming, EMT, and stemness in regenerating nerves. *Glia* 67, 421–437. doi: 10.1002/glia.23532

Ji, M., Li, W., He, G., Zhu, D., Lv, S., Tang, W., et al. (2019). Zinc-alpha2-glycoprotein 1 promotes EMT in colorectal cancer by filamin A mediated focal adhesion pathway. *J. Cancer* 10, 5557–5566. doi: 10.7150/jca.35380

Jia, H., Francois, F., Bourien, J., Eybalin, M., Lloyd, R. V., Van De Water, T. R., et al. (2016). Prevention of trauma-induced cochlear fibrosis using intracochlear application of anti-inflammatory and antiproliferative drugs. *Neuroscience* 316, 261–278. doi: 10.1016/j.neuroscience.2015.12.031

Johnen, N., Francart, M., Thelen, N., Cloes, M., and Thiry, M. (2012). Evidence for a partial epithelial–mesenchymal transition in postnatal stages of rat auditory organ morphogenesis. *Histochem. Cell Biol.* 138, 477–488. doi: 10.1007/s00418-012-0969-5

Kalluri, R., and Weinberg, R. A. (2009). The basics of epithelial-mesenchymal transition. *J. Clin. Invest.* 119, 1420–1428. doi: 10.1172/JCI39104

Keller, L., Werner, S., and Pantel, K. (2019). Biology and clinical relevance of EpCAM. *Cell Stress* 3, 165–180. doi: 10.15698/cst2019.06.188

Kim, Y. H., and Raphael, Y. (2007). Cell division and maintenance of epithelial integrity in the deafened auditory epithelium. *Cell Cycle* 6, 612–619. doi: 10.4161/cc.6.5.3929

King, D., Yeomanson, D., and Bryant, H. E. (2015). PI3King the lock: targeting the PI3K/Akt/mTOR pathway as a novel therapeutic strategy in neuroblastoma. *J. Pediatr. Hematol. Oncol.* 37, 245–251. doi: 10.1097/mph.0000000000000329

Kobayashi, Y., Nakamura, H., and Funahashi, J. (2008). Epithelial-Mesenchymal Transition as a Possible Mechanism of Semicircular Canal Morphogenesis in Chick Inner Ear. *Tohoku J. Exp. Med.* 215, 207–217. doi: 10.1620/tjem.215.207

Ladrech, S., Eybalin, M., Puel, J. L., and Lenoir, M. (2017). Epithelial-mesenchymal transition, and collective and individual cell migration regulate epithelial changes in the amikacin-damaged organ of Corti. *Histochem. Cell Biol.* 148, 129–142. doi: 10.1007/s00418-017-1548-6

Lamouille, S., Xu, J., and Derynck, R. (2014). Molecular mechanisms of epithelial–mesenchymal transition. *Nat. Rev. Mol. Cell Biol.* 15, 178–196. doi: 10.1038/nrm3758

Li, C. W., Xia, W., Lim, S. O., Hsu, J. L., Huo, L., Wu, Y., et al. (2016). AKT1 Inhibits Epithelial-to-Mesenchymal Transition in Breast Cancer through Phosphorylation-Dependent Twist1 Degradation. *Cancer Res.* 76, 1451–1462. doi: 10.1158/0008-5472.CAN-15-1941

Li, X. W., Tuergan, M., and Abulizi, G. (2015). Expression of MAPK1 in cervical cancer and effect of MAPK1 gene silencing on epithelial-mesenchymal transition, invasion and metastasis. *Asian Pac. J. Trop. Med.* 8, 937–943. doi: 10.1016/j.apjtm.2015.10.004

Lin, G., Yu, B., Liang, Z., Li, L., Qu, S., Chen, K., et al. (2018). Silencing of c-jun decreases cell migration, invasion, and EMT in radioresistant human nasopharyngeal carcinoma cell line CNE-2R. *Onco Targets Ther.* 11, 3805–3815. doi: 10.2147/OTT.S162700

Liu, F., Song, S., Yi, Z., Zhang, M., Li, J., Yang, F., et al. (2017). HGF induces EMT in non-small-cell lung cancer through the hBVR pathway. *Eur. J. Pharmacol.* 811, 180–190. doi: 10.1016/j.ejphar.2017.05.040

McCall, A. A., Ishiyama, G. P., Lopez, I. A., Bhuta, S., Vetter, S., and Ishiyama, A. (2009). Histopathological and ultrastructural analysis of vestibular endorgans in Meniere's disease reveals basement membrane pathology. *BMC Ear Nose Throat Disord.* 9:4. doi: 10.1186/1472-6815-9-4

Mendus, D., Sundaresan, S., Grillet, N., Wangsawihardja, F., Leu, R., Muller, U., et al. (2014). Thrombospondins 1 and 2 are important for afferent synapse formation and function in the inner ear. *Eur. J. Neurosci.* 39, 1256–1267. doi: 10.1111/ejn.12486

Murphy-Ullrich, J. E., and Poczatek, M. (2000). Activation of latent TGF-beta by thrombospondin-1: mechanisms and physiology. *Cytokine Growth Factor Rev.* 11, 59–69. doi: 10.1016/s1359-6101(99)00029-5

Nadol, J., and Eddington, D. (2006). Histopathology of the inner ear relevant to cochlear implantation. *Adv. Otorhinolaryngol.* 64, 31–49.

Nieto, M. A., Huang, R. Y., Jackson, R. A., and Thiery, J. P. (2016). Emt: 2016. *Cell* 166, 21–45. doi: 10.1016/j.cell.2016.06.028

Oesterle, E. C., Sarthy, P. V., and Rubel, E. W. (1990). Intermediate filaments in the inner ear of normal and experimentally damaged guinea pigs. *Hear. Res.* 47, 1–16. doi: 10.1016/0378-5955(90)90162-i

Puram, S. V., Parikh, A. S., and Tirosh, I. (2018). Single cell RNA-seq highlights a role for a partial EMT in head and neck cancer. *Mol. Cell Oncol.* 5:e1448244. doi: 10.1080/23723556.2018.1448244

Ritzenthaler, J. D., Han, S., and Roman, J. (2008). Stimulation of lung carcinoma cell growth by fibronectin-integrin signalling. *Mol. Biosyst.* 4, 1160–1169. doi: 10.1039/b800533h

Sen, T., Dutta, A., Maity, G., and Chatterjee, A. (2010). Fibronectin induces matrix metalloproteinase-9 (MMP-9) in human laryngeal carcinoma cells by involving multiple signaling pathways. *Biochimie* 92, 1422–1434. doi: 10.1016/j.biochi.2010.07.005

Shannon, P., Markiel, A., Ozier, O., Baliga, N., Wang, J., Ramage, D., et al. (2003). Cytoscape: a software environment for integrated models of biomolecular interaction networks. *Genome Res.* 13, 2498–2504. doi: 10.1101/gr.1239303

Shen, X., Xu, X., Xie, C., Liu, H., Yang, D., Zhang, J., et al. (2020). YAP promotes the proliferation of neuroblastoma cells through decreasing the nuclear location of p27(Kip1) mediated by Akt. *Cell Prolif.* 53:e12734. doi: 10.1111/cpr.12734

Shu, Y., Li, W., Huang, M., Quan, Y. Z., Scheffer, D., Tian, C., et al. (2019). Renewed proliferation in adult mouse cochlea and regeneration of hair cells. *Nat. Commun.* 10:5530. doi: 10.1038/s41467-019-13157-7

Simonneau, L., Gallego, M., and Pujol, R. (2003). Comparative expression patterns of T-, N-, E-cadherins, beta-catenin, and polysialic acid neural cell adhesion molecule in rat cochlea during development: implications for the nature of Kolliker's organ. *J. Comp. Neurol.* 459, 113–126. doi: 10.1002/cne.10604

Takahashi, M., Yamamoto-Fukuda, T., Akiyama, N., Motegi, M., Yamamoto, K., Tanaka, Y., et al. (2019). Partial Epithelial–Mesenchymal Transition Was Observed Under p63 Expression in Acquired Middle Ear Cholesteatoma and Congenital Cholesteatoma. *Otol. Neurotol.* 40, e803–e811. doi: 10.1097/mao.0000000000002328

Teufert, K., Linthicum, F. J., and Connell, S. (2006). The Effect of Organ of Corti Loss on Ganglion Cell Survival in Humans. *Otol. Neurotol.* 27, 1146–1151. doi: 10.1097/01.mao.0000232006.16363.44

Thiery, J. P., Acloque, H., Huang, R. Y., and Nieto, M. A. (2009). Epithelial-mesenchymal transitions in development and disease. *Cell* 139, 871–890. doi: 10.1016/j.cell.2009.11.007

Van De Water, T. R., Lallemend, F., Eshraghi, A. A., Ahsan, S., He, J., Guzman, J., et al. (2004). Caspases, the enemy within, and their role in oxidative stress-induced apoptosis of inner ear sensory cells. *Otol. Neurotol.* 25, 627–632. doi: 10.1097/00129492-200407000-00035

Varela-Nieto, I., Morales-Garcia, J. A., Vigil, P., Diaz-Casares, A., Gorospe, I., Sanchez-Galiano, S., et al. (2004). Trophic effects of insulin-like growth factor-I (IGF-I) in the inner ear. *Hear. Res.* 196, 19–25. doi: 10.1016/j.heares.2003.12.022

Wang, G. P., Basu, I., Beyer, L. A., Wong, H. T., Swiderski, D. L., Gong, S. S., et al. (2017). Severe streptomycin ototoxicity in the mouse utricle leads to a flat epithelium but the peripheral neural degeneration is delayed. *Hear. Res.* 355, 33–41. doi: 10.1016/j.heares.2017.09.004

Wang, H., and Unternaehrer, J. (2019). Epithelial-mesenchymal Transition and Cancer Stem Cells: at the Crossroads of Differentiation and Dedifferentiation. *Dev. Dyn.* 248, 10–20. doi: 10.1002/dvdy

Wang, T., Chai, R., Kim, G. S., Pham, N., Jansson, L., Nguyen, D. H., et al. (2015). Lgr5+ cells regenerate hair cells via proliferation and direct transdifferentiation in damaged neonatal mouse utricle. *Nat. Commun.* 6:6613. doi: 10.1038/ncomms7613

Wang, X., Wang, B., Xie, J., Hou, D., Zhang, H., and Huang, H. (2018). Melatonin inhibits epithelial-to-mesenchymal transition in gastric cancer cells

via attenuation of IL-1β/NF-κB/MMP2/MMP9 signaling. *Int. J. Mol. Med.* 42, 2221–2228. doi: 10.3892/ijmm.2018.3788

Wu, D. K., and Kelley, M. W. (2012). Molecular mechanisms of inner ear development. *Cold Spring Harb. Perspect. Biol.* 4:a008409. doi: 10.1101/cshperspect.a008409

Xiao, W., Tang, H., Wu, M., Liao, Y., Li, K., Li, L., et al. (2017). Ozone oil promotes wound healing by increasing the migration of fibroblasts via PI3K/Akt/mTOR signaling pathway. *Biosci. Rep.* 37:BSR20170658. doi: 10.1042/BSR20170658

Xu, W., Yang, Z., and Lu, N. (2015). A new role for the PI3K/Akt signaling pathway in the epithelial-mesenchymal transition. *Cell Adh. Migr.* 9, 317–324. doi: 10.1080/19336918.2015.1016686

Yin, S., Cheryan, V. T., Xu, L., Rishi, A. K., and Reddy, K. B. (2017). Myc mediates cancer stem-like cells and EMT changes in triple negative breast cancers cells. *PLoS One* 12:e0183578. doi: 10.1371/journal.pone.0183578

You, D., Guo, L., Li, W., Sun, S., Chen, Y., Chai, R., et al. (2018). Characterization of Wnt and Notch-Responsive Lgr5+ Hair Cell Progenitors in the Striolar Region of the Neonatal Mouse Utricle. *Front. Mol. Neurosci.* 11:137. doi: 10.3389/fnmol.2018.00137

Yousef, E. M., Furrer, D., Laperriere, D. L., Tahir, M. R., Mader, S., Diorio, C., et al. (2017). MCM2: an alternative to Ki-67 for measuring breast cancer cell proliferation. *Mod. Pathol.* 30, 682–697. doi: 10.1038/modpathol.2016.231

Yu, J. S., and Cui, W. (2016). Proliferation, survival and metabolism: the role of PI3K/AKT/mTOR signalling in pluripotency and cell fate determination. *Development* 143, 3050–3060. doi: 10.1242/dev.137075

Zarzynska, J. M. (2014). Two faces of TGF-beta1 in breast cancer. *Mediators Inflamm.* 2014:141747. doi: 10.1155/2014/141747

Zhang, H., Sun, J. D., Yan, L. J., and Zhao, X. P. (2016). PDGF-D/PDGFRbeta promotes tongue squamous carcinoma cell (TSCC) progression via activating p38/AKT/ERK/EMT signal pathway. *Biochem. Biophys. Res. Commun.* 478, 845–851. doi: 10.1016/j.bbrc.2016.08.035

Zhang, Y., Zhang, S., Zhang, Z., Dong, Y., Ma, X., Qiang, R., et al. (2020). Knockdown of Foxg1 in Sox9+ supporting cells increases the trans-differentiation of supporting cells into hair cells in the neonatal mouse utricle. *Aging* 12, 19834–19851. doi: 10.18632/aging.104009

Zhang, Z., Wang, Y., Zhang, J., Zhong, J., and Yang, R. (2018). COL1A1 promotes metastasis in colorectal cancer by regulating the WNT/PCP pathway. *Mol. Med. Rep.* 17, 5037–5042. doi: 10.3892/mmr.2018.8533

Zhou, M., Liu, X., Li, Z., Huang, Q., Li, F., and Li, C. Y. (2018). Caspase-3 regulates the migration, invasion and metastasis of colon cancer cells. *Int. J. Cancer* 143, 921–930. doi: 10.1002/ijc.31374

Zhu, X., Luo, X., Jiang, S., and Wang, H. (2020). Bone Morphogenetic Protein 1 Targeting COL1A1 and COL1A2 to Regulate the Epithelial-Mesenchymal Transition Process of Colon Cancer SW620 Cells. *J. Nanosci. Nanotechnol.* 20, 1366–1374. doi: 10.1166/jnn.2020.17362

Conflict of Interest: The authors declare that the research was conducted in the absence of any commercial or financial relationships that could be construed as a potential conflict of interest.

Publisher's Note: All claims expressed in this article are solely those of the authors and do not necessarily represent those of their affiliated organizations, or those of the publisher, the editors and the reviewers. Any product that may be evaluated in this article, or claim that may be made by its manufacturer, is not guaranteed or endorsed by the publisher.

frontiers in Molecular Neuroscience

ORIGINAL RESEARCH
published: 10 January 2022
doi: 10.3389/fnmol.2021.757831

A Novel *in vitro* Model Delineating Hair Cell Regeneration and Neural Reinnervation in Adult Mouse Cochlea

Wenyan Li[1,2,3,4†], Yizhou Quan[1,2†], Mingqian Huang[1,2], Wei Wei[1,2], Yilai Shu[1,2,3,4], Huawei Li[3,4] and Zheng-Yi Chen[1,2*]*

[1] Department of Otolaryngology-Head and Neck Surgery, Graduate Program in Speech and Hearing Bioscience and Technology and Program in Neuroscience, Harvard Medical School, Boston, MA, United States, [2] Eaton-Peabody Laboratory, Massachusetts Eye and Ear Infirmary, Boston, MA, United States, [3] ENT Institute and Otorhinolaryngology Department of Eye & ENT Hospital, State Key Laboratory of Medical Neurobiology and MOE Frontiers Center for Brain Science, Fudan University, Shanghai, China, [4] Institutes of Biomedical Sciences, Fudan University, Shanghai, China

OPEN ACCESS

Edited by:
Yu Sun,
Huazhong University of Science and Technology, China

Reviewed by:
Lukas D. Landegger,
Medizinische Universität Wien, Austria
Jiri Popelar,
Institute of Experimental Medicine (ASCR), Czechia
Alan G. Cheng,
Stanford University, United States

***Correspondence:**
Huawei Li
hwli@shmu.edu.cn
Zheng-Yi Chen
Zheng-Yi_Chen@meei.harvard.edu

[†] These authors have contributed equally to this work

Specialty section:
This article was submitted to Molecular Signalling and Pathways, a section of the journal Frontiers in Molecular Neuroscience

Received: 12 August 2021
Accepted: 07 December 2021
Published: 10 January 2022

Citation:
Li W, Quan Y, Huang M, Wei W, Shu Y, Li H and Chen Z-Y (2022) A Novel in vitro Model Delineating Hair Cell Regeneration and Neural Reinnervation in Adult Mouse Cochlea.
Front. Mol. Neurosci. 14:757831.
doi: 10.3389/fnmol.2021.757831

The study of an adult mammalian auditory system, such as regeneration, has been hampered by the lack of an *in vitro* system in which hypotheses can be tested efficiently. This is primarily due to the fact that the adult inner ear is encased in the toughest bone of the body, whereas its removal leads to the death of the sensory epithelium in culture. We hypothesized that we could take advantage of the integral cochlear structure to maintain the overall inner ear architecture and improve sensory epithelium survival in culture. We showed that by culturing adult mouse cochlea with the (surrounding) bone intact, the supporting cells (SCs) survived and almost all hair cells (HCs) degenerated. To evaluate the utility of the explant culture system, we demonstrated that the overexpression of *Atoh1*, an HC fate-determining factor, is sufficient to induce transdifferentiation of adult SCs to HC-like cells (HCLCs). Transdifferentiation-derived HCLCs resemble developmentally young HCs and are able to attract adult ganglion neurites. Furthermore, using a damage model, we showed that degenerated adult ganglions respond to regenerated HCLCs by directional neurite outgrowth that leads to HCLC-neuron contacts, strongly supporting the intrinsic properties of the HCLCs in establishing HCLC-neuron connections. The adult whole cochlear explant culture is suitable for diverse studies of the adult inner ear including regeneration, HC-neuron pathways, and inner ear drug screening.

Keywords: hair cell, adult, regeneration, novel model, cochlea

INTRODUCTION

Hearing deficits affect one in 500 newborn babies and half of the senior population over 70 years of age in the world (Morton and Nance, 2006; Muller and Barr-Gillespie, 2015). Loss of the auditory hair cells (HCs) that detect sound is the major cause of hearing loss. Furthermore, the mammalian cochlea completely lacks the capacity to regenerate HCs in adulthood, which leads to permanent deafness (Liu et al., 2012).

In adult lower vertebrates including zebrafish, amphibians, and birds, supporting cells (SCs) spontaneously proliferate and transdifferentiate into new HCs after the damage of existing HCs which leads to restoration of hearing (Corwin and Cotanche, 1988; Ryals and Rubel, 1988; Jones and Corwin, 1993; Dooling et al., 1997). To study regeneration in mammals, the neonatal mouse cochlear culture system has been developed and used extensively (Zheng and Gao, 1999, 2000; Zheng et al., 2000). As a result, signaling pathways involving mammalian cochlear HC regeneration by SC-to-HC transdifferentiation with potential in therapeutics have been identified in neonatal mice (Zheng and Gao, 2000, Shou et al., 2003; White et al., 2006; Diensthuber et al., 2009; Mizutari et al., 2013; Bramhall et al., 2014). A general approach to culture neonatal mouse cochleae involves the isolation of the sensory epithelium, which is cultured by adhering to the surface of a culture dish. A similar approach for adult cochleae requires the disruption of the ossified cochlear bone followed by removing the sensory epithelium for culture. Under this condition, the sensory epithelium inevitably dies shortly later. *In vivo* HC regeneration has been reported (Arnold et al., 2010; Walters et al., 2017; Kong et al., 2020). However, an *in vitro* culture system for adult mouse cochleae is yet to be established to allow studies ranging from regeneration and HC-neuron interactions to drug screening Chan and Rouse, 2016. The construction of transgenic animal models has become a dominant method to study those aspects in the adult mammalian inner ear, which is time-consuming in addition to other limitations. We hypothesized that the integral cochlear structure is important to the survival of the adult cochlear sensory epithelial cells. By culturing adult mouse cochlea with the intact bone, some sensory epithelial cells may survive long-term within well-preserved cochlear architecture suitable for the study of adult mammalian cochleae in culture.

In this study, for the first time, we developed a novel *in vitro* adult mouse cochlear culture system that includes the sensory epithelium with the surrounding bony structure. With the adult mouse cochlear explant culture system, a majority of adult SCs are viable in culture for up to 3 weeks. We further demonstrated the utility of the culture system in the regeneration of HC-like cells (HCLCs) through SC-to-HC transdifferentiation by overexpression of an HC induction gene *Atoh1*. We illustrated that the system can be used to study the auditory pathway by establishing connections between regenerated HCLCs and adult ganglion neurons in culture.

RESULTS

Adult Mouse Cochlear Sensory Epithelium Degenerates Rapidly With the Conventional Culture Method

Few studies have been carried out successfully using cultured adult mouse cochleae due to the difficulty in retrieving the sensory epithelia from the ossified cochlea, especially those from the mid-to-base turn. In this study, we first tested the dissection of the adult cochlear sensory epithelium according to the protocol established for culturing neonatal mouse cochleae (Parker et al., 2010; Landegger et al., 2017). Only the apical region of the sensory epithelium could be preserved using this method (**Supplementary Figures 1a1, a2**). After 2 weeks in culture, the whole sensory epithelium folded and degenerated, as shown by the disruption of the overall structure, loss of all HCs, and severely reduced the number of $SOX2^+$ SCs (**Supplementary Figures 1b1–b3**). Thus, using the conventional method, the adult cochlear sensory epithelium cannot be cultured long-term.

Culture of the Intact Adult Cochlea

We reasoned that the degeneration and cell death in cultured adult cochlear sensory epithelia are due to the lack of the structure of the organ of Corti, which supports communications among cells and their environment and promotes cell survival. To test the hypothesis, we cultured adult (P30) mouse cochleae with the surrounding bone, which maintained the overall cochlear structure. We created openings, one in the apex and one in the base, and separated the entire cochlea from the vestibular part of the bony inner ear with forceps. Reissner's membrane and the stria vascularis were carefully removed with a microprobe without touching the sensory epithelium, to expose the organ of Corti and allow the culture medium to pass through the endolymphatic space (**Figure 1** and **Supplementary Video 1**).

To characterize HC survival in cultured adult cochleae, we performed time-lapse recording using a reporter mouse model, *Gfi1*-Cre-Tm-red, in which tdTomato (Tm-red) expression was induced by *Gfi1* promoter-driven Cre activity (*Gfi1*-Cre). In *Gfi1*-Cre-Tm-red cochleae, Tm-red is induced in the cochlear HCs at the age of E12, with the Tm-red signal persisting throughout adulthood. Due to the difficulty of exposing the delicate structures of cultured adult sensory epithelia within the spatial bony structure, we evaluated the survival of the sensory epithelial cells based on the fluorescence signal (Tm-red). We observed rapid outer HC (OHC) death starting at 30 min from the beginning of the culture. The loss of OHCs continued and, by 24 h, all OHCs were virtually lost throughout the cochlea. To confirm the result, we stained existing HCs with Myosin VIIa (MYO7A)/Phalloidin 1 week after culture and noticed that nearly all OHCs died by this time point. Condensed and shrunken nuclei indicated dead OHCs, though some undegraded MYO7A protein could still be detected in the OHC region of the apex. In contrast, many inner HCs (IHCs) survived 1 week after culture, an indication of IHC resistance to cell death in culture (**Figure 2**).

To study SC survival in adult cochlear culture, we used a reporter mouse model, Sox2-CreER-Tm-red, in which *Sox2* promoter-driven Cre activity induces Tm-red after tamoxifen exposure (Sox2-CreER) in culture. After 14 days in culture, abundant $SOX2^+$ cells were identified along the whole length of the cultured cochlear explant. Strong SC loss in the base and moderate SC loss in other regions only occurred at 21 days, indicating long-term survival of adult SCs in our culture system (**Figure 3**).

We studied the details of the cultured adult mouse cochleae from 5 to 21 days and found our whole cochlear explant

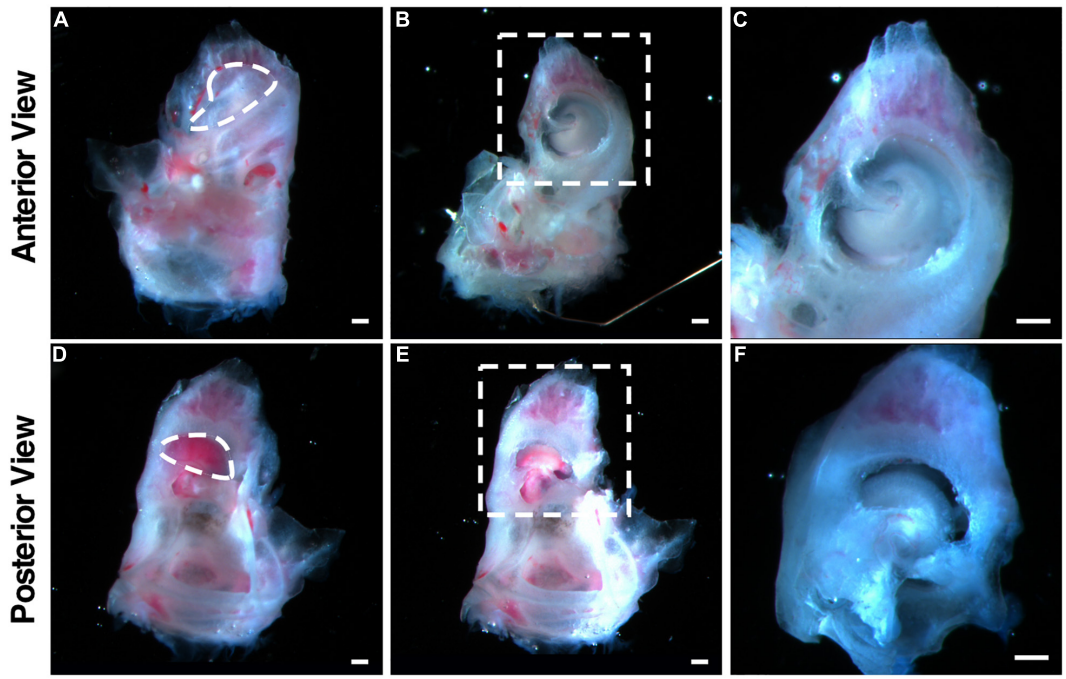

FIGURE 1 | Illustration of the dissection procedure that maintains the architecture of the adult cochleae used in explant culture. **(A–C)** Freshly dissected adult mouse cochlea viewed from the anterior. The dotted circle in **(A)** indicates the openings to be created by removing the bony shell in the apex. **(B)** The cochlea after removing the bony shell with the exposure of the apex. **(C)** The enlarged image of the dotted box shown in **(B)**. **(D–F)** Freshly dissected adult mouse cochlea viewed from the posterior. The dotted circle in **(D)** indicates the openings to be created by removing the bony shell in the base. **(E)** The cochlea after removing the bony shell with the exposure of the base. **(F)** The enlarged image of the dotted box shown in **(E)**. Scale bars: 0.2 mm.

culture method drastically improved the preservation of the overall structure of the organ of Corti and the integrity of the sensory epithelium. After 14 days in culture, the inner pillar cells (IPCs) and outer pillar cells (OPCs) were separated by the tunnel of Corti, similar to freshly dissected adult cochleae (**Figures 3a, b** and **Supplementary Video 2**). Due to HC death, SOX2 + SC nuclei could be seen as disorganized compared to a freshly dissected adult cochlea (**Supplementary Video 2**). We quantified the number of SCs in cultured adult cochleae. After 14 days in culture, ∼70% of SCs in the apex and ∼60% of SCs in the base survived, whereas, by 21 days, ∼50% of SCs in the apex and ∼13% in the base survived (**Figures 3e–j**), an indication of major SC loss in particular in the base between 14 and 21 days in culture. Approximately 30% of IHCs in the cultured adult cochleae could survive for 7 days, while only ∼10% of IHCs could survive for 14 days, and there is no significant difference between the cochlear turns. Nevertheless, even in the group with the longest culture time, the overall structure of the organ of Corti was maintained, in contrast to previous studies with a total loss of cochlear structure and $SOX2^+$ SCs using the conventional method (**Supplementary Figures 1b1–b3**). We concluded that our new adult cochlear explant culture system maintains the overall structure of the organ of Corti with improved cell survival of SCs.

One important application of adult cochlear explant culture is the ability to study SCs in their relatively native status. To determine if adult SCs drastically change their properties, we examined multiple SC markers in the cultured adult cochlea. By immunolabeling with the SC markers of SOX2, JAG1, and S100A1, we found that the SCs in culture continued to express *Sox2*. JAG1 and S100A1 were detected in a subset of SCs in the cultured cochlea that resembled the patterns in the freshly dissected adult cochlea (**Supplementary Figures 2a1–a3, c1–c3**). There was a general diffusion of signals of JAG1 and S100A1 in cultured SCs, likely reflecting the disorganization of SCs after HC death (**Supplementary Figures 2b1–b3, d1–d3**).

Expression of Exogenous Genes in Cultured Adult Cochlear Explants by a Viral Infection

It has been reported that the recombinant, replication-deficient Adenovirus (Ad) could efficiently infect the HCs and SCs in the neonatal mouse cochlea (Shu et al., 2016). We investigated the ability of adenovirus to infect cultured adult cochleae to express exogenous genes. Two weeks after adding the adenovirus containing CMV promoter-driven GFP (Ad-GFP) to the culture media with adult mouse cochleae, we observed robust GFP signals in both the sensory epithelial and the spiral limbus regions (**Figure 4a**). In the sensory epithelial region, 39.36 ± 5.70% of the $SOX2^+$ SCs were GFP^+, whereas 28.87 ± 11.79% of the remaining $MYO7A^+$ IHCs expressed GFP (**Figures 4a–f**). We further compared the infection efficiency among different

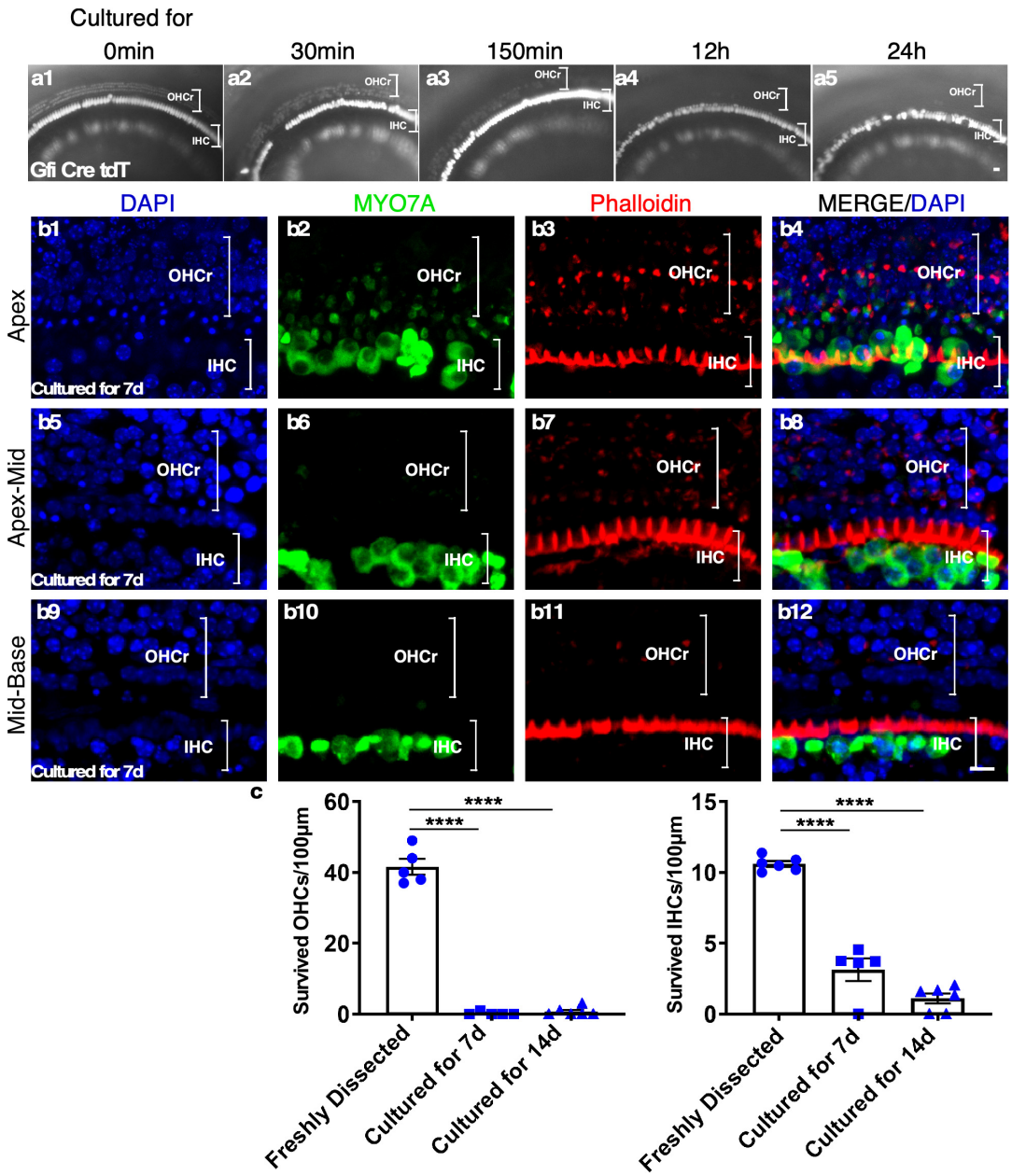

FIGURE 2 | The rapid loss of outer hair cells (OHCs) in adult cochlear culture. **(a1–a5)** The loss of OHCs *in vitro*. In adult Gfi-Cre-Tm-red cochlear culture (apex), the loss of OHCs (by the absence of the Tm-red signals) started as early as 30 min in culture **(a2)**. By 12 h **(a4)**, no OHC signal was detectable, an indication of complete OHC loss. In contrast, many inner HCs (IHCs) survived 7 days in culture **(b1–b12)**. **(c)** Quantification of surviving OHCs and IHCs from apex to base of the adult cochlear culture system. ****$p < 0.0001$, two-tailed unpaired Student's *t*-test. Error bar, mean ± SEM, $n = 5–6$. *n* is the number of biologically independent cochlea samples. Scale bars: 10 μm.

SC subtypes by dividing SCs into the inner and outer regions that are separated by the tunnel of Corti (**Figure 4d**). The SCs in the inner region were composed of inner border cells (IBCs), inner phalangeal cells (IPhCs), and IPCs, while the SCs in the outer region consisted of OPCs, Deiters' cells (DCs), Hensen cells and Claudius cells. Judging by the position, most SC subtypes including IPCs, OPCs, and DCs in cultured adult cochlear epithelia were infected by Ad-GFP (**Figures 4c,d**), and the infection efficiency of the SCs in the outer region was higher than that of the inner region (44.52 ± 9.06% in the outer region vs. 17.23 ± 3.39% in the inner region, $n = 4$, $p < 0.05$) (**Figure 4g**). We further cultured adult *Sox2*-CreER-Tm-red cochleae in the presence of tamoxifen to activate Tm-red in SOX2^{+} SCs for lineage tracing. After Ad-GFP infection and tamoxifen treatment, Tm-red^{+} SCs were co-localized with GFP, demonstrating GFP expression in the

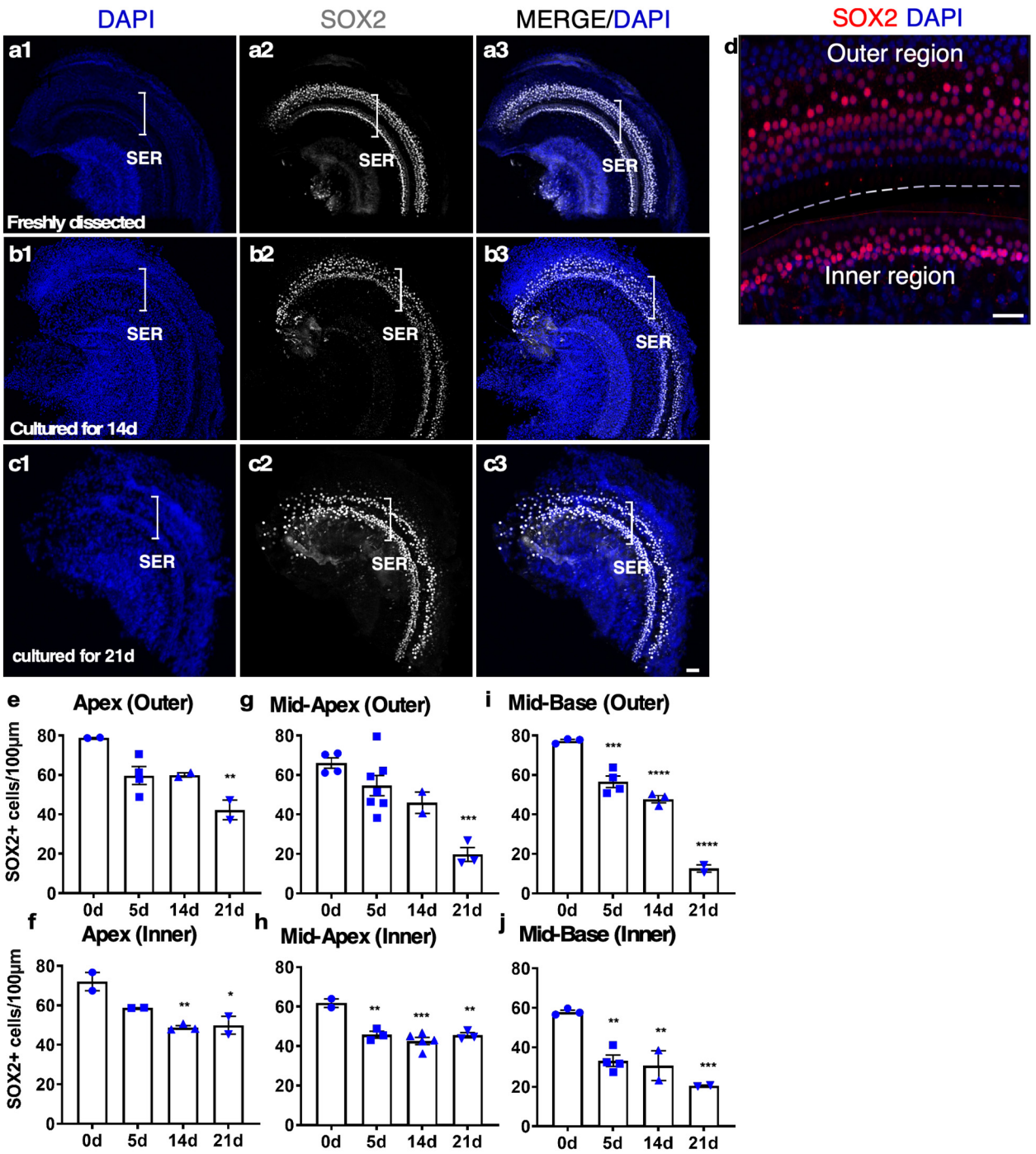

FIGURE 3 | The survival of SOX2$^+$ supporting cells (SCs) in adult cochlear explant culture. **(a–c)** Fresh and cultured wild-type adult cochlea (apex). **(a1–a3)** In a freshly dissected adult cochlea labeled with an anti-SOX2 antibody, SOX2$^+$ SCs were confined to the sensory epithelial region (SER, bracket). **(b1–b3)** After 14 days in culture, the overall structure of the organ of Corti was intact with the survival of most of the SCs. **(c1–c3)** By 21 days, the loss of SOX2$^+$ SCs became apparent yet the organ of Corti structure was maintained. **(d)** A freshly dissected sample to show the SCs in the inner and outer hair cell regions. **(e–j)** Quantification of SCs in the outer and inner SER (**d**, demarcated by a dashed line) along the cochlear turns showed similar patterns of survival of SCs in the apex and mid-turns for up to 14 days, and a diminished number of SCs in the base at 21 days in culture. $^*p < 0.05$, $^{**}p < 0.01$, $^{***}p < 0.001$, $^{****}p < 0.0001$. One-way ANOVA comparison of the data obtained on days 5, 14, and 21 with the data obtained day 0. Error bar, mean ± SEM, n = 2–7 in each group. n is the number of biologically independent cochlea samples. Scale bars: 50 µm.

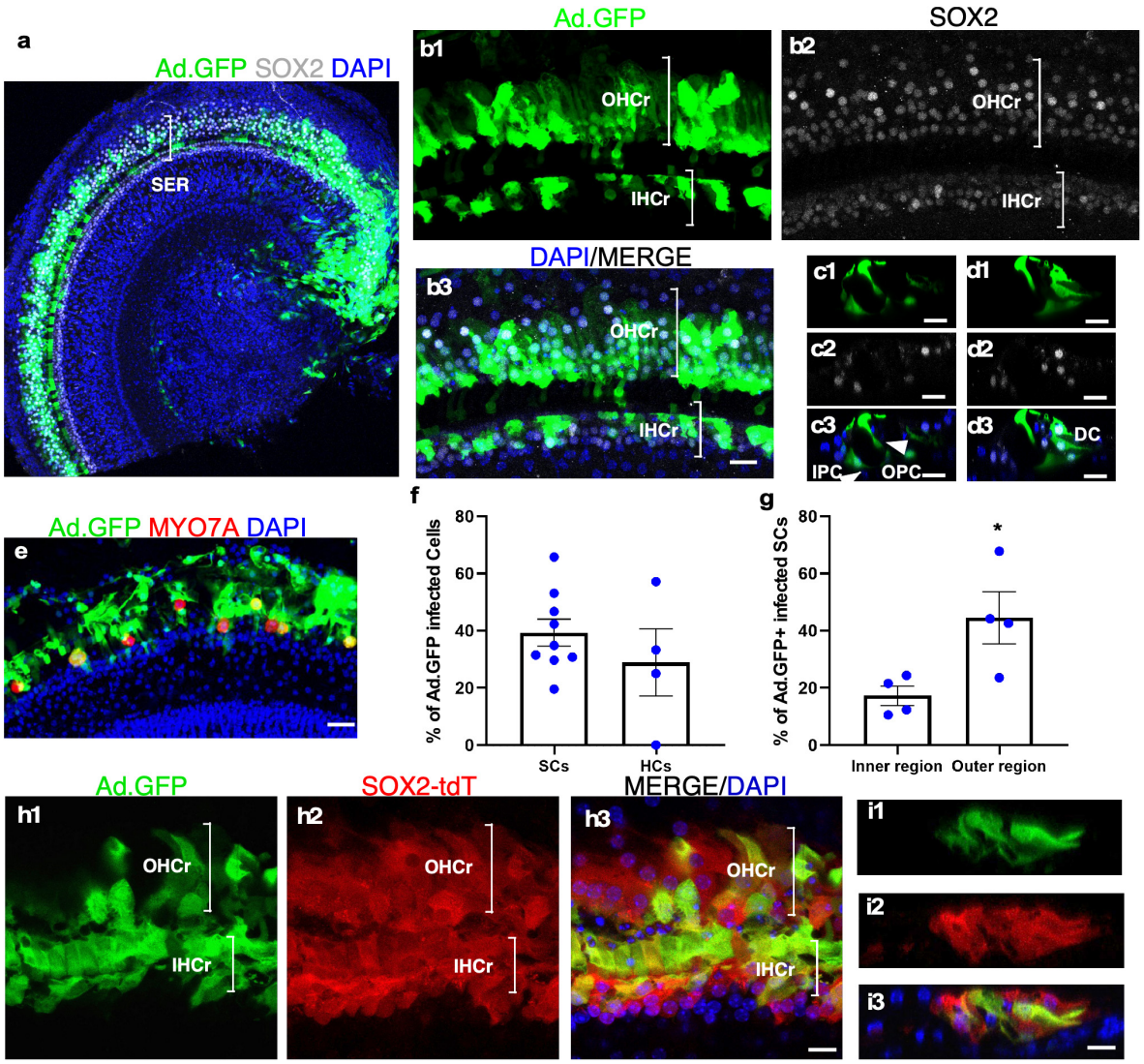

FIGURE 4 | Adenovirus infects cultured adult SC subtypes and IHCs. **(a)** A surface view of a cultured adult cochlea (apical and part of the middle turn) infected by Ad-GFP with the production of GFP mainly in the SER with fewer infected cells in the limbus region. **(b1–b3)** The enlarged SER shows GFP$^+$ SCs (SOX2$^+$/GFP$^+$). **(c,d)** Cross-sections of the SER to show the infected SC subtypes (SOX2$^+$/GFP$^+$) according to their positions in the organ of Corti, including inner and outer pillar Cells (IPCs and OPCs), Deiters' cells (DCs), and inner phalangeal cells (IPhCs). **(e)** Surviving IHCs were infected by Ad-GFP (MYO7A$^+$/GFP$^+$). **(f,g)** Quantification and comparison of Ad-GFP-infected SCs vs. IHCs and infected SCs in the inner vs. outer SERs. **(h1–h3)** A lineage tracing study is shown in a cultured adult SOX2-CreER-Tm-red mouse cochlea treated by tamoxifen and infected by Ad-GFP. Tm-red and GFP were co-localized in the SCs in the sensory epithelium. **(i1–i3)** Cross-sections of the SER in **(h)** to show co-localization of Tm-red and GFP in the SCs. *$p < 0.05$, Student's t-test. Error bar, mean ± SEM, n = 4–9. n is the number of biologically independent cochlea samples. Scale bars: 10 μm.

SCs infected by Ad-GFP (**Figures 4h,i**). Efficient adenovirus-mediated SC infection and expression of exogenous genes in cultured adult cochlear explant provided an important tool to study gene functions.

In vitro Regeneration of Hair Cell-Like Cells With *Atoh1* Overexpression in Cultured Adult Cochlear Explants

It has been established that overexpression of *Atoh1*, an HC fate determinant, is sufficient to transdifferentiate SCs to HCs in neonatal mouse cochleae and adult mouse vestibular system, yet transdifferentiation from SCs to HCs in adult cochleae *in vivo* remains controversial (Zheng and Gao, 2000; Kawamoto et al., 2003; Kelly et al., 2012; Liu et al., 2012; Yang et al., 2012). The capacity to culture adult mouse cochleae provides a unique opportunity to study adult HC regeneration *in vitro*. In adult cochleae cultured for more than 7 days, we did not observe any HCs in the OHC region due to the death of all OHCs in the culture and the lack of spontaneous HC regeneration. Rare IHCs survived in the culture (**Figure 4e**).

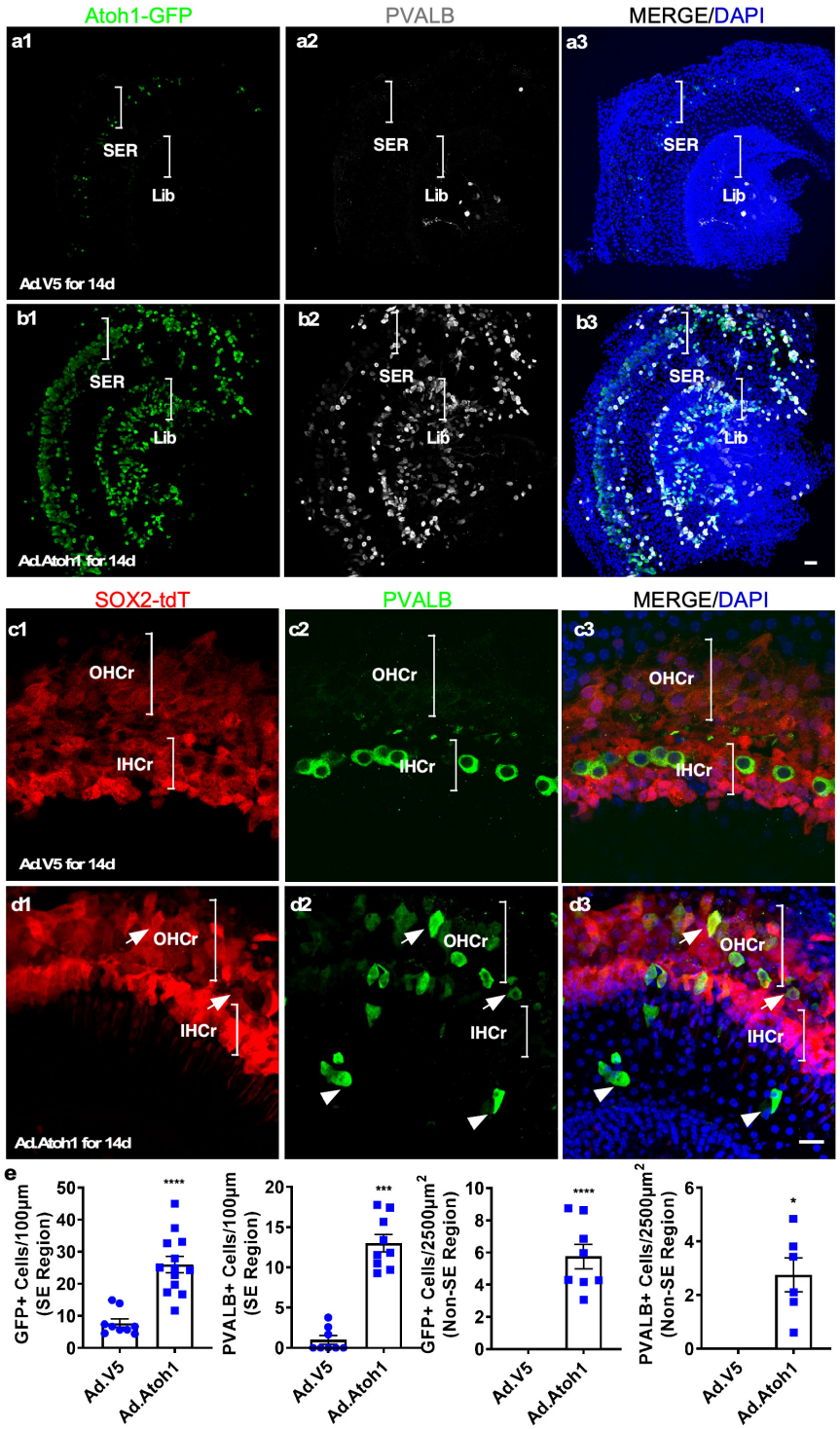

FIGURE 5 | Transdifferentiation of Ad-Atoh1-infected cells and lineage tracing in cultured adult cochleae. **(a1–a3)** In cultured adult Atoh1-GFP cochleae (apex), control Ad-V5 infection-induced only a few GFP$^+$ cells in the SER (bracket). There was no induction of GFP in the limbus region (Lib, bracket). **(b1–b3)** In cultured adult Atoh1-GFP cochleae (apex), Ad-Atoh1 infection-induced many GFP$^+$ cells in the SER (bracket) and Lib (bracket). **(c,d)** SC origin of regenerated HC-like cells (HCLCs) by lineage tracing. **(c1–c3)** In the apex of the cultured adult Sox2-CreER-Tm-red cochleae infected with Ad-V5, no PVALB$^+$ cells were detected in the OHC region whereas the surviving IHCs were Tm-red negative. **(d1–d3)** HCLCs (PVALB$^+$) were detected in the OHC region that was co-localized with Tm-red signal (arrows) as well as in the non-sensory region (arrowheads) that were devoid of Tm-red after Ad-Atoh1 infection in cultured adult Sox2-CreER-Tm-red cochleae. **(e)** Quantification of GFP+ cells and new HCLCs from apex, apex-mid, and base in Ad-V5 and Ad-Atoh1 groups. *$p < 0.05$, ***$p < 0.001$, ****$p < 0.0001$, Student's *t*-test. Error bar, mean ± SEM, $n = 3$–13. *n* is the number of biologically independent cochlea samples. Scale bars: 20 μm.

To test the utility of the explant culture system for HC regeneration *in vitro*, we cultured adult cochleae from the *Atoh1*-GFP transgenic mice, in which GFP expression was under the control of the 3′ enhancer of *Atoh1* (Lumpkin et al., 2003) and induced by *Atoh1* expression. We used adenovirus carrying CMV promoter-driven human *ATOH1* (Ad-Atoh1) to infect cultured adult *Atoh1*-GFP transgenic mouse cochleae, whereas adenovirus carrying a V5 tag (Ad-V5) was used as the control for infection. In Ad-V5-infected *Atoh1*-GFP cochleae that were subsequently cultured for 14 days, a few weak GFP^+ cells were detected both in surviving IHCs and in the SCs vicinity of surviving IHCs in the explants (7.77 ± 1.30 GFP^+ cells/100 μm, n = 9, **Figures 5a1–a3** and **Supplementary Figures 5a1–a4**), reflecting the weak endogenous ATOH1 activity. In adult *Atoh1*-GFP cochleae infected with Ad-Atoh1 followed by culture for 14 days, quantitatively more GFP^+ cells were detected throughout the sensory epithelium as well as in the spiral limbus region in the explants (26.07 ± 2.54 GFP^+ cells/100 μm for sensory epithelium, n = 13, and 5.75 ± 0.76 GFP^+ cells/2,500 μm^2 for spiral limbus region, n = 11, **Figures 5b,e**). These GFP^+ cells were the cells with *Atoh1* transcriptional activity due to Ad-Atoh1 infection.

To investigate whether cells with increased *Atoh1* activity transdifferentiate into HCs, we examined the co-expression of MYO7A and GFP in the infected adult cochlear explants. There were significantly more $MYO7A^+/GFP^+$ cells in the explants infected by Ad-Atoh1 (4.03 ± 0.66/100 μm sensory epithelium, n = 13, 0.64 ± 0.14 cells/2,500 μm^2 spiral limbus region, n = 11, **Supplementary Figures 3c1–c4**) than in the explants infected by Ad-V5 (1.04 ± 0.47 cells/100 μm sensory epithelium, n = 9, **Supplementary Figures 3a1–a4, b1–b4**). We noticed that only a small portion of GFP^+ cells turned out to be $MYO7A^+$ HCLCs in both the sensory epithelial region and the limbus region after the infection of Ad-Atoh1 (16.00 ± 2.18% for the sensory epithelium, 12.57 ± 3.29% for the spiral limbus region) (**Supplementary Figures 3d,e**).

To further confirm the identity of regenerated HCs, we investigated the expression of the HC marker Parvalbumin (PVALB). After Ad-V5 infection of the cochlear explants from *Atoh1*-GFP transgenic mice, $PVALB^+$ IHCs were observed in the sensory region of cultured cochlear explants, an indication of surviving existing IHCs (2.67 ± 0.61 cells/100 μm sensory epithelium, n = 3, **Figure 5a**), some $PVALB^+$ spiral ganglion neurons (SGNs) were also found (Fischer et al., 2019). After Ad-Atoh1 infection, the number of $PVALB^+$ cells was significantly increased in both the sensory epithelium (13.02 ± 1.076 cells/100 μm sensory epithelium, n = 9, **Figures 5a, b** and **Supplementary Figures 5a, b**) and the limbus region (2.76 ± 0.63 cells/2,500 μm^2 limbus region, n = 6, **Figures 5a, b**). Of all the GFP^+ cells, significantly more cells were $PVALB^+/GFP^+$ (60.64 ± 10.32% in the sensory region, n = 3 and 73.23 ± 11.81% in the limbus region, n = 3) than $MYO7A^+/GFP^+$.

To further determine the origin of HCLCs, we performed lineage tracing by using the *Sox2*-CreER-Tm-red mice. After injecting tamoxifen daily for 3 days, adult SCs were permanently labeled with tdTomato ($Tm\text{-}red^+$). Cochleae from tamoxifen-injected adult mice were cultured and infected with either Ad-Atoh1 or Ad-V5. Fourteen days after Ad-V5 infection, we did not observe any $PVALB^+$ HCLCs in the OHC region, and the remaining existing IHCs were negative for Tm-red (**Figure 5c**). In contrast, $PVALB^+$ HCLCs were detected in the OHC region after Ad-Atoh1 infection and all of them were $Tm\text{-}red^+$ (**Figure 5d**). We concluded that *Atoh1* overexpression resulted in regeneration of HCLCs in the OHC region from $SOX2^+$ SC transdifferentiation and in the limbus region due to transdifferentiation of SOX2-negative cells.

Regenerated Hair Cell-Like Cells Have Young Hair Cell Properties

What are the characteristics of new HCLCs? Are they relatively mature HCs resulting from formation in the adult cochlea, or are they developmentally young HCs due to recent transdifferentiation from SCs? Using immunostaining with markers including PVALB, PTPRQ, espin (ESPN), and acetylated tubulin, we studied the presence of HC stereocilia in the regenerated HCLCs. Staining of PTPRQ, a marker for young HCs (Goodyear et al., 2003), was identified within the stereocilia-like structures of $PVALB^+$ HCLCs, but not in the existing IHCs in control cochleae infected by Ad-V5 (**Figures 6a,b**). The kinocilium is a transient structure for directing the orientation of stereocilia during early cochlear HC development, and it is no longer detectable after postnatal day 21 (Cotanche and Corwin, 1991; Tilney et al., 1992). We observed acetylated tubulin-labeled kinocilia in the $ESPN^+$ HCLCs in the Ad-Atoh1-infected cochlea but not in the existing IHCs from Ad-V5-infected control cochleae (**Figures 6c,d**). The detection of immature HC markers in the HCLCs but not in the existing surviving adult HCs strongly supports that regenerated HCLCs resemble developmentally young, immature HCs.

The Survival of Adult Neurons in Cultured Cochlear Explants

Spiral ganglion neurons relay the information generated by mechanotransduction of HCs to the brainstem. The ability to culture adult SGNs concomitantly with cochlear explants presents an opportunity to study SGNs and their interactions with the HCs that are essential in the auditory pathway for hearing. The whole cochlear explant culture enabled us to assess the survival of SGNs housed in the bony structure of the modiolus. We examined the density of SGNs within the modiolus by the labeling of TUJ1 (TUBB3), a neuronal marker, and quantified the number of $TUJ1^+$ SGN somas from the frozen sections of cultured adult cochleae. Compared to the freshly dissected adult cochleae, 86 and 77% of $TUJ1^+$ SGNs were maintained after 5 and 14 days in culture, respectively, demonstrating long-term survival of adult SGNs *in vitro* (**Figure 7**).

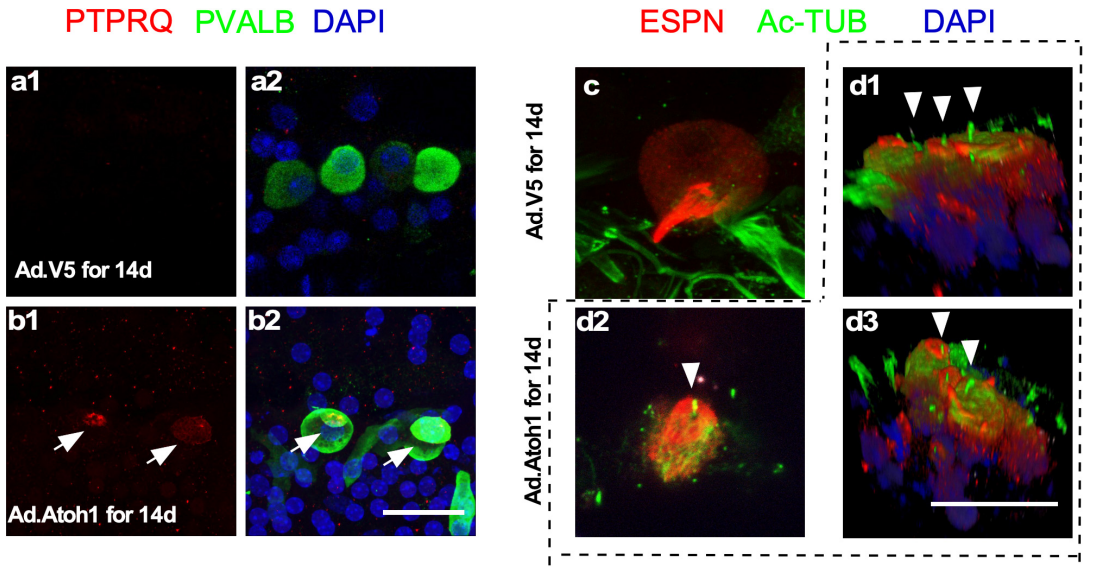

FIGURE 6 | Regenerated HCLCs resemble developmentally young, immature HCs. **(a1,a2)** In control cultured adult cochleae infected with Ad-V5, an early HC marker PTPRQ was not detected in the existing surviving IHCs. **(b1,b2)** In Ad-Atoh1-infected adult cochleae in culture, PTPRQ was seen in the stereocilia structures in the regenerated HCLCs (arrows). **(c)** Kinocilia were not detected in control cochlear IHCs by acetylated tubulin (Ac-TUB) labeling after Ad-V5 infection in cultured adult cochleae. **(d1–d3)** Ac-TUB labeled kinocilia were observed in regenerated ESPN$^+$ HCLCs after Ad-Atoh1 infection in cultured adult cochleae (arrowheads). Scale bars: 25 μm.

Reinnervation in the Cultured Adult Cochleae

It has been established that after *in vivo* injection with ototoxic drugs including kanamycin in combination with diuretic drug furosemide, there is significant OHC loss that is accompanied by subsequent retraction of the ganglion neurites (Oesterle and Campbell, 2009). We used the model of kanamycin and furosemide injection in adult wild-type mice to induce OHC death. Examination of the cochleae 9 days post-injection showed a complete OHC loss and the absence of neurites in the OHC region (**Figure 8b**). In the IHC region, fewer neurites labeled with TUJ1 were observed medial to the IHCs in comparison to the freshly dissected untreated adult cochleae (**Figures 8a,b**).

We cultured adult wild-type cochleae 9 days postkanamycin/furosemide injection and infected one group with Ad-Atoh1 and the other group with Ad-V5 as control. In the Ad-V5-infected control after 14 days in culture, we observed surviving IHCs (MYO7A$^+$) in the vicinity of the remnants of ganglion neurites, with occasional IHC to neurite connections (**Figure 8c**). No HCs or neurites were detected in the OHC region. In contrast, in the Ad-Atoh1-infected group, MYO7A$^+$ HCLCs were detected in the OHC region (**Figure 8d**). Strikingly, numerous adult neurites migrated across the medial line to form connections with regenerated HCLCs in the OHC region. Furthermore, there were clusters of disorganized neurites surrounding the IHCs, many of which were in direct contact with the IHCs (**Figure 8d** and **Supplementary Video 3**).

We noticed that some regenerated MYO7A$^+$ HCLCs in the OHC and IHC regions were also labeled with TUJ1, a neuronal marker. In fact, TUJ1$^+$ cells were abundant in the sensory epithelia (20.87 ± 4.85/100 μm sensory epithelium, n = 5, **Figures 8d,f**) of the Ad-Atoh1-infected cultured adult cochleae. TUJ1 was mainly detected in cells with weak or absent MYO7A signal (arrowheads, **Figure 8d**), whereas cells with prominent MYO7A staining generally lacked TUJ1 (arrows, **Figure 8d**), suggesting that the expression of TUJ1 may be associated with early regenerated HCLCs transdifferentiated from SCs. Significantly, TUJ1$^+$ cells were able to form connections with the SGN neurites irrespective of *Myo7a* expression (arrowheads, **Figure 8d**). To confirm the result, we treated the adult wild-type cochleae with Ad.Atoh1-mCherry, the adenovirus expressing both human *ATOH1* and mCherry marker under CMV promoter (**Supplementary Figures 4b, 6**). Notably, numerous neurites connected to Ad.Atoh1-mCherry$^+$/TUJ1$^+$ cells were detected in the culture system while no new TUJ1$^+$ cells were detected in the Ad-V5 treated control samples (**Supplementary Figures 4a1–a3, b1–b3**). Besides, the triple labeling of Ad.Atoh1-mCherry$^+$/ESPN$^+$/TUJ1$^+$ HCLCs was detected (**Supplementary Figure 6**). Furthermore, we infected Atoh1-GFP mouse cochleae with Ad-Atoh1 and detected GFP$^+$ cells co-labeled with TUJ1. In addition, these GFP$^+$/TUJ1$^+$ cells form connections to the TUJ1$^+$ SGN neurites (**Figure 8e**). The connections between neurites and regenerated HCLCs can be seen in a movie with the 3D-reconstructed images (**Supplementary Videos 3, 4**). Taken together, the results strongly indicated that the HCLCs promote neurite outgrowth and the

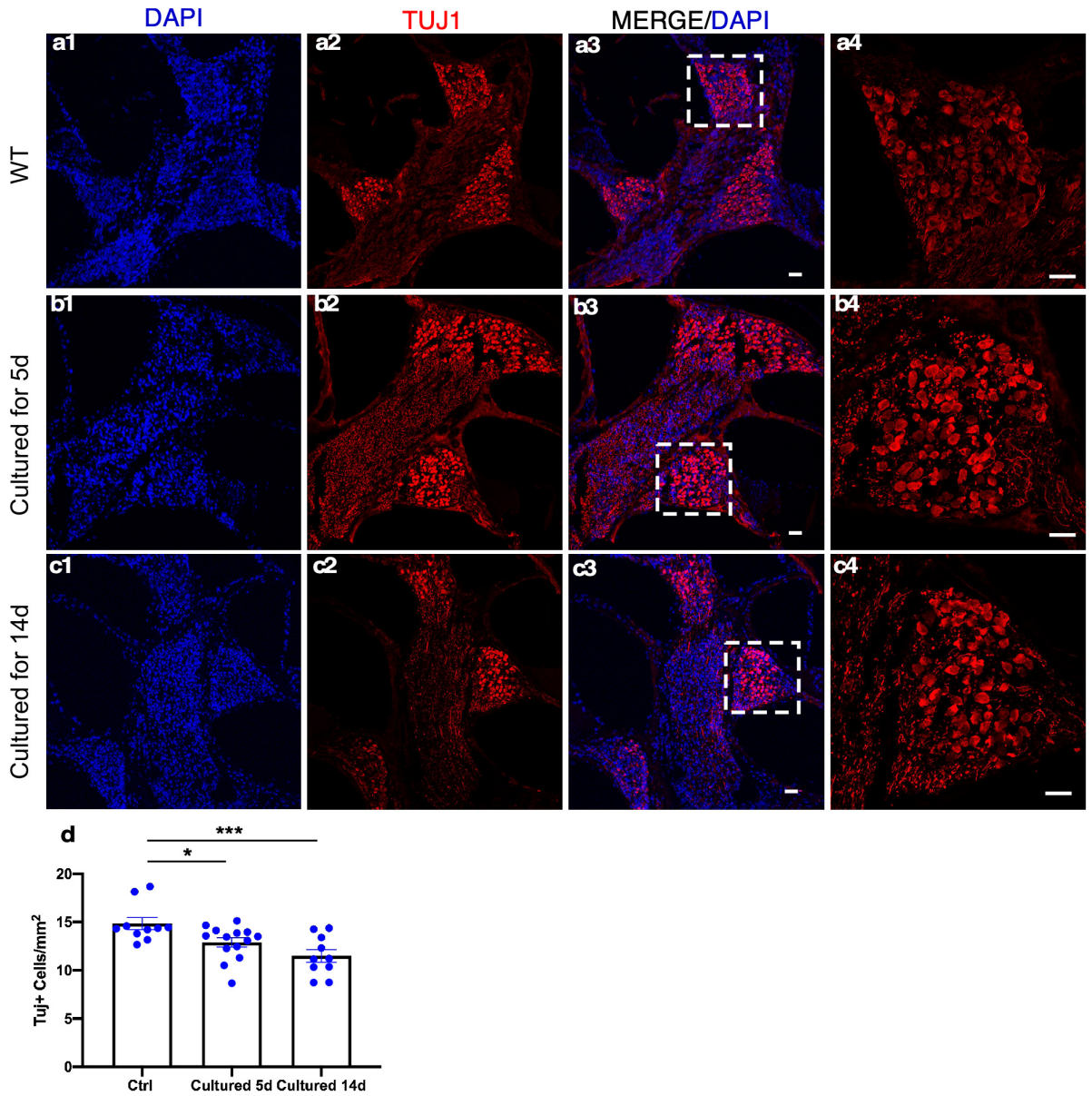

FIGURE 7 | Spiral ganglion neurons (SGNs) survive in adult cochlear explant culture. **(a1–a4)** In the freshly dissected adult cochleae, SGNs in the modiolus were detected by TUJ1 labeling. After 5 **(b1–b4)** or 14 days **(c1–c4)** in culture, abundant TUJ1$^+$ SGNs were seen in the modiolus with a well-maintained structure. **(d)** Quantification showed the survival of a majority of adult SGNs in the apical turn even after 14 days in culture. $^*p < 0.05$, $^{***}p < 0.001$, and one-way ANOVA comparison of the mean of each column with the mean of a control column. Error bar, mean ± SEM, and n = 10–14. n is the number of biologically independent cochlea samples. Scale bars: 25 μm.

likely formation of new connections between the SGN and HCs at an early stage of HC formation.

DISCUSSION

Embryonic or neonatal mouse cochleae can be cultured, which has led to studies to generate a wealth of information related to development, regeneration, and mechanisms underlying deafness (Zheng and Gao, 1999, 2000; Zheng et al., 2000; Shou et al., 2003; Woods et al., 2004; White et al., 2006; Dabdoub et al., 2008; Diensthuber et al., 2009; Mizutari et al., 2013; Bramhall et al., 2014). However, adult mature mammalian cochleae have characteristics that are fundamentally different from young cochleae. Since even newborn human inner ears are fully mature, studies in adult mature cochleae are necessary to understand disease progression, identify potential drugs, and develop regeneration therapy for the treatment of hearing loss. The lack of a system to study adult mammalian cochleae *in vitro* has been a major hurdle to efficiently test scientific hypotheses

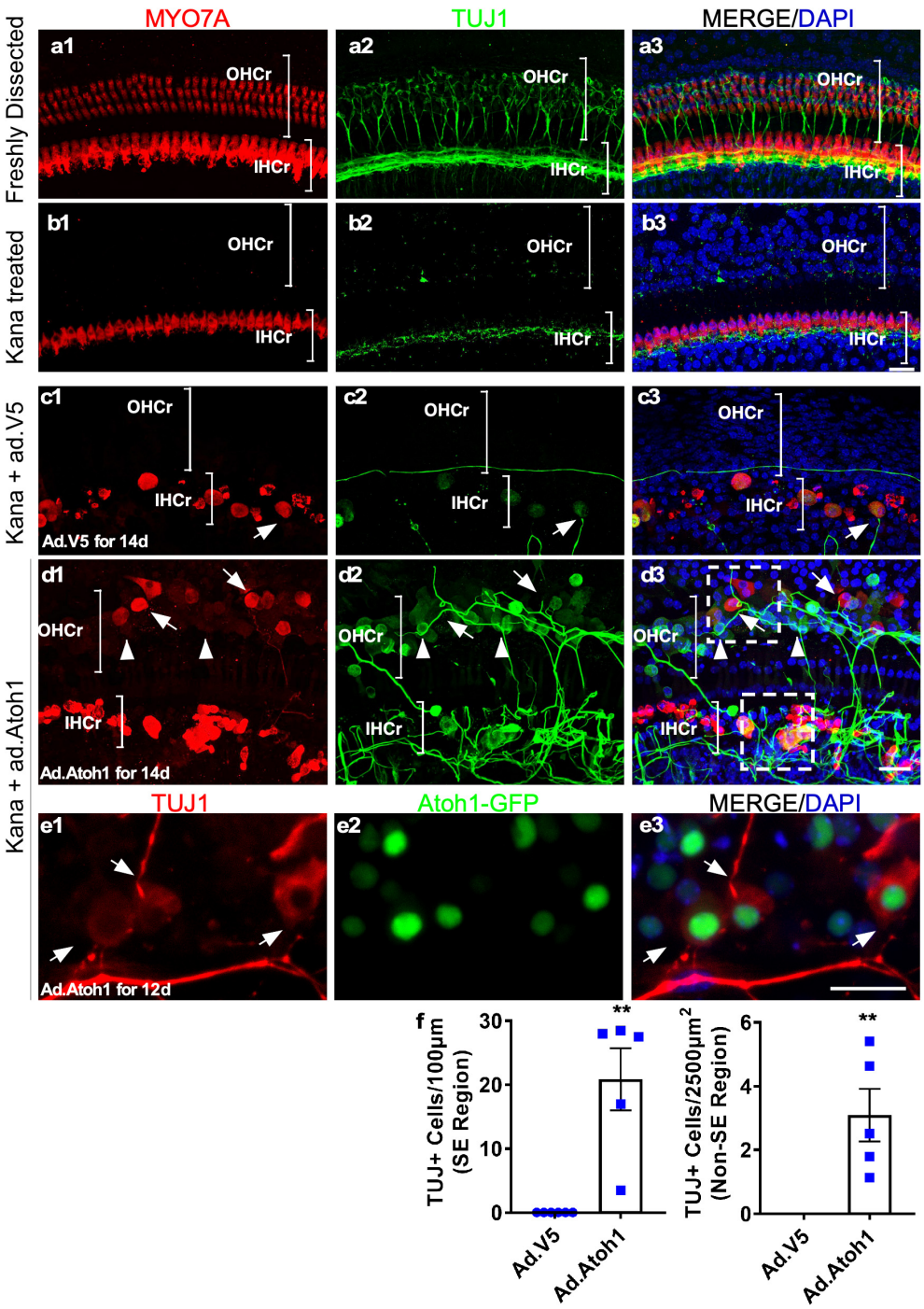

FIGURE 8 | Promotion of outgrowth of adult SGN neurites and formation of connections with regenerated HCLCs in adult cochlear explant culture. **(a1–a3)** A freshly dissected apex of the adult cochlea showed the distribution of neurites labeled with TUJ1. **(b1–b3)** Nine days postkanamycin/furosemide injection *in vivo* (d0 in culture), there was a complete loss of OHCs and an absence of neurites in the OHC region (OHCr, bracket). Neurites with lower density were scattered beneath the surviving IHCs. **(c1–c3)** Nine days postkanamycin/furosemide injection *in vivo* and 14 days after Ad-V5 infection in culture (d14), adult cochleae showed no HCs or neurites in the OHC region. There was a loss of a majority of neurites in the IHC region (IHCr, bracket). Some surviving IHCs were in direct contact with remaining neurites (arrow). **(d1–d3)** Nine days postkanamycin/furosemide injection *in vivo* and 14 days after Ad-Atoh1 infection in culture, adult cochleae showed regenerated HCLCs and neurites in the OHC region, and numerous disorganized neurites in the IHC region. HCLCs (MYO7A$^+$) were in direct contact with neurites (arrows). Many cells in the OHC region were TUJ1$^+$ with weak or absent MYO7A signals, yet were in direct contact with neurites (arrowheads). The box areas in panel d3 refer to **Supplementary Videos 3, 4**. **(e1–e3)** Atoh1–GFP cochlea samples 12 days after Ad-Atoh1 infection. The Atoh1-GFP$^+$ cells began to express TUJ1 marker and connect to neural fibers (arrows). **(f)** Quantification showed an increase of TUJ1$^+$ cells after Ad-Atoh1 infection in culture. $^{**}p < 0.01$, Student's *t*-test. Error bar, mean ± SEM, $n = 5$–6. *n* is the number of biologically independent cochlea samples. Scale bars: 20 μm.

and screen new drugs for inner ear disorders. In this study, we established an adult mouse cochlear explant culture system and demonstrated its utility in a case study of HC regeneration and interaction between SGNs and HCs.

The major difference between our adult explant culture system and previous attempts to establish an adult cochlear explant culture lies in the fact that we purposefully retained the bony structure of the cochlea, maintaining cells in their endogenous environment that promotes cell survival. The overall architecture of the cochlea is important to cell survival as it is increasingly realized that mature cell types generally survive better in a 3D environment (Edmondson et al., 2014). Our culture system provides an integral architecture that sustains the relative positions of different adult cochlear cell types, which likely results in the maintenance of the cell-to-cell and cell-to-ECM interactions. The openings at the apex and the base of the cochlea facilitate access to the medium. Our results strongly support that a majority of adult cochlear cell types have the intrinsic capacity to survive long-term in explant culture, which allows the studies of individual cell types and their interactions.

In culture, adult OHCs undergo rapid cell death and, by 24 h, all OHCs are virtually lost (**Figure 2**). It is known that OHCs are sensitive to endolymph with high ionic concentration, and changes in the microenvironment lead to OHC death (Zenner, 1986; Dulon et al., 1987; Zenner et al., 1994). However, additional unknown factors are likely to contribute to cell death as OHCs die quickly even in artificial endolymph with a similar ionic environment to endogenous endolymph. Rapid OHC death in culture provides an opportunity to study HC regeneration in the OHC region as we have shown that all HCLCs in the OHC region are from regeneration rather than the survival of existing OHCs. The explant culture system should serve as an excellent model to screen potential drugs that attenuate OHC death in culture, which could lead to important hearing loss treatments by developing drugs that protect against HC death. In contrast to OHCs, some adult IHCs survive long-term (14 days) in culture, which may provide clues about mechanisms for their resistance to cell death. We are currently conducting experiments to profile gene expression in surviving IHCs by RNA-Seq to address the issue.

In the adult cultured explant, the overall cochlear structure is well maintained for up to 14 days (**Supplementary Videos 1, 2**) with the survival of a majority of SC types including Claudius cells, Hensen's cells, DCs, pillar cells, IPhCs, IBCs, and inner sulcus cells. By studying SC markers, it is evident that SCs largely maintain their identities, i.e., SCs do not undergo a major dedifferentiation process with the perturbation of SC gene expression. Infection of diverse adult SC subtypes in culture by adenovirus provides an opportunity to activate or inhibit gene expression efficiently and temporally by methods, such as genome editing and siRNAs, and evaluate the effects on various activities including regeneration, treatment of genetic hearing loss, and SC biological roles (Shu et al., 2019; Niggemann et al., 2020).

In the current adult cochlear explant culture system, all OHCs and some IHCs, as well as a portion of SCs die. There is the reorganization of the sensory epithelium in cultured adult cochleae. Our explant culture system presents a damaged model. However, as it has been shown in our study, it can serve as a valuable tool to study different aspects of the adult cochlea in culture.

Reproducible regeneration of HCLCs in cultured adult cochlear explants by adenovirus-mediated *Atoh1* overexpression highlights the utility of the system. By activation of *Atoh1* in cultured adult mouse cochleae, we demonstrated that adult cochlear SCs can transdifferentiate into HCLCs, with the expression of multiple HC markers. In contrast, in our recent study, Ad-Atoh1 overexpression in adult cochlear SCs has never resulted in the regeneration of HCLCs *in vivo* (Shu et al., 2019). *In vivo* regeneration of HCLCs could only be achieved through reprogramming by transient activation of *Myc* and *Notch* followed by *Atoh1* overexpression (Shu et al., 2019). Therefore, it is highly likely that the explant culture itself provides a degree of reprogramming that enables adult SCs to respond to *Atoh1* induction signals and transdifferentiate to HCs *in vitro*. This is consistent with the evidence that mature cell types undergo reprogramming in culture by selective downregulation of mature genes and upregulation of developmental genes (Alizadeh et al., 2001; Mantikou et al., 2016). The cochlear explant culture system further illustrates that HCLCs can be regenerated from non-sensory epithelial regions, such as the limbus, providing evidence that additional adult cochlear non-sensory cell types have the capacity to transdifferentiate into HCs in culture in the presence of *Atoh1* signaling. Identification of signaling pathways in culture-mediated reprogramming in adult SCs should shed light on the process with potential improvement in HC regeneration efficiency.

Our study is the first in which adult SGNs were cultured for an extended period of time and were studied in the context of degeneration and reinnervation. In adult cochleae, the loss of HCs leads to retraction of neurites (Sugawara et al., 2005; Kujawa and Liberman, 2009). Furthermore, damage to HCs leads to the loss of synapses by the way of synaptopathy that contributes to "hidden hearing loss," the reduced capacity to recognize speech in noisy environments. Efforts to reestablish new synapses after HC noise damage, including NT3 overexpression, have had limited success (Wan et al., 2014). However, it is not known if adult SGNs retain their potential for outgrowth and reestablishment of connections with HCs once they are retracted as the consequence of HC damage or death. The adult cochlear explant culture demonstrates the feasibility of adult SGN outgrowth which likely results in reestablishing connections with regenerated HCLCs. Future studies will involve optimization of the culture condition so that the culture time can be further extended, which would allow for the study of the behavior of type I and II ganglion neurons and synaptogenesis in adult cochleae *in vitro*.

Insightfully, we found that during HC regeneration, Ad-Atoh1-infected cells start to express *Tuj1*, a neuronal marker, before the expression of HC genes including *Myo7a*. At this stage, $TUJ1^+$ neurites have migrated toward the $TUJ1^+$ cells induced by Ad-Atoh1 infection to form likely connections (**Figures 8d,e**, **Supplementary Figure 4**, and **Supplementary Videos 3, 4**). Thus, the signals that promote neurite outgrowth and formation of connections may have been produced at

a very early stage during HC regeneration. Identification of the signals responsible for the process will have a major impact on neurite outgrowth and synaptogenesis that are essential in developing potential therapy to reconnect SGNs with existing or regenerated HCs. A previous study on spontaneous HC regeneration in chicks has also identified early new HCs labeled with TUJ1 (Stone and Rubel, 2000), which is consistent with our observations during HC regeneration in adult cochleae *in vitro*. Expression of *Tuj1*, however, is transient, in regenerated HCLCs expressing mature markers, such as *Myo7a*. We noticed that there were only a small number of TUJ1+ cells that weakly express HC markers, such as Myo7a, and that these may represent prosensory cells before they more strongly express Myo7a and become HCLCs. For example, the triple labeling of Ad.Atoh1-mCherry+/ESPN+/TUJ1+ HCLCs was detected (**Supplementary Figure 6**). Furthermore, we infected Atoh1-GFP mouse cochleae with Ad-Atoh1 and detected GFP+ cells co-labeled with TUJ1. In addition, these GFP+/TUJ1+ cells form connections to the TUJ1+ SGN neurites (**Figure 8e**). The intermediate TUJ1 expression in early regenerated HCLCs may be unique to HC regeneration, as TUJ1 is not involved in normal HC development (Stone et al., 1996; Molea et al., 1999). Our data illustrate the application of the adult cochlear explant culture system to uncover novel biological processes.

Recent progress with inner ear organoids has provided new opportunities to study inner ear cell types including HCs *in vitro* (Koehler et al., 2013, 2017). The adult cochlear explant culture system is complementary to inner ear organoids for the study of the inner ear *in vitro*. The explant culture system uses adult cochleae, thus providing critical information on the capacity of mature inner ear cells to regenerate and develop cell-to-cell interactions. Furthermore, the regenerated HCs have properties that resemble the auditory HCs since the explant culture system uses adult cochleae. This has been illustrated by our recent study of Myc/Notch activation in combination with HC regeneration that leads to the production of HCLCs expressing *Slc26a5* (Prestin) and *Slc17a8* (Vglut3), an OHC marker and an IHC marker, respectively (Shu et al., 2019). The ability to study adult whole cochleae in their native architecture and in the presence of diverse inner ear cell types (cells from sensory and non-sensory regions as well as the SGNs) provides a unique opportunity to build an auditory system *in vitro*. It is possible that our approach can be extended to other mammalian species including pigs and humans so that the study can be carried out with results that are directly relevant to clinical applications.

MATERIALS AND METHODS

Mouse Models

Sox2-CreER transgenic mice and tdTomato reporter mice were from Jackson Laboratory (Stock# 017593 and 007914, respectively); We also used a strain expressing tdTomato under the control of *Gfi1* promoter (Gfi1 $^{TM1(Cre)Gan}$; R26tdTomato). *Atoh1*-nGFP mice are from Jane Johnson, University of Texas Southwestern Medical Center, Dallas, TX, United States. The wild-type mice were C57BL/6 from Charles River Laboratories. All experiments were performed in compliance with ethical regulations and approved by the Animal Care Committees of Massachusetts Eye and Ear and Harvard Medical School.

Adult Cochlear Culture and Viral Infection *in vitro*

Different from the neonatal cochlea culture method, in which the cochleae were disassociated from the bone, adult mouse cochleae (6–8 weeks old) were dissected with the bone attached. The bulla was first removed from the skull and then, in brief, dipped in 70% ethanol before being placed in ice-cold Hanks' Balanced Salt Solution (HBSS). The vestibular region was also removed. Under a dissecting microscope, the middle ear, vessels, and debris were removed from the bulla. The bone covering the apical turn was chipped off, and round window and oval window membranes were opened to allow media exchange with the cochlea fluids. The ligament portion and Reissner's membrane at each end of the cochlea were also removed to facilitate the access of medium to the sensory cells. The cochleae were maintained in floating culture in DMEM/F12 (Invitrogen) supplemented with N2 and B27 (both from Invitrogen) for 5–21 days. For infection, adenovirus was added to the culture at a titer of 5×10^{10} pfu/ml overnight before replacement with fresh medium. Ad-*Atoh1* and Ad-*V5* were purchased from SignaGen Laboratories, Rockville, MD, United States. Ad-GFP was purchased from the Vector Lab, Baylor College of Medicine, Houston, TX, United States. To label proliferating cells, EdU was added at a final concentration of 10 μM for varying time points.

Lineage Tracing

Notably, 6-week-old Sox2-CreER/tdT$^{f/f}$ mice were injected with tamoxifen (75 mg/kg) daily for 3 days before the cochleae were dissected for culture. Each virus was added to the medium for 16 h at a concentration of 5×10^{10} pfu/ml.

Immunohistochemistry

Mouse cochleae were fixed in 4% paraformaldehyde at 4°C overnight, followed by decalcification in 120 mM EDTA for 1–2 days. The decalcified cochleae were used for whole-mount immunohistochemistry following a standard procedure (Huang et al., 2013). The antibodies used are shown in **Supplementary Table**-antibody.

Confocal Microscopy

Confocal microscopy was performed using a Leica TCS SP8 with Leica Application Suite Advanced Fluorescence (LAS AF) software version 2.6.0 (Leica Microsystems Inc., Buffalo Grove, IL, United States). Sequential scanning with different laser channels was used for image acquisitions. Confocal images were processed using the ImageJ package

(National Institutes of Health, Bethesda, MD, United States)[1]. For Z-stacks, equal numbers of images of adjacent optical sections, 0.5 μm in thickness, were used for processing with identical parameters, including median filtering and adjustment of brightness and contrast, between experimental and control groups.

Statistical Analysis

The Prism 8 statistical package (GraphPad Software, Inc., San Diego, CA, United States) was used in the data processing. The number of $SOX2^+$ cells was counted as an SC number. The average number of $SOX2^+$ SCs per 100 μm was calculated as SC density for each cochlea and was used for statistical analysis. Data were presented as mean ± SEM. ANOVA analysis with Tukey's multiple comparisons test was used to compare three or more groups ($p < 0.05$ was considered significant).

DATA AVAILABILITY STATEMENT

The original contributions presented in the study are included in the article/**Supplementary Material**, further inquiries can be directed to the corresponding authors.

ETHICS STATEMENT

The animal study was reviewed and approved by the Massachusetts Eye & Ear Infirmary IACUC.

AUTHOR CONTRIBUTIONS

WL and YQ designed and performed the experiments, analyzed the data, interpreted the results, and drafted the manuscript. MH, WW, and YS performed the experiments and analyzed the data. HL analyzed the data. Z-YC conceived the project, designed the experiments, analyzed the data, interpreted the results, and wrote the manuscript. All authors edited the manuscript.

FUNDING

The authors acknowledged funding from NIH R01DC006908, R56DC006908, UG3TR002636 (Z-YC), DOD W81XWH1810331 (Z-YC), Fredrick and Ines Yeatts hair cell regeneration fellowship (Z-YC) and David-Shulsky Foundation (Z-YC), the National Key R&D Program of China No. 2017YFA0103900 (HL), the National Science Foundation for outstanding young people 81922018 (WL), the National Natural Science Foundation of China 81771011 (WL), and the Key Laboratory of Hearing Medicine, National Health and Family Planning Commission, Shanghai, China (HL).

[1]https://imagej.nih.gov/ij/

SUPPLEMENTARY MATERIAL

The Supplementary Material for this article can be found online at: https://www.frontiersin.org/articles/10.3389/fnmol.2021.757831/full#supplementary-material

Supplementary Figure 1 | Adult cochlear sensory epithelium degenerates in culture with the conventional method. **(a1,a2)** Epifluorescent picture of the apical turn of the freshly dissected wild-type adult mouse cochlea according to the protocol established for culturing neonatal mouse cochlea (Parker et al., 2010; Landegger et al., 2017). Only the very apical region of the sensory epithelium could be preserved with this method. Panel **(a2)** is the box area in panel **(a1)**, with the sensory epithelial regions (SER) marked with a bracket. **(b1–b3)** Fluorescent picture of the apical turn of an adult mouse cochlea using the traditional culture method. After 2 weeks in culture, the whole sensory epithelium folded and degenerated, with the loss of virtually all $SOX2^+$ cells. Scale bars: 50 μ m.

Supplementary Figure 2 | Maintenance of supporting cell (SC) markers in cultured adult cochleae. **(a1–a3)** In a freshly dissected adult cochlea (middle turn), markers SOX2 and JAG1 were co-localized in the SCs. **(b1–b3)** After 5 days in culture, a subset of $SOX2^+$ cells was co-labeled with JAG1. Notice disorganization of SCs compared with the freshly dissected sample. **(c1–c3)** Co-localization of SOX2 and S100A1 in a subset of SCs of a freshly dissected adult cochlea. **(d1–d3)** SOX2 and S100A1 were similarly co-localized in a subset of SCs of adult cochleae after 5 days in culture. Again, the disorganization of SCs was evident in culture. Scale bars: 50 μ m.

Supplementary Figure 3 | *In vitro* regeneration of hair cell-like cells (HCLCs) with *Atoh1* overexpression. **(a1–a4)** In cultured adult *Atoh1*-GFP cochleae infected with Ad-V5, a few GFP^+ cells were observed mainly in the existing inner HCs (IHCs), but not in other sensory epithelial regions. In cultured adult *Atoh1*-GFP cochleae infected with Ad-Atoh1, increased numbers of GFP^+ cells were observed across the sensory epithelial region **(b1–b4)** and the limbus region **(c1–c4)**. Some GFP^+ cells were co-labeled with MYO7A, indicating regeneration of HCLCs in those areas. **(d,e)** Quantification data showed more $MYO7A^+$ HCLCs that were detected in both the sensory epithelial region and the limbus region in cultured adult *Atoh1*-GFP cochleae infected by Ad-Atoh1 than by Ad-V5 infection. $^{**}p < 0.01$, $^{***}p < 0.001$, Student's *t*-test. Error bar, mean ± SEM, $n = 9$–13. *n* is the number of biologically independent cochlea samples. Scale bars: 20 μ m.

Supplementary Figure 4 | Atoh1 overexpression generates $TUJ1^+$ cells in adult cochlear explant culture. **(a1–a3)** Nine days postkanamycin/furosemide injection *in vivo* and 12 days after Ad-V5 infection in culture (d12), and there was a loss of a majority of neurites in the IHC region (IHCr, bracket). **(b1–b3)** Nine days postkanamycin/furosemide injection *in vivo* and 12 days after Ad-Atoh1-mCherry infection in culture, adult cochleae showed regenerated $TUJ1^+$/$mCherry^+$ cells in the OHC region (OHCr, bracket), and significantly more neurites in the IHC region. $TUJ1^+$ cells were co-labeled with mCherry (arrows). Scale bars: 20 μ m.

Supplementary Figure 5 | *In vitro* regeneration of HCLCs with *Atoh1* overexpression. Enlarged picture of the apex of a cultured adult *Atoh1*-GFP cochlea infected with Ad-V5/Ad-Atoh1. The samples were incubated with antibodies against GFP/MYO7A/PVALB. **(a1–a4)** In cultured adult *Atoh1*-GFP cochleae infected with Ad-V5 (the enlarged image of **Supplementary Figure 3a**), a few weak GFP^+ cells were observed mainly inside and surrounding the existing IHCs, indicating the weak endogenous ATOH1 activity. **(b1–b4)** Many strong GFP^+ cells were observed across the sensory epithelial region. Most GFP^+ cells were co-labeled with PVALB. Scale bars: 10 μ m.

Supplementary Figure 6 | Atoh1 overexpression generates $TUJ1^+$/$ESPN^+$ HCLCs in adult cochlear explant culture. **(a1–a4)** (Low magnification) and **(b1–b4)** (high magnification). Twelve days after Ad-Atoh1-mCherry infection of cultured WT adult cochleae, regenerated $mCherry^+$/$TUJ1^+$/$ESPN^+$ HCLCs in the sensory region of apex were detected. $Atoh1mCherry^+$/$TUJ1^+$ cells were co-labeled with an HC marker ESPN (arrows). Scale bars: 10 μ m.

REFERENCES

Alizadeh, M., Wada, M., Gelfman, C. M., Handa, J. T., and Hjelmeland, L. M. (2001). Downregulation of differentiation specific gene expression by oxidative stress in ARPE-19 cells. *Invest. Ophthalmol. Visual Sci.* 42, 2706–2713.

Arnold, H. J., Muller, M., Waldhaus, J., Hahn, H., and Lowenheim, H. (2010). A novel buoyancy technique optimizes simulated microgravity conditions for whole sensory organ culture in rotating bioreactors. *Tissue Eng. Part C Methods* 16, 51–61. doi: 10.1089/ten.TEC.2009.0028

Bramhall, N. F., Shi, F., Arnold, K., Hochedlinger, K., and Edge, A. S. (2014). Lgr5-positive supporting cells generate new hair cells in the postnatal cochlea. *Stem Cell Rep.* 2, 311–322. doi: 10.1016/j.stemcr.2014.01.008

Chan, D. K., and Rouse, S. L. (2016). Sound-induced intracellular Ca2+ dynamics in the adult hearing cochlea. *PLoS One* 11:e0167850. doi: 10.1371/journal.pone.0167850

Corwin, J. T., and Cotanche, D. A. (1988). Regeneration of sensory hair cells after acoustic trauma. *Science* 240, 1772–1774. doi: 10.1126/science.3381100

Cotanche, D. A., and Corwin, J. T. (1991). Stereociliary bundles reorient during hair cell development and regeneration in the chick cochlea. *Hear. Res.* 52, 379–402. doi: 10.1016/0378-5955(91)90027-7

Dabdoub, A., Puligilla, C., Jones, J. M., Fritzsch, B., Cheah, K. S., Pevny, L. H., et al. (2008). Sox2 signaling in prosensory domain specification and subsequent hair cell differentiation in the developing cochlea. *Proc. Natl. Acad. Sci. U.S.A.* 105, 18396–18401. doi: 10.1073/pnas.0808175105

Diensthuber, M., Oshima, K., and Heller, S. (2009). Stem/progenitor cells derived from the cochlear sensory epithelium give rise to spheres with distinct morphologies and features. *J. Assoc. Res. Otolaryngol.* 10, 173–190. doi: 10.1007/s10162-009-0161-3

Dooling, R. J., Ryals, B. M., and Manabe, K. (1997). Recovery of hearing and vocal behavior after hair-cell regeneration. *Proc. Natl. Acad. Sci. U.S.A.* 94, 14206–14210. doi: 10.1073/pnas.94.25.14206

Dulon, D., Aran, J. M., and Schacht, J. (1987). Osmotically induced motility of outer hair cells: implications for Meniere's disease. *Arch. Otorhinolaryngol.* 244, 104–107. doi: 10.1007/BF00458558

Edmondson, R., Broglie, J. J., Adcock, A. F., and Yang, L. (2014). Three-dimensional cell culture systems and their applications in drug discovery and cell-based biosensors. *Assay Drug Dev. Technol.* 12, 207–218. doi: 10.1089/adt.2014.573

Fischer, N., Johnson Chacko, L., Majerus, A., Potrusil, T., Schmutzhard, J., Schrott-Fischer, A., et al. (2019). Age-dependent calcium-binding protein expression in the spiral ganglion and hearing performance of C57BL/6J and 129/SvJ Mice. *ORL J. Otorhinolaryngol. Relat. Spec.* 81, 138–154. doi: 10.1159/000499472

Goodyear, R. J., Legan, P. K., Wright, M. B., Marcotti, W., Oganesian, A., Coats, S. A., et al. (2003). A receptor-like inositol lipid phosphatase is required for the maturation of developing cochlear hair bundles. *J. Neurosci.* 23, 9208–9219. doi: 10.1523/JNEUROSCI.23-27-09208.2003

Huang, M., Kantardzhieva, A., Scheffer, D., Liberman, M. C., and Chen, Z. Y. (2013). Hair cell overexpression of Islet1 reduces age-related and noise-induced hearing loss. *J. Neurosci.* 33, 15086–15094. doi: 10.1523/JNEUROSCI.1489-13.2013

Jones, J. E., and Corwin, J. T. (1993). Replacement of lateral line sensory organs during tail regeneration in salamanders: identification of progenitor cells and analysis of leukocyte activity. *J. Neurosci.* 13, 1022–1034. doi: 10.1523/JNEUROSCI.13-03-01022.1993

Kawamoto, K., Ishimoto, S., Minoda, R., Brough, D. E., and Raphael, Y. (2003). Math1 gene transfer generates new cochlear hair cells in mature guinea pigs in vivo. *J. Neurosci.* 23, 4395–4400. doi: 10.1523/JNEUROSCI.23-11-04395.2003

Kelly, M. C., Chang, Q., Pan, A., Lin, X., and Chen, P. (2012). Atoh1 directs the formation of sensory mosaics and induces cell proliferation in the postnatal mammalian cochlea in vivo. *J. Neurosci.* 32, 6699–6710. doi: 10.1523/JNEUROSCI.5420-11.2012

Koehler, K. R., Mikosz, A. M., Molosh, A. I., Patel, D., and Hashino, E. (2013). Generation of inner ear sensory epithelia from pluripotent stem cells in 3D culture. *Nature* 500, 217–221. doi: 10.1038/nature12298

Koehler, K. R., Nie, J., Longworth-Mills, E., Liu, X. P., Lee, J., Holt, J. R., et al. (2017). Generation of inner ear organoids containing functional hair cells from human pluripotent stem cells. *Nat. Biotechnol.* 35, 583–589. doi: 10.1038/nbt.3840

Kong, L., Xin, Y., Chi, F., Chen, J., and Yang, J. (2020). Developmental and functional hair cell-like cells induced by atoh1 overexpression in the adult mammalian cochlea in vitro. *Neural Plastic.* 2020:8885813. doi: 10.1155/2020/8885813

Kujawa, S. G., and Liberman, M. C. (2009). Adding insult to injury: cochlear nerve degeneration after "temporary" noise-induced hearing loss. *J. Neurosci.* 29, 14077–14085. doi: 10.1523/JNEUROSCI.2845-09.2009

Landegger, L. D., Dilwali, S., and Stankovic, K. M. (2017). Neonatal murine cochlear explant technique as an in vitro screening tool in hearing research. *J. Vis. Exp.* 124:e55704. doi: 10.3791/55704

Liu, Z., Dearman, J. A., Cox, B. C., Walters, B. J., Zhang, L., Ayrault, O., et al. (2012). Age-dependent in vivo conversion of mouse cochlear pillar and Deiters' cells to immature hair cells by Atoh1 ectopic expression. *J. Neurosci.* 32, 6600–6610. doi: 10.1523/JNEUROSCI.0818-12.2012

Lumpkin, E. A., Collisson, T., Parab, P., Omer-Abdalla, A., Haeberle, H., Chen, P., et al. (2003). Math1-driven GFP expression in the developing nervous system of transgenic mice. *Gene Expr. Patterns* 3, 389–395. doi: 10.1016/s1567-133x(03)00089-9

Mantikou, E., Jonker, M. J., Wong, K. M., van Montfoort, A. P., de Jong, M., Breit, T. M., et al. (2016). Factors affecting the gene expression of in vitro cultured human preimplantation embryos. *Hum. Reprod.* 31, 298–311. doi: 10.1093/humrep/dev306

Mizutari, K., Fujioka, M., Hosoya, M., Bramhall, N., Okano, H. J., Okano, H., et al. (2013). Notch inhibition induces cochlear hair cell regeneration and recovery of hearing after acoustic trauma. *Neuron* 77, 58–69. doi: 10.1016/j.neuron.2012.10.032

Molea, D., Stone, J. S., and Rubel, E. W. (1999). Class III beta-tubulin expression in sensory and nonsensory regions of the developing avian inner ear. *J. Comp. Neurol.* 406, 183–198. doi: 10.1002/(sici)1096-9861(19990405)406:2<183::aid-cne4>3.0.co;2-k

Morton, C. C., and Nance, W. E. (2006). Newborn hearing screening–a silent revolution. *N. Engl. J. Med.* 354, 2151–2164. doi: 10.1056/nejmra050700

Muller, U., and Barr-Gillespie, P. G. (2015). New treatment options for hearing loss. *Nat. Rev. Drug Discov.* 14, 346–365. doi: 10.1038/nrd4533

Niggemann, P., Gyorgy, B., and Chen, Z. Y. (2020). Genome and base editing for genetic hearing loss. *Hear. Res.* 394:107958. doi: 10.1016/j.heares.2020.107958

Oesterle, E. C., and Campbell, S. (2009). Supporting cell characteristics in long-deafened aged mouse ears. *J. Assoc. Res. Otolaryngol.* 10, 525–544. doi: 10.1007/s10162-009-0183-x

Parker, M., Brugeaud, A., and Edge, A. S. (2010). Primary culture and plasmid electroporation of the murine organ of Corti. *J. Vis. Exp.* 36:e1685. doi: 10.3791/1685

Ryals, B. M., and Rubel, E. W. (1988). Hair cell regeneration after acoustic trauma in adult *Coturnix* quail. *Science* 240, 1774–1776. doi: 10.1126/science.3381101

Shou, J., Zheng, J. L., and Gao, W. Q. (2003). Robust generation of new hair cells in the mature mammalian inner ear by adenoviral expression of Hath1. *Mol. Cell. Neurosci.* 23, 169–179. doi: 10.1016/s1044-7431(03)00066-6

Shu, Y., Li, W., Huang, M., Quan, Y. Z., Scheffer, D., Tian, C., et al. (2019). Renewed proliferation in adult mouse cochlea and regeneration of hair cells. *Nat. Commun.* 10:5530. doi: 10.1038/s41467-019-13157-7

Shu, Y., Tao, Y., Li, W., Shen, J., Wang, Z., and Chen, Z. Y. (2016). Adenovirus vectors target several cell subtypes of mammalian inner ear in vivo. *Neural Plastic.* 2016:9409846. doi: 10.1155/2016/9409846

Stone, J. S., and Rubel, E. W. (2000). Temporal, spatial, and morphologic features of hair cell regeneration in the avian basilar papilla. *J. Comp. Neurol.* 417, 1–16. doi: 10.1002/(SICI)1096-9861(20000131)417:1<1::AID-CNE1>3.0.CO;2-E

Stone, J. S., Leano, S. G., Baker, L. P., and Rubel, E. W. (1996). Hair cell differentiation in chick cochlear epithelium after aminoglycoside toxicity: in vivo and in vitro observations. *J. Neurosci.* 16, 6157–6174. doi: 10.1523/JNEUROSCI.16-19-06157.1996

Sugawara, M., Corfas, G., and Liberman, M. C. (2005). Influence of supporting cells on neuronal degeneration after hair cell loss. *J. Assoc. Res. Otolaryngol.* 6, 136–147. doi: 10.1007/s10162-004-5050-1

Tilney, L. G., Cotanche, D. A., and Tilney, M. S. (1992). Actin filaments, stereocilia and hair cells of the bird cochlea. VI. How the number and arrangement of stereocilia are determined. *Development* 116, 213–226.

Walters, B. J., Coak, E., Dearman, J., Bailey, G., Yamashita, T., Kuo, B., et al. (2017). In vivo interplay between p27(Kip1), GATA3, ATOH1, and POU4F3 converts non-sensory cells to hair cells in adult mice. *Cell Rep.* 19, 307–320. doi: 10.1016/j.celrep.2017.03.044

Wan, G., Gomez-Casati, M. E., Gigliello, A. R., Liberman, M. C., and Corfas, G. (2014). Neurotrophin-3 regulates ribbon synapse density in the cochlea and induces synapse regeneration after acoustic trauma. *eLife* 3:e03564. doi: 10.7554/eLife.03564

White, P. M., Doetzlhofer, A., Lee, Y. S., Groves, A. K., and Segil, N. (2006). Mammalian cochlear supporting cells can divide and trans-differentiate into hair cells. *Nature* 441, 984–987. doi: 10.1038/nature04849

Woods, C., Montcouquiol, M., and Kelley, M. W. (2004). Math1 regulates development of the sensory epithelium in the mammalian cochlea. *Nat. Neurosci.* 7, 1310–1318. doi: 10.1038/nn1349

Yang, S. M., Chen, W., Guo, W. W., Jia, S., Sun, J. H., Liu, H. Z., et al. (2012). Regeneration of stereocilia of hair cells by forced Atoh1 expression in the adult mammalian cochlea. *PLoS One* 7:e46355. doi: 10.1371/journal.pone.0046355

Zenner, H. P. (1986). K+-induced motility and depolarization of cochlear hair cells. Direct evidence for a new pathophysiological mechanism in Meniere's disease. *Arch. Otorhinolaryngol.* 243, 108–111. doi: 10.1007/BF00453760

Zenner, H. P., Reuter, G., Zimmermann, U., Gitter, A. H., Fermin, C., and LePage, E. L. (1994). Transitory endolymph leakage induced hearing loss and tinnitus: depolarization, biphasic shortening and loss of electromotility of outer hair cells. *Eur. Arch. Otorhinolaryngol.* 251, 143–153. doi: 10.1007/BF00181826

Zheng, J. L., and Gao, W. Q. (1999). Concanavalin A protects hair cells against gentamicin ototoxicity in rat cochlear explant cultures. *J. Neurobiol.* 39, 29–40. doi: 10.1002/(sici)1097-4695(199904)39:1<29::aid-neu3>3.0.co;2-e

Zheng, J. L., and Gao, W. Q. (2000). Overexpression of Math1 induces robust production of extra hair cells in postnatal rat inner ears. *Nat. Neurosci.* 3, 580–586. doi: 10.1038/75753

Zheng, J. L., Shou, J., Guillemot, F., Kageyama, R., and Gao, W. Q. (2000). Hes1 is a negative regulator of inner ear hair cell differentiation. *Development* 127, 4551–4560. doi: 10.1242/dev.127.21.4551

Conflict of Interest: Z-YC has a financial interest in Salubritas Therapeutics, LLC, which is developing treatments for hearing loss including genome editing, inner ear regeneration, novel delivery, and gene therapy.

The remaining authors declare that the research was conducted in the absence of any commercial or financial relationships that could be construed as a potential conflict of interest.

Publisher's Note: All claims expressed in this article are solely those of the authors and do not necessarily represent those of their affiliated organizations, or those of the publisher, the editors and the reviewers. Any product that may be evaluated in this article, or claim that may be made by its manufacturer, is not guaranteed or endorsed by the publisher.

frontiers in Molecular Neuroscience

REVIEW
published: 20 January 2022
doi: 10.3389/fnmol.2021.829564

Regulation of Spiral Ganglion Neuron Regeneration as a Therapeutic Strategy in Sensorineural Hearing Loss

*Man Wang, Lei Xu, Yuechen Han, Xue Wang, Fang Chen, Junze Lu, Haibo Wang and Wenwen Liu**

Department of Otolaryngology-Head and Neck Surgery, Shandong Provincial ENT Hospital, Cheeloo College of Medicine, Shandong University, Jinan, China

In the mammalian cochlea, spiral ganglion neurons (SGNs) are the primary neurons on the auditory conduction pathway that relay sound signals from the inner ear to the brainstem. However, because the SGNs lack the regeneration ability, degeneration and loss of SGNs cause irreversible sensorineural hearing loss (SNHL). Besides, the effectiveness of cochlear implant therapy, which is the major treatment of SNHL currently, relies on healthy and adequate numbers of intact SGNs. Therefore, it is of great clinical significance to explore how to regenerate the SGNs. In recent years, a number of researches have been performed to improve the SGNs regeneration strategy, and some of them have shown promising results, including the progress of SGN regeneration from exogenous stem cells transplantation and endogenous glial cells' reprogramming. Yet, there are challenges faced in the effectiveness of SGNs regeneration, the maturation and function of newly generated neurons as well as auditory function recovery. In this review, we describe recent advances in researches in SGNs regeneration. In the coming years, regenerating SGNs in the cochleae should become one of the leading biological strategies to recover hearing loss.

Keywords: hearing loss, spiral ganglion neurons, regeneration, stem cells transplantation, glial cells

OPEN ACCESS

Edited by:
Yu Sun,
Huazhong University of Science and Technology, China

Reviewed by:
Zuhong He,
Wuhan University, China
Guoqiang Wan,
Nanjing University, China

****Correspondence:***
Wenwen Liu
wenwenliu_1@yahoo.com

Specialty section:
This article was submitted to Molecular Signalling and Pathways, a section of the journal Frontiers in Molecular Neuroscience

Received: *06 December 2021*
Accepted: *27 December 2021*
Published: *20 January 2022*

Citation:
Wang M, Xu L, Han Y, Wang X, Chen F, Lu J, Wang H and Liu W (2022) Regulation of Spiral Ganglion Neuron Regeneration as a Therapeutic Strategy in Sensorineural Hearing Loss. Front. Mol. Neurosci. 14:829564. doi: 10.3389/fnmol.2021.829564

INTRODUCTION

The first world report of hearing released in 2021 warned that nearly 2.5 billion people, or one in four people in the world, will be living with some degree of hearing loss by 2050. Hearing loss affects many aspects of life, including communication, cognition, education, and even mental health, with significant detrimental effects economically on society. Among all hearing loss, sensorineural hearing loss (SNHL) is the most common type and accounts for the vast majority of them. The inner ear core parts are composed of hair cells (HCs) and spiral ganglion neurons (SGNs). The HCs function in transducing the sound mechanical stimulation into the primary acoustic signals (Liu Y. et al., 2019; Zhou et al., 2020), while the SGNs are primary afferent neurons in the auditory conduction pathway, and they transmit acoustic signals from the inner HCs of the cochlea to the central cochlear nucleus in the brainstem (Liu et al., 2021; Wang et al., 2021; Wei et al., 2021). Both HCs and SGNs can be injured by excessive noise exposure (Liberman, 2017; Guo L. et al., 2021), ototoxic drugs (Lang et al., 2005; He et al., 2017; Liu W. et al., 2019), aging (Bao and Ohlemiller, 2010; Kujawa and Liberman, 2015; He et al., 2021), genetic factors (Lv et al., 2021) and

infections (Zhang et al., 2021), and thus leading to the SNHL.The SGNs in the cochlea can be divided into two subgroups-type I SGNs and type II SGNs, by their morphological structure, cell body, myelin sheath, and biological function. Type I SGNs, which account for the majority of auditory neurons in the inner ear, are myelinated, large, bipolar cells and primarily innervate the inner HCs, while the type II SGNs are unmyelinated, small, and innervate the outer HCs. More recently, single-cell profiling has been performed and three subpopulations of type I SGNs have been identified on the basis of transcriptional profiling (Shrestha et al., 2018; Sun et al., 2018). At the developmental level, the SGNs belong to terminally differentiated cells and can hardly regenerate by self-proliferation spontaneously and thus the damage of SGNs results in permanent SNHL (Guo et al., 2016, 2020). Besides, cochlear implant, which is the main clinical procedure for SNHL treatment, plays the role of restoring hearing by giving direct electrical stimulation to the viable SGNs (Guo et al., 2019, 2021b), and the effectiveness of cochlear implant therapy relies on healthy and adequate numbers of intact SGNs.

Therefore, prompting the strategies for regenerating SGNs is of great clinical significance for further advances in deafness treatment. In recent years, important advances have been made in a better understanding of the mechanisms involved in the regeneration of SGNs, which is a significant step toward the ultimate goal of improved hearing. In this review, we summarize the new discoveries about SGNs regeneration in recent years.

STEM CELLS DERIVED FROM EXOGENOUS SOURCES DIFFERENTIATE TOWARD SGNs

With the development of the inner ear after birth, the neuronal stem cell characteristics of the original stem cells continue to decline, and it lacks the endogenous cellular source for SGNs regeneration in the adult inner ear. Exogenous stem cells transplantation is an attractive alternative for adult SGNs regeneration. In recent years, studies have shown that many kinds of stem cells derived from exogenous sources, such as the induced pluripotent stem cells (iPSCs; Chen et al., 2017), mesenchymal stem cells (MSCs; Cho et al., 2011; Kil et al., 2016), and neural stem cells (NSCs; He et al., 2014), transplanted into the cochlea *in vivo* or *in vitro* could be differentiated toward SGNs. In addition, as the unique pluripotent cells, embryonic stem cells (ESCs) possess great differentiation potential and can differentiate into almost all cell types that make up the body. ESCs from the mouse or humans have been transplanted into the inner ear to replace the damaged SGNs (Corrales et al., 2006; Reyes et al., 2008; Hackelberg et al., 2017). Chang et al. (2021) found successful survival and migration of transplanted ESCs in the cochlea, and the transplanted ESC cells increased the auditory connection to the central auditory pathway in the hearing loss mice model.

Due to the cochlea's special cavity-like structure, delivery of therapeutics to the inner ear becomes complicated due to their inaccessible location (Nyberg et al., 2019). The efficiency of regenerating SGNs and the survival of newly generated neurons are related to the transplantation method of exogenous stem cells, and thus it is necessary to find a suitable route for stem cell transplantation. Recently, transplantation through a small hole drilled into the scala tympani (ST), a fluid-filled lumen adjacent to the cochlear duct epithelium, has been widely used for its technically easier implementation (Hu et al., 2005; Lee et al., 2017; Chang et al., 2020). Besides, stem cell transplantation through the cochlear lateral wall was also found to be precise and safe, which has more efficacy to enter the Rosenthal's canal (RC) compared with transplantation *via* the ST (Zhang et al., 2013).

Novel scaffolds could contribute to regulating neural stem cell proliferation, differentiation, and the oriented growth of derived neurons (Liu et al., 2018; Yan et al., 2018; Xia et al., 2020; Guo et al., 2021a). Hackelberg et al. (2017) present novel nanofibrous scaffolds for the guidance of stem cell-derived neurons for auditory nerve regeneration. The human ESC-derived neural precursor cells (NPC) implanted into the aligned nanofiber mats were efficiently differentiated into glutamatergic neurons and were guided into their target location of the cochlea in deafened guinea pigs. However, no improvement in eABR thresholds, or any functional improvement was found in mice implanted scaffolds with NPC compared with the cell-free (without NPC) scaffolds transplantation group (Hackelberg et al., 2017).

Collectively, researches have shown that the stem cells transplanted into cochlea could survive and acquiresome neuronal features, thus suggesting stem cell-based therapy might be a promising approach for auditory nerve regeneration. However, solid evidences for significant auditory function recovery after stem cell transplantation are still very limited (Fu et al., 2009; Chen et al., 2012, 2017; Hackelberg et al., 2017; Chang et al., 2021), and whether these exogenous cells can differentiate into functional SGNs and promote hearing recovery remain an open question. Meanwhile, proper integration of exogenous cells into the auditory circuit remains a fundamental challenge, and there are still some inevitable risks of transplanting stem cells into the inner ear, such as tumor formation, immune response (Nishimura et al., 2012), as well as ethical arguments regarding ESC cells transplantation. It is still necessary to develop safe and effective stem cell-based therapy for the clinical monitoring of cell transplantation.

GLIAL CELLS WITHIN THE INNER EAR ARE POTENT PROGENITORS FOR SGN REPROGRAMMING

In the central nervous system (CNS), glial cells have been proved to be able to reprogram into functional neurons directly (Heins et al., 2002; Heinrich et al., 2010). Glial cells in the inner ear consist of Schwann cells that distribute along the fibers of SGNs and satellite glial cells that reside in RC surrounding SGNs cell bodies. It has been reported that glial cells in the inner ear play an irreplaceable role in protecting SGNs from

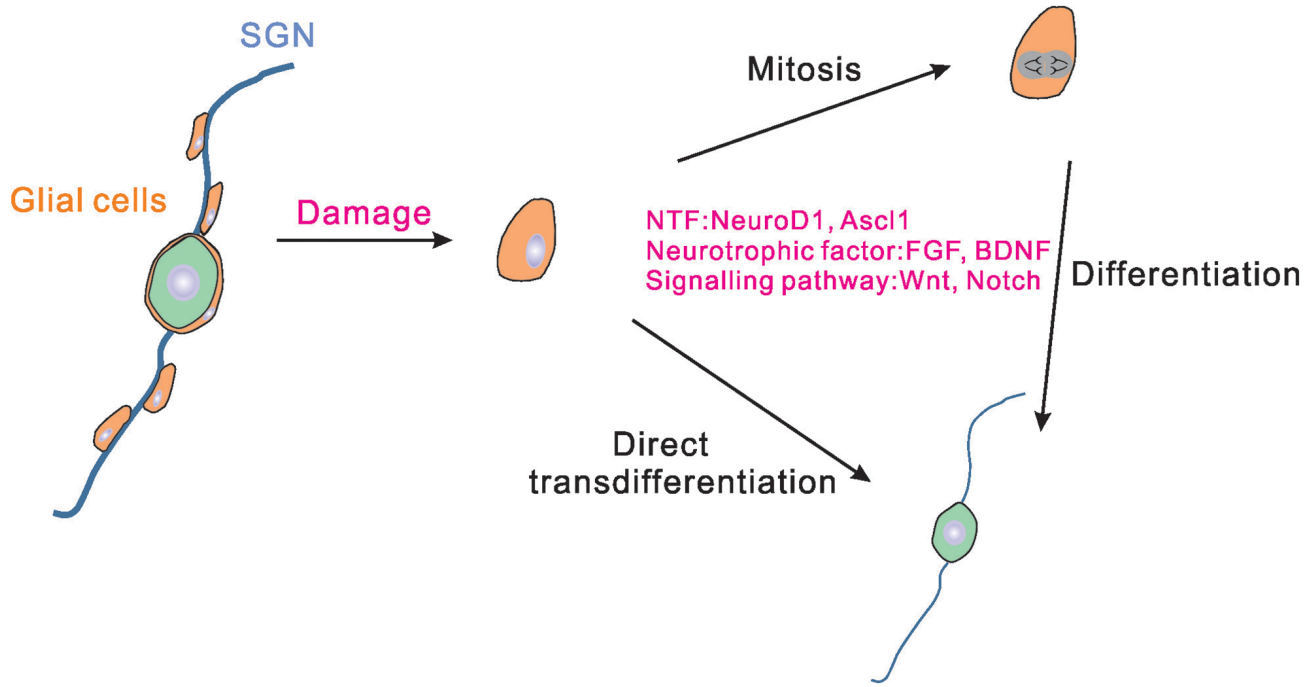

FIGURE 1 | Schematic drawing of the endogenous glial cells regenerating SGNs. In the cochlea, satellite glial cells exist around SGNs. Satellite glial cells may proliferate and differentiate into SGNs when the SGNs are damaged. Some of the glial cells can also be directly transdifferentiated into SGNs. Neurogenic transcription factors, neurotrophic factors, and signal pathways could regulate the process of glial cells proliferation and differentiation. NTF, neurogenic transcription factors; SGNs, spiral ganglion neurons.

degeneration and helping the SGNs to perform normal functions (Liu et al., 2014; Akil et al., 2015). The Schwann cells along the neuronal fibers express multiple neurotrophins, including the brain-derived neurotrophic factor (BDNF) and neurotrophin-3 (NT-3) that induce the development and survival of SGNs (Hansen et al., 2001). Recent studies found that the abundant glial cells in the inner ear could also become a promising resource for SGNs regeneration. McLean et al. (2016) reported that the separated proteolipid protein (PLP1) positive glial cells derived from the newborn mouse spiral ganglion could give rise to multiple cell types *in vitro*, including glial cells and neurons, and thus the PLP1 positive glial cells existing in the inner ear were identified as neural progenitors. Li X. et al. (2020) also found that glial cells in the mice inner ears started to express SGNs markers *in vivo* 6 days after Neurog1 (Ngn1) and Neurod1 ectopic expression. Moreover, a part of the newly generated SGNs exhibited a similar cellular phenotype (such as large round somas) to that of native SGNs and these SGNs could survive until postnatal day 42 (Li X. et al., 2020). In addition, it was found that even the spiral glial cells separated from adult human or rodent cochleae cultured *in vitro* could produce neurospheres and were capable of differentiating into neurons (Rask-Andersen et al., 2005; Lang et al., 2015). These studies revealed the stem cell potential of glial cells in the inner ear (**Figure 1**). Single cell RNA-sequencing analysis showed that satellite glial cells in the inner ear share many characteristics with CNS astrocytes (Tasdemir-Yilmaz et al., 2021), suggesting the important role of satellite glial cells in SGN regeneration. However, because of lack of an effective method for separating Schwann cells and satellite glial cells in the inner ear, the respective function of Schwann cells and satellite glial cells in SGNs regeneration remains to be defined.

Under normal conditions, the proliferation and regeneration ability of glial cells in the inner ear are really weak. Therefore, it is necessary to find ways to improve the ability of glial cells to regenerate SGNs. Neurogenic transcription factors have been utilized widely in many studies trying to reprogram glial cells into SGNs. The current advanced researches on viral vectors make it more convenient and effective to use virus-mediated neurogenic transcription factors expression to reprogram glial cells into neurons. For example, Chen et al. (2020) demonstrated that adeno-associated virus-mediated NeuroD1 ectopic overexpression contributed to astrocyte-to-neuron conversion in adult mammalian brains. Through NeuroD1-based gene therapy, a good deal of functional new neurons were generated in the ischemic injured cortex and brain function was repaired after ischemic injury (Chen et al., 2020). In addition to NeuroD1 and Ngn1 (Li X. et al., 2020), Ascl1 was also proved to be able to reprogram the spiral ganglion cells into induced SGNs (Nishimura et al., 2014; Noda et al., 2018). It is worth noting that the combination of two factors results in better reprogramming of reactive glial cells to neurons than using one single copy alone (**Figure 1**).

SGNs DAMAGE INDUCES GLIAL CELLS PROLIFERATION

Activation of astrocytes (reactive gliosis) has been considered as the sign of a lesion to the nervous system in conditions such as mechanical damage to the brain or neurodegenerative diseases (de Melo et al., 2012; Pekny et al., 2014). Similar to the survival characteristics of glial cells in the CNS, glial cells in the inner ear also presented greater survival traits than SGNs (Wise et al., 2017). Wise et al. (2017) found that 6 weeks after deafness duration, the morphology of glial cells was altered following the SGNs soma loss. The soma of Schwann cell assumed an "astrocyte-like" morphology and dedifferentiation might have occurred in the Schwann cells. Studies showed that moderate ouabain administration could selectively cause SGNs damage and abolish hearing without influencing HCs (Lang et al., 2005; Yuan et al., 2013). This drug that specifically damages endogenous SGNs allows scientists to better focus on the responses of inner ear cells after SGNs damage. Lang et al. (2011) found that ouabain application to the round window caused a significant up-regulation in glial cells proliferation and increase of Sox2 protein expression, which is the marker of neural progenitor. In addition, after ouabain exposure, the morphology of glial cells nuclei also changed, becoming enlarged and rounded in shape, similar to the nuclei of SGNs (Lang et al., 2015). Furthermore, Kempfle et al. (2020) found that ouabain treatment in adult mouse inner ear induced SGNs damage and the transient overexpression of Lin28 in Plp1-positive glial cells led to increased proliferation and neural conversion. Thus, these results demonstrated that the damage of SGNs induced inner ear glial cells proliferation and morphological changes, while the proliferative glial cells may be poised to regenerate the auditory nerve when given appropriate stimuli.

NEUROTROPHIC FACTORS AND SIGNALING PATHWAYS ENHANCE THE SGNs REGENERATION

Some growth factors and neurotrophins, such as fibroblast growth factor (FGF), BDNF, glial cell-derived neurotrophic factor (GDNF), and NT-3, play important roles during SGNs development and survival (Johnson Chacko et al., 2017). Treatment of mature BDNF and proBDNF in SGNs cultures with a concentration as low as ng/ml-range could exert a protective effect on SGNs against degeneration (Schulze et al., 2020). Previous studies also found that FGF, GDNF, and NT-3 promoted the outgrowth of neurites from cultured SGNs, which indicated that these molecules may also have trophic functions in SGNs regeneration (Wei et al., 2007; Wang and Green, 2011; Garcia-Hernandez et al., 2013). Currently, a combination administration of stem cells and different growth factors or neurotrophic molecules was evolved in hearing loss studies. In *in vivo* experiments, transducing the mesenchymal cells within perilymphatic compartments of the cochlea with a recombinant plasmid gene that drives BDNF expression stimulated the regeneration of spiral ganglion neurites (Pinyon et al., 2014). With BDNF overexpression, the regenerated spiral ganglion neurites could extend to the area of cochlear implant electrodes, with localized ectopic branching (Pinyon et al., 2014). The success in regenerating SGNs in rodents by combined administration of neurotrophic factors with stem cells has led to great developments in cochlea implant technology (Scheper et al., 2019).

On the delivery system of neurotrophic factors, coating the artificial cochlea with ultra-high viscous alginate containing BDNF-overexpressing MSCs resulted in increased SGNs density in the inner ear of deafened animal (Scheper et al., 2019). In order to improve the survival of stem cells in the inner ear and increase the efficiency of SGNs generation, Chang et al. (2020) cultured human ESC-derived spheroids in an artificial three-dimensional (3D) microenvironment composed of specific hydrogel combined with a sustained release BDNF delivery system (PODS-hBDNF). The transplanted human ESC-derived otic neuronal progenitors spheroids survived and neuronally differentiated into otic neuronal lineages *in vitro* and *in vivo* and also extended neurites toward the bony wall of the cochlea (Chang et al., 2020). In some studies exploring the differentiation of glial cells into SGNs, neurotrophic factors are generally added to the culture medium to promote the regeneration of SGNs and maintain the survival of newly generated neurons (Diensthuber et al., 2014; McLean et al., 2016). In a word, supplementation of neurotrophic factors could enhance the regeneration of SGNs.

Moreover, modulation of some specific signaling pathways also promoted robust neuronal differentiation. For example, Zong et al. (2014) found that the Wnt signaling pathway plays a critical role in stimulating the differentiation of amniotic fluid-derived stem cells into functional neurons. The role of Wnt signaling in triggering neurogenesis in the gentamicin-lesioned cochlear cultures was also proved by Bas et al. (2014). Pharmacologic activation of Wnt/β-catenin pathway together with human nasal MSC treatment could induce robust differentiation of SGNs. In addition, Notch signaling also had a significant role in the inner ear stem cells fate decision. Different from the role in HCs differentiation, continued Notch signaling increased the expansion of neuronal progenitors and promoted progenitor cells to enter a neuronal lineage by directly increasing Ngn1 expression (Jeon et al., 2011). The PI3K/Akt signaling pathway was verified to be involved in promoting neuron differentiation in the inner ears (Zhang et al., 2016). Recently, Perny et al. (2017) developed a protocol based on 3D organoid culture systems, which guided mouse ESCs differentiating into otic sensory neurons by activating the bone morphogenetic protein (BMP) signaling and concomitantly inhibiting the transforming growth factor beta (TGFβ) signaling. In this study, BDNF and NT-3 were also supplemented into the culture to guide neuronal maturation (Perny et al., 2017). The neurotrophic factors and certain signaling pathways found to promote proliferation and neural differentiation may reveal the mechanisms underlying stem cell differentiation (**Figure 1**).

TRANSCRIPTOME ANALYSIS AND SGNs REGENERATION

By comparing similarities and differences of transcriptional regulatory networks in multiple events during sensory cell development or regeneration, key factors or cell signaling pathways could be found to be involved in the modulation of cell regeneration (Atkinson et al., 2015). In 2016, Kwan introduced the single-cell transcriptome analysis application in SGNs regeneration (Kwan, 2016). Transcriptome profiling of cells at different stages of SGNs differentiation, including exogenous stem cell-derived and endogenous glial cell-derived SGNs regeneration, could provide useful information about the molecular processes involved. Most recently, the emerging cell transcriptome analysis such as single-cell RNA sequencing and bulk RNA-sequencing have been applied in identifying the subtypes of SGNs and inner ear glial cells, characterizing the dynamic expression pattern of SGN genes, and analyzing the transcriptome of the induced neurons after regeneration (Shrestha et al., 2018; Sun et al., 2018; Li C. et al., 2020; Chen et al., 2021; Tasdemir-Yilmaz et al., 2021). For example, Li C. et al. (2020) compared the transcriptomes of SGNs and two other inner ear cell types, HCs and glia to identify genes that were expressed specifically in SGNs within the cochlea and exhibited either constant (e.g., Scrt2) or dynamic (e.g., Celf4) expression patterns. These genes might represent promising candidate regulators of SGN cell-fate determination and/or differentiation. Chen et al. (2021) performed transcriptomic analysis of the glial cells-derived SGNs under different stimuli conditions *in vitro* and found that the small molecules cocktail FIBCL treatment promoted the newborn SGNs maturation. Despite the transcriptome analysis of the inner ear cells still facing some challenges such as a limited number of cells obtained from the cochleae, the lower cell viability, etc. it is predicted to play a great role in enhancing the SGNs regeneration research in the future.

THE FUNCTION OF NEWLY REGENERATED NEURONS

In most of the *in vitro* studies about SGNs regeneration, the newly generated neurons were confirmed by neuronal morphology or by immunostaining of several neuronal markers, including TUJ1, MAP2, Prox1, Gata3, etc. (Diensthuber et al., 2014; Rousset et al., 2020). The electrophysiological characteristic function of newly generated neurons was also identified to determine whether newborn neurons have electrophysiological functions. For example, recording the whole-cell current of the newly generated neurons; using specific Na^+ channel antagonist tetrodotoxin (TTX) to prove whether there are Na^+ channels on the newborn neurons and recording the glutamate induced-current on neurons to confirm whether newborn neurons responding to the main neurotransmitter in the cochlea (Crozier and Davis, 2014; Davis and Crozier, 2015). In the induced newborn neurons, Nishimura et al. (2014) measured the dynamics of neuronal-like membrane potential. Ascl1 and NeuroD1 double overexpressed cochlear epithelial cells exhibit neuronal firing on days *in vitro* 8 and the inward membrane currents could be reduced by the treatment of TTX, which indicates the existence of a robust membrane Na^+ current (Nishimura et al., 2014).

In *in vivo* study, functional analyses of the peripheral auditory system can be investigated using audiological tests. ABR is a reflection of the neural activity transmitted from the scalp that reflects synchronous neural activity within the auditory nerve, and subsequently to the brainstem. A previous study has shown that the ABR wave I latency and amplitude were related to the corresponding SGNs density and function (Li et al., 2016; Zhang et al., 2018).

CONCLUSION AND FUTURE PERSPECTIVES

According to these foundational studies of SGNs regeneration in recent years, the reprogramming of exogenous stem cells or endogenous inner ear cells into SGNs seems to be a promising strategy. The application of some neurogenic transcription factors helps the glial cells proliferation and reprogramming. Combined transplantation of stem cells and neurotrophic factors enhances the effectiveness of SGNs regeneration and improves the survival of newly generated neurons. In addition, modulation of some signaling pathways also promotes neural differentiation. Although it is still necessary to clarify details about SGNs regeneration in humans, the early success of these interventions increases our expectation about the auditory nerve regeneration in human patients in the future.

Still, more efforts are needed to improve the effectiveness of SGNs regeneration, especially to promote the maturation of newly generated neurons. The newly generated SGNs are needed to not only present neuronal morphology and express neuronal protein markers, but also to possess electrophysiological functions, generate action potentials as well as form synaptic connections with HCs in the inner ear and with conductive neurons in the brain stem. As type I and type II SGNs perform different functions in the cochlea and the appearance of the three subtypes of type I SGN indicates the maturity of neurons, differentiating these cells into the desired mature subtypes is also crucial.

AUTHOR CONTRIBUTIONS

MW, LX, YH, XW, FC, JL, HW, and WL drafted and wrote the manuscript. All authors contributed to the article and approved the submitted version.

FUNDING

This work was supported by Taishan Scholars Program of Shandong Province (No. ts20130913, No. tsqn201909189), the Shandong Province Science Foundation for Youths (No. ZR2020QH153), and the Major Fundamental Research Program of the Natural Science Foundation of Shandong Province, China (ZR2020ZD39, ZR2021ZD40).

REFERENCES

Akil, O., Sun, Y., Vijayakumar, S., Zhang, W., Ku, T., Lee, C. K., et al. (2015). Spiral ganglion degeneration and hearing loss as a consequence of satellite cell death in saposin B-deficient mice. *J. Neurosci.* 35, 3263–3275. doi: 10.1523/JNEUROSCI.3920-13.2015

Atkinson, P. J., Huarcaya Najarro, E., Sayyid, Z. N., and Cheng, A. G. (2015). Sensory hair cell development and regeneration: similarities and differences. *Development* 142, 1561–1571. doi: 10.1242/dev.114926

Bao, J., and Ohlemiller, K. K. (2010). Age-related loss of spiral ganglion neurons. *Hear. Res.* 264, 93–97. doi: 10.1016/j.heares.2009.10.009

Bas, E., Van De Water, T. R., Lumbreras, V., Rajguru, S., Goss, G., Hare, J. M., et al. (2014). Adult human nasal mesenchymal-like stem cells restore cochlear spiral ganglion neurons after experimental lesion. *Stem Cells Dev.* 23, 502–514. doi: 10.1089/scd.2013.0274

Chang, H. T., Heuer, R. A., Oleksijew, A. M., Coots, K. S., Roque, C. B., Nella, K. T., et al. (2020). An engineered three-dimensional stem cell niche in the inner ear by applying a nanofibrillar cellulose hydrogel with a sustained-release neurotrophic factor delivery system. *Acta Biomater.* 108, 111–127. doi: 10.1016/j.actbio.2020.03.007

Chang, S. Y., Jeong, H. W., Kim, E., Jung, J. Y., and Lee, M. Y. (2021). Distribution and afferent effects of transplanted mESCs on cochlea in acute and chronic neural hearing loss models. *Biomed Res. Int.* 2021:4956404. doi: 10.1155/2021/4956404

Chen, J., Guan, L., Zhu, H., Xiong, S., Zeng, L., and Jiang, H. (2017). Transplantation of mouse-induced pluripotent stem cells into the cochlea for the treatment of sensorineural hearing loss. *Acta Otolaryngol.* 137, 1136–1142. doi: 10.1080/00016489.2017.1342045

Chen, Z., Huang, Y., Yu, C., Liu, Q., Qiu, C., and Wan, G. (2021). Cochlear Sox2(+) glial cells are potent progenitors for spiral ganglion neuron reprogramming induced by small molecules. *Front. Cell Dev. Biol.* 9:728352. doi: 10.3389/fcell.2021.728352

Chen, W., Jongkamonwiwat, N., Abbas, L., Eshtan, S. J., Johnson, S. L., Kuhn, S., et al. (2012). Restoration of auditory evoked responses by human ES-cell-derived otic progenitors. *Nature* 490, 278–282. doi: 10.1038/nature11415

Chen, Y. C., Ma, N. X., Pei, Z. F., Wu, Z., Do-Monte, F. H., Keefe, S., et al. (2020). A neuroD1 AAV-based gene therapy for functional brain repair after ischemic injury through *in vivo* astrocyte-to-neuron conversion. *Mol. Ther.* 28, 217–234. doi: 10.1016/j.ymthe.2019.09.003

Cho, Y. B., Cho, H. H., Jang, S., Jeong, H. S., and Park, J. S. (2011). Transplantation of neural differentiated human mesenchymal stem cells into the cochlea of an auditory-neuropathy guinea pig model. *J. Korean Med. Sci.* 26, 492–498. doi: 10.3346/jkms.2011.26.4.492

Corrales, C. E., Pan, L., Li, H., Liberman, M. C., Heller, S., and Edge, A. S. (2006). Engraftment and differentiation of embryonic stem cell-derived neural progenitor cells in the cochlear nerve trunk: growth of processes into the organ of Corti. *J. Neurobiol.* 66, 1489–1500. doi: 10.1002/neu.20310

Crozier, R. A., and Davis, R. L. (2014). Unmasking of spiral ganglion neuron firing dynamics by membrane potential and neurotrophin-3. *J. Neurosci.* 34, 9688–9702. doi: 10.1523/JNEUROSCI.4552-13.2014

Davis, R. L., and Crozier, R. A. (2015). Dynamic firing properties of type I spiral ganglion neurons. *Cell Tissue Res.* 361, 115–127. doi: 10.1007/s00441-014-2071-x

de Melo, J., Miki, K., Rattner, A., Smallwood, P., Zibetti, C., Hirokawa, K., et al. (2012). Injury-independent induction of reactive gliosis in retina by loss of function of the LIM homeodomain transcription factor Lhx2. *Proc. Natl. Acad. Sci. U S A* 109, 4657–4662. doi: 10.1073/pnas.1107488109

Diensthuber, M., Zecha, V., Wagenblast, J., Arnhold, S., Edge, A. S., and Stover, T. (2014). Spiral ganglion stem cells can be propagated and differentiated into neurons and glia. *Biores. Open Access* 3, 88–97. doi: 10.1089/biores.2014.0016

Fu, Y., Wang, S., Liu, Y., Wang, J., Wang, G., Chen, Q., et al. (2009). Study on neural stem cell transplantation into natural rat cochlea *via* round window. *Am. J. Otolaryngol.* 30, 8–16. doi: 10.1016/j.amjoto.2007.12.006

Garcia-Hernandez, S., Potashner, S. J., and Morest, D. K. (2013). Role of fibroblast growth factor 8 in neurite outgrowth from spiral ganglion neurons *in vitro*. *Brain Res.* 1529, 39–45. doi: 10.1016/j.brainres.2013.07.030

Guo, L., Cao, W., Niu, Y., He, S., Chai, R., and Yang, J. (2021). Autophagy regulates the survival of hair cells and spiral ganglion neurons in cases of noise, ototoxic drug and age-induced sensorineural hearing loss. *Front. Cell. Neurosci.* 15:760422. doi: 10.3389/fncel.2021.760422

Guo, R., Li, J., Chen, C., Xiao, M., Liao, M., Hu, Y., et al. (2021a). Biomimetic 3D bacterial cellulose-graphene foam hybrid scaffold regulates neural stem cell proliferation and differentiation. *Colloids Surf. B Biointerfaces* 200:111590. doi: 10.1016/j.colsurfb.2021.111590

Guo, R., Liao, M., Ma, X., Hu, Y., Qian, X., Xiao, M., et al. (2021b). Cochlear implant-based electric-acoustic stimulation modulates neural stem cell-derived neural regeneration. *J. Mater. Chem. B.* 9, 7793–7804. doi: 10.1039/d1tb01029h

Guo, R., Ma, X., Liao, M., Liu, Y., Hu, Y., Qian, X., et al. (2019). Development and application of cochlear implant-based electric-acoustic stimulation of spiral ganglion neurons. *ACS Biomater. Sci. Eng.* 5, 6735–6741. doi: 10.1021/acsbiomaterials.9b01265

Guo, R., Xiao, M., Zhao, W., Zhou, S., Hu, Y., Liao, M., et al. (2020). 2D $Ti_3C_2T_x$MXene couples electrical stimulation to promote proliferation and neural differentiation of neural stem cells. *Acta Biomater.* doi: 10.1016/j.actbio.2020.12.035. [Online ahead of print].

Guo, R., Zhang, S., Xiao, M., Qian, F., He, Z., Li, D., et al. (2016). Accelerating bioelectric functional development of neural stem cells by graphene coupling: implications for neural interfacing with conductive materials. *Biomaterials* 106, 193–204. doi: 10.1016/j.biomaterials.2016.08.019

Hackelberg, S., Tuck, S. J., He, L., Rastogi, A., White, C., Liu, L., et al. (2017). Nanofibrous scaffolds for the guidance of stem cell-derived neurons for auditory nerve regeneration. *PLoS One* 12:e0180427. doi: 10.1371/journal.pone.0180427

Hansen, M. R., Vijapurkar, U., Koland, J. G., and Green, S. H. (2001). Reciprocal signaling between spiral ganglion neurons and Schwann cells involves neuregulin and neurotrophins. *Hear. Res.* 161, 87–98. doi: 10.1016/s0378-5955(01)00360-4

He, Z., Guo, L., Shu, Y., Fang, Q., Zhou, H., Liu, Y., et al. (2017). Autophagy protects auditory hair cells against neomycin-induced damage. *Autophagy* 13, 1884–1904. doi: 10.1080/15548627.2017.1359449

He, Z. H., Li, M., Fang, Q. J., Liao, F. L., Zou, S. Y., Wu, X., et al. (2021). FOXG1 promotes aging inner ear hair cell survival through activation of the autophagy pathway. *Autophagy* 17, 4341–4362. doi: 10.1080/15548627.2021.1916194

He, Y., Zhang, P. Z., Sun, D., Mi, W. J., Zhang, X. Y., Cui, Y., et al. (2014). Wnt1 from cochlear schwann cells enhances neuronal differentiation of transplanted neural stem cells in a rat spiral ganglion neuron degeneration model. *Cell Transplant.* 23, 747–760. doi: 10.3727/096368913X669761

Heinrich, C., Blum, R., Gascon, S., Masserdotti, G., Tripathi, P., Sanchez, R., et al. (2010). Directing astroglia from the cerebral cortex into subtype specific functional neurons. *PLoS Biol.* 8:e1000373. doi: 10.1371/journal.pbio.1000373

Heins, N., Malatesta, P., Cecconi, F., Nakafuku, M., Tucker, K. L., Hack, M. A., et al. (2002). Glial cells generate neurons: the role of the transcription factor Pax6. *Nat. Neurosci.* 5, 308–315. doi: 10.1038/nn828

Hu, Z., Wei, D., Johansson, C. B., Holmstrom, N., Duan, M., Frisen, J., et al. (2005). Survival and neural differentiation of adult neural stem cells transplanted into the mature inner ear. *Exp. Cell Res.* 302, 40–47. doi: 10.1016/j.yexcr.2004.08.023

Jeon, S. J., Fujioka, M., Kim, S. C., and Edge, A. S. (2011). Notch signaling alters sensory or neuronal cell fate specification of inner ear stem cells. *J. Neurosci.* 31, 8351–8358. doi: 10.1523/JNEUROSCI.6366-10.2011

Johnson Chacko, L., Blumer, M. J. F., Pechriggl, E., Rask-Andersen, H., Dietl, W., Haim, A., et al. (2017). Role of BDNF and neurotrophic receptors in human inner ear development. *Cell Tissue Res.* 370, 347–363. doi: 10.1007/s00441-017-2686-9

Kempfle, J. S., Luu, N. C., Petrillo, M., Al-Asad, R., Zhang, A., and Edge, A. S. B. (2020). Lin28 reprograms inner ear glia to a neuronal fate. *Stem Cells* 38, 890–903. doi: 10.1002/stem.3181

Kil, K., Choi, M. Y., and Park, K. H. (2016). *In vitro* differentiation of human wharton's jelly-derived mesenchymal stem cells into auditory hair cells and neurons. *J. Int. Adv. Otol.* 12, 37–42. doi: 10.5152/iao.2016.1190

Kujawa, S. G., and Liberman, M. C. (2015). Synaptopathy in the noise-exposed and aging cochlea: primary neural degeneration in acquired sensorineural hearing loss. *Hear. Res.* 330, 191–199. doi: 10.1016/j.heares.2015.02.009

Kwan, K. Y. (2016). Single-cell transcriptome analysis of developing and regenerating spiral ganglion neurons. *Curr. Pharmacol. Rep.* 2, 211–220. doi: 10.1007/s40495-016-0064-z

Lang, H., Li, M., Kilpatrick, L. A., Zhu, J., Samuvel, D. J., Krug, E. L., et al. (2011). Sox2 up-regulation and glial cell proliferation following degeneration of spiral ganglion neurons in the adult mouse inner ear. *J. Assoc. Res. Otolaryngol.* 12, 151–171. doi: 10.1007/s10162-010-0244-1

Lang, H., Schulte, B. A., and Schmiedt, R. A. (2005). Ouabain induces apoptotic cell death in type I spiral ganglion neurons, but not type II neurons. *J. Assoc. Res. Otolaryngol.* 6, 63–74. doi: 10.1007/s10162-004-5021-6

Lang, H., Xing, Y., Brown, L. N., Samuvel, D. J., Panganiban, C. H., Havens, L. T., et al. (2015). Neural stem/progenitor cell properties of glial cells in the adult mouse auditory nerve. *Sci. Rep.* 5:13383. doi: 10.1038/srep13383

Lee, M. Y., Hackelberg, S., Green, K. L., Lunghamer, K. G., Kurioka, T., Loomis, B. R., et al. (2017). Survival of human embryonic stem cells implanted in the guinea pig auditory epithelium. *Sci. Rep.* 7:46058. doi: 10.1038/srep46058

Li, X., Bi, Z., Sun, Y., Li, C., Li, Y., and Liu, Z. (2020). *In vivo* ectopic Ngn1 and Neurod1 convert neonatal cochlear glial cells into spiral ganglion neurons. *FASEB J.* 34, 4764–4782. doi: 10.1096/fj.201902118R

Li, C., Li, X., Bi, Z., Sugino, K., Wang, G., Zhu, T., et al. (2020). Comprehensive transcriptome analysis of cochlear spiral ganglion neurons at multiple ages. *eLife* 9:e50491. doi: 10.7554/eLife.50491

Li, X., Shi, X., Wang, C., Niu, H., Zeng, L., and Qiao, Y. (2016). Cochlear spiral ganglion neuron apoptosis in neonatal mice with murine cytomegalovirus-induced sensorineural hearing loss. *J. Am. Acad. Audiol.* 27, 345–353. doi: 10.3766/jaaa.15061

Liberman, M. C. (2017). Noise-induced and age-related hearing loss: new perspectives and potential therapies. *F1000Res.* 6:927. doi: 10.12688/f1000research.11310.1

Liu, W., Glueckert, R., Linthicum, F. H., Rieger, G., Blumer, M., Bitsche, M., et al. (2014). Possible role of gap junction intercellular channels and connexin 43 in satellite glial cells (SGCs) for preservation of human spiral ganglion neurons : a comparative study with clinical implications. *Cell Tissue Res.* 355, 267–278. doi: 10.1007/s00441-013-1735-2

Liu, Y., Qi, J., Chen, X., Tang, M., Chu, C., Zhu, W., et al. (2019). Critical role of spectrin in hearing development and deafness. *Sci. Adv.* 5:eaav7803. doi: 10.1126/sciadv.aav7803

Liu, Z., Tang, M., Zhao, J., Chai, R., and Kang, J. (2018). Looking into the future: toward advanced 3D biomaterials for stem-cell-based regenerative medicine. *Adv. Mater.* 30:e1705388. doi: 10.1002/adma.201705388

Liu, W., Xu, L., Wang, X., Zhang, D., Sun, G., Wang, M., et al. (2021). PRDX1 activates autophagy *via* the PTEN-AKT signaling pathway to protect against cisplatin-induced spiral ganglion neuron damage. *Autophagy* 17, 4159–4181. doi: 10.1080/15548627.2021.1905466

Liu, W., Xu, X., Fan, Z., Sun, G., Han, Y., Zhang, D., et al. (2019). Wnt signaling activates TP53-induced glycolysis and apoptosis regulator and protects against cisplatin-induced spiral ganglion neuron damage in the mouse cochlea. *Antioxid. Redox Signal.* 30, 1389–1410. doi: 10.1089/ars.2017.7288

Lv, J., Fu, X., Li, Y., Hong, G., Li, P., Lin, J., et al. (2021). Deletion of Kcnj16 in mice does not alter auditory function. *Front. Cell Dev. Biol.* 9:630361. doi: 10.3389/fcell.2021.630361

McLean, W. J., McLean, D. T., Eatock, R. A., and Edge, A. S. (2016). Distinct capacity for differentiation to inner ear cell types by progenitor cells of the cochlea and vestibular organs. *Development* 143, 4381–4393. doi: 10.1242/dev.139840

Nishimura, K., Nakagawa, T., Sakamoto, T., and Ito, J. (2012). Fates of murine pluripotent stem cell-derived neural progenitors following transplantation into mouse cochleae. *Cell Transplant.* 21, 763–771. doi: 10.3727/096368911X623907

Nishimura, K., Weichert, R. M., Liu, W., Davis, R. L., and Dabdoub, A. (2014). Generation of induced neurons by direct reprogramming in the mammalian cochlea. *Neuroscience* 275, 125–135. doi: 10.1016/j.neuroscience.2014.05.067

Noda, T., Meas, S. J., Nogami, J., Amemiya, Y., Uchi, R., Ohkawa, Y., et al. (2018). Direct reprogramming of spiral ganglion non-neuronal cells into neurons: toward ameliorating sensorineural hearing loss by gene therapy. *Front. Cell Dev. Biol.* 6:16. doi: 10.3389/fcell.2018.00016

Nyberg, S., Abbott, N. J., Shi, X., Steyger, P. S., and Dabdoub, A. (2019). Delivery of therapeutics to the inner ear: the challenge of the blood-labyrinth barrier. *Sci. Transl. Med.* 11:eaao0935. doi: 10.1126/scitranslmed.aao0935

Pekny, M., Wilhelmsson, U., and Pekna, M. (2014). The dual role of astrocyte activation and reactive gliosis. *Neurosci. Lett.* 565, 30–38. doi: 10.1016/j.neulet.2013.12.071

Perny, M., Ting, C. C., Kleinlogel, S., Senn, P., and Roccio, M. (2017). Generation of otic sensory neurons from mouse embryonic stem cells in 3D culture. *Front. Cell. Neurosci.* 11:409. doi: 10.3389/fncel.2017.00409

Pinyon, J. L., Tadros, S. F., Froud, K. E., AC, Y. W., Tompson, I. T., Crawford, E. N., et al. (2014). Close-field electroporation gene delivery using the cochlear implant electrode array enhances the bionic ear. *Sci. Transl. Med.* 6:233ra254. doi: 10.1126/scitranslmed.3008177

Rask-Andersen, H., Bostrom, M., Gerdin, B., Kinnefors, A., Nyberg, G., Engstrand, T., et al. (2005). Regeneration of human auditory nerve. *in vitro*/in video demonstration of neural progenitor cells in adult human and guinea pig spiral ganglion. *Hear. Res.* 203, 180–191. doi: 10.1016/j.heares.2004.12.005

Reyes, J. H., O'Shea, K. S., Wys, N. L., Velkey, J. M., Prieskorn, D. M., Wesolowski, K., et al. (2008). Glutamatergic neuronal differentiation of mouse embryonic stem cells after transient expression of neurogenin 1 and treatment with BDNF and GDNF: *in vitro* and *in vivo* studies. *J. Neurosci.* 28, 12622–12631. doi: 10.1523/JNEUROSCI.0563-08.2008

Rousset, F., V, B. C. K., Sipione, R., Schmidbauer, D., Nacher-Soler, G., Ilmjarv, S., et al. (2020). Intrinsically self-renewing neuroprogenitors from the A/J mouse spiral ganglion as virtually unlimited source of mature auditory neurons. *Front. Cell. Neurosci.* 14:395. doi: 10.3389/fncel.2020.599152

Scheper, V., Hoffmann, A., Gepp, M. M., Schulz, A., Hamm, A., Pannier, C., et al. (2019). Stem cell based drug delivery for protection of auditory neurons in a guinea pig model of cochlear implantation. *Front. Cell. Neurosci.* 13:177. doi: 10.3389/fncel.2019.00177

Schulze, J., Staecker, H., Wedekind, D., Lenarz, T., and Warnecke, A. (2020). Expression pattern of brain-derived neurotrophic factor and its associated receptors: implications for exogenous neurotrophin application. *Hear. Res.* doi: 10.1016/j.heares.2020.108098. [Online ahead of print].

Shrestha, B. R., Chia, C., Wu, L., Kujawa, S. G., Liberman, M. C., and Goodrich, L. V. (2018). Sensory neuron diversity in the inner ear is shaped by activity. *Cell* 174, 1229–1246.e17. doi: 10.1016/j.cell.2018.07.007

Sun, S., Babola, T., Pregernig, G., So, K. S., Nguyen, M., Su, S.-S. M., et al. (2018). Hair cell mechanotransduction regulates spontaneous activity and spiral ganglion subtype specification in the auditory system. *Cell* 174, 1247–1263.e15. doi: 10.1016/j.cell.2018.07.008

Tasdemir-Yilmaz, O. E., Druckenbrod, N. R., Olukoya, O. O., Dong, W., Yung, A. R., Bastille, I., et al. (2021). Diversity of developing peripheral glia revealed by single-cell RNA sequencing. *Dev. Cell* 56, 2516–2535.e8. doi: 10.1016/j.devcel.2021.08.005

Wang, Q., and Green, S. H. (2011). Functional role of neurotrophin-3 in synapse regeneration by spiral ganglion neurons on inner hair cells after excitotoxic trauma *in vitro*. *J. Neurosci.* 31, 7938–7949. doi: 10.1523/JNEUROSCI.1434-10.2011

Wang, M., Han, Y., Wang, X., Liang, S., Bo, C., Zhang, Z., et al. (2021). Characterization of EGR-1 expression in the auditory cortex following kanamycin-induced hearing loss in mice. *J. Mol. Neurosci.* 71, 2260–2274. doi: 10.1007/s12031-021-01791-0

Wei, H., Chen, Z., Hu, Y., Cao, W., Ma, X., Zhang, C., et al. (2021). Topographically conductive butterfly wing substrates for directed spiral ganglion neuron growth. *Small* 17:e2102062. doi: 10.1002/smll.202102062

Wei, D., Jin, Z., Järlebark, L., Scarfone, E., and Ulfendahl, M. (2007). Survival, synaptogenesis and regeneration of adult mouse spiral ganglion neurons*in vitro*. *J. Neurobiol.* 67, 108–122. doi: 10.1002/dneu.20336

Wise, A. K., Pujol, R., Landry, T. G., Fallon, J. B., and Shepherd, R. K. (2017). Structural and ultrastructural changes to type I spiral ganglion neurons and schwann cells in the deafened guinea pig cochlea. *J. Assoc. Res. Otolaryngol.* 18, 751–769. doi: 10.1007/s10162-017-0631-y

Xia, L., Shang, Y., Chen, X., Li, H., Xu, X., Liu, W., et al. (2020). Oriented neural spheroid formation and differentiation of neural stem cells guided by anisotropic inverse opals. *Front. Bioeng. Biotechnol.* 8:848. doi: 10.3389/fbioe.2020.00848

Yan, W., Liu, W., Qi, J., Fang, Q., Fan, Z., Sun, G., et al. (2018). A three-dimensional culture system with matrigel promotes purified spiral ganglion neuron survival and function *in vitro*. *Mol. Neurobiol.* 55, 2070–2084. doi: 10.1007/s12035-017-0471-0

Yuan, Y., Shi, F., Yin, Y., Tong, M., Lang, H., Polley, D. B., et al. (2013). Ouabain-induced cochlear nerve degeneration: synaptic loss and plasticity in a mouse model of auditory neuropathy. *J. Assoc. Res. Otolaryngol.* 15, 31–43. doi: 10.1007/s10162-013-0419-7

Zhang, Z. J., Guan, H. X., Yang, K., Xiao, B. K., Liao, H., Jiang, Y., et al. (2018). Estimation of the status of spiral ganglion neurons and Schwann cells in the auditory neural degeneration mouse using the auditory brainstem response. *Acta Otolaryngol.* 138, 603–609. doi: 10.1080/00016489.2018.1436766

Zhang, Y., He, Q., Dong, J., Jia, Z., Hao, F., and Shan, C. (2016). Effects of epigallocatechin-3-gallate on proliferation and differentiation of mouse cochlear neural stem cells: involvement of PI3K/Akt signaling pathway. *Eur. J. Pharm. Sci.* 88, 267–273. doi: 10.1016/j.ejps.2016.03.017

Zhang, P. Z., He, Y., Jiang, X. W., Chen, F. Q., Chen, Y., Shi, L., et al. (2013). Stem cell transplantation *via* the cochlear lateral wall for replacement of degenerated spiral ganglion neurons. *Hear. Res.* 298, 1–9. doi: 10.1016/j.heares.2013.01.022

Zhang, Y., Li, Y., Fu, X., Wang, P., Wang, Q., Meng, W., et al. (2021). The detrimental and beneficial functions of macrophages after cochlear injury. *Front. Cell Dev. Biol.* 9:631904. doi: 10.3389/fcell.2021.631904

Zhou, H., Qian, X., Xu, N., Zhang, S., Zhu, G., Zhang, Y., et al. (2020). Disruption of Atg7-dependent autophagy causes electromotility disturbances, outer hair cell loss and deafness in mice. *Cell Death Dis.* 11:913. doi: 10.1038/s41419-020-03110-8

Zong, L., Chen, K., Zhou, W., Jiang, D., Sun, L., Zhang, X., et al. (2014). Inner ear stem cells derived feeder layer promote directional differentiation of amniotic fluid stem cells into functional neurons. *Hear. Res.* 316, 57–64. doi: 10.1016/j.heares.2014.07.012

Conflict of Interest: The authors declare that the research was conducted in the absence of any commercial or financial relationships that could be construed as a potential conflict of interest.

Publisher's Note: All claims expressed in this article are solely those of the authors and do not necessarily represent those of their affiliated organizations, or those of the publisher, the editors and the reviewers. Any product that may be evaluated in this article, or claim that may be made by its manufacturer, is not guaranteed or endorsed by the publisher.

frontiers in Molecular Neuroscience

BRIEF RESEARCH REPORT
published: 15 February 2022
doi: 10.3389/fnmol.2022.829204

BAIAP2L2 Inactivation Does Not Affect Stereocilia Development or Maintenance in Vestibular Hair Cells

Keji Yan[1], Chengli Qu[1], Yanfei Wang[1], Wen Zong[2] and Zhigang Xu[1,3]**

[1] Shandong Provincial Key Laboratory of Animal Cell and Developmental Biology, School of Life Sciences, Shandong University, Qingdao, China, [2] State Key Laboratory of Microbial Technology, Shandong University, Qingdao, China, [3] Shandong Provincial Collaborative Innovation Center of Cell Biology, Shandong Normal University, Jinan, China

Hair cells are mechanosensitive cells in the inner ear, characterized by dozens to hundreds of actin-based stereocilia and one tubulin-based kinocilium on the apical surface of each cell. Two types of hair cells, namely cochlear hair cells and vestibular hair cells (VHCs), are responsible for the sensation of sound and balancing information, respectively. In each hair cell, the stereocilia are organized into rows of increasing heights with the mechano-electrical transduction (MET) channels localized at the tips of shorter-row stereocilia. A so-called "row 2 protein complex" also localizes at the tips of shorter-row mechanotransducing stereocilia, which plays important roles in the maintenance of mechanotransducing stereocilia. Recently, we and others identified BAIAP2L2 as a new component of row 2 complex. *Baiap2l2* inactivation causes degeneration of the mechanotransducing stereocilia in cochlear hair cells, and leads to profound hearing loss in mice. In the present work, we examined the role of BAIAP2L2 in the VHC stereocilia. Confocal microscopy reveals that BAIAP2L2 immunoreactivity is localized at the tips of shorter-row stereocilia in VHCs. However, stereocilia development and maintenance are unaffected in *Baiap2l2*$^{-/-}$ VHCs. Meanwhile, MET function of VHCs as well as vestibular functions are also unaffected in *Baiap2l2*$^{-/-}$ mice. Further investigations show that the stereociliary tip localization of CAPZB2, another known row 2 complex component, is not affected in *Baiap2l2*$^{-/-}$ VHCs, consistent with the unaltered stereocilia morphology. Taken together, our present data show that BAIAP2L2 inactivation does not affect vestibular hair cell stereocilia.

Keywords: inner ear, vestibular hair cells, stereocilia, BAIAP2L2, CAPZB2

OPEN ACCESS

Edited by:
Dongdong Ren,
Fudan University, China

Reviewed by:
Jeremy Duncan,
Western Michigan University, United States
Sangyong Jung,
*Institute of Molecular and Cell Biology (A*STAR), Singapore*

****Correspondence:***
Wen Zong
wenzong@sdu.edu.cn
Zhigang Xu
xuzg@sdu.edu.cn

Specialty section:
This article was submitted to Molecular Signalling and Pathways, a section of the journal Frontiers in Molecular Neuroscience

Received: *05 December 2021*
Accepted: *26 January 2022*
Published: *15 February 2022*

Citation:
Yan K, Qu C, Wang Y, Zong W and Xu Z (2022) BAIAP2L2 Inactivation Does Not Affect Stereocilia Development or Maintenance in Vestibular Hair Cells. Front. Mol. Neurosci. 15:829204. doi: 10.3389/fnmol.2022.829204

INTRODUCTION

Hair cells are the mechanosensory cells in the inner ear, responsible for converting the mechanical signals into electrical signals, a process referred to as mechano-electrical transduction (MET). Each hair cell harbors dozens to hundreds of actin-based stereocilia and one microtubule-based kinocilium at the apical surface, collectively named hair bundle (Flock and Cheung, 1977). The stereocilia play a pivotal role in MET, whereas the kinocilium is important for hair bundle development (Hudspeth and Jacobs, 1979; Jones et al., 2008).

There are two different types of hair cells in the mammalian inner ear, namely cochlear hair cells and vestibular hair cells (VHCs), which are responsible for the sensation of sound and balancing information, respectively. In each mammalian cochlear hair cell, stereocilia are organized into

three rows of increasing heights, forming a characteristic staircase-like pattern (Tilney et al., 1980). Similarly, the stereocilia in mammalian VHCs form a staircase-like pattern with more rows of increasing heights (Krey and Barr-Gillespie, 2019). The MET channels are localized at the tips of shorter-row stereocilia, which are therefore referred to as mechanotransducing stereocilia (Beurg et al., 2009). In either type of hair cells, the development and maintenance of stereocilia is tightly regulated, and several proteins have been identified to play important roles in regulating stereocilia length (Barr-Gillespie, 2015; McGrath et al., 2017; Krey and Barr-Gillespie, 2019; Velez-Ortega and Frolenkov, 2019).

At the tips of the tallest-row stereocilia, there is a so-called "row 1 protein complex" that controls the identity and development of the tallest-row stereocilia (Tadenev et al., 2019; Krey et al., 2020). Meanwhile, at the tips of shorter-row mechanotransducing stereocilia resides a "row 2 protein complex", which consists of MYO15A-L, EPS8L2, TWF2, and CAPZB2 (Peng et al., 2009; Rzadzinska et al., 2009; Furness et al., 2013; Fang et al., 2015; Avenarius et al., 2017). Evidences suggest that deficiency of row 2 complex components leads to degeneration of the mechanotransducing stereocilia (Furness et al., 2013; Fang et al., 2015). Recently, we and others identified BAI1-associated protein 2-like 2 (BAIAP2L2, also known as Pinkbar) as a new component of row 2 complex (Carlton et al., 2021; Yan et al., 2021). BAIAP2L2 inactivation causes degeneration of the mechanotransducing stereocilia in cochlear hair cells, and leads to profound hearing loss in mice (Carlton et al., 2021; Yan et al., 2021). Furthermore, the stereociliary tip localization of the known row 2 complex component, CAPZB2, is abolished in *Baiap2l2* knockout mice, suggesting that BAIAP2L2 is indispensable for the formation of row 2 complex in cochlear hair cells (Yan et al., 2021).

In the present work, we further investigate the role of BAIAP2L2 in VHC stereocilia. Surprisingly, our results show that albeit localizing at the tips of shorter-row VHC stereocilia, BAIAP2L2 is not required for the development or maintenance of VHC stereocilia, which is in sharp contrast to the results observed in cochlear hair cells.

MATERIALS AND METHODS

Mice

Animal experiments were approved by the Animal Ethics Committee of Shandong University School of Life Sciences (Permit Number: SYDWLL-2020-31) and performed accordingly. *Baiap2l2* and *Lhfpl5* knockout mice were established and maintained as previously reported (Xiong et al., 2012; Yan et al., 2021).

Whole-Mount Immunostaining

Utricles and saccules were dissected out and fixed with 4% paraformaldehyde (PFA) in PBS for 20 min, followed by permeabilization and blocking with PBT1 (0.1% Triton X-100, 1% BSA, and 5% heat-inactivated goat serum in PBS, pH 7.3) for 40 min. Afterwards, the samples were incubated with primary antibody in PBT1 overnight at 4°C, followed by incubation with corresponding secondary antibody in PBT2 (0.1% Triton X-100 and 0.1% BSA in PBS) for 2 h. After incubation with TRITC-conjugated phalloidin (Sigma-Aldrich, Cat. No. P1951) in PBS for 30 min, the samples were mounted in PBS/glycerol (1:1) and imaged using a confocal microscope with a 1.4NA/63 × Kort M27 objective lens (LSM 900, Zeiss, Germany). The antibodies used in the present study are as follows: rabbit anti-BAIAP2L2 antibody (Sigma-Aldrich, Cat. No. HPA003043); rabbit anti-CAPZB2 antibody (Merck, Cat. No. AB6017); mouse anti-EPS8 antibody (BD Biosciences, Cat. No. 610143); Alexa Fluor 488-conjugated donkey anti-rabbit IgG (Thermo Fisher Scientific, Cat. No. A21206); Alexa Fluor 488-conjugated donkey anti-mouse IgG (Thermo Fisher Scientific, Cat. No. A21202).

Scanning Electron Microscopy

Mouse temporal bone was dissected out and fixed with 2.5% glutaraldehyde in 0.1 M phosphate buffer overnight at 4°C. Then the utricle and saccule were taken out of the temporal bone and post-fixed with 1% osmium tetroxide in 0.1 M phosphate buffer at 4°C for 2 h. After dehydration in ethanol and critically point drying using a Leica EM CPD300 (Leica, Germany), samples were mounted and sputter coated with platinum (15 nm) using a Cressington 108 sputter coater (Cressington, United Kingdom). Images were taken using a Quanta250 field-emission scanning electron microscope (FEI, Netherlands).

FM1-43FX Uptake

The sensory epithelia of utricle and saccule were dissected out and incubated with 3 μM FM 1-43FX (Thermo Fisher, Cat. No. F35355) in PBS for 40 s, then fixed with 4% PFA at room temperature for 20 min. After mounting in PBS-glycerol (1:1), the samples were imaged using a confocal microscope with a 0.8NA/20 × Kort M27 objective lens using identical settings (LSM 700, Zeiss, Germany). The relative fluorescence intensity of individual hair cell was measured and analyzed using ImageJ software.

Vestibular Function Examination

Vestibular function of mice was evaluated as described previously (Li et al., 2021). Circling stereotyped movement was counted to record compulsive circles around the animal's hips. Swimming test was performed to observe swimming behavior ranging from normal swimming to drowning. Swimming test scores were defined as follows: 0, normal swimming; 1, irregular swimming; 2, immobile floating; and 3, underwater tumbling. For rotarod test, mice were placed on the rod apparatus (HB-600, Ruanlong, China) that was set to accelerate from 0 to 50 rpm over a 3-min period. Mice were trained for seven consecutive days and the time before dropping was recorded on day 4–7. Four trials were performed on each day and the second, third and fourth trials were measured and analyzed.

Statistical Analysis

All experiments were performed at least three times independently. Data were shown as means ± standard error of mean (SEM). Student's two-tailed unpaired *t* test was used to

determine statistical significance when the results show normal distribution; otherwise, Mann-Whitney *U* test is used. $P < 0.05$ was considered statistically significant.

RESULTS

BAIAP2L2 Is Localized at the Tips of Shorter-Row Stereocilia in Vestibular Hair Cells

We first examined the localization of BAIAP2L2 in the VHC stereocilia by performing whole-mount immunostaining and confocal microscopy using a specific anti-BAIAP2L2 antibody. The stereociliary F-actin core was visualized by TRITC-conjugated phalloidin. The results reveal that BAIAP2L2 immunoreactivity is localized at the tips of utricular hair cell stereocilia at postnatal day 8 (P8) (**Figure 1A** and **Supplementary Figure 1A**, top panel). Noticeably, BAIAP2L2 immunoreactivity is more enriched at the tips of the shorter-row stereocilia (**Figure 1A**, top panel). Similar results were obtained in P30 utricular hair cells (**Figure 1A** and **Supplementary Figure 1A**, middle panel). No BAIAP2L2 immunoreactivity is detected in the homozygous *Baiap2l2* knockout mice, confirming the specificity of the antibody (**Figure 1A** and **Supplementary Figure 1A**, bottom panel). Similar expression pattern was also observed in saccular hair cells (**Figure 1B** and **Supplementary Figure 1B**).

Loss of BAIAP2L2 Does Not Affect the Development or Maintenance of Vestibular Hair Cell Stereocilia

Phalloidin staining reveals largely unaffected stereocilia morphology in *Baiap2l2*$^{-/-}$ VHCs (**Figures 1A,B**). Scanning electron microscopy (SEM) was then employed to further examine the morphology of VHC stereocilia in *Baiap2l2* knockout mice. When examined at P8, the morphology of both utricular and saccular VHC stereocilia in *Baiap2l2*$^{-/-}$ mice is indistinguishable from that in control mice (**Figures 2A,B**). Similar results were observed in *Baiap2l2*$^{-/-}$ mice at P30 (**Figures 2C,D**). Taken together, our present data suggest that loss of BAIAP2L2 does not affect the development or maintenance of VHC stereocilia.

Loss of BAIAP2L2 Does Not Affect the Mechano-Electrical Transduction Function of Vestibular Hair Cells

The unaffected stereocilia morphology suggests that MET function might be normal in *Baiap2l2*$^{-/-}$ VHCs. We then examined the MET function of *Baiap2l2*$^{-/-}$ VHCs by performing FM 1-43FX uptake experiment. FM 1-43FX is a fixable fluorescent dye that could enter hair cells through MET channels when applied briefly, therefore is often used as an indicator of hair cell MET function (Gale et al., 2001; Meyers et al., 2003). The results show that FM 1-43FX dye uptake of utricular VHCs in *Baiap2l2*$^{-/-}$ mice at P8 is comparable to that in control mice (**Supplementary Figures 2A,B**). Similar results were obtained in P8 saccular VHCs (**Supplementary Figures 2C,D**). We then examined the MET function of adult VHCs at P30 by performing FM 1-43FX uptake experiment, which also did not reveal any difference between *Baiap2l2*$^{-/-}$ and control mice (**Figures 3A–D**). Therefore, our present data suggest that the MET function of VHCs is not affected by loss of BAIAP2L2.

Loss of BAIAP2L2 Does Not Affect Vestibular Function in Mice

We then moved on to examine the vestibular function of *Baiap2l2*$^{-/-}$ mice. Mutation in *Lhfpl5* gene, which encodes for MET component LHFPL5, leads to deafness and balance

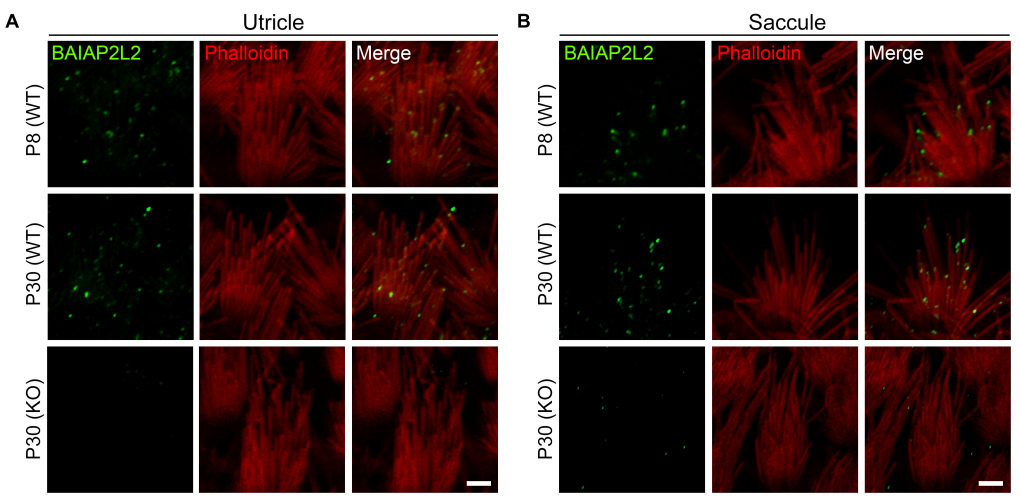

FIGURE 1 | BAIAP2L2 is localized at the tips of shorter-row stereocilia in VHCs. Whole-mount immunostaining using a specific anti-BAIAP2L2 antibody (green) was performed to examine the localization of BAIAP2L2 in the stereocilia of utricular **(A)** and saccular **(B)** hair cells. Steoreociliary F-actin core was visualized using TRITC-conjugated phalloidin (red). The genotypes and ages of mice are indicated. Scale bar, 2 μm.

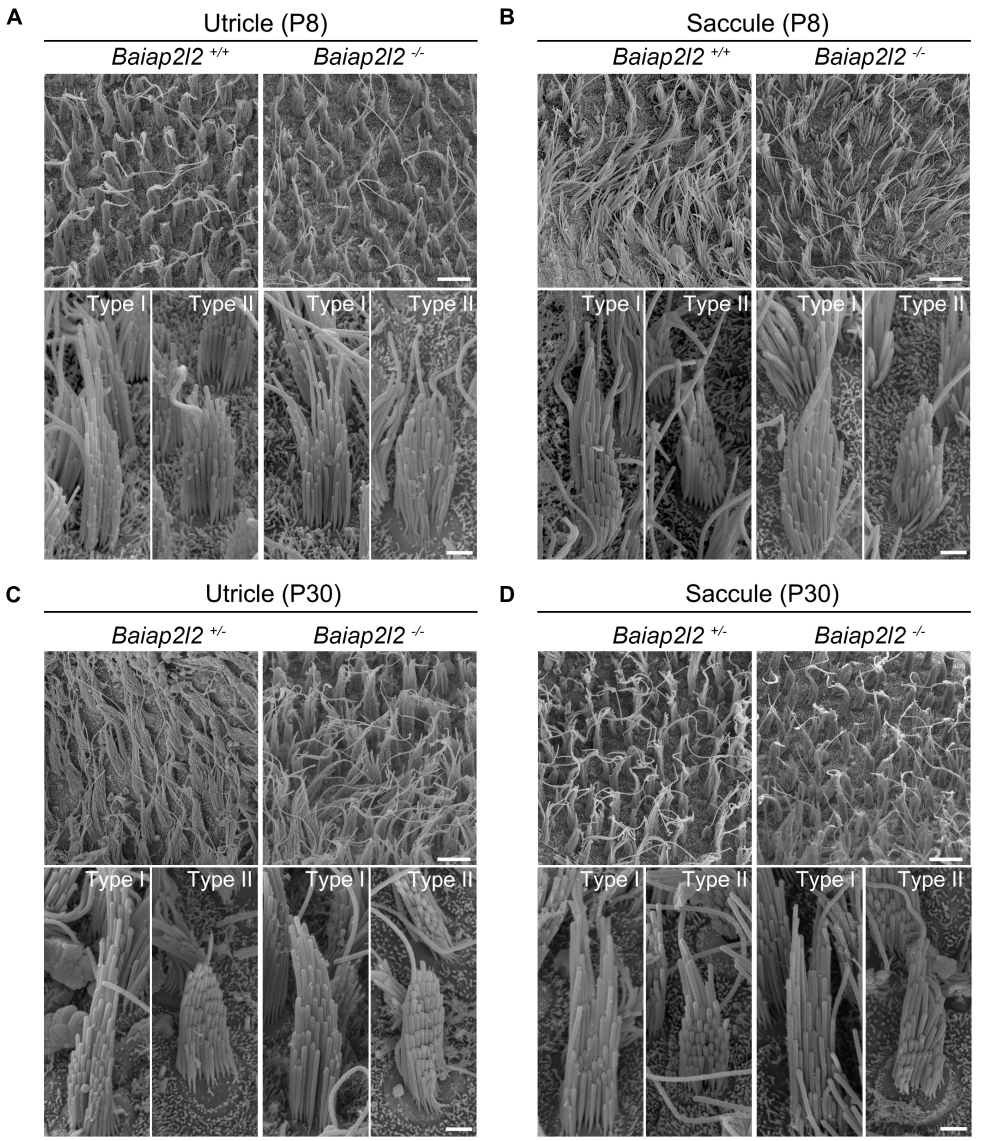

FIGURE 2 | Stereocilia morphology is unaffected in VHCs of *Baiap2l2* knockout mice. SEM was performed to examine the stereocilia morphology of P8 utricle **(A)**, P8 saccule **(B)**, P30 utricle **(C)**, and P30 saccule **(D)** in mice of different genotypes as indicated. In each panel, low-magnification images and high magnification images of type I and II VHCs are shown at the top and bottom, respectively. Scale bar, 5 μm (in low-magnification images) and 1 μm (in high-magnification images).

dysfunction (Longo-Guess et al., 2005). Therefore, *Lhfpl5*$^{-/-}$ mice were included in the present experiments as positive control. Consistent with the previous report, *Lhfpl5*$^{-/-}$ mice show typical circling stereotyped movement, suggesting of balance dysfunction (**Figure 3E**). However, *Baiap2l2*$^{-/-}$ mice at ages of up to 12 months do not show any circling stereotyped movement (**Figure 3E**).

The vestibular function of *Baiap2l2*$^{-/-}$ mice was further evaluated by swimming test and rotarod test. In both tests, *Baiap2l2*$^{-/-}$ mice at ages of up to 12 months perform indistinguishably from control *Baiap2l2*$^{+/-}$ mice (**Figures 3F,G**). In contrast, *Lhfpl5*$^{-/-}$ mice show abnormal swimming behavior and are easier to fall off the rotarod (**Figures 3F,G**). Taken together, our present data suggest that the vestibular function is not affected by loss of BAIAP2L2.

Loss of BAIAP2L2 Does Not Affect the Stereociliary Tip Localization of CAPZB2 or EPS8 in Vestibular Hair Cells

To explore the possible reason why loss of BAIAP2L2 does not affect VHC stereocilia or vestibular function, we tried to examine the stereociliary localization of other row 2 complex components in VHCs by performing whole-mount immunostaining and confocal microscopy. Here, we focused on CAPZB2 since its stereociliary tip localization in cochlear hair cells has been shown

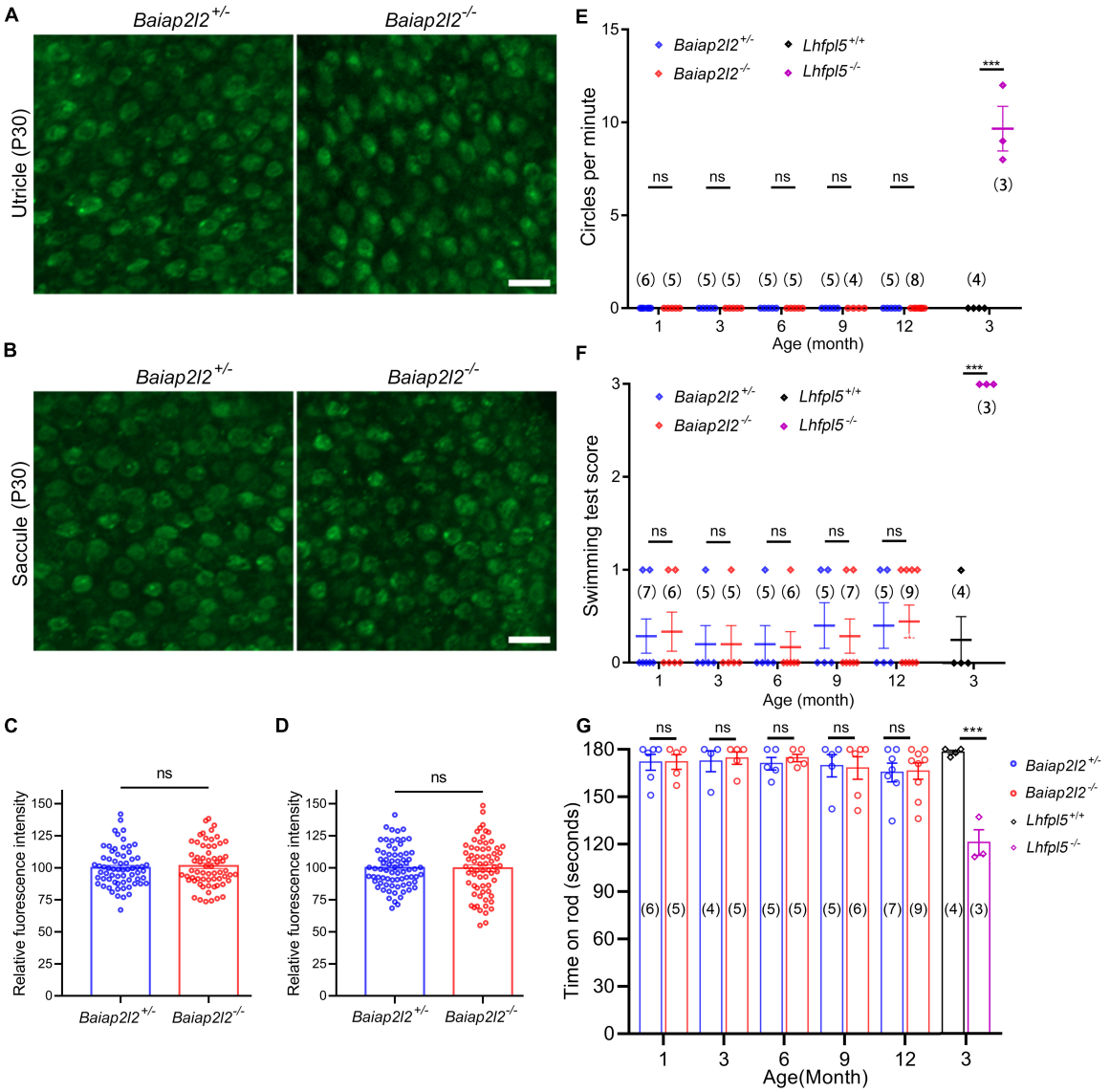

FIGURE 3 | Vestibular function is unaffected in *Baiap2l2* knockout mice. **(A,B)** FM1-43FX uptake by P30 utricular **(A)** and saccular **(B)** hair cells from *Baiap2l2*$^{+/-}$ or *Baiap2l2*$^{-/-}$ mice was examined using confocal microscope. Scale bars, 10 μm. **(C,D)** FM1-43FX uptake was quantified according to the results from **(A,B)**, respectively. **(E–G)** The vestibular function of *Baiap2l2*$^{+/-}$ or *Baiap2l2*$^{-/-}$ mice of different ages was evaluated by examining circling stereotyped movement **(E)**, swimming test **(F)**, and rotarod test **(G)**. *Lhfpl5*$^{-/-}$ mice were included as positive control. Numbers of animals in each group are indicated in brackets. ns, not significant; ***$p < 0.001$.

to depend on BAIAP2L2 (Yan et al., 2021). The results show that in the utricle of P30 control mice, CAPZB2 immunoreactivity is localized at the tips of shorter-row stereocilia as reported previously (Avenarius et al., 2017; **Figure 4A**, top panel). Interestingly, CAPZB2 immunoreactivity is unaffected in the utricle of *Baiap2l2*$^{-/-}$ mice (**Figure 4A**, bottom panel), which is consistent with the normal development and maintenance of VHC stereocilia in *Baiap2l2*$^{-/-}$ mice. Similar results were observed in the saccule (**Figure 4B**).

EPS8 is a row 1 complex component and is responsible for the stereociliary tip localization of BAIAP2L2 in cochlear hair cells (Carlton et al., 2021). Our results show that EPS8 immunoreactivity is localized at the tips of the taller-row stereocilia in the utricle or saccule of both *Baiap2l2*$^{+/+}$ and *Baiap2l2*$^{-/-}$ mice (**Figures 4C,D**). Taken together, the present data show that row 1 and row 2 complex are largely unaffected in the VHC stereocilia of *Baiap2l2*$^{-/-}$ mice.

DISCCUSSION

BAIAP2L2 is a recently identified row 2 complex component that localizes at the tips of shorter-row mechanotransducing stereocilia in cochlear hair cells (Carlton et al., 2021;

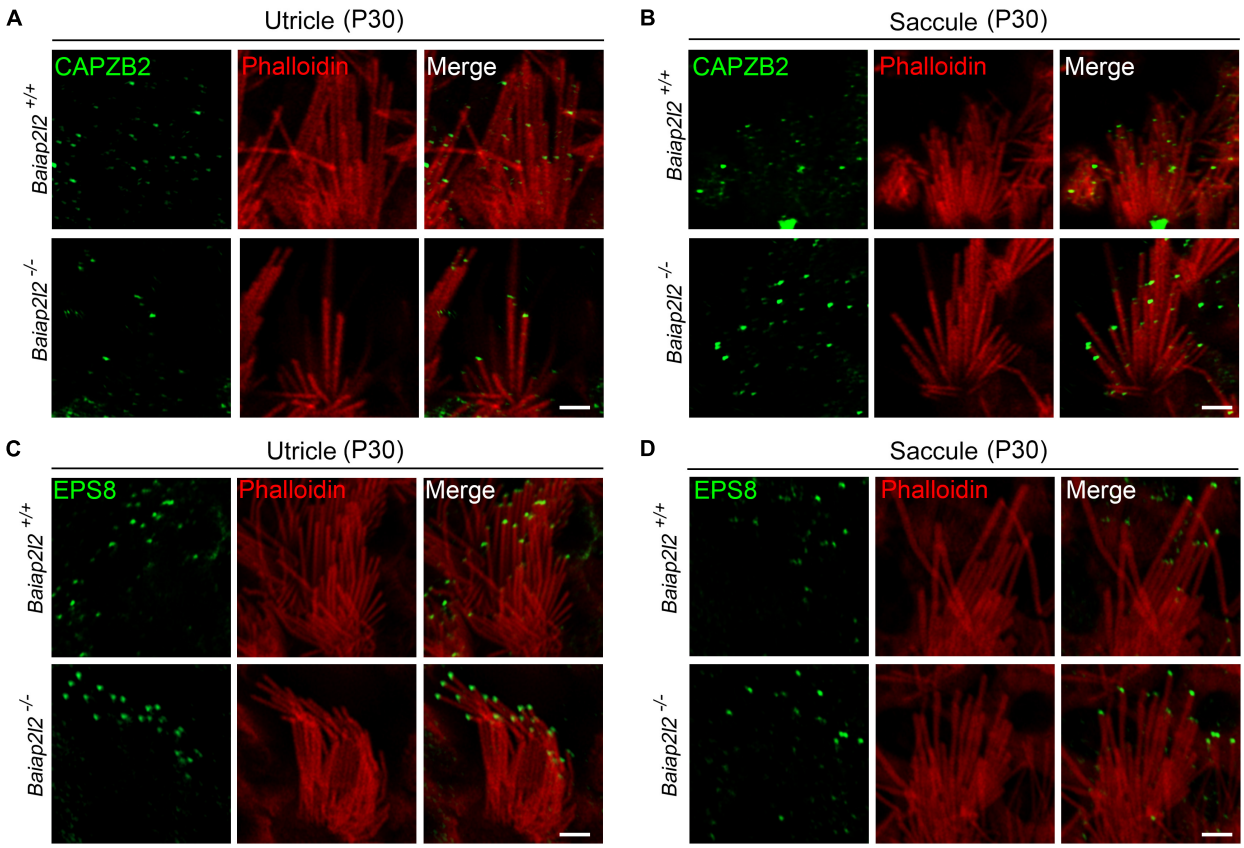

FIGURE 4 | Stereociliary tip localization of CAPZB2 and EPS8 is unaffected in VHCs of *Baiap2l2* knockout mice. Whole-mount immunostaining and confocal microscopy were performed to examine the localization of CAPZB2 in utricular **(A)** and saccular **(B)** hair cells of P30 *Baiap2l2*$^{+/+}$ or *Baiap2l2*$^{-/-}$ mice. Similar experiments were performed to examine the localization of EPS8 in utricular **(C)** and saccular **(D)** hair cells of P30 *Baiap2l2*$^{+/+}$ or *Baiap2l2*$^{-/-}$ mice. TRITC-conjugated phalloidin was used to visualize stereociliary F-actin core. Scale bars, 2 μm.

Yan et al., 2021). BAIAP2L2 inactivation results in mechanotransducing stereocilia degeneration in cochlear hair cells, and leads to profound hearing loss (Carlton et al., 2021; Yan et al., 2021). In the present work, we show that BAIAP2L2 is also localized at the tips of shorter-row stereocilia in VHCs. Unexpectedly, our data reveal that BAIAP2L2 inactivation does not affect the development/maintenance of VHC stereocilia as well as vestibular function.

There are evidences suggesting that deficiency of row 2 complex components might affect cochlear and vestibular hair cells differently. For example, EPS8L2 or MYO15A-L inactivation results in degeneration of the mechanotransducing stereocilia in cochlear hair cells, but does not significantly affect vestibular function and/or VHC stereocilia morphology (Furness et al., 2013; Fang et al., 2015). ESP8L2 localizes at the tips of most VHC stereocilia including the taller ones (Furness et al., 2013; Avenarius et al., 2017). Meanwhile, row 1 complex component EPS8 is mostly enriched at the tips of taller-row VHC stereocilia, raising the possibility that row 1 and 2 complex components might work cooperatively in VHC stereocilia and compensate for the loss of each other (Furness et al., 2013; Avenarius et al., 2017). Our present results suggest that similar functional compensation might also happen in *Baiap2l2* knockout mice, which awaits further investigations.

One of the candidates responsible for this possible compensation is its homolog BAIAP2L1 (also known as IRTKS), whose expression has been detected in the hair cells through transcriptome studies (umgear.org). In the gut, BAIAP2L1 could localize EPS8 to the developing microvilli of the brush border and regulate their growth (Postema et al., 2018). Examination of the precise localization of BAIAP2L1 in the stereocilia of cochlear and vestibular hair cells, and analysis of *Baiap2l1* knockout mice and *Baiap2l1*/*Baiap2l2* double knockout mice will help to address this question.

Similarly to BAIAP2L2, CAPZB2 and TWF2 are more enriched at the tips of shorter-row VHC stereocilia (Avenarius et al., 2017). CAPZB2 is a capping protein that binds to the barbed ends of F-actin and prevents both actin polymerization and depolymerization (Caldwell et al., 1989). CAPZB2 functions as a heterodimer formed together with CAPZA1/2, both of which are detected at the tips of stereocilia (Shin et al., 2013; Avenarius et al., 2017). In sharp contrast to BAIAP2L2/EPS8L2/MYO15A-L, CAPZB2 inactivation leads to VHC stereocilia deficits as well as compromised vestibular function (Avenarius et al., 2017).

Capzb2-deficient VHC stereocilia are normal when examined at P2, but become severely disrupted at P7-P9 in some VHCs (Avenarius et al., 2017). A common phenotype in *Capzb2*-deficient VHCs at P7-P9 is missing of the shortest stereocilia, with the intermediate or highest stereocilia largely unaffected (Avenarius et al., 2017). Consistent with the important role of CAPZB2 in VHC stereocilia, the stereociliary tip localization of CAPZB2 is unaffected in *Baiap2l2*-deficient VHCs. In contrast, in the cochlear hair cells, the stereociliary tip localization of CAPZB2 is dependent on functional BAIAP2L2 (Yan et al., 2021). The different dependency of CAPZB2 localization on BAIAI2L2 in cochlear and vestibular hair cells might explain the different auditory and balancing phenotypes in *Baiap2l2* knockout mice. Detailed examination of the localization of row 2 proteins in VHC stereocilia using super-resolution microscopy might help to learn more about the underlying mechanism (Liu et al., 2019; Qi et al., 2019, 2020).

DATA AVAILABILITY STATEMENT

The original contributions presented in the study are included in the article/**Supplementary Material**, further inquiries can be directed to the corresponding authors.

ETHICS STATEMENT

The animal study was reviewed and approved by the Animal Ethics Committee of Shandong University School of Life Sciences.

AUTHOR CONTRIBUTIONS

WZ and ZX: study concept and design. KY, CQ, YW, and WZ: acquisition of data. KY, CQ, YW, WZ, and ZX: analysis and interpretation of data. KY, WZ, and ZX: drafting the manuscript. All authors contributed to the article and approved the submitted version.

FUNDING

This work was supported by grants from the National Natural Science Foundation of China (82071051 and 81771001), Shandong Provincial Natural Science Foundation (ZR2020ZD39), and Start-up funds from Shandong University (2019GN115).

ACKNOWLEDGMENTS

We thank Wei Xiong (Tsinghua University) for *Lhfpl5* knockout mice. We also thank Sen Wang, Xiaomin Zhao, and Haiyan Yu from the core facilities for Life and Environmental Sciences, Shandong University for the technical support in SEM and confocal microscopy.

SUPPLEMENTARY MATERIAL

The Supplementary Material for this article can be found online at: https://www.frontiersin.org/articles/10.3389/fnmol.2022.829204/full#supplementary-material

REFERENCES

Avenarius, M. R., Krey, J. F., Dumont, R. A., Morgan, C. P., Benson, C. B., Vijayakumar, S., et al. (2017). Heterodimeric capping protein is required for stereocilia length and width regulation. *J. Cell Biol.* 216, 3861–3881. doi: 10.1083/jcb.201704171

Barr-Gillespie, P. G. (2015). Assembly of hair bundles, an amazing problem for cell biology. *Mol. Biol. Cell* 26, 2727–2732. doi: 10.1091/mbc.E14-04-0940

Beurg, M., Fettiplace, R., Nam, J. H., and Ricci, A. J. (2009). Localization of inner hair cell mechanotransducer channels using high-speed calcium imaging. *Nat. Neurosci.* 12, 553–558. doi: 10.1038/nn.2295

Caldwell, J. E., Heiss, S. G., Mermall, V., and Cooper, J. A. (1989). Effects of CapZ, an actin capping protein of muscle, on the polymerization of actin. *Biochemistry* 28, 8506–8514. doi: 10.1021/bi00447a036

Carlton, A. J., Halford, J., Underhill, A., Jeng, J. Y., Avenarius, M. R., Gilbert, M. L., et al. (2021). Loss of Baiap2l2 destabilizes the transducing stereocilia of cochlear hair cells and leads to deafness. *J. Physiol.* 599, 1173–1198. doi: 10.1113/JP280670

Fang, Q., Indzhykulian, A. A., Mustapha, M., Riordan, G. P., Dolan, D. F., Friedman, T. B., et al. (2015). The 133-kDa N-terminal domain enables myosin 15 to maintain mechanotransducing stereocilia and is essential for hearing. *Elife* 4:e08627. doi: 10.7554/eLife.08627

Flock, A., and Cheung, H. C. (1977). Actin filaments in sensory hairs of inner ear receptor cells. *J. Cell Biol.* 75, 339–343. doi: 10.1083/jcb.75.2.339

Furness, D. N., Johnson, S. L., Manor, U., Ruttiger, L., Tocchetti, A., Offenhauser, N., et al. (2013). Progressive hearing loss and gradual deterioration of sensory hair bundles in the ears of mice lacking the actin-binding protein Eps8L2. *Proc. Natl. Acad. Sci. U. S. A.* 110, 13898–13903. doi: 10.1073/pnas.1304644110

Gale, J. E., Marcotti, W., Kennedy, H. J., Kros, C. J., and Richardson, G. P. (2001). FM1-43 dye behaves as a permeant blocker of the hair-cell mechanotransducer channel. *J. Neurosci.* 21, 7013–7025. doi: 10.1523/Jneurosci.21-18-07013.2001

Hudspeth, A. J., and Jacobs, R. (1979). Stereocilia mediate transduction in vertebrate hair cells. *Proc. Natl. Acad. Sci. U. S. A.* 76, 1506–1509. doi: 10.1073/pnas.76.3.1506

Jones, C., Roper, V. C., Foucher, I., Qian, D., Banizs, B., Petit, C., et al. (2008). Ciliary proteins link basal body polarization to planar cell polarity regulation. *Nat. Genet.* 40, 69–77. doi: 10.1038/ng.2007.54

Krey, J. F., and Barr-Gillespie, P. G. (2019). Molecular composition of vestibular hair bundles. *Cold Spring Harb. Perspect. Med.* 9:a033209. doi: 10.1101/cshperspect.a033209

Krey, J. F., Chatterjee, P., Dumont, R. A., O'Sullivan, M., Choi, D., Bird, J. E., et al. (2020). Mechanotransduction-dependent control of stereocilia dimensions and row identity in inner hair cells. *Curr. Biol.* 30, 442–454. doi: 10.1016/j.cub.2019.11.076

Li, N., Xi, Y., Du, H., Zhou, H., and Xu, Z. (2021). Annexin A4 is dispensable for hair cell development and function. *Front. Cell Dev. Biol.* 9:680155. doi: 10.3389/fcell.2021.680155

Liu, Y., Qi, J., Chen, X., Tang, M., Chu, C., Zhu, W., et al. (2019). Critical role of spectrin in hearing development and deafness. *Sci. Adv.* 5:eaav7803. doi: 10.1126/sciadv.aav7803

Longo-Guess, C. M., Gagnon, L. H., Cook, S. A., Wu, J., Zheng, Q. Y., and Johnson, K. R. (2005). A missense mutation in the previously undescribed gene Tmhs underlies deafness in hurry-scurry (hscy) mice. *Proc. Natl. Acad. Sci. U. S. A.* 102, 7894–7899. doi: 10.1073/pnas.0500760102

McGrath, J., Roy, P., and Perrin, B. J. (2017). Stereocilia morphogenesis and maintenance through regulation of actin stability. *Semin. Cell Dev. Biol.* 65, 88–95. doi: 10.1016/j.semcdb.2016.08.017

Meyers, J. R., MacDonald, R. B., Duggan, A., Lenzi, D., Standaert, D. G., Corwin, J. T., et al. (2003). Lighting up the senses: fM1-43 loading of sensory cells through nonselective ion channels. *J. Neurosci.* 23, 4054–4065. doi: 10.1523/JNEUROSCI.23-10-04054.2003

Peng, A. W., Belyantseva, I. A., Hsu, P. D., Friedman, T. B., and Heller, S. (2009). Twinfilin 2 regulates actin filament lengths in cochlear stereocilia. *J. Neurosci.* 29, 15083–15088. doi: 10.1523/JNEUROSCI.2782-09.2009

Postema, M. M., Grega-Larson, N. E., Neininger, A. C., and Tyska, M. J. (2018). IRTKS (BAIAP2L1) elongates epithelial microvilli using EPS8-dependent and independent mechanisms. *Curr. Biol.* 28, 2876–2888. doi: 10.1016/j.cub.2018.07.022

Qi, J., Liu, Y., Chu, C., Chen, X., Zhu, W., Shu, Y., et al. (2019). A cytoskeleton structure revealed by super-resolution fluorescence imaging in inner ear hair cells. *Cell. Discov.* 5:12. doi: 10.1038/s41421-018-0076-4

Qi, J., Zhang, L., Tan, F., Liu, Y., Chu, C., Zhu, W., et al. (2020). Espin distribution as revealed by super-resolution microscopy of stereocilia. *Am. J. Transl. Res.* 12, 130–141.

Rzadzinska, A. K., Nevalainen, E. M., Prosser, H. M., Lappalainen, P., and Steel, K. P. (2009). MyosinVIIa interacts with Twinfilin-2 at the tips of mechanosensory stereocilia in the inner ear. *PLoS One* 4:e7097. doi: 10.1371/journal.pone.0007097

Shin, J. B., Krey, J. F., Hassan, A., Metlagel, Z., Tauscher, A. N., Pagana, J. M., et al. (2013). Molecular architecture of the chick vestibular hair bundle. *Nat. Neurosci.* 16, 365–374. doi: 10.1038/nn.3312

Tadenev, A. L. D., Akturk, A., Devanney, N., Mathur, P. D., Clark, A. M., Yang, J., et al. (2019). GPSM2-GNAI specifies the tallest stereocilia and defines hair bundle row identity. *Curr. Biol.* 92:e924. doi: 10.1016/j.cub.2019.01.051

Tilney, L. G., Derosier, D. J., and Mulroy, M. J. (1980). The organization of actin filaments in the stereocilia of cochlear hair cells. *J. Cell Biol.* 86, 244–259. doi: 10.1083/jcb.86.1.244

Velez-Ortega, A. C., and Frolenkov, G. I. (2019). Building and repairing the stereocilia cytoskeleton in mammalian auditory hair cells. *Hear. Res.* 376, 47–57. doi: 10.1016/j.heares.2018.12.012

Xiong, W., Grillet, N., Elledge, H. M., Wagner, T. F. J., Zhao, B., Johnson, K. R., et al. (2012). TMHS is an integral component of the mechanotransduction machinery of cochlear hair cells. *Cell* 151, 1283–1295. doi: 10.1016/j.cell.2012.10.041

Yan, K., Zong, W., Du, H., Zhai, X., Ren, R., Liu, S., et al. (2021). BAIAP2L2 is required for the maintenance of mechanotransducing stereocilia of cochlear hair cells. *J. Cell. Physiol.* Epub Online ahead of print. doi: 10.1002/jcp.30545

Conflict of Interest: The authors declare that the research was conducted in the absence of any commercial or financial relationships that could be construed as a potential conflict of interest.

Publisher's Note: All claims expressed in this article are solely those of the authors and do not necessarily represent those of their affiliated organizations, or those of the publisher, the editors and the reviewers. Any product that may be evaluated in this article, or claim that may be made by its manufacturer, is not guaranteed or endorsed by the publisher.

frontiers in Molecular Neuroscience

ORIGINAL RESEARCH
published: 24 February 2022
doi: 10.3389/fnmol.2022.829642

Shikonin Attenuates Cochlear Spiral Ganglion Neuron Degeneration by Activating Nrf2-ARE Signaling Pathway

Hongjie Du[1,2], Xuanchen Zhou[1], Lei Shi[1], Ming Xia[1], Yajie Wang[1], Na Guo[1], Houyang Hu[1], Pan Zhang[1], Huiming Yang[1], Fangyuan Zhu[1], Zhenxiao Teng[1,3], Chengcheng Liu[4] and Miaoqing Zhao[5]**

[1] Department of Otolaryngology, Shandong Provincial Hospital Affiliated to Shandong First Medical University, Jinan, China, [2] Qilu Pharmaceutical Co., Ltd., Jinan, China, [3] Department of Otolaryngology, Shandong Provincial Hospital, Cheeloo College of Medicine, Shandong University, Jinan, China, [4] Central Laboratory, Shandong Provincial Hospital Affiliated to Shandong First Medical University, Jinan, China, [5] Department of Pathology, Shandong Provincial Hospital Affiliated to Shandong First Medical University, Jinan, China

OPEN ACCESS

Edited by:
Dongdong Ren,
Fudan University, China

Reviewed by:
Haibo Shi,
Shanghai Jiao Tong University Affiliated Sixth People's Hospital, China
Xun Wang,
University of Texas Southwestern Medical Center, United States

***Correspondence:**
Chengcheng Liu
LCcheng211314@126.com
Miaoqing Zhao
zhaomqsd@163.com

Specialty section:
This article was submitted to Molecular Signalling and Pathways, a section of the journal Frontiers in Molecular Neuroscience

Received: 06 December 2021
Accepted: 04 February 2022
Published: 24 February 2022

Citation:
Du H, Zhou X, Shi L, Xia M, Wang Y, Guo N, Hu H, Zhang P, Yang H, Zhu F, Teng Z, Liu C and Zhao M (2022) Shikonin Attenuates Cochlear Spiral Ganglion Neuron Degeneration by Activating Nrf2-ARE Signaling Pathway. Front. Mol. Neurosci. 15:829642. doi: 10.3389/fnmol.2022.829642

The molecular mechanisms that regulate the proliferation and differentiation of inner ear spiral ganglion cells (SGCs) remain largely unknown. Shikonin (a naphthoquinone pigment isolated from the traditional Chinese herbal medicine comfrey root) has anti-oxidation, anti-apoptosis and promoting proliferation and differentiation effects on neural progenitor cells. To study the protective effect of shikonin on auditory nerve damage, we isolated spiral ganglion neuron cells (SGNs) and spiral ganglion Schwann cells (SGSs) that provide nutrients *in vitro* and pretreated them with shikonin. We found that shikonin can reduce ouabain, a drug that can selectively destroy SGNs and induce auditory nerve damage, caused SGNs proliferation decreased, neurite outgrowth inhibition, cells apoptosis and mitochondrial depolarization. In addition, we found that shikonin can increase the expression of Nrf2 and its downstream molecules HO-1 and NQO1, thereby enhancing the antioxidant capacity of SGNs and SGSs, promoting cells proliferation, and inhibiting cells apoptosis by activating the Nrf2/antioxidant response elements (ARE) signal pathway. However, knockdown of Nrf2 rescued the protective effect of shikonin on SGNs and SGSs damage. In addition, we injected shikonin pretreatment into mouse that ouabain-induced hearing loss and found that shikonin pretreatment has a defensive effect on auditory nerve damage. In summary, the results of this study indicate that shikonin could attenuate the level of oxidative stress in SGNs and SGSs through the Nrf2-ARE signaling pathway activated, induce the proliferation and differentiation of SGNs, and thereby improve the neurological hearing damage in mice. Therefore, shikonin may be a candidate therapeutic drug for endogenous antioxidants that can be used to treat neurological deafness.

Keywords: shikonin, spiral ganglion cells, auditory nerve damage, Nrf2-ARE, ouabain

INTRODUCTION

Sensorineural hearing loss is a sensorineural disorder that affects human physical and mental health and quality of life. The pathological feature of sensorineural hearing loss is corti organ dysfunction (Chen et al., 2021; Fu et al., 2021a; He Z. H. et al., 2021) and spiral ganglion neuron degeneration subsequently (White et al., 2000; Liu et al., 2019a). Spiral Ganglion Neuron (SGN), as the first afferent neuron in the auditory pathway, transmits mechanical sound signals received from the outside world from hair cells to cochlear sensory neurons for processing, thereby establishing the bridge between physics and perceptual world of sound (Reijntjes and Pyott, 2016; Tan et al., 2019; Wei et al., 2021). Drugs, noise, and hypoxia can easily cause SGN damage (Guo et al., 2021a; Liu et al., 2021), which can lead to hearing loss, age-related hearing loss and even auditory neuropathy (Waqas et al., 2017; Liu et al., 2019b). Studies have shown that because SGNs cannot regenerate, the loss of cochlear signals can lead to irreversible hearing damage (Liu et al., 2019a; Ding et al., 2020). Thus, recently many studies have focusd on the regeneration of SGN via neural stem cells (Guo et al., 2021b; He Z. et al., 2021). Spiral ganglion Schwann cells (SGSs) are glial cells responsible for myelination in the peripheral nervous system (Wise et al., 2017; Meas et al., 2018). When the spiral ganglion cells are damaged, it can provide the spiral ganglion cells with the nutrient factors needed for growth, help the damaged neurons to repair, and promote the growth of neurites (Wang et al., 2009; Provenzano et al., 2011). The existence of SGSs can greatly improve the survival rate of SGNs and the repair ability of neurons (Pettingill et al., 2008; Provenzano et al., 2011; Lei and Tang, 2017). Therefore, Schwann cells play an irreplaceable role in the development of the cochlear nervous system, especially in the recovery and protection of the damaged nervous system.

Exogenous factors such as ototoxic drugs and noise can induce SGNs oxidative stress and mitochondrial dysfunction, resulting in abnormal SGNs proliferation and differentiation, apoptosis or programed cells death (He et al., 2016; Sun et al., 2016). These cellular processes and the resulting SGNs dysfunction and degradation are the most important causes of hearing loss. The loss of function and neurological degeneration of SGN impairs the transmission of nerve signals that carry sound information. The use of therapeutic drugs with ototoxic side effects, such as aminoglycoside antibiotics (Selimoglu, 2007), ouabain (Zhang et al., 2017), and cisplatin (Liu et al., 2019b), can cause the damage or loss of mammalian SGNs, which can lead to permanent deafness. Ototoxic drugs can cause cochlear neurons to produce reactive oxygen species (ROS), which promotes cell apoptosis in turn (Tabuchi et al., 2011). The oxidative stress response in SGNs is triggered by oxidative imbalance, which leads to oxidative damage, which in turn causes hearing loss (Kim et al., 2020). Currently, cochlear implants can be used to restore the hearing of patients with severe sensorineural hearing loss (Buchman et al., 2020). The survival and protection of SGNs are necessary for cochlear implantation and patient hearing recovery (Guo R. et al., 2019; Guo et al., 2021c). SGSs can proliferate during neuronal regeneration after injury, and their cellular proliferation, differentiation, and myelination depend on interactions with axons (Kobayashi et al., 2012). The identification of signals that mediate SGN-SGS cells interactions is relevant not only to normal auditory nerve development, but also to its maintenance and possible repair (Castelnovo et al., 2017). If the degradation of SGNs can be slowed, the effect of cochlear implants will be further optimized. Therefore, preventing or reducing the damage and degeneration of cochlear SGN is essential for the recovery of sensorineural hearing loss.

Noise-induced hearing loss, ototoxic drugs, and age-related factors are always related to the increase in autophagy and oxidative stress in the mouse cochlea SGN, which ultimately leads to SGN cell apoptosis (Fu et al., 2021b; Zhang et al., 2021). Studies have shown that antioxidant drugs can reduce SGN loss and hearing damage, indicating that the oxidative stress level of SGN can affect hearing status (Guo et al., 2021a). Shikonin is the main component of the extract of the Chinese herbal medicine comfrey. It has anti-bacterial, anti-tumor, anti-oxidation, anti-inflammatory, and anti-apoptosis effect (Gwon et al., 2020; Wang et al., 2020; Zhou et al., 2020). Research data has shown that shikonin induces antioxidants and protects cells from oxidative stress by reducing the level of free radicals and cytotoxic substances in cell (Guo H. et al., 2019; Gwon et al., 2020). Recently, studies have shown that shikonin has neuroprotective activity against traumatic or ischemic neuronal damage regulated by oxidative stress and apoptosis pathways (Wang et al., 2010). Previous studies have also proved that shikonin can reduce spinal cord ischemia-reperfusion injury by improving the level of mitochondrial oxidative stress (Wang et al., 2010). However, there is no report on the anti-apoptosis and antioxidant effects of shikonin on SGNs caused by ototoxic drugs.

Nrf2 is a redox-sensitive transcription factor that plays a key role in the regulation of oxidative stress (Ma, 2013). Under oxidative stress conditions, Nrf2 accumulates in the nucleus and activates the expression of antioxidant response elements (ARE) dependent genes, including heme oxygenase 1 (HO-1), superoxide dismutase (SOD), and peroxidase, catalase (CAT), glutathione synthase (GS), glutathione reductase (GR), glutathione peroxidase (GPX) and glutathione-*S*-transferase (GST) (Albarakati et al., 2020). It is reported that age-related hearing loss is accelerated in SOD1 knockout mice, and SOD1 knockout mice are more prone to hearing loss when affected by noise (Ohlemiller et al., 1999). Tempol (a SOD simulator) can prevent noise from causing damage to hearing (Minami et al., 2007). In addition, HO1 can also effectively protect the inner ear from damage caused by oxidative stress (Kim et al., 2006). There is enhanced evidence that the regulation of the Nrf2/ARE signaling pathway plays an important role in neurological deafness.

In this study, we used the ototoxic drug ouabain to establish a mouse model of neurological deafness and observe the damage to the hearing and SGCs of the mice. To find the pathogenic mechanism of ouabain's ototoxicity, we isolated and cultured mouse SGNs and SGSs *in vitro* and detected that ouabain inhibits SGNs proliferation and neurite growth, and promotes cell mitochondrial depolarization. The increase in the level of oxidative stress in SGNs eventually leads to an increase in the level of cell apoptosis, which in turn leads to the occurrence of

neurological deafness. Shikonin, the main component of comfrey extract, can activate the Nrf2/ARE signaling pathway, thereby alleviating ouabain-induced increase in the level of oxidative stress in SGNs, cells apoptosis and hearing loss in mice. It provides a new choice of antioxidant drugs for the treatment of neurological deafness.

MATERIALS AND METHODS

Animals

All animal experiments were approved by the Ethics Committee of Shandong Provincial Hospital Affiliated to Shandong First Medical University Permit Number: No.2020-422 and were performed in accordance with the relevant guidelines and regulations. Keep animals in a controlled environment with constant temperature and humidity, and provide enough sterile food and water.

Reagants

Ouabain (Cat. No. S4016) was obtained from Selleck. Shikonin (Cat. No. 517-89-5) and ML385 (Cat. No. 846557-71-9) were purchased from Merck (Billerica, United States). Rabbit polyclonal anti-Nrf2 antibody (Cat. No. sc-173), anti-NeuN (Cat. No. ab177487), anti-Tuj1 (Cat. No. ab52623) and anti-Nestin (Cat. No. ab254048) was from Abcam (Cambridge, United Kingdom). Rabbit polyclonal anti-LC3B antibody (Cat. No. A19665), anti-Bax (Cat. No.A19684), anti-Casepase3 (Cat. No. A11319) and anti-Actin (Cat. No. AC026) was from Abclonal (Wuhan, China), and rabbit polyclonal anti-Bcl2 antibody (Cat. No. 12789-1-AP) and anti-SQSTM1 antibody (Cat. No. 18420-1-AP), was from Proteintech (Wuhan, China). The primary mouse anti-S100 antibody (Cat. No. S2532) obtained from Sigma (St. Louis, United States). Rabbit monoclonal anti-VGLUT1 (Cat. No. #12331), anti-GAT1 (Cat. No. #37342) was from Cell Signaling Technology (Boston, MA, United States). Mouse polyclonal anti-HO-1 antibody (Cat. No. 66743-1-Ig) and anti-NQO1 antibody (Cat. No. 67240-1-Ig) was from Proteintech (Wuhan, China).

Primary Explants and Cells Isolation Culture of Mouse Cochlear Spiral Ganglion

Decapitated inner cochlea of P3 C57BL/6 J WT mice and placed in pre-cooled PBS. Then, the volute, spiral ligament and stria vascularis are removed. Finally, the removed spiral ganglion tissue explant was placed on a glass cover slip, which was pre-coated with CellTaK (Corning, Cat. No.354240). Add DMEM/F12 (Gibco, 11,330,032), which contains epithelial growth factor (EGF, 20 ng/ml), N2 additives (Gibco, catalog number 17502-048) and 1% ampicillin (Sigma-Aldrich, St. Louis, United States) in the petri dish. We then obtain spiral ganglion cells. After the cells were cultured for 48 h, 10 μM cytarabine was added for treatment, and then the cells were replaced with a medium without N2 and serum, and the culture was continued to obtain Schwann cells. After the cells were cultured for 48 h, 10 μM cytarabine was added for treatment, and then the cells were replaced with a medium without N2 and serum, and the culture was continued to obtain Schwann cells.

Transfer the dissected spiral ganglion explants into a sterile tube equipped with pre-cooled D-hanks. After washing twice with D-hanks, add a digestion solution containing 0.25% trypsin and 0.001% DNase. After digestion in a 37°C incubator for 20 min, add a serum-containing medium to terminate the digestion, gently pipette to form single cells, inoculate them into a culture dish containing the above medium, and cultivate in a 37°C and 5% CO_2 incubator.

In vivo Drug Treatments

All mouse experiments were performed using 8-month-old female C57BL/6 WT mice *in vitro*. As stated in the text: ouabain (3 mM) was injected for 5 consecutive days, recovered for 3 days, and then injected for 5 consecutive days; Shikonin (10 mM) was injected 3 days in advance for pretreatment, and ML385(30 mg/Kg) was injected 1 day before for pretreatment; Control mice were replaced with the same dose of saline at the same time point.

Apoptosis and Cell Cycle Analysis

The cell cycle and apoptosis were analyzed by flow cytometry. PI staining assesses cell cycle distribution. Seed the cells in a 6-well tissue culture plate (40,0000 cells/well). After 24 h of culture, drugs were added for another 24 h, and the cells were collected and added RNase A solution, incubate the cells at 37°C. Finally, add 400 μL of PI and incubate at room temperature for 30 min. The DNA content was detected by flow cytometry, and the percentage of cells in G1, S, and G2/M phases was analyzed.

According to the manufacturer's instructions, the AnnexinV-FITC/PI apoptosis detection kit was used to evaluate the apoptosis rate. After cells treatment, the cells were collected in binding buffer. Then, Annexin V-FITC and PI were added and incubated at room temperature in the dark. The level of apoptosis was analyzed by flow cytometry.

Oxidative Stress Level Detection

Spiral ganglion neuron cells were inoculated into a 6-well tissue culture plate (40,0000 cells/well), after 24 h of culture, drugs were added for another 24 h. According to the manufacturer's instructions, use a reactive oxygen detection kit (Cat. No. S0033S, Beyotime) to detect ROS levels, a total SOD activity detection kit (WST-8 method, Cat. No. S0101S, Beyotime) to detect SOD levels, and Lipid Peroxidation (MDA) Assay Kit (Cat. No. K739-100, Biovision) detects MDA levels, and total glutathione (GSH) detection kit (Cat. No. S0052, Beyotime) detects GSH levels.

Auditory Brainstem Response Measurements

The hearing status of mice was detected by the auditory brainstem response (ABR) threshold. In brief, animal were anesthetized with pentobarbital intraperitoneal injection (8.4 mg/100 g). Place the mouse on a constant temperature pad and keep the body temperature at 37°C. Insert electrodes on the top, subcutaneously at the outer auricle, and back of the mouse's

skull. RZ6 workstation and BioSig software (Tucker-Davis Technologies, Inc., Alachua, FL, United States) were used for ABR data collection and generation. At each sound level, 512 responses are sampled and averaged. The minimum detectable threshold of all ABR waves is determined by gradually reducing the stimulus intensity from 90 dB SPL to 10 dB SPL, so as to obtain the ABR threshold of each animal.

Transfection and Gene Expression Silencing

Small hairpin RNA (shRNA) was used to silence Nrf2 gene expression. Nrf2 siRNAs were obtained from Invitrogen (Nrf2-si-1: siRNA ID 68238; Nrf2-si-2: siRNA ID 156499; and Nrf2-si-3: siRNA ID 156501). For effective gene silencing, siRNAs were transfected twice. In short, according to the manufacturer's instructions, use jetPRIME® Transfection Agent (Polyplus) to transfect cells with 30 nM negative control (NC) siRNA and Nrf2-siRNA. After 24 h of incubation, a second transfection was performed.

Cell Proliferation Assay

MTT assay was performed to measure the cell proliferation. Spiral ganglion cells were seeded in a 96-well plate at 10,000 cells/well in five replicates. After 24 h, the cells were pretreated with DHC and SHI for 2 h, and then added with ouabain for another 22 h. Then discard the supernatant and replace with fresh serum-free medium. According to the instructions of the MTT Proliferation Assay Kit (ab211091), add MTT to the cell culture medium and incubate it in a 37°C incubator. Subsequently, MTT solvent was added to the cell culture medium, and the 96-well plate was shaken for 5 min in the dark, and the absorbance was read at OD = 570 nm, and then the cell proliferation was evaluated.

Analysis of Mitochondrial Membrane Potential

JC-1 assay kit (C2006, Beyotime) was used for JC-1 analysis according to the manufacturer's instructions. Brief, the cultured cells were washed once with PBS, and then fresh cell culture medium was added. Add an equal volume of JC-1 staining working solution to the culture solution, mix well, put it into the cell culture incubator, and incubate at 37°C for 20 min. Then discard the supernatant and wash twice with JC-1 staining buffer. Collect the processed cells, and then use the flow cytometer to detect and analyze.

Immunofluorescence

The spiral ganglion primary tissues or cells were cultured on glass coverslips coated with gelatin and incubated at 37°C for 24 h, and then treated with ouabain for another 24 h. The cell supernatant was discarded and washed twice with PBS, then fixed with 4% paraformaldehyde (PFA) for 15 min, and then washed with PBS. After permeating the cell membrane with 0.2% TritonX-100, it was blocked with goat serum. Add the primary antibody and incubate overnight at 4°C. The next day, the corresponding fluorescent secondary antibody was added, and after incubating for 1 h at room temperature, the nuclei were stained with DAPI (Gen-View Scientific Inc., Galveston, TX, United States) and mounted. Finally, the cells were imaged and observed using an upright fluorescent confocal microscope (LSM 700, Zeiss). The measurement of nerve cell dendrites is the straight-line distance from the center of the nerve cell body to the tip of the longest dendrite.

Quantitative Real-Time Polymerase Chain Reaction

RNeasy Micro Kits (Qiagen) was used to extract total RNA from mouse spiral ganglion cells or tissues according to the manufacturer's instructions. Subsequently, reverse transcription was performed using a reverse transcription kit (Invitrogen), and the cDNA obtained by reverse transcription was used as a template to perform real-time quantitative PCR using the SYBR® Premix Ex Taq^{TM} system (Perfect Real Time, Thermo Fisher Scientific, Waltham, MA, United States). The primer sequences used in the study are shown in **Table 1**. In order to obtain the best sensitivity and specificity, the PCR reaction set is set to: The initial cycle of 95°C for 30 s, followed by 40 cycles of 95°C for 5 s, 58°C for 20 s, and the final cycle is 95°C for 15 s, 62°C for 1 min, and 95°C for 15 s. The negative control is a sample without template and processed in the same procedure. All reactions were performed in triplicate. Melting curve analysis was used to verify the specificity of amplification. The relative expression of mRNA of each gene was calculated by the $2^{-\Delta\Delta CT}$ method.

Western Blotting

Dissect mouse spiral ganglion tissue or cultured cells, wash with pre-cooled PBS, add RIPA lysis buffer containing protease inhibitor Cocktail (Merck, Millipore 539131-1VL), and lyse on ice. After centrifugation at 4°C, the supernatant was collected and the protein concentration was determined with the BCA Protein Assay Kit (P0011, Beyotime). Add protein loading buffer for sample preparation, then perform polyacrylamide gel electrophoresis (PAGE), and transfer the protein to PVDF membrane. After blocking with skimmed milk powder, add the corresponding primary antibody and incubate overnight

TABLE 1 | Sequences of primers used for quantitative real-time polymerase chain reaction (qRT-PCR).

Gene	Sense primer	Anti-sense primer	Lengths
Nrf2	5′-ATTCTGCTTTCATAG CAGAG -3′	5′-ACTCGTGTTCAGTGA AATG -3′	196 bp
HO-1	5′-TACCTGGGTGACCT CTCA-3′	5′-ATAGAGCTGTTTGA ACTT-3′	138 bp
NQO1	5′-TAAGGAAGGACGCC TGAG-3′	5′-AGCAGTCTCTCAAAC-3′	134 bp
VGLUT1	5′-TTGGCTTTGCCATTG TGGC-3′	5′-GACTCCGTTCTAA GGGA-3′	173 bp
GAT1	5′-TTGGACTGGAAAG GTGGT-3′	5′-ACAGCTTTCGGAAGTT-3′	136 bp
β-*actin*	5′-CTCCATCCTGGCCTCG CTGT-3′	5′-GCTGTCACCTTCACCG TTCC-3′	268 bp

at 4°C. The next day, add the corresponding secondary antibody and incubate at room temperature for 1 h. The signal band was then detected by the chemiluminescent detection method (Amersham ECL).

Statistical Analysis

In the statistical analysis of the data, GraphPad Prism9 software was used. All data are shown as the mean ± SD (standard error of the mean) from at least 3 independently performed experiments, and '*n*' represents the number of samples. A two-tailed unfit Student's *t*-test was used to determine statistical significance of two sets of data. For statistical analysis of multiple sets of data, two-way analysis of variance and post-event Student–Newman–Keuls test are used for significance analysis. And $P < 0.05$ is considered statistically significant.

RESULTS

Ouabain Damages the Hearing of Mice and Activates Spiral Ganglion Schwann Cells Apoptosis and Autophagy

To evaluate the damage effect of ouabain on the hearing of mice, we used different concentrations of ouabain to continuously inject 8-week-old C57BL/6 mice for 5 days, and detect the changes in the hearing threshold of the mice on the 7th day. Zhang et al. (2017) showed that ouabain was dose-dependent on spiral ganglion neurons and Schwann cells in mice, and the optimal dose ranged from 0.5 mM to 3. Therefore, we chose 0–3 mM ouabain to stimulate spiral ganglion neurons and Schwann cells in mice. The hearing brainstem response (ABR) results of mice showed that with the increase of ouabain concentration, the hearing threshold of mice gradually increased (**Figures 1A,B**). Ouabain has obvious damage to the hearing of mice.

The existence of SGSs is essential to the maintenance of SGNs function, and studies have shown that SGN dysfunction and degeneration are the most important causes of hearing loss (Chai et al., 2017). In order to observe the damage effect of ouabain on mouse spiral ganglion tissue, we dissect and culture SGSs explants from P3 newborn mice *in vivo*, then treat them with different concentrations of ouabain. Considering that cells cultured *in vitro* are more sensitive to drugs than *in vivo*, the concentration of drug treatment is reduced accordingly. S100 is highly expressed in mature Schwann cells (Fregoso and Hoover, 2012), so we labeled Schwann cells with S100. Immunofluorescence results showed that, compared with the control group, as the concentration of ouabain increased, the SGSs explants gradually appeared cell death, and the morphological damage was gradually serious (**Figure 1C**). Subsequently, we examined the changes in the level of apoptosis in mouse SGSs explants. The expression of apoptosis marker proteins Caspase 3 and Bax was significantly increased, while the expression of anti-apoptotic protein Bcl-2 was significantly decreased (**Figures 1D,E**). In addition, the autophagy marker proteins LC3B and SQSTM were also tested, and the results showed that the level of autophagy was also significantly increased (**Figures 1D,E**). The above results suggest that ouabain can cause hearing damage in mice, and spiral ganglion damage plays an important role in this process.

Ouabain Affects the Differentiation of Spiral Ganglion Neuron Cells Into Glutamatergic and GABAergic Neuronal Groups

In order to observe the effect of ouabain on the cell morphology of spiral ganglion cells (SGNs) more clearly, we separated spiral ganglion cells by enzymatic hydrolysis and performed immunofluorescence staining with NeuN, a specific marker for screening and identifying neurons (Duan et al., 2016). The results showed that with the increase of ouabain concentration, SGNs cells gradually changed from elongated to elliptical, and the synapse length was significantly shortened (**Figures 2A,B**). Furthermore, the cellular viability of SGNs decreased and the level of apoptosis increased with increasing ouabain concentration (**Figure 2C** and **Supplementary Figure 1**). Glutamatergic and GABAergic neurons in the cochlear nerve cells secrete excitatory and inhibitory neurotransmitters, respectively, to regulate the transmission of nerve impulses in the cochlea. We tried to explore the effect of ouabain on the transmission of nerve impulses in SGNs by detecting the effect of ouabain on the differentiation of glutamatergic and GABAergic neurons. Western blot results showed that the addition of ouabain inhibited the expression of glutamate transporter 1 (VGLUT1) and promoted the expression of GAT1 protein (GABAergic neurons) (**Figures 2D–F**). The rate of VGLUT1 positive cells was also significantly lower than that of GAT1 positive cells (**Figures 2G,H**). The above results suggest that ouabain can damage the morphology and differentiation of spiral ganglia and inhibit neuronal excitation.

Shikonin Can Relieve Ouabain's Damage to the Growth and Proliferation of Spiral Ganglion Schwann Cells

Shikonin is an extract component of comfrey (**Figure 3G**). A large number of studies have shown that shikonin has obvious anti-inflammatory, anti-oxidant and anti-apoptotic effects. We tried to explore whether shikonin has a protective effect on cell death caused by ouabain. We pretreated the SGSs explants with ouabain with a gradient concentration of shikonin, and then observed the cell morphology. Immunofluorescence results showed that as the concentration of shikonin increased, the cell damage of SGSs explants was reduced after ouabain treatment. However, when the concentration of shikonin exceeded a certain limit, the protective effect on the cells gradually disappeared (**Figure 3A**). We speculate that the effect of shikonin may be bifacial, with low concentrations promoting cell survival and high concentrations inhibiting cell growth. In this regard, we isolated SGNs to detect the effect of different concentrations of shikonin on cell survival and growth. In addition to NeuN, we used Nestin, a neural stem cell marker specifically expressed in adult mammalian neural stem cells known to support mitotic activity (Ernst and Christie, 2006), to co-identify and label spiral ganglion cells (**Figure 3B**). Subsequently, the cell viability, cell

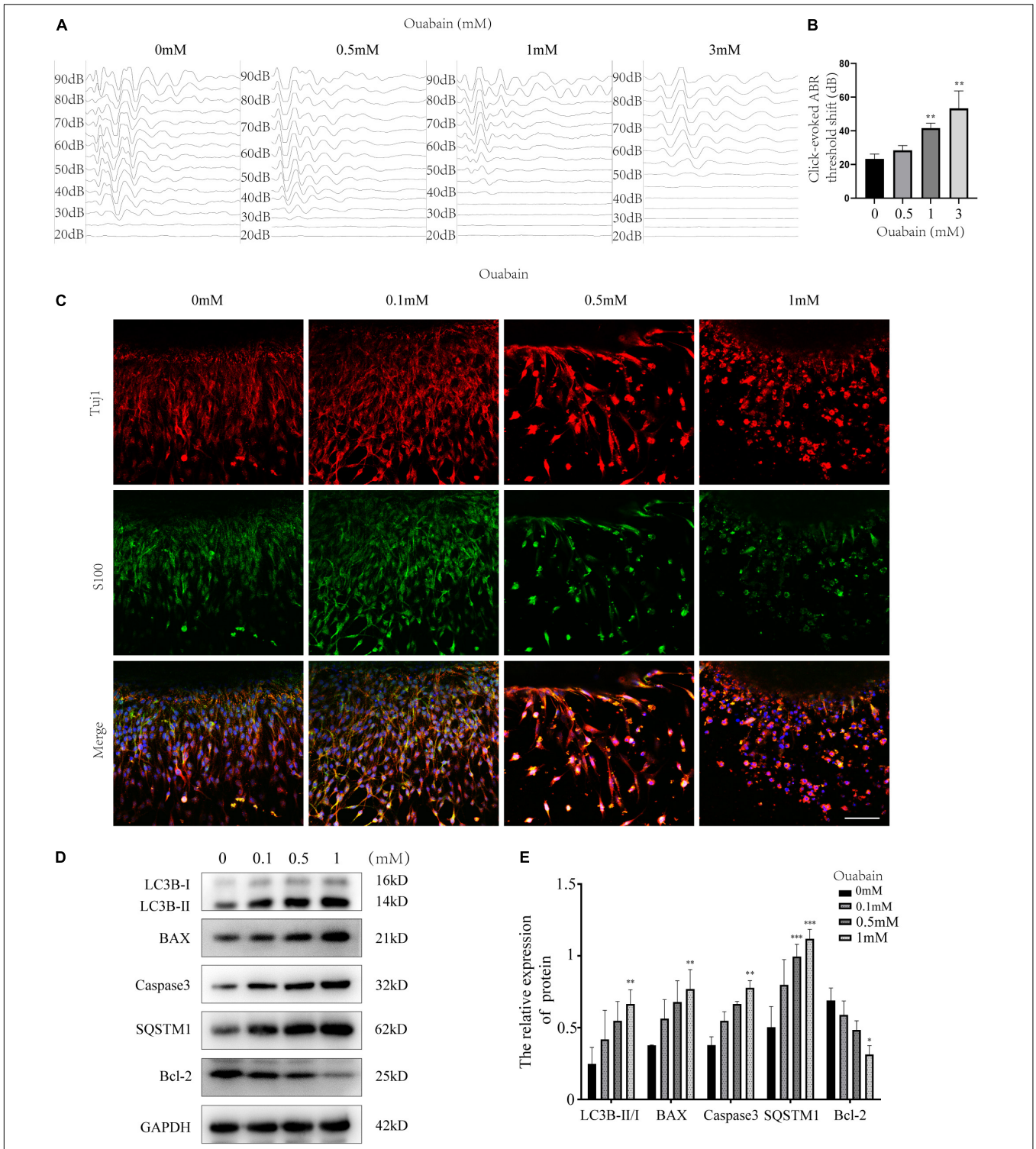

FIGURE 1 | Ouabain damages the hearing of mice and activates SGSs apoptosis and autophagy. **(A)** Ouabain drugs of different concentrations (0.5, 1.0, and 3 mM) were treated for 7 days, and the auditory brainstem response waveforms of the mice were detected ($n = 3$). In the control group, the mice were injected with the same dose of saline. **(B)** Statistical histogram of mouse hearing threshold. **(C)** Immunofluorescence observed the changes in cell morphology of SGSs explants treated with different concentrations of ouabain (0.1, 0.5, and 1 mM) for 24 h. Red fluorescence represents Tuj1 staining, green fluorescence represents S100 staining, and blue fluorescence represents nuclear (DAPI) staining, bar = 50 μm. **(D)** After SGNs were treated with different concentrations of ouabain drugs (0.1, 0.5, and 1 mM) for 24 h, cell proteins were collected, and Western Blot was used to detect cell apoptosis and autophagy protein level changes. **(E)** Statistical histogram of relative protein expression levels. $^{*}P < 0.05$, $^{**}P < 0.01$, $^{***}P < 0.001$.

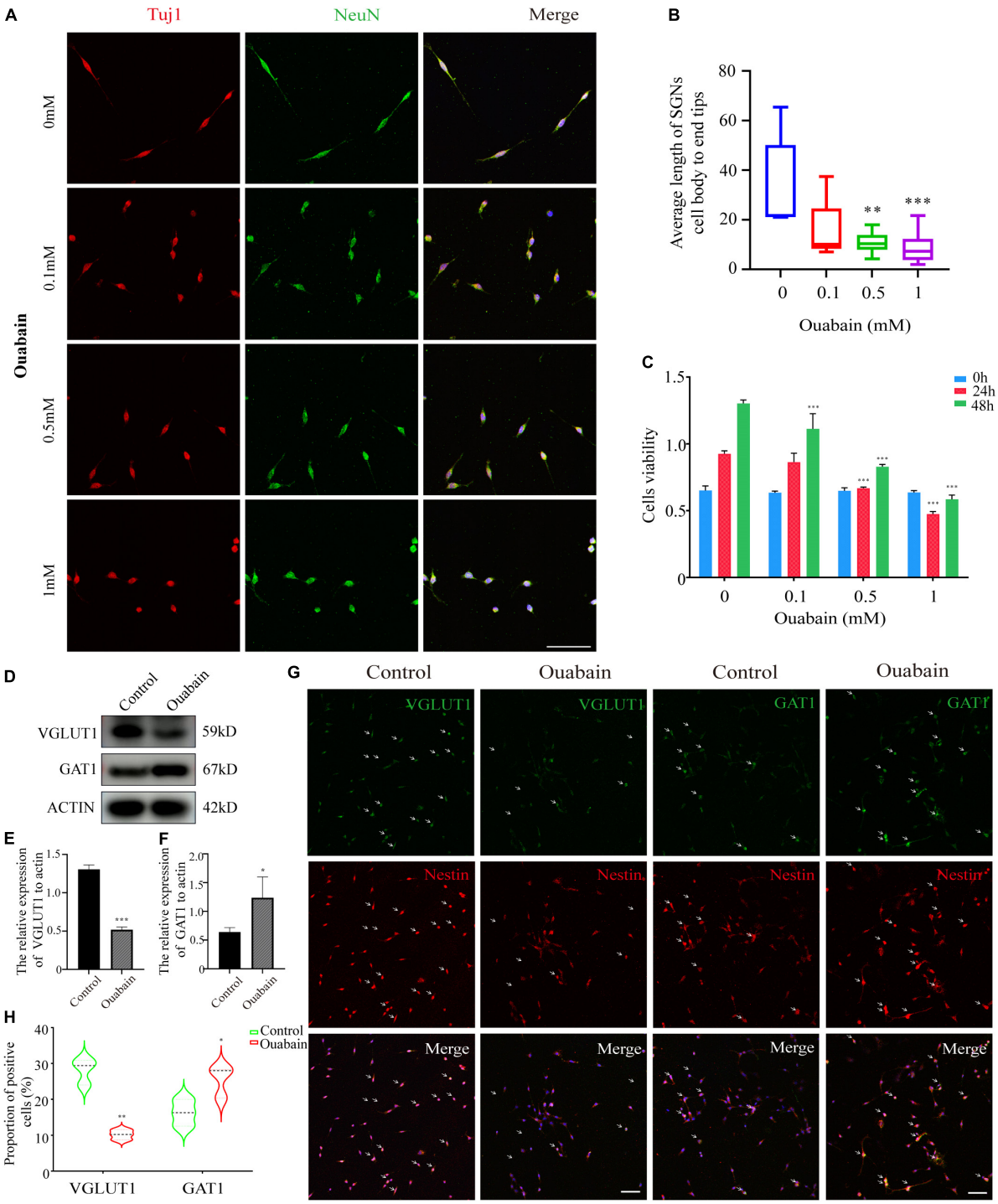

FIGURE 2 | Ouabain affects the differentiation of SGNs into glutamatergic and GABAergic neuronal groups. **(A)** After separating the SGNs, they were treated with different concentrations of ouabain (0.5, 1.0, and 3 mM) for 24 h, and the cell morphology changes were observed by immunofluorescence. Red represents Tuj1 staining, green fluorescence represents NeuN staining, blue fluorescence represents nuclear (DAPI) staining, bar = 50 μm. **(B)** Statistics of the average length of SGNs cell body to the apex of the longer synapse after treatment with different concentrations of ouabain. **(C)** Cell viability (0, 24, and 48 h) after treatment with different concentrations of ouabain was detected by MTT. **(D)** The expression of VGLUT1 and GAT1 proteins was detected after 24 h of treatment with 0.5 mM ouabain. **(E)** Statistical histogram of relative expression of VGLUT1 protein. **(F)** Statistical histogram of the relative expression of GAT1 protein. **(G)** Immunofluorescence observation of the number of VGLUT1 and GAT1 positive cells after ouabain treatment. Red fluorescence represents Nestin staining, green fluorescence represents VGLUT1 or GAT1 staining, blue fluorescence represents nuclear (DAPI) staining, white arrows represent positive cells, bar = 50 μm. **(H)** Statistical histogram of the proportion of VGLUT1 and GAT1 positive cells. $^{*}P < 0.05$, $^{**}P < 0.01$, $^{***}P < 0.001$.

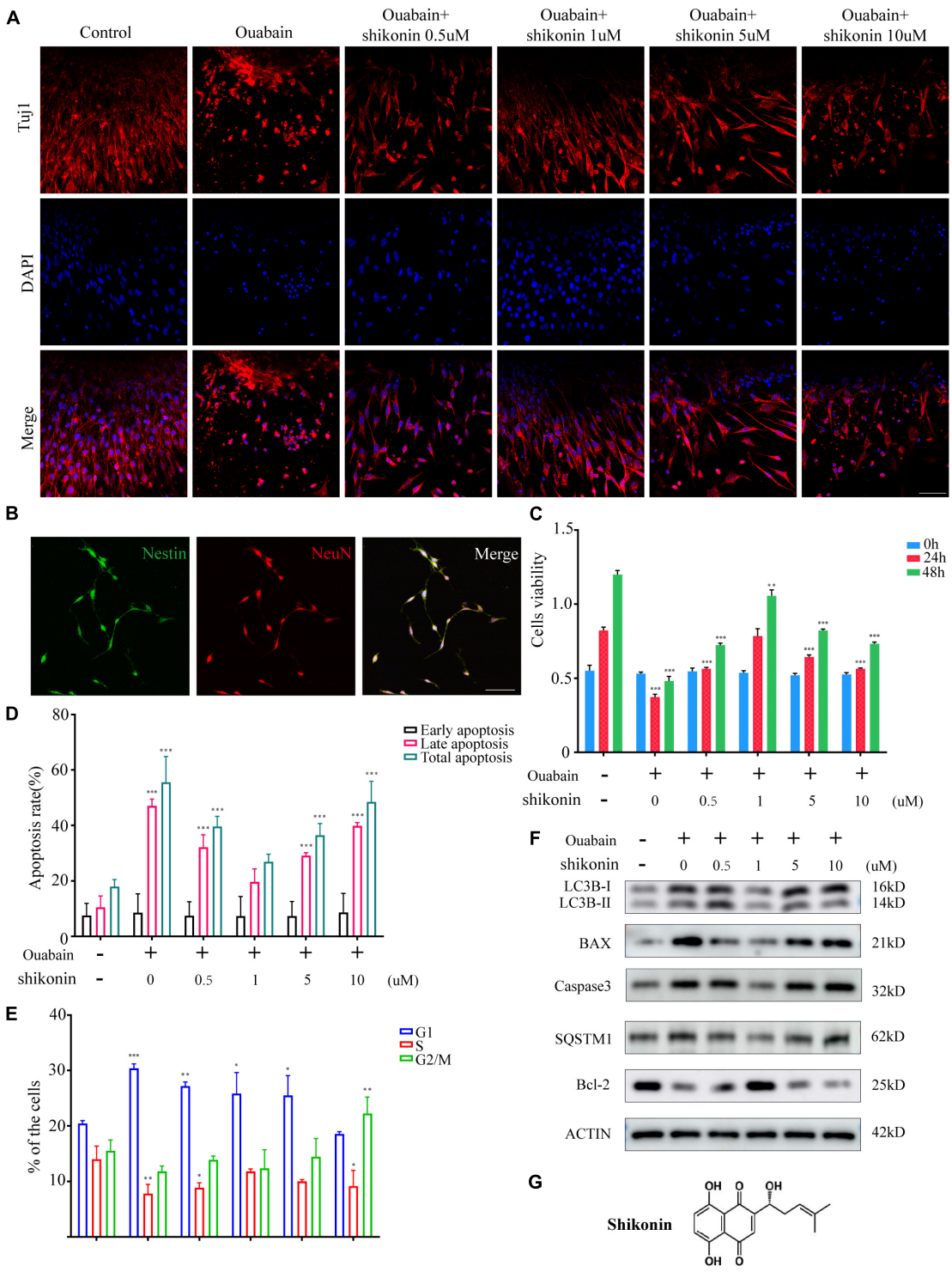

FIGURE 3 | Shikonin can relieve ouabain's damage to the growth and proliferation of SGNs and SGSs. After pretreatment of SGSs explants with different concentrations of shikonin (0.5, 1, 5, and 10 μM) for 2 h, 0.5 mM ouabain continued treatment for another 22 h. **(A)** The morphology of SGSs was observed by immunofluorescence. Red fluorescence represents Tuj1 staining, blue fluorescence represents nuclear (DAPI) staining, bar = 50 μm. **(B)** Nestin and NeuN perform nerve cell labeling. Among them, red represents NeuN staining, green fluorescence represents Nestin staining, and blue fluorescence represents nuclear (DAPI) staining, bar = 50 μm. **(C)** After treatment with shikonin and ouabain, cell viability detection (0, 24, and 48 h). Flow cytometry was used to detect the changes of apoptosis **(D)** and cell cycle **(E)** after treatment with shikonin and ouabain. **(F)** The effects of shikonin pretreatment on apoptosis and autophagy were detected by Western blot. **(G)** Structural diagram of shikonin. $^{*}P < 0.05$, $^{**}P < 0.01$, $^{***}P < 0.001$.

cycle and apoptosis of SGNs stimulated by ouabain pretreated with different concentrations of shikonin were tested. The results showed that compared with the pretreatment group without shikonin, shikonin at a concentration of 1 μM can increase the cell activity and cell cycle of SGNs inhibited by ouabain, and increase the proportion of S-phase cells (**Figures 3C,E**). At the same time, it reduces the proportion of late apoptotic cells (**Figure 3D**), and had a protective effect on ouabain-induced apoptosis of SGNs (**Figure 3F**). The above results suggest that shikonin has a significant protective effect on SGNs cell damage stimulated by ouabain. However, the shikonin concentration has the most obvious protective effect on ouabain damage when appropriate, and the cytoprotective effect of ouabain is reduced when the concentration is lower or too high.

Shikonin Can Rescue the Effect of Ouabain on the Differentiation of Spiral Ganglion Neuron Cells

Next, in order to explore whether shikonin can alleviate the suppression of nerve impulse transmission in SGNs caused by ouabain, we measured the changes in the dendritic length of SGNs and the distribution of cell differentiation populations after shikonin treatment. The results showed that compared with the non-pretreatment group with shikonin, shikonin can significantly reduce the length damage of SGNs dendrites caused by ouabain, and can better maintain the cell morphology of SGNs (**Figures 4A,B**). In addition, shikonin pretreatment can significantly improve the decrease of VGLUT1 expression and the increase of GAT1 expression caused by ouabain, promote the differentiation of glutamatergic neurons, and relieve the inhibition of neuronal excitability caused by ouabain (**Figures 4C,D**). However, the effects of shikonin above also have the same dose-dependent effect.

Nrf2/Antioxidant Response Elements Signaling Pathway Inhibited by Ouabain Can Be Activated by Shikonin, Reducing Oxidative Stress in Spiral Ganglion Neuron Cells

More and more evidences show that reactive oxygen species (ROS) are involved in the pathogenesis of multiple cochlear injuries, especially the apoptosis of SGNs induced by reactive oxygen species (Xiong et al., 2011; Zhuang et al., 2018). The protection of neurons from oxidative damage depends on the up-regulation of antioxidant response mediated by Nrf2/ARE. The redox-sensitive transcription factor Nrf2 and the anti-oxidant ARE response element dependent genes (GST, HO-1, SOD, etc.) play a vital role in the regulation of oxidative stress in cochlear SGNs. We detected the expression of Nrf2 and downstream HO-1 and NQO1 in SGSs after ouabain treatment. The results showed that ouabain treatment significantly inhibited the expression of Nrf2, HO-1 and NQO1 in SGSs, and was time-dependent (**Figures 5A–C**). However, we found that the addition of shikonin pretreatment can alleviate the inhibition of Nrf2/ARE signal pathway activity caused by ouabain, and significantly increase the expression of Nrf2 (**Figure 6A**). Subsequently, we tested the changes in mitochondrial membrane potential and oxidative stress levels. The results show that ouabain promotes the depolarization of mitochondrial membrane potential, while shikonin can significantly alleviate the sharp increase in mitochondrial depolarization caused by ouabain (**Figures 6B,C**). In addition, shikonin pretreatment can also significantly reduce the high levels of reactive oxygen species (ROS) and malondialdehyde (MDA) in SGNs caused by ouabain, and increase the levels of superoxide dismutase (SOD) and reduced glutathione (GSH) expression and secretion (**Figure 6D**). Therefore, shikonin may activate the Nrf2-ARE signal pathway inhibited by ouabain, thereby reducing the oxidative stress level of SGNs.

Knockdown of Nrf2 Reduces the Protective Effect of Shikonin on Spiral Ganglion Neuron Cells Differentiation

Next, to explore the role of Nrf2/ARE signal pathway in the function of SGNs, we used specific small interfering RNA to knock down the expression of Nrf2 in SGNs. According to the knockout efficiency of small interfering RNA (**Figures 7A,B**), we choose siNrf2-2 for follow-up experiments. The results of the study show that knockdown of Nrf2 will significantly affect the expression of downstream factors HO-1 and NQO1 (**Figures 7C,E**). More importantly, the mitigation effect of shikonin on the inhibition of Nrf2, HO-1 and NQO1 expression caused by ouabain will also be lost due to the knockdown of Nrf2 (**Figures 7C,E**). In addition, the knockdown of Nrf2 will also hinder the regulation of shikonin on the differentiation of SGNs after ouabain injury. The suppression of VGLUT1 expression and the increase of GAT expression caused by ouabain improved by shikonin are lost (**Figures 7D,E**). The above results indicate that Nrf2 plays an irreplaceable role in the protection and regulation of shikonin on the function of SGNs.

Shikonin Has Protective Effects on Ouabain-Induced Hearing Damage in Mice

Considering that small interfering RNA transfection in mice *in vitro* has low efficiency and difficult operation, we choose Nrf2/ARE signaling pathway inhibitor ML385 to inhibit the activity of Nrf2/ARE signaling pathway in mice. ML385 can directly interact with Nrf2 protein and bind to the Neh1 binding region of Nrf2, thus preventing the binding of Nrf2-Mafg complex to the promoter ARE sequence and reducing transcriptional activity (Singh et al., 2016). Shikonin, inhibitors and ouabain need to be treated multiple times. In order to prevent multiple surgical damages from affecting the hearing and life status of mice, we chose intraperitoneal injection. The mouse hearing damage model and the time point of drug pretreatment are shown in **Figure 8A**. The control group was replaced by injection of the same amount of drug solvent. We tested the hearing changes of mice at 7, 14, and 30 days after drug injection. The results showed that the hearing loss of mice in the shikonin pretreatment group was significantly

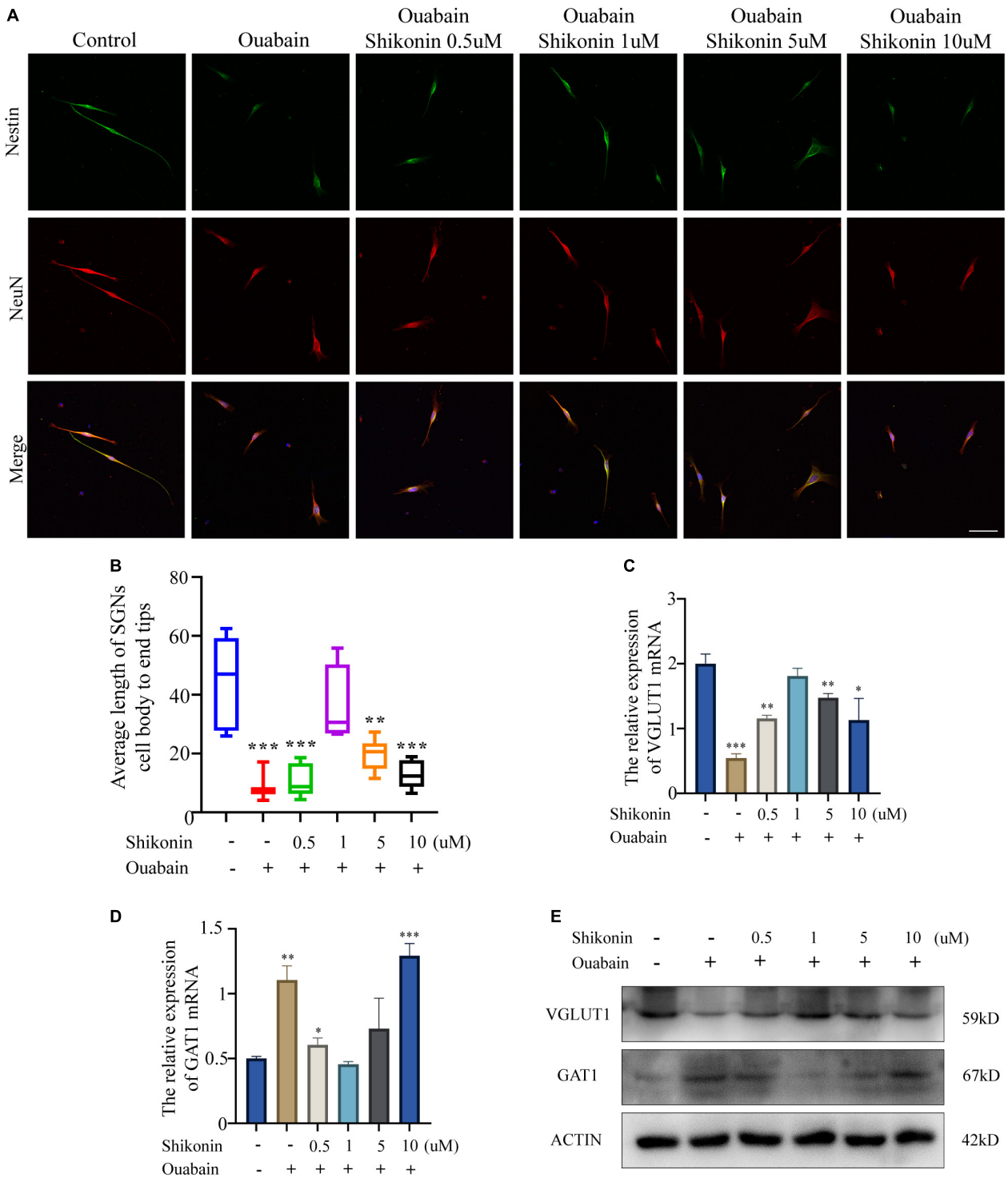

FIGURE 4 | Shikonin can rescue the effect of ouabain on the differentiation of SGNs. After pretreatment of SGNs with different concentrations of shikonin (0.5, 1, 5, and 10 μM) to separate the cells for 2 h, 0.5 mM ouabain continued treatment for another 22 h. **(A)** The morphology of SGNs was observed by immunofluorescence. Red represents NeuN staining, green fluorescence represents Nestin staining, blue fluorescence represents nuclear (DAPI) staining, bar = 50 μm. **(B)** Statistics of the average length of SGNs from the cell body to the apex of the longer synapse in different treatment groups. After collecting cells in different treatment groups, RNA was extracted, and the relative mRNA expression levels of VGLUT1 **(C)** and GAT1 **(D)** were detected by qPCR, and β-antin was used as an internal reference gene. **(E)** The cells of different treatment groups were subjected to protein extraction to detect the expression of VGLUT1 and GAT1 proteins. $^{*}P < 0.05$, $^{**}P < 0.01$, $^{***}P < 0.001$.

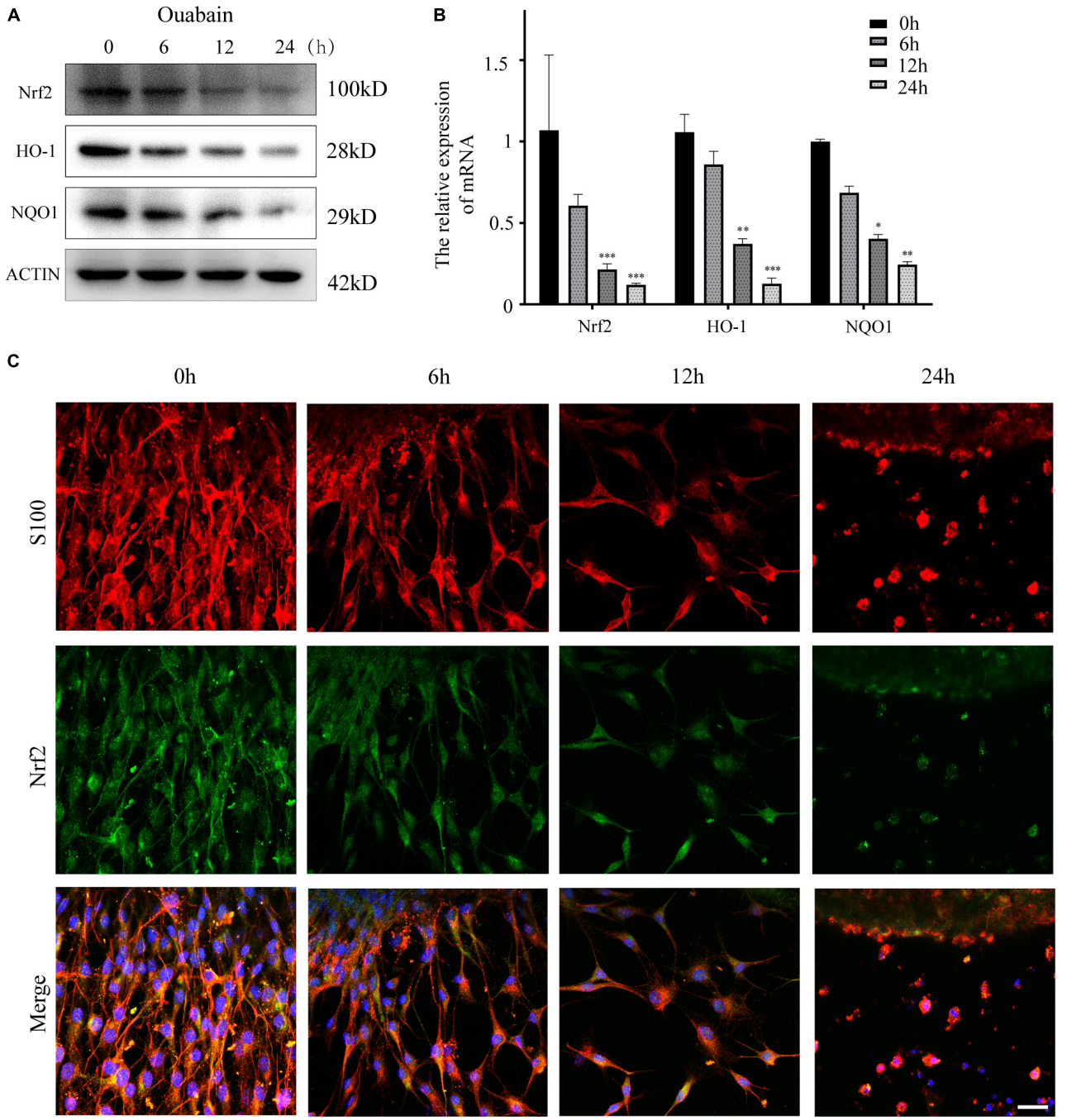

FIGURE 5 | Shikonin can activate the Nrf2/ARE signaling pathway inhibited by ouabain in SGSs. **(A)** After 0.5 mM ouabain was treated with SGSs explants for different times, cell proteins were collected and the protein expression changes of Nrf2/ARE signaling pathway proteins (Nrf2, HO-1 and NQO1) were detected. **(B)** Extract the RNA of each group of cells, and detect the relative expression of Nrf2, HO-1 and NQO1 mRNA by qPCR. **(C)** Immunofluorescence staining to detect the protein expression of Nrf2 after ouabain treatment. Among them, red represents S100 staining, green fluorescence represents Nrf2 staining, blue fluorescence represents nuclear (DAPI) staining, bar = 50 μm. $^{*}P < 0.05$, $^{**}P < 0.01$, $^{***}P < 0.001$.

less than that of the mice without shikonin pretreatment, and Nrf2/ARE signaling pathway inhibitor ML385 pretreatment will greatly reduce the protective effect of shikonin on the hearing of mice (**Figure 8B**). Subsequently, we detected the expression of Nrf2/ARE signaling pathway proteins in mouse cochlea SGNs. The results showed that the expression of Nrf2, HO-1 and NQO1 in mouse cochlea SGNs in the ouabain treatment group was significantly reduced. Shikonin pretreatment can alleviate the ouabain-induced Inhibition of Nrf2/ARE signaling pathway protein expression (**Figures 8C,E**). The expression of VGLUT1

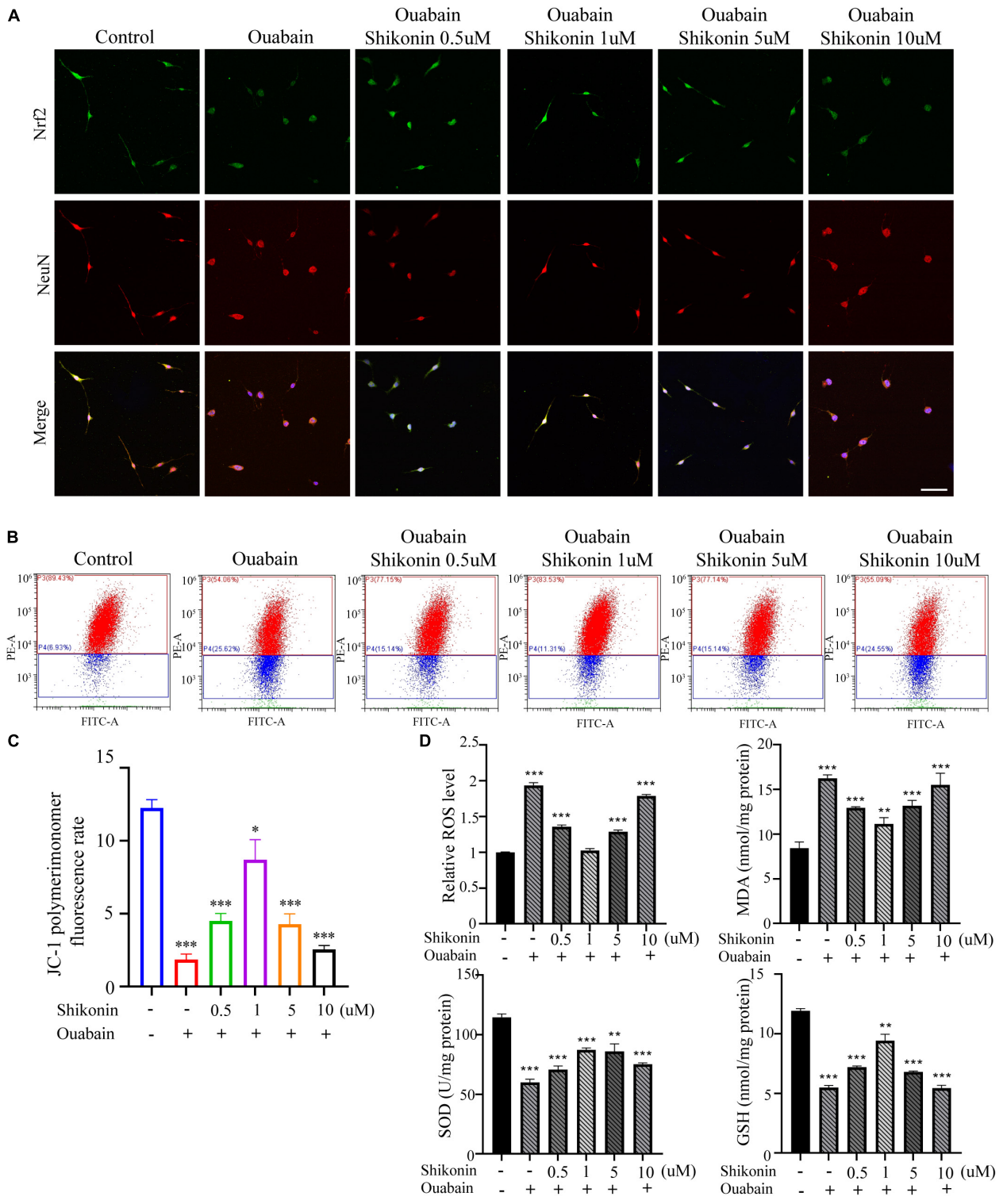

FIGURE 6 | Shikonin can reduce the oxidative stress level of SGNs caused by ouabain. After pretreatment of SGNs with different concentrations of shikonin (0.5, 1, 5, and 10 μM) to separate the cells for 2 h, 0.5 mM ouabain continued treatment for another 22 h. **(A)** After treatment, the morphology of SGNs cells and the expression of Nrf2 protein were observed. Among them, red represents NeuN staining, green fluorescence represents Nrf2 staining, blue fluorescence represents nuclear (DAPI) staining, bar = 50 μm. **(B)** The level of mitochondrial depolarization was measured by flow cytometry to detect the JC-1 polymer/monomer fluorescence ratio. Red represents the fluorescence ratio of JC-1 polymer, and blue represents the fluorescence ratio of JC-1 monomer. **(C)** Different treatment groups, JC-1 red fluorescence/green fluorescence ratio statistical histogram. **(D)** Detection of secretion levels of oxidative factors ROS and MDA and antioxidant factors SOD and GSH in cells of different treatment groups. $^{*}P < 0.05$, $^{**}P < 0.01$, $^{***}P < 0.001$.

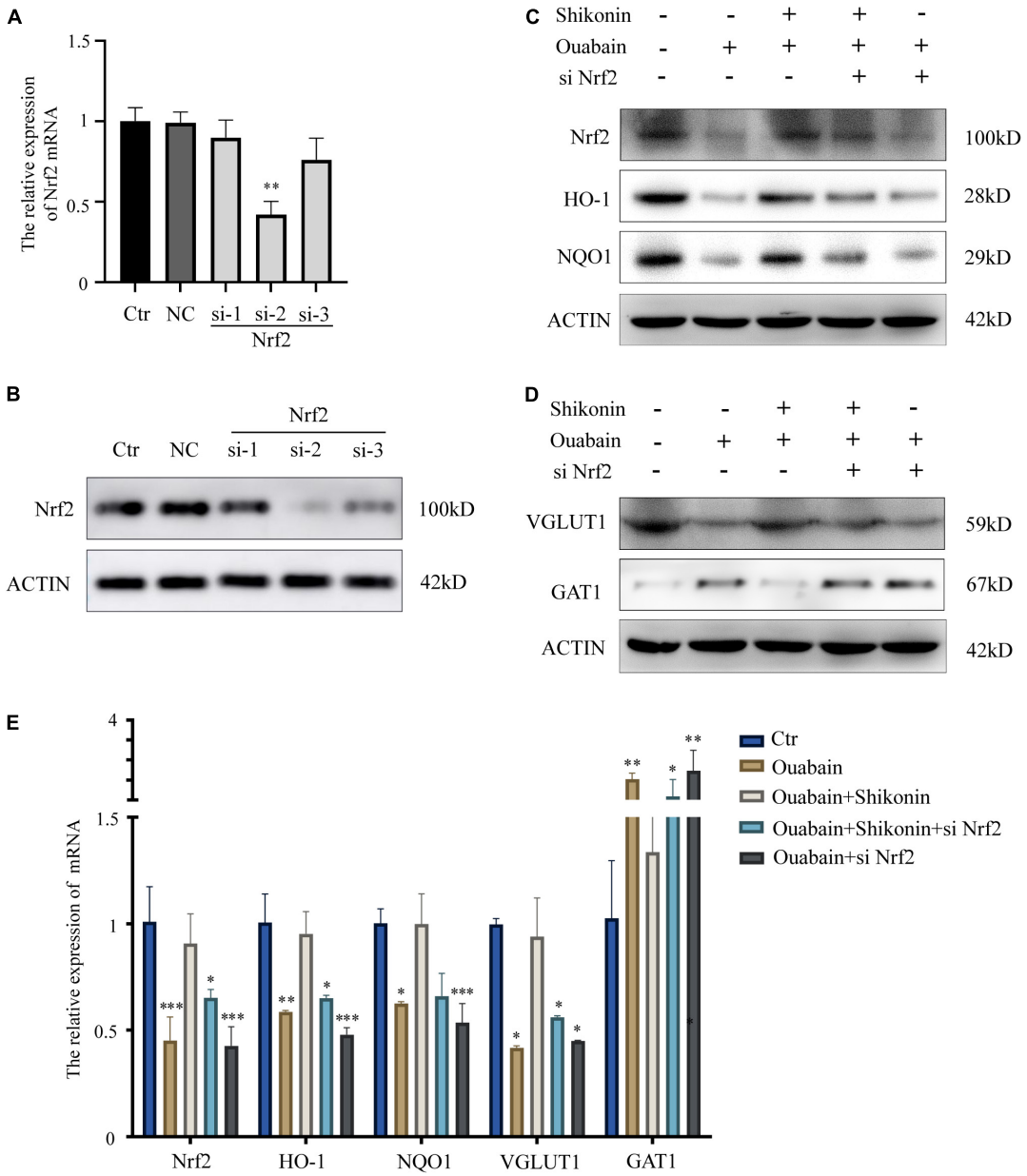

FIGURE 7 | Knockdown of Nrf2 reduces the protective effect of shikonin on SGNs differentiation. **(A)** The specificity and efficiency of siRNA against Nrf2 were tested by quantitative PCR. **(B)** The knockout efficiency of Nrf2 siRNA was detected at the protein level by Western blot. SGNs were transfected with Nrf2 siRNA for 24 h, pretreated with shikonin, and then treated with ouabain for another 22 h. To detect the expression changes of Nrf2/ARE signal pathway (Nrf2, HO-1, and NQO1) protein **(C)** and mRNA **(E)** in SGNs. As well as the protein **(D)** and mRNA **(E)** expression changes of glutamatergic neurons VGLUT1 and GABAergic neurons GAT1. $^{*}P < 0.05$, $^{**}P < 0.01$, $^{***}P < 0.001$.

in the cochlea SGNs of mice in the ouabain treatment group was significantly reduced, and the expression of GAT1 was significantly increased. Shikonin pretreatment can significantly improve the differentiation imbalance of glutamatergic and GABAergic neurons in SGNs caused by ouabain (**Figures 8D,E**). In addition, the inhibition of the Nrf2/ARE signaling pathway will weaken the regulation of shikonin on the expression of differentiation proteins in mouse SGNs (**Figures 8D,E**). In summary, shikonin has a protective effect on ouabain-induced hearing damage in mice, and this protective effect depends on the activation of the Nrf2/ARE signaling pathway.

DISCUSSION

The spiral ganglion (SGN) is the first transfer station in the cochlear auditory pathway. It converts the external sound mechanical stimulus received by the hair cells into electrical

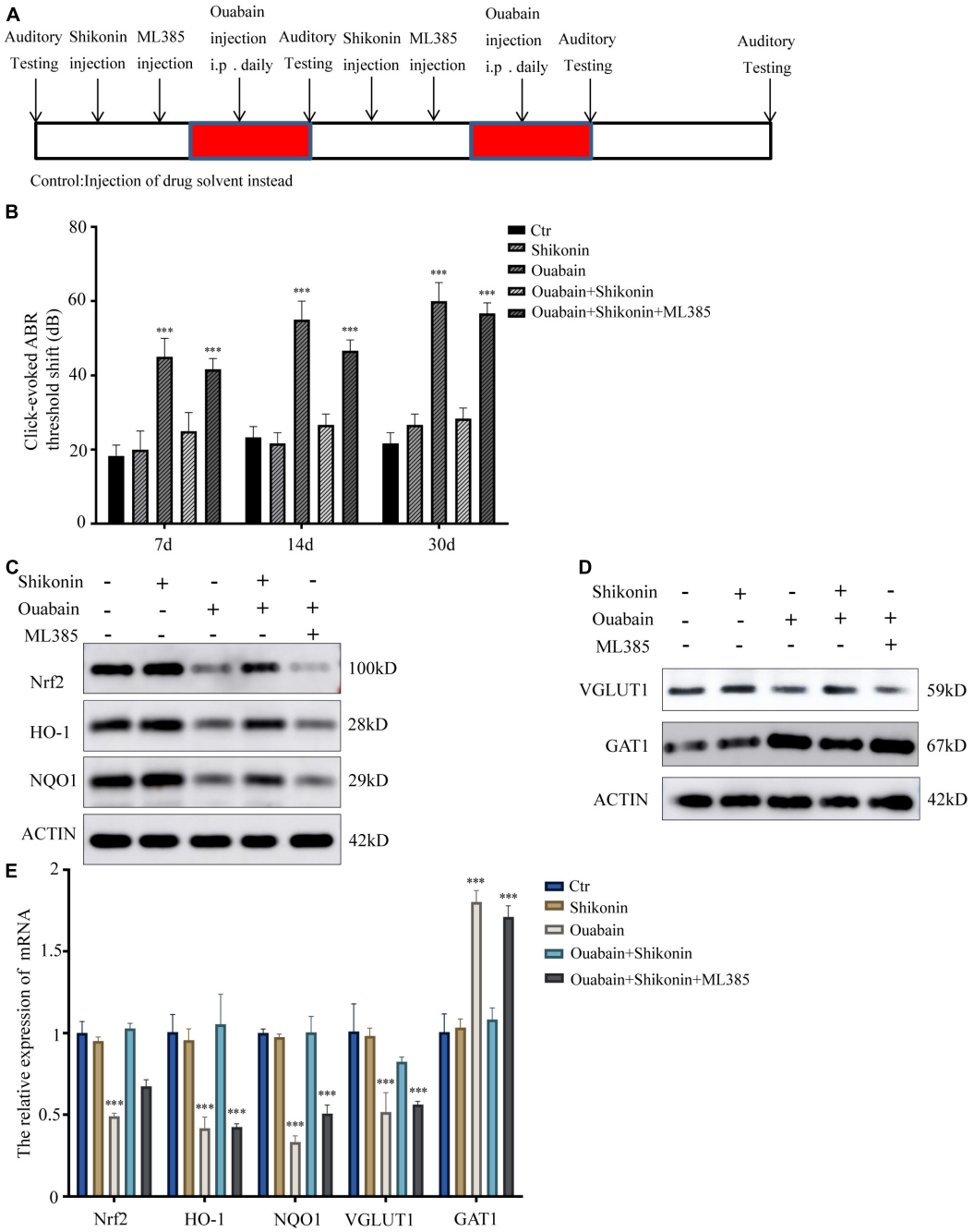

FIGURE 8 | Shikonin has protective effects on ouabain-induced hearing damage in mice. **(A)** Experimental procedure of drug injection in mice. The arrow represents the drug injection point. The red bars represent the time period of continuous drug injection. The mice in the control group were injected with the same amount of normal saline or drug solvent at the same time point. **(B)** The statistical histogram of the hearing brainstem response of mice at 7, 14, and 30 days after drug injection ($n = 3$). After 14 days of drug treatment, detect the expression of Nrf2/ARE signal pathway (Nrf2, HO-1, and NQO1) protein **(C)** and mRNA **(E)** in mouse SGN tissue protein. And detect the protein **(D)** and mRNA **(E)** expressions of glutamatergic neurons VGLUT1 and GABAergic neurons GAT1. $^{***}P < 0.001$.

signals, and then transmits them to the auditory center of the brain, completing the conversion of sound from the physical world into the perceptual world (Reijntjes and Pyott, 2016). The survival of spiral ganglion Schwann cells (SGSs) has attracted more and more attention of researchers due to the protective effect of the secreted factors on spiral ganglia. At present, the degeneration and death of SGN in the inner ear mainly include primary neurodegeneration and secondary neurodegeneration (the consequence of loss of hair cells) (Kujawa and Liberman, 2015; Guo J. et al., 2019). Due to the

stimulation of ototoxic drugs, SGNs and SGSs in the cochlea gradually undergo morphological changes after being injured, including axons retreat, auditory nerve endings degenerate into neuron cell bodies, and finally neurons die. Schwann cells myelinize the peripheral processes, the initial part of the central axon, and the neuronal cell bodies of spiral ganglion neurons (SGNs) (Rangaraju et al., 2009), and the development, maintenance and regeneration of peripheral nerves involve dynamic interactions between neurons and Schwann cells (Sugiura and Lin, 2011). The search for drugs that can alleviate SGNs and SGSs retrograde degeneration caused by ototoxic drugs and lead to cell death is very important for hearing protection.

In clinical drug applications, many drugs have greatly limited their clinical applications due to ototoxic side effects (such as ouabain, cisplatin, etc.) (Liu et al., 2016; He et al., 2017), and many researchers have tried to reduce their ototoxicity (Gao et al., 2019; Zhang et al., 2019). Ouabain is a cardiac glycoside that can block the activity of Na+/K+-ATPase through specific binding (Lelkes, 2020). Studies have shown that ouabain can specifically damage SGNs when acting on the round window of the cochlea, but has little effect on the morphology and function of sensory epithelial hair cells and stria vascularis cells. Therefore, this study established a mouse model of neurological deafness with ouabain. In this study, we chose to inject ouabain through the intraperitoneal cavity of the mouse instead of directly administering the mouse by opening the round window in the ear to establish a mouse model of deafness. On the one hand, considering that the pretreatment of therapeutic drugs requires multiple administrations, the increased frequency of operations will have a greater impact on the survival of mice; On the other hand, it is more suitable to establish a non-acute deafness model and make the deafness model more stable. Another advantage is that the operation is simple and easy. Our research results show that ouabain can significantly increase the hearing threshold of mouse ABR and significantly damage the morphology of SGSs (**Figure 1**).

In the cochlea, the balance maintenance of inhibitory and excitatory neurotransmitters is one of the key regulatory factors for the physiological functions of the cochlea. Neurons in the cochlea can be divided into glutamatergic neurons and GABAergic neurons according to the neurotransmitters they produce (Wang et al., 2015; Huang et al., 2019). Among them, glutamatergic neurons produce excitatory neurotransmitters, and GABAergic neurons inhibit glutamatergic impulses (Huang et al., 2018). Our research results show that ouabain inhibits the differentiation of neurons into glutamatergic neurons, promotes the differentiation of GABAergic neurons, reduces the generation of excitatory nerve impulses, and reduces the sensitivity of the cochlea to sound stimulation (**Figure 2**). Ouabain affects VGLUT1 and GAT1 expression through regulation of neural cell differentiation but not cell proliferation.

Considering that the death of mouse cochlea SGSs is often caused by increased levels of autophagy, apoptosis, and oxidative stress. We tested the levels of autophagy and apoptosis in SGSs cells after ouabain treatment, and the results showed that with the gradual increase in the concentration of ouabain treatment, the levels of apoptosis and autophagy in SGSs increased (**Figure 1**). Although there are reports that shikonin is an ideal antioxidant, anti-apoptotic agent, and anti-inflammatory agent, it has not been reported whether shikonin has a protective effect on ototoxicity of drugs (such as ouabain). We speculate that shikonin has a protective effect on SGCs damage. In order to verify our hypothesis, we pretreated with shikonin before ouabain stimulated SGNs or SGSs. The results showed that shikonin pretreatment can significantly increase the survival rate of SGNs and SGSs after ouabain treatment, and reduce the apoptosis, autophagy and oxidative stress levels of SGNs and SGSs (**Figures 3**, **6**). In addition, shikonin pretreatment also improves the potential of SGNs to differentiate into glutamatergic, promotes the generation and transmission of excitatory nerve impulses, and prepares for improving the sensitivity of sound stimulation (**Figure 4**).

Antioxidant drugs can reduce the damage of SGCs and protect SGCs from degeneration. Nrf2 regulates the transcription of genes encoding antioxidants, detoxification enzymes, and other vital factors for cell survival by regulating the antioxidant response element (ARE) (Hoshino et al., 2011). Studies have shown that intraperitoneal injection of rosmarinic acid can activate the Nrf-2/heme oxygenase-1 (HO-1) signaling pathway in the cochlea of rats, thereby reducing the production of superoxide and lipid peroxidation caused by noise (Fetoni et al., 2015). In order to explore whether the increase in oxidative stress levels in degraded SGCs after ouabain treatment is regulated by the Nrf2/ARE signaling pathway, we analyzed the expression of Nrf2, HO-1 and NQO1 after ouabain treatment, which are widely recognized Nrf2/ARE signals Pathway markers. The results showed that ouabain significantly inhibited the activity of the Nrf2/ARE signaling pathway (**Figure 5**), and Shikonin can alleviate ouabain's damage to SGNs through the activation of the Nrf2/ARE signaling pathway (**Figure 6**); Knockdown or inhibition of Nrf2 can hinder the protective effect of shikonin on SGNs damage (**Figures 7**, **8**).

CONCLUSION

To conclude our research, we have proved through *in vitro* and *in vivo* experiments that ouabain can damage the growth and differentiation of SGNs, and promote cell apoptosis by increasing the level of oxidative stress in SGNs and SGSs. As an antioxidant, shikonin has a significant protective effect on ototoxicity caused by ouabain. In the cochlea, SGCs damage is regulated by complex signaling pathways. Shikonin can inhibit the increase of oxidative stress and abnormal cell differentiation caused by ouabain by activating the activity of the Nrf2/ARE signaling pathway. For the protection of ototoxic drugs-induced neurological degeneration of SGCs, shikonin may be a better candidate antioxidant drug.

DATA AVAILABILITY STATEMENT

The original contributions presented in the study are included in the article/**Supplementary Material**, further inquiries can be directed to the corresponding authors.

ETHICS STATEMENT

The animal study was reviewed and approved by the Ethics Committee of the Affiliated Hospital of Shandong First Medical University. Written informed consent was obtained from the owners for the participation of their animals in this study.

AUTHOR CONTRIBUTIONS

HD drafted the important content of the manuscript and explained it, and carried out rigorous conception and design of the subject. XZ, MX, and LS carried out a detailed analysis of the data in the article. YW, NG, and HH carried out the collection of clinical samples. HY, ZT, FZ, and PZ conducted experimental operations. MZ and CL provided the subject ideas and careful proofreading of the manuscript. All authors contributed to the article and approved the submitted version.

FUNDING

This work was supported by the grants from the Medical Science and Technology Innovation Center, Shandong First Medical University and Shandong Academy of Medical Sciences, the National Natural Science Foundation of China (#81770979, #82071035, and #81900922), Natural Science Foundation of Shandong Province (#ZR2019BH019), Shandong Joint Fund (ZR202108050034), and Taishan Scholar Foundation of Shandong Province (#tsqn201812134).

SUPPLEMENTARY MATERIAL

The Supplementary Material for this article can be found online at: https://www.frontiersin.org/articles/10.3389/fnmol.2022.829642/full#supplementary-material

Supplementary Figure 1 | Ouabain can induce autophagy and apoptosis in SGNs cells. Western Blot was used to detect the changes of apoptosis and autophagy protein levels in SGNs after ouabain treatment.

REFERENCES

Albarakati, A. J. A., Baty, R. S., Aljoudi, A. M., Habotta, O. A., Elmahallawy, E. K., Kassab, R. B., et al. (2020). Luteolin protects against lead acetate-induced nephrotoxicity through antioxidant, anti-inflammatory, anti-apoptotic, and Nrf2/HO-1 signaling pathways. *Mol. Biol. Rep.* 47, 2591–2603. doi: 10.1007/s11033-020-05346-1

Buchman, C. A., Gifford, R. H., Haynes, D. S., Lenarz, T., O'Donoghue, G., Adunka, O., et al. (2020). Unilateral cochlear implants for severe, profound, or moderate sloping to profound bilateral sensorineural hearing loss: a systematic review and consensus statements. *JAMA Otolaryngol. Head Neck Surg.* 146, 942–953. doi: 10.1001/jamaoto.2020.0998

Castelnovo, L. F., Bonalume, V., Melfi, S., Ballabio, M., Colleoni, D., and Magnaghi, V. (2017). Schwann cell development, maturation and regeneration: a focus on classic and emerging intracellular signaling pathways. *Neural Regener. Res.* 12, 1013–1023. doi: 10.4103/1673-5374.211172

Chai, R., Li, G. L., Wang, J., and Zou, J. (2017). Hearing loss: reestablish the neural plasticity in regenerated spiral ganglion neurons and sensory hair cells. *Neural Plast.* 2017:1807581.

Chen, Y., Gu, Y., Li, Y., Li, G. L., Chai, R., Li, W., et al. (2021). Generation of mature and functional hair cells by co-expression of Gfi1, Pou4f3, and Atoh1 in the postnatal mouse cochlea. *Cell Rep.* 35:109016. doi: 10.1016/j.celrep.2021.109016

Ding, Y., Meng, W., Kong, W., He, Z., and Chai, R. (2020). The role of FoxG1 in the inner ear. *Front. Cell Dev. Biol.* 8:614954. doi: 10.3389/fcell.2020.614954

Duan, W., Zhang, Y. P., Hou, Z., Huang, C., Zhu, H., Zhang, C. Q., et al. (2016). Novel insights into NeuN: from neuronal marker to splicing regulator. *Mol. Neurobiol.* 53, 1637–1647. doi: 10.1007/s12035-015-9122-5

Ernst, C., and Christie, B. R. (2006). The putative neural stem cell marker, nestin, is expressed in heterogeneous cell types in the adult rat neocortex. *Neuroscience* 138, 183–188. doi: 10.1016/j.neuroscience.2005.10.065

Fetoni, A. R., Paciello, F., Rolesi, R., Eramo, S. L., Mancuso, C., Troiani, D., et al. (2015). Rosmarinic acid up-regulates the noise-activated Nrf2/HO-1 pathway and protects against noise-induced injury in rat cochlea. *Free Radic. Biol. Med.* 85, 269–281. doi: 10.1016/j.freeradbiomed.2015.04.021

Fregoso, S. P., and Hoover, D. B. (2012). Development of cardiac parasympathetic neurons, glial cells, and regional cholinergic innervation of the mouse heart. *Neuroscience* 221, 28–36. doi: 10.1016/j.neuroscience.2012.06.061

Fu, X., An, Y., Wang, H., Li, P., Lin, J., Yuan, J., et al. (2021a). Deficiency of Klc2 induces low-frequency sensorineural hearing loss in C57BL/6 J mice and human. *Mol. Neurobiol.* 58, 4376–4391. doi: 10.1007/s12035-021-02422-w

Fu, X., Wan, P., Li, P., Wang, J., Guo, S., Zhang, Y., et al. (2021b). Mechanism and prevention of ototoxicity induced by aminoglycosides. *Front. Cell. Neurosci.* 15:692762. doi: 10.3389/fncel.2021.692762

Gao, S., Cheng, C., Wang, M., Jiang, P., Zhang, L., Wang, Y., et al. (2019). Blebbistatin inhibits neomycin-induced apoptosis in hair cell-like HEI-OC-1 cells and in cochlear hair cells. *Front. Cell. Neurosci.* 13:590. doi: 10.3389/fncel.2019.00590

Guo, H., Sun, J., Li, D., Hu, Y., Yu, X., Hua, H., et al. (2019). Shikonin attenuates acetaminophen-induced acute liver injury via inhibition of oxidative stress and inflammation. *Biomed. Pharmacother. Biomed. Pharmacother.* 112:108704. doi: 10.1016/j.biopha.2019.108704

Guo, J., Chai, R., Li, H., and Sun, S. (2019). Protection of hair cells from ototoxic drug-induced hearing loss. *Adv. Exp. Med. Biol.* 1130, 17–36. doi: 10.1007/978-981-13-6123-4_2

Guo, L., Cao, W., Niu, Y., He, S., Chai, R., and Yang, J. (2021a). Autophagy regulates the survival of hair cells and spiral ganglion neurons in cases of noise, ototoxic drug, and age-induced sensorineural hearing loss. *Front. Cell. Neurosci.* 15:760422. doi: 10.3389/fncel.2021.760422

Guo, R., Li, J., Chen, C., Xiao, M., Liao, M., Hu, Y., et al. (2021b). Biomimetic 3D bacterial cellulose-graphene foam hybrid scaffold regulates neural stem cell proliferation and differentiation. *Colloids Surf. B Biointerf.* 200:111590. doi: 10.1016/j.colsurfb.2021.111590

Guo, R., Liao, M., Ma, X., Hu, Y., Qian, X., Xiao, M., et al. (2021c). Cochlear implant-based electric-acoustic stimulation modulates neural stem cell-derived neural regeneration. *J. Mater. Chem. B* 9, 7793–7804. doi: 10.1039/d1tb01029h

Guo, R., Ma, X., Liao, M., Liu, Y., Hu, Y., Qian, X., et al. (2019). Development and application of cochlear implant-based electric-acoustic stimulation of spiral ganglion neurons. *ACS Biomater. Sci. Eng.* 5, 6735–6741. doi: 10.1021/acsbiomaterials.9b01265

Gwon, S. Y., Ahn, J., Jung, C. H., Moon, B., and Ha, T. Y. (2020). Shikonin attenuates hepatic steatosis by enhancing beta oxidation and energy expenditure via AMPK activation. *Nutrients* 12:1133. doi: 10.3390/nu12041133

He, Z., Ding, Y., Mu, Y., Xu, X., Kong, W., Chai, R., et al. (2021). Stem cell-based therapies in hearing loss. *Front. Cell Dev. Biol.* 9:730042. doi: 10.3389/fcell.2021.730042

He, Z., Guo, L., Shu, Y., Fang, Q., Zhou, H., Liu, Y., et al. (2017). Autophagy protects auditory hair cells against neomycin-induced damage. *Autophagy* 13, 1884–1904. doi: 10.1080/15548627.2017.1359449

He, Z., Zhang, S., Song, Q., Li, W., Liu, D., Li, H., et al. (2016). The structural development of primary cultured hippocampal neurons on a graphene

substrate. *Colloids Surf. B Biointerf.* 146, 442–451. doi: 10.1016/j.colsurfb.2016.06.045

He, Z. H., Li, M., Fang, Q. J., Liao, F. L., Zou, S. Y., Wu, X., et al. (2021). FOXG1 promotes aging inner ear hair cell survival through activation of the autophagy pathway. *Autophagy* 17, 4341–4362. doi: 10.1080/15548627.2021.1916194

Hoshino, T., Tabuchi, K., Nishimura, B., Tanaka, S., Nakayama, M., Ishii, T., et al. (2011). Protective role of Nrf2 in age-related hearing loss and gentamicin ototoxicity. *Biochem. Biophys. Res. Commun.* 415, 94–98. doi: 10.1016/j.bbrc.2011.10.019

Huang, X., Liu, J., Wu, W., Hu, P., and Wang, Q. (2019). Taurine enhances mouse cochlear neural stem cell transplantation via the cochlear lateral wall for replacement of degenerated spiral ganglion neurons via sonic hedgehog signaling pathway. *Cell Tissue Res.* 378, 49–57. doi: 10.1007/s00441-019-03018-6

Huang, X., Wu, W., Hu, P., and Wang, Q. (2018). Taurine enhances mouse cochlear neural stem cells proliferation and differentiation to sprial gangli through activating sonic hedgehog signaling pathway. *Organogenesis* 14, 147–157. doi: 10.1080/15476278.2018.1477462

Kim, H. J., So, H. S., Lee, J. H., Lee, J. H., Park, C., Park, S. Y., et al. (2006). Heme oxygenase-1 attenuates the cisplatin-induced apoptosis of auditory cells via down-regulation of reactive oxygen species generation. *Free Radic. Biol. Med.* 40, 1810–1819. doi: 10.1016/j.freeradbiomed.2006.01.018

Kim, Y. Y., Chao, J. R., Kim, C., Kim, B., Thi-Thanh Nguyen, P., Jung, H., et al. (2020). Hearing loss through apoptosis of the spiral ganglion neurons in apolipoprotein E knockout mice fed with a western diet. *Biochem. Biophys. Res. Commun.* 523, 692–698. doi: 10.1016/j.bbrc.2019.12.100

Kobayashi, M., Ishibashi, S., Tomimitsu, H., Yokota, T., and Mizusawa, H. (2012). Proliferating immature Schwann cells contribute to nerve regeneration after ischemic peripheral nerve injury. *J. Neuropathol. Exp. Neurol.* 71, 511–519. doi: 10.1097/NEN.0b013e318257fe7b

Kujawa, S. G., and Liberman, M. C. (2015). Synaptopathy in the noise-exposed and aging cochlea: primary neural degeneration in acquired sensorineural hearing loss. *Hear. Res.* 330, 191–199. doi: 10.1016/j.heares.2015.02.009

Lei, L., and Tang, L. (2017). Schwann cells genetically modified to express S100A4 increases GAP43 expression in spiral ganglion neurons in vitro. *Bioengineered* 8, 404–410. doi: 10.1080/21655979.2016.1238534

Lelkes, Z. (2020). Ouabain, a Na-K-ATPase inhibitor, enhances wakefulness in rats. *Neuropharmacology* 176:108224. doi: 10.1016/j.neuropharm.2020.108224

Liu, L., Chen, Y., Qi, J., Zhang, Y., He, Y., Ni, W., et al. (2016). Wnt activation protects against neomycin-induced hair cell damage in the mouse cochlea. *Cell Death Dis.* 7:e2136.

Liu, W., Wang, X., Wang, M., and Wang, H. (2019a). Protection of spiral ganglion neurons and prevention of auditory neuropathy. *Adv. Exp. Med. Biol.* 1130, 93–107. doi: 10.1007/978-981-13-6123-4_6

Liu, W., Xu, X., Fan, Z., Sun, G., Han, Y., Zhang, D., et al. (2019b). Wnt signaling activates TP53-induced glycolysis and apoptosis regulator and protects against cisplatin-induced spiral ganglion neuron damage in the mouse cochlea. *Antioxid. Redox Signal.* 30, 1389–1410. doi: 10.1089/ars.2017.7288

Liu, W., Xu, L., Wang, X., Zhang, D., Sun, G., Wang, M., et al. (2021). PRDX1 activates autophagy via the PTEN-AKT signaling pathway to protect against cisplatin-induced spiral ganglion neuron damage. *Autophagy* 17, 4159–4181. doi: 10.1080/15548627.2021.1905466

Ma, Q. (2013). Role of nrf2 in oxidative stress and toxicity. *Annu. Rev. Pharmacol. Toxicol.* 53, 401–426.

Meas, S. J., Nishimura, K., Scheibinger, M., and Dabdoub, A. (2018). In vitro methods to cultivate spiral ganglion cells, and purification of cellular subtypes for induced neuronal reprogramming. *Front. Neurosci.* 12:822. doi: 10.3389/fnins.2018.00822

Minami, S. B., Yamashita, D., Ogawa, K., Schacht, J., and Miller, J. M. (2007). Creatine and tempol attenuate noise-induced hearing loss. *Brain Res.* 1148, 83–89. doi: 10.1016/j.brainres.2007.02.021

Ohlemiller, K. K., McFadden, S. L., Ding, D. L., Flood, D. G., Reaume, A. G., Hoffman, E. K., et al. (1999). Targeted deletion of the cytosolic Cu/Zn-superoxide dismutase gene (Sod1) increases susceptibility to noise-induced hearing loss. *Audiol. Neuro Otol.* 4, 237–246. doi: 10.1159/000013847

Pettingill, L. N., Minter, R. L., and Shepherd, R. K. (2008). Schwann cells genetically modified to express neurotrophins promote spiral ganglion neuron survival in vitro. *Neuroscience* 152, 821–828. doi: 10.1016/j.neuroscience.2007.11.057

Provenzano, M. J., Minner, S. A., Zander, K., Clark, J. J., Kane, C. J., Green, S. H., et al. (2011). p75(NTR) expression and nuclear localization of p75(NTR) intracellular domain in spiral ganglion Schwann cells following deafness correlate with cell proliferation. *Mol. Cell. Neurosci.* 47, 306–315. doi: 10.1016/j.mcn.2011.05.010

Rangaraju, S., Hankins, D., Madorsky, I., Madorsky, E., Lee, W. H., Carter, C. S., et al. (2009). Molecular architecture of myelinated peripheral nerves is supported by calorie restriction with aging. *Aging cell* 8, 178–191. doi: 10.1111/j.1474-9726.2009.00460.x

Reijntjes, D. O. J., and Pyott, S. J. (2016). The afferent signaling complex: regulation of type I spiral ganglion neuron responses in the auditory periphery. *Hear. Res.* 336, 1–16. doi: 10.1016/j.heares.2016.03.011

Selimoglu, E. (2007). Aminoglycoside-induced ototoxicity. *Curr. Pharm. Des.* 13, 119–126.

Singh, A., Venkannagari, S., Oh, K. H., Zhang, Y. Q., Rohde, J. M., Liu, L., et al. (2016). Small molecule inhibitor of NRF2 selectively intervenes therapeutic resistance in KEAP1-deficient NSCLC tumors. *ACS Chem. Biol.* 11, 3214–3225. doi: 10.1021/acschembio.6b00651

Sugiura, Y., and Lin, W. (2011). Neuron-glia interactions: the roles of Schwann cells in neuromuscular synapse formation and function. *Biosci. Rep.* 31, 295–302. doi: 10.1042/BSR20100107

Sun, G., Liu, W., Fan, Z., Zhang, D., Han, Y., Xu, L., et al. (2016). The three-dimensional culture system with matrigel and neurotrophic factors preserves the structure and function of spiral ganglion neuron in vitro. *Neural Plast.* 2016:4280407. doi: 10.1155/2016/4280407

Tabuchi, K., Nishimura, B., Nakamagoe, M., Hayashi, K., Nakayama, M., and Hara, A. (2011). Ototoxicity: mechanisms of cochlear impairment and its prevention. *Curr. Med. Chem.* 18, 4866–4871. doi: 10.2174/092986711797535254

Tan, F., Chu, C., Qi, J., Li, W., You, D., Li, K., et al. (2019). AAV-ie. *Nat. Commun.* 10:3733. doi: 10.1038/s41467-019-11687-8

Wang, F., Mayca Pozo, F., Tian, D., Geng, X., Yao, X., Zhang, Y., et al. (2020). Shikonin inhibits cancer through P21 upregulation and apoptosis induction. *Front. Pharmacol.* 11:861. doi: 10.3389/fphar.2020.00861

Wang, Q., Zhu, G. H., Xie, D. H., Wu, W. J., and Hu, P. (2015). Taurine enhances excitability of mouse cochlear neural stem cells by selectively promoting differentiation of glutamatergic neurons over GABAergic neurons. *Neurochem. Res.* 40, 924–931. doi: 10.1007/s11064-015-1546-9

Wang, S. J., Furusho, M., D'Sa, C., Kuwada, S., Conti, L., Morest, D. K., et al. (2009). Inactivation of fibroblast growth factor receptor signaling in myelinating glial cells results in significant loss of adult spiral ganglion neurons accompanied by age-related hearing impairment. *J. Neurosci. Res.* 87, 3428–3437. doi: 10.1002/jnr.22164

Wang, Z., Liu, T., Gan, L., Wang, T., Yuan, X., Zhang, B., et al. (2010). Shikonin protects mouse brain against cerebral ischemia/reperfusion injury through its antioxidant activity. *Eur. J. Pharmacol.* 643, 211–217. doi: 10.1016/j.ejphar.2010.06.027

Waqas, M., Sun, S., Xuan, C., Fang, Q., Zhang, X., Islam, I. U., et al. (2017). Bone morphogenetic protein 4 promotes the survival and preserves the structure of flow-sorted Bhlhb5+ cochlear spiral ganglion neurons in vitro. *Sci. Rep.* 7:3506. doi: 10.1038/s41598-017-03810-w

Wei, H., Chen, Z., Hu, Y., Cao, W., Ma, X., Zhang, C., et al. (2021). Topographically conductive butterfly wing substrates for directed spiral ganglion neuron growth. *Small* 17:e2102062. doi: 10.1002/smll.202102062

White, J. A., Burgess, B. J., Hall, R. D., and Nadol, J. B. (2000). Pattern of degeneration of the spiral ganglion cell and its processes in the C57BL/6J mouse. *Hear. Res.* 141, 12–18. doi: 10.1016/s0378-5955(99)00204-x

Wise, A. K., Pujol, R., Landry, T. G., Fallon, J. B., and Shepherd, R. K. (2017). Structural and ultrastructural changes to type I spiral ganglion neurons and schwann cells in the deafened guinea pig cochlea. *J. Assoc. Res. Otolaryngol.* 18, 751–769. doi: 10.1007/s10162-017-0631-y

Xiong, M., He, Q., Lai, H., and Wang, J. (2011). Oxidative stress in spiral ganglion cells of pigmented and albino guinea pigs exposed to impulse noise. *Acta Oto Laryngol.* 131, 914–920. doi: 10.3109/00016489.2011.577448

Zhang, Y., Li, W., He, Z., Wang, Y., Shao, B., Cheng, C., et al. (2019). Pre-treatment with fasudil prevents neomycin-induced hair cell damage by reducing the accumulation of reactive oxygen species. *Front. Mol. Neurosci.* 12:264. doi: 10.3389/fnmol.2019.00264

Zhang, Y., Li, Y., Fu, X., Wang, P., Wang, Q., Meng, W., et al. (2021). The detrimental and beneficial functions of macrophages after cochlear injury. *Front. Cell Dev. Biol.* 9:631904. doi: 10.3389/fcell.2021.631904

Zhang, Z. J., Guan, H. X., Yang, K., Xiao, B. K., Liao, H., Jiang, Y., et al. (2017). Dose-dependent effects of ouabain on spiral ganglion neurons and Schwann cells in mouse cochlea. *Acta Oto Laryngol.* 137, 1017–1023. doi: 10.1080/00016489.2017.1324217

Zhou, L., Wang, J., Zhao, J., Kuai, F., and Yang, H. (2020). Shikonin promotes osteogenesis and suppresses osteoclastogenesis in vitro. *Am. J. Transl. Res.* 12, 8099–8110.

Zhuang, W., Wang, C., Shi, X., Qiu, S., Zhang, S., Xu, B., et al. (2018). MCMV triggers ROS/NLRP3-associated inflammasome activation in the inner ear of mice and cultured spiral ganglion neurons, contributing to sensorineural hearing loss. *Int. J. Mol. Med.* 41, 3448–3456. doi: 10.3892/ijmm.2018.3539

Conflict of Interest: HD was employed by the company Qilu Pharmaceutical Co., Ltd.

The remaining authors declare that the research was conducted in the absence of any commercial or financial relationships that could be construed as a potential conflict of interest.

Publisher's Note: All claims expressed in this article are solely those of the authors and do not necessarily represent those of their affiliated organizations, or those of the publisher, the editors and the reviewers. Any product that may be evaluated in this article, or claim that may be made by its manufacturer, is not guaranteed or endorsed by the publisher.

frontiers in Molecular Neuroscience

ORIGINAL RESEARCH
published: 04 March 2022
doi: 10.3389/fnmol.2022.850035

Autophagy-Mediated Synaptic Refinement and Auditory Neural Pruning Contribute to Ribbon Synaptic Maturity in the Developing Cochlea

Rui Guo[1†], Yice Xu[2†], Wei Xiong[1], Wei Wei[3], Yue Qi[1], Zhengde Du[1], Shusheng Gong[1], Zezhang Tao[4] and Ke Liu[1*]*

[1] Department of Otolaryngology Head and Neck Surgery, Beijing Friendship Hospital, Capital Medical University, Beijing, China, [2] Department of Otolaryngology Head and Neck Surgery, Xiaogan Central Hospital, Wuhan University of Science and Technology, Xiaogan, China, [3] Department of Otology, Shengjing Hospital, China Medical University, Shenyang, China, [4] Department of Otolaryngology Head and Neck Surgery, Renmin Hospital of Wuhan University, Wuhan, China

OPEN ACCESS

Edited by:
Yu Sun,
Huazhong University of Science and Technology, China

Reviewed by:
Renjie Chai,
Southeast University, China
Hao Xiong,
Sun Yat-sen Memorial Hospital, China

***Correspondence:**
Shusheng Gong
gongss@ccmu.edu.cn
Ke Liu
Liuke@ccmu.edu.cn

[†] These authors have contributed equally to this work and share first authorship

Specialty section:
This article was submitted to Molecular Signalling and Pathways, a section of the journal Frontiers in Molecular Neuroscience

Received: 07 January 2022
Accepted: 28 January 2022
Published: 04 March 2022

Citation:
Guo R, Xu Y, Xiong W, Wei W, Qi Y, Du Z, Gong S, Tao Z and Liu K (2022) Autophagy-Mediated Synaptic Refinement and Auditory Neural Pruning Contribute to Ribbon Synaptic Maturity in the Developing Cochlea. Front. Mol. Neurosci. 15:850035. doi: 10.3389/fnmol.2022.850035

In rodents, massive initial synapses are formed in the auditory peripheral nervous system at the early postnatal stage, and one of the major phenomena is that the number of afferent synapses in the cochlea is significantly reduced in the duration of development. This raises the hypothesis that the number of cochlear ribbon synapses are dramatically changed with hearing development and maturation. In this study, several tracers identifying activities of autophagy were applied to estimate the level of autophagy activity in the process of ribbon synapse development in mice; further, changes in the synaptic number and spiral ganglion nerve (SGN) fibers were quantitatively measured. We found robust expression of LC3B and lysosomal-associated membrane protein 1 as well as LysoTracker in or near inner hair cells and cochlear ribbon synapses in the early stage of postnatal development. Moreover, we found a significant loss in the intensity of SGN fibers at ribbon synaptic development and hearing onset. Thus, this study demonstrates that ribbon synaptic refinement and SGN fibers pruning are closely associated with the morphological and functional maturation of ribbon synapses and that synaptic refinement and SGN fiber pruning are regulated by the robust activities of autophagy in the earlier stages of auditory development.

Keywords: auditory development, cochlear ribbon synapses, autophagy, synaptic refinement, neural fibers pruning

INTRODUCTION

Acoustic signals are sensed by cochlear hair cells and transmit information to the central nervous system *via* the spiral ganglion neurons (SGNs) (Liu et al., 2019; Wei et al., 2021). In mammals, this task is accomplished by using several synaptic structures with special features along the hearing pathway (Raphael and Altschuler, 2003; Wichmann and Moser, 2015). Among these synapses, ribbon synapses are the first synaptic structures formed between inner hair cells (IHCs) and SGNs, which have their own morphological and electrophysiological properties, ensuring rapid,

accurate, and reliable signal transmission from the ear to the brain (Fuchs et al., 2003; Wichmann and Moser, 2015). Electron microscopy evidence has shown that a lack of synaptic ribbons can cause a reduction in the compound action potential and sound-evoked firing rates of SGNs (Jean et al., 2018).

Mice are born without hearing and begin to develop auditory capacity approximately 2 weeks after birth (Ehret, 1985; Safieddine et al., 2012). In the developing cochlea, ribbon synapses undergo robust changes both in morphology and function. During the early stage of postnatal development, excess synapses are formed, which are subsequently significantly eliminated to achieve optimal synaptic connectivity (Sobkowicz et al., 1982; Roux et al., 2009; Huang et al., 2012). Furthermore, studies have reported that lysosomal and autophagy activities are remarkably involved and contribute to the pruning of neural fibers (He et al., 2019), and synaptic elimination is a secondary change after axon or fiber pruning (Rowland et al., 2006; Song et al., 2008; Shen and Ganetzky, 2009; Ban et al., 2013; Chen et al., 2013; Xiong et al., 2020a), providing an insight into the possible mechanisms underlying the development and maturation of ribbon synapses in the developing cochlea. Consistently, the ribbon synapses in the developing cochlea were also found to undergo refinement coupled with exocytosis and Ca^{2+} influx (Moser and Beutner, 2000; Beutner and Moser, 2001; Johnson et al., 2005; Beurg et al., 2010; Wong et al., 2014). Our previous study showed that autophagy is required for the remodeling of cochlear ribbon synapses in postnatal mice (Xiong et al., 2020a). Despite this evidence, however, synaptic refinement and SGN fiber pruning have not yet been fully explored; moreover, it is still unclear whether synaptic refinement and SGN fiber pruning are fully mediated *via* dynamic autophagy flux (Ding et al., 2020; Zhou et al., 2020; Fu et al., 2021; Guo et al., 2021). Thus, in this study, we applied multiple markers to trace autophagy flux coupled with synaptic changes in the developing cochlea of mice, and hearing and synaptic function were estimated *via* auditory brainstem response (ABR) threshold detection and wave I amplitude analysis. Our study showed that quantitative reduction and functional facilitation of ribbon synapses, as well as density loss of SGN fibers, are regulated by dynamic autophagy flux, suggesting that both ribbon synaptic refinement and auditory neural fiber pruning are regulated *via* the dynamic activities of autophagy, which plays a key role in the development and construction of cochlear ribbon synapses.

MATERIALS AND METHODS

Animals

Postnatal male C57BL/6J mice with documented at the age of P1, P7, P14, and P28 were purchased from Vital River Laboratory Animal Technology, Beijing, China. A total of 60 animals were used in the experiment. All animal experiments were approved by the Animal Ethics Committee of Capital Medical University. And all the efforts were aimed to minimize animals' suffering and the number of mice which was sacrificed in the experiment.

Drug Administration

3-MA (Millipore, 3089588) was dissolved in 0.9% saline as a stock solution (30 mg/ml) and stored at −20°C. The solution was heated to 60°C to completely dissolved and then cool at room temperature before being used. Experimental mice received intraperitoneal injections of 3-MA at a dose of 30 mg/kg daily from P7 to P14 consecutively, the controls were administered by the same amount of saline.

Auditory Brainstem Responses

Auditory brainstem responses detected auditory function of mice at P1, P7, P14, and P28, respectively. All animals were anesthetized *via* intraperitoneal injection of ketamine (100 mg/kg, Gutian Pharmaceutical Co., Ltd., Fujian, China) plus xylazine (10 mg/kg, Sigma-Aldrich Co., Llc., United States). Needle electrodes were placed subcutaneously beneath the pinna of the test ear (−) and at the vertex (+), with a ground electrode placed in the contralateral ear over neck muscles. ABR threshold was recorded in a double-walled, electrically shielded, and radio frequency-shielded sound booth. ABR stimulus frequencies of 4, 8, 16, and 32 kHz and clicks (100 μs) were tested with System 3 hardware (Tucker Davis Technologies, Alachua, FL, United States) and SigGen/BioSig software (Tucker Davis Technologies). The stimulus level was calibrated and a probe tube microphone was tightly fitted into the external auditory canal. The ABR threshold was obtained for each animal by reducing the stimulus intensity in 10 dB steps and then 5 dB steps to identify the lowest intensity eliciting a response. The ABR threshold was defined as the lowest stimulus intensity that produced reliable and reproducible (in at least two trials) ABR waves. The amplitude of the wave I was identified as the difference between the first peak in the waveform and the baseline.

Immunofluorescence

Mice were sacrificed after anesthesia with xylazine and ketamine (ketamine, 100 mg/kg and xylazine, 10 mg/kg). The acidotropic agent LysoTracker Red DND-99 (LysoT; Molecular Probes) was freshly diluted in growth medium to a final concentration of 100 nM. Cochlear tissues were dissected and preincubated with LysoT for 30 min at 37°C. And the tissues were subsequently harvested and fixed in 4% paraformaldehyde for 1h at room temperature. After fixation, tissues were permeabilized in 30% sucrose for 20 min, blocked in 0.3% TritonX-100 (Sigma, United States) for 30 min and 10% normal goat serum (ZSGB-BIO, China) for 1 h, then incubated overnight at 4°C with primary antibodies including: mouse anti-CtBP2 (1:500, Abcam, ab204663), rabbit anti-LC3B (1:100, CST 3868T), rat anti-lamp1 (1:300, Abcam, ab25245), chicken anti-NF200 (neurofilament 200) antibody (1:600, Chemicon, AB5539). The following day the preparations were washed three times in PBS for 5 min each and incubated with species-appropriate secondary antibodies. All the secondary antibodies were conjugated with Alexa Fluor TM 488, 568 (1:300, Invitrogen/Molecular Probes, Carlsbad, CA, United States catalog number: A21131, A21124). Specimens were subsequently washed three times in PBS and then mounted on glass slides using fluorescent mounting (ZSGB-BIO, ZLI-9557).

Confocal Microscope Imaging

Images were acquired with a 63 oil-immersion, high-resolution confocal microscope (TCS SP8 II; Leica Microsystems, Wetzlar, Germany). Scanning was performed from top to bottom with an interval of 0.35 μm/layer, and images were then superimposed. Specimens were observed using optimal excitation wavelengths of 488 nm (green) and 568 nm (red). DAPI was observed using an optimal excitation wavelength of 358 nm (blue).

Calculation of the Number and Size of Ribbon Synapses

Quantification of LC3B puncta, LAMP1 puncta, LysoT puncta, auditory nerve fibers (ANF) (labeled by anti-NF200) and ribbon synapses (labeled by anti-CtBP2) was performed at P1, P7, P14, and P28, respectively. In addition, ribbon synapses were quantified in the cochlear apex turn, middle turn and basal turn. We selected five samples in each group to calculate the average number of fluorescent puncta per IHC. The areas of presynaptic ribbons were measured in Adobe Photoshop CS6 software by segmenting the synaptic elements from the whole image into a single area then the area of the synapse was obtained by the measurement area tool.

Measurement of the Distance Between Ribbon Synaptic Spots and Nucleus of Inner Hair Cell

The distance from ribbon synapses to nucleus center of IHCs was measured by using the scale tool in Adobe Photoshop CS6 software. In this study, the distance has been defined as the length from the synaptic immunostained spot to the nearest IHC. The actual distance was obtained by conversion with the image scale.

Statistical Analysis

Statistical analysis was performed using GraphPad Prism 8 software (GraphPad Software Inc., La Jolla, CA, United States). Normally distributed continuous variables were presented as means ± standard error of the mean (SEM). Statistical differences between groups in ABR threshold, ABR wave I amplitude, fluorescent puncta (LC3B, LAMP1, LysoT, NF200, and ribbon synapses) per IHC were analyzed using two-way analysis of variance (ANOVA), followed by Bonferroni's multiple comparisons test. $^{*}p < 0.05$, $^{**}p < 0.01$, $^{***}p < 0.001$, and $^{****}p < 0.0001$.

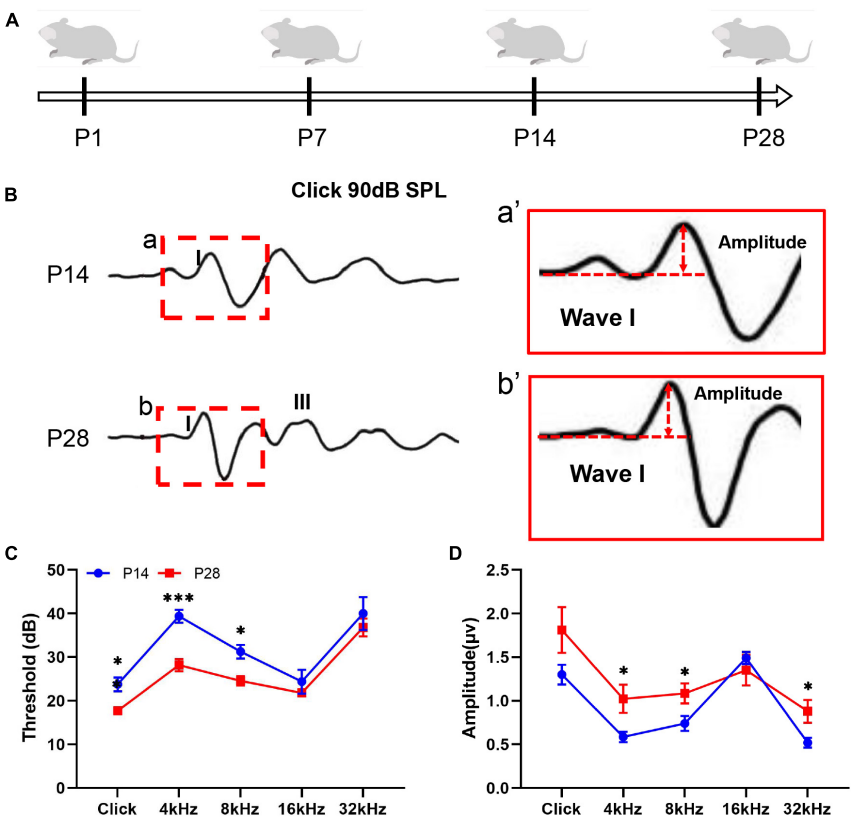

FIGURE 1 | Hearing detection corresponding to developing cochlea. **(A)** Schematic diagram of the experimental procedure and time points for hearing detection. Hearing function in the mice was estimated by detecting the ABR threshold and ABR wave I amplitude at P14 and P28. **(B,a,b)** A visible ABR waveform was observed at P14 and P28; the red dashed frame indicates ABR wave I. **(a′,b′)** A larger amplitude of ABR wave I was found at P28 than at P14. **(C)** Compared with P14, significantly reduced ABR thresholds at P28 were identified at click, 4 kHz, and 8 kHz ($^{*}p < 0.05$; $^{***}p < 0.001$). **(D)** Compared with P14, significantly increased ABR wave I amplitudes were observed at P28 at 4, 8, and 32 kHz ($^{*}p < 0.05$). ABR, auditory brainstem response.

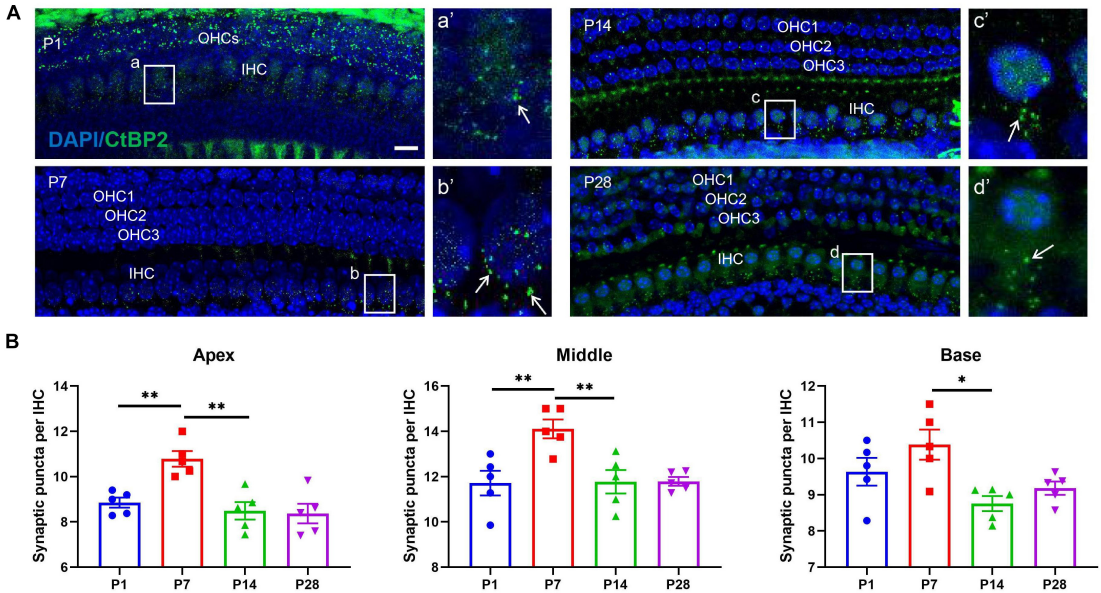

FIGURE 2 | Alterations in the number of ribbon synapses in the developing cochlea. **(A)** Whole mount of immunostaining at P1, P7, P14, and P28. Ribbon synapses were identified beneath the nuclei of IHCs using anti-CtBP2/RIBEYE (green, white arrow), and the nuclei of IHCs and OHCs were identified using DAPI staining (blue). A number of synaptic spots can be seen at P1 [**(a)** white frame indicated; **(a′)** enlarged image of panel **(a)**], and the highest number of synaptic puncta was identified at P7 [**(b)**, white frame indicated; **(b′)** enlarged image of panel **(b)**]. In contrast, reduced puncta of ribbon synapses appeared at P14 [**(c)**, white frame indicated; **(c′)** enlarged image of panel **(c)**] and P28 [**(d)** white frame indicated; **(d′)** enlarged image of panel **(d)**]. Scale bar = 5 μm. **(B)** Quantitative analysis of changes in ribbon synaptic numbers in developing cochlea. Correspondingly, the largest number of ribbon synaptic puncta was found at P7 across the cochlear frequency (including the apex, middle, and basal turns), and a significantly reduced number of synaptic spots was observed at P14 and P28 (*$p < 0.05$; **$p < 0.01$). IHC, inner hair cell; OHC, outer hair cell.

RESULTS

Auditory Detection in the Developing Cochlea of Mice

To investigate the hearing development profile, we first detected changes in the ABR threshold and amplitude of ABR wave I (**Figures 1A–D**). In this study, a visible ABR waveform was first recorded at P14, and a clearer ABR waveform appeared at P28 (**Figures 1A,B**). Because the amplitude of the ABR wave I has been demonstrated to roughly reflect the function of cochlear ribbon synapses (Qi et al., 2019; Xiong et al., 2020b), we then estimated the changes in the amplitude of the ABR wave I and found a significantly increased amplitude of the ABR wave I at P28 at 4, 8, and 32 kHz compared with that at P14 (**Figures 1a′,b′,D**). Thus, our study suggested a gradual change in hearing construction coupled with ribbon synaptic maturity in the developing cochlea of mice.

Changes in the Number of Ribbon Synapses in the Developing Cochlea

First, we measured quantitative changes in the cochlear ribbon synapses in the developing cochlea. In this study, cochlear ribbon synapses were labeled with anti-CtBP2 (Liu et al., 2009; Wang and Green, 2011; Wong et al., 2014). Before onset of hearing, at P1, the immunostaining positive puncta of CtBP2/RIBEYE were 8.85 ± 0.22 (apex), 11.71 ± 0.54 (middle), 9.64 ± 0.38 (base), respectively; At P7, the numbers were 10.78 ± 0.35 (apex), 14.11 ± 0.42 (middle), 10.38 ± 0.42 (base) respectively; At P14, the numbers were 8.49 ± 0.39 (apex), 11.78 ± 0.52 (middle), 8.76 ± 0.21 (base); And at P28, the numbers were 8.37 ± 0.43 (apex), 11.79 ± 0.19 (middle), 9.18 ± 0.18 (base), respectively (**Figure 2**). In this study, the largest number of synaptic puncta appeared at P7 and was significantly reduced at P14 and P28, suggesting that the number of ribbon synapses may undergo robust synaptic elimination during cochlear development.

Changes in the Sizes of Ribbon Synapses and the Distances From the Synapses to the Nuclei of Inner Hair Cells

To explore whether ribbon synaptic size undergoes significant alterations, we next estimated the changes in ribbon synaptic size at P1, P7, P14, and P28 using Adobe Photoshop CS6 software (San Jose, CA, United States). At P1, the mean sizes of synaptic spot were 0.42 ± 0.05 (apex), 0.42 ± 0.08 (middle), 0.47 ± 0.04 (base), respectively; At P7, the mean sizes were 0.42 ± 0.04 (apex), 0.40 ± 0.04 (middle), 0.44 ± 0.03 (base) respectively; At P14, the sizes were 0.36 ± 0.05 (apex), 0.24 ± 0.03 (middle), 0.30 ± 0.05 (base); And at P28, the sizes were 0.19 ± 0.01 (apex), 0.21 ± 0.01 (middle), 0.17 ± 0.01 (base), respectively; The largest synaptic spots appeared at

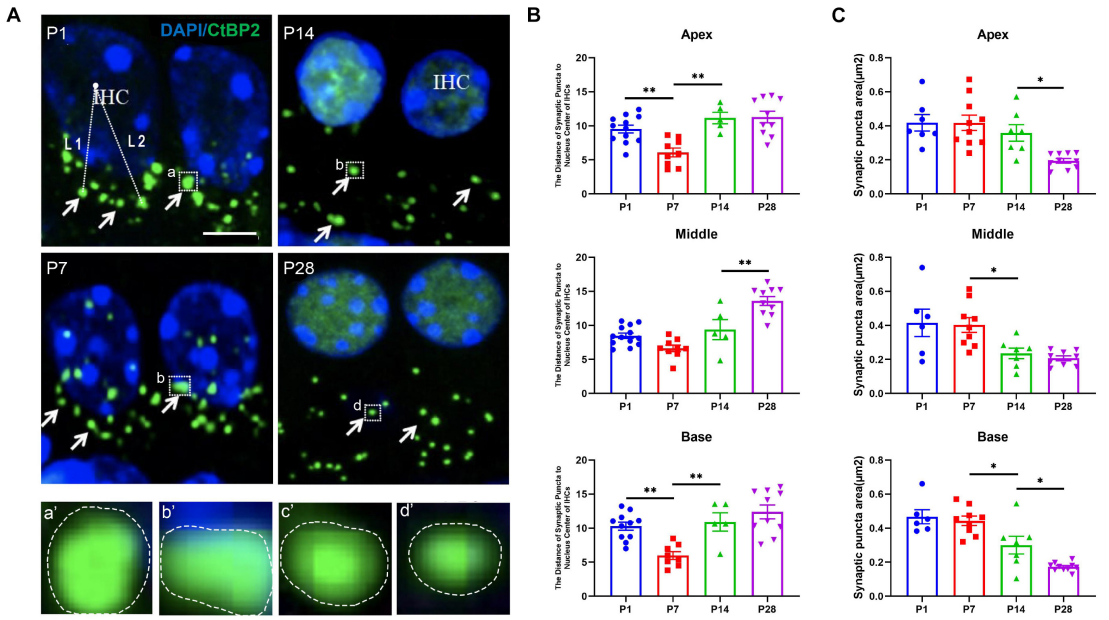

FIGURE 3 | Calculation of the size of synaptic spots and the distance between synaptic puncta and the nucleic center in adjacent IHCs. **(A)** DAPI staining of the nuclei of IHCs (blue) and ribbon synaptic puncta was performed using anti-CtBP2 (green, white indicated). The white dashed line indicates the distance from the synaptic puncta to the nucleic center of the adjacent IHC (L1, L2); **(a–d)** represent different sizes of synaptic puncta at P1, P7, P14, and P28 (white dashed frame); **(a′–d′)** are enlarged images of panels **(a–d)**, respectively. Scale bar = 5 μm. **(B)** Quantitative analysis of the distance between synaptic puncta and the nucleic center of adjacent IHCs. Compared with P1, a significantly increased distance was observed at P14 and P28 (**$p < 0.01$, apical and basal), and a more significantly enhanced distance appeared at P28 (**$p < 0.01$, middle). **(C)** Quantitative analysis of synaptic spot size. The sizes of the synaptic puncta at P1 and P7 were significantly larger than those at P14 and P28 (*$p < 0.05$, middle and basal); at the apex, the sizes at P1, P7, and P14 were significantly larger than those at P28 (*$p < 0.05$, apex). IHC, inner hair cell.

P1 and P7, and a significant reduction in synaptic size was found at P14 and P28, suggesting that the size of synaptic puncta undergoes a similar refinement in the developing cochlea (**Figure 3**). Next, we estimated the changes in the distance from the synaptic puncta to the nuclei of the IHCs. At P1, the distances from the synaptic puncta to nuclei center of adjacent IHCs were 9.53 ± 0.58 μm (apex), 8.48 ± 0.39 μm (middle), 10.29 ± 0.60um (base); At P7, the distances were 6.09 ± 0.65 μm (apex), 6.63 ± 0.48 μm (middle), 5.98 ± 0.57 μm (base), respectively; At P14, the distances were 11.15 ± 0.84 μm (apex), 9.39 ± 1.48 μm (middle), 10.91 ± 1.34 μm (base); At P28, the distances were 11.30 ± 0.86 μm (apex), 13.59 ± 0.66 μm (middle), 12.39 ± 1.02 μm (base), respectively. The distance at the P7 apex and middle turn was significantly shorter than that at P14 and P28 (**$p < 0.01$), and the distance at the P14 basal turn was also significantly shorter than that at P28 (**$p < 0.01$) (**Figure 3**), suggesting a remarkable retraction of the postsynaptic neural fibers during ribbon synaptic maturation.

LC3B Detection in the Region of Ribbon Synapses in the Developing Cochlea

To investigate whether autophagy flux undergoes remarkable alterations during cochlear development, we measured the level of LC3B, the current major recognized marker of autolysosomes (Barth et al., 2010; Aburto et al., 2012; Yuan et al., 2015; He et al., 2020, 2021; Liu et al., 2021), at P1, P7, P14, and P28, respectively. At P1, the number of positive immunostaining LC3B puncta were 7.59 ± 0.16 (apex), 8.30 ± 0.09 (middle), 7.45 ± 0.08 (base); At P7, the numbers were 9.44 ± 0.38 (apex), 11.88 ± 0.56 (middle), 10.60 ± 0.44 (base), respectively; At P14, the numbers were 5.21 ± 0.62 (apex), 6.30 ± 0.19 (middle), 4.60 ± 0.55 (base); At P28, the numbers were 2.31 ± 0.20 (apex), 4.60 ± 0.29 (middle), 2.31 ± 0.11 (base), respectively (**Figures 4A,B**). The highest number of LC3B puncta was observed at P7, suggesting the highest level of autophagic activity. Our study also showed decreased autophagy flux after P7 as a significantly reduced number of LC3B puncta were found at P14 and P28, and the smallest number of LC3B spots appeared at P28, suggesting that the level of autophagy was dramatically reduced when the cochlea was developed (**Figures 4A,B**).

Lamp1 Detection in the Developing Cochlea

To further confirm the autophagic activities in the developing cochlea, we examined additional autophagy-associated markers, such as lysosomal-associated membrane protein1 (LAMP1). LAMP1 has been used as a marker of autophagic flux (Yuan et al., 2015). At P1, the number of Lamp1 staining spots were 9.36 ± 0.17 (apex), 10.20 ± 0.13 (middle), 8.98 ± 0.20 (base); At P7, the numbers were 12.47 ± 0.40 (apex), 14.80 ± 0.52

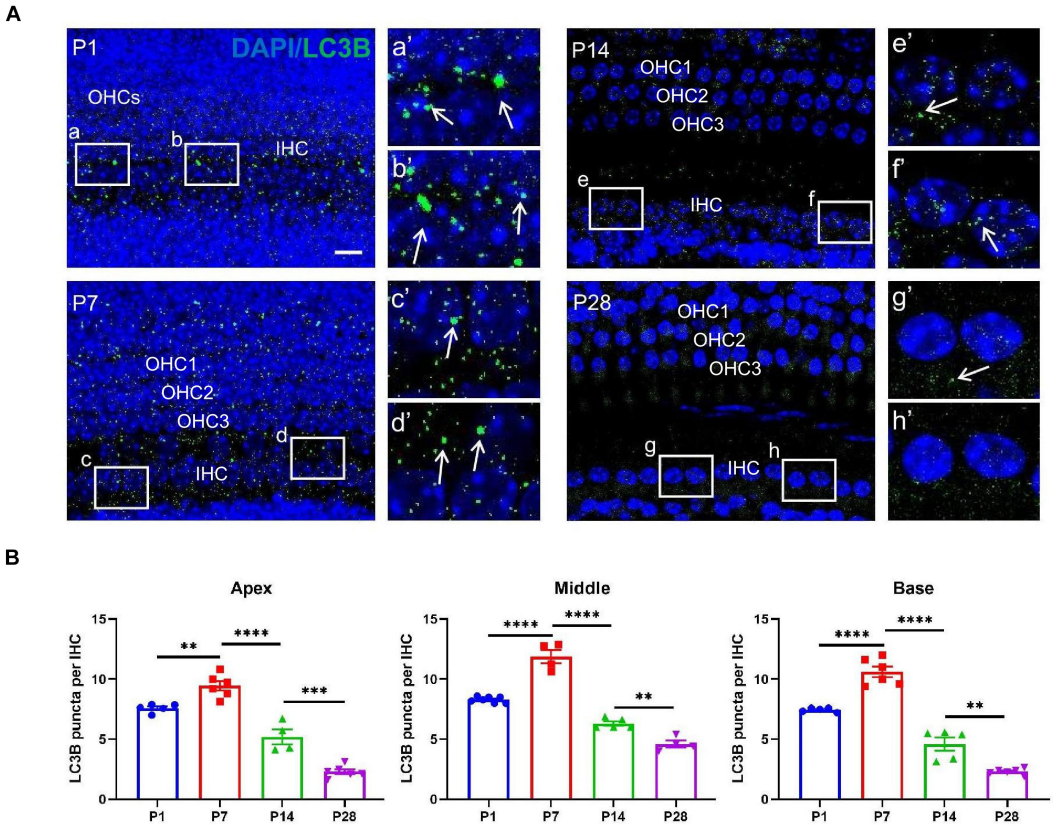

FIGURE 4 | LC3B detection in the ribbon synapses regions. **(A)** Autophagic flux was identified using anti-CtBP2 (green, white arrows). White frames at P1 **(a,b)**, P7 **(c,d)**, P14 **(e,f)**, and P28 **(g,h)** indicate the regions of ribbon synapses; **(a′–h′)** are enlarged images of panels **(a–h)**, respectively. Scale bar = 5 μm. **(B)** Quantitative analysis of the number of LC3B puncta at P1, P7, P14, and P28. The highest number of LC3B puncta was identified at P7, and significant reductions in LC3B puncta were observed at P14 and P28 (*$p < 0.01$; ***$p < 0.001$; ****$p < 0.0001$).

(middle), 10.96 ± 0.24 (base), respectively; At P14, the numbers were 7.60 ± 0.27 (apex), 8.45 ± 0.14 (middle), 7.41 ± 0.22 (base); At P28, the numbers were 4.25 ± 0.57 (apex), 6.45 ± 0.25 (middle), 2.37 ± 0.22 (base), respectively. Consistent with LC3B detection, the highest level of LAMP1 at or near the IHC region was found at P7, and the level decreased gradually at P14 and P28 (**Figures 5A,B**).

Detection of LysoTracker Red and Examination of Co-localization Between Ribbon Synapses and Auditory Nerve Fibers

LysoTracker Red dye, a type of lysosome marker, is used as a probe to track the formation of autolysosome-like structures and to indicate autophagic activity in the living tissues of various organisms by labeling acidic organelles such as autolysosomes (Aburto et al., 2012). Moreover, LysoTracker Red has been used to identify lysosomal activity, with positive staining indicating neuronal pruning (Song et al., 2008; He et al., 2021).

Our study showed that lysosome-mediated auditory neuronal axon pruning was initially observed at P1, beginning with LysoTracker particles distributed at or near the bottom of the axon bulb (**Figure 6A**). At P7, the activity of lysosome-mediated axon pruning was significantly enhanced, and a large amount of LysoTracker was visible in the axon and neuronal fibers (**Figures 6A,B**). After the onset of hearing, LysoTracker staining almost vanished around the axon bulb between P14 and P28 (**Figures 6A,B**). These results suggest that robust lysosome-mediated auditory neuronal axon pruning occurred before the onset of hearing, and axon pruning was significantly decreased after hearing onset.

Next, we co-labeled CtBP2 and neurofilament 200 (NF200) using immunostaining. Only small amounts of NF200 puncta connected with the IHCs were observed at P1, and CtBP2-positive spots occurred in the vicinity of the IHCs. Most importantly, the two types of signals were clearly separated, and no merged signals could be found (**Figures 6C,a,b,a′,b′**). AtP7, excessive neuronal fibers and ribbon synapses were found to form, and merged signals increased significantly (**Figures 6C,c,d,c′,d′**). At P14 and P28, merged signals formed byanti-NF200- and anti-CtBP2-stained puncta increased robustly (**Figures 6C,e–h,e′–h′**). These results indicate that afferent neuron fibers undergo changes analogous to those of ribbon synapses.

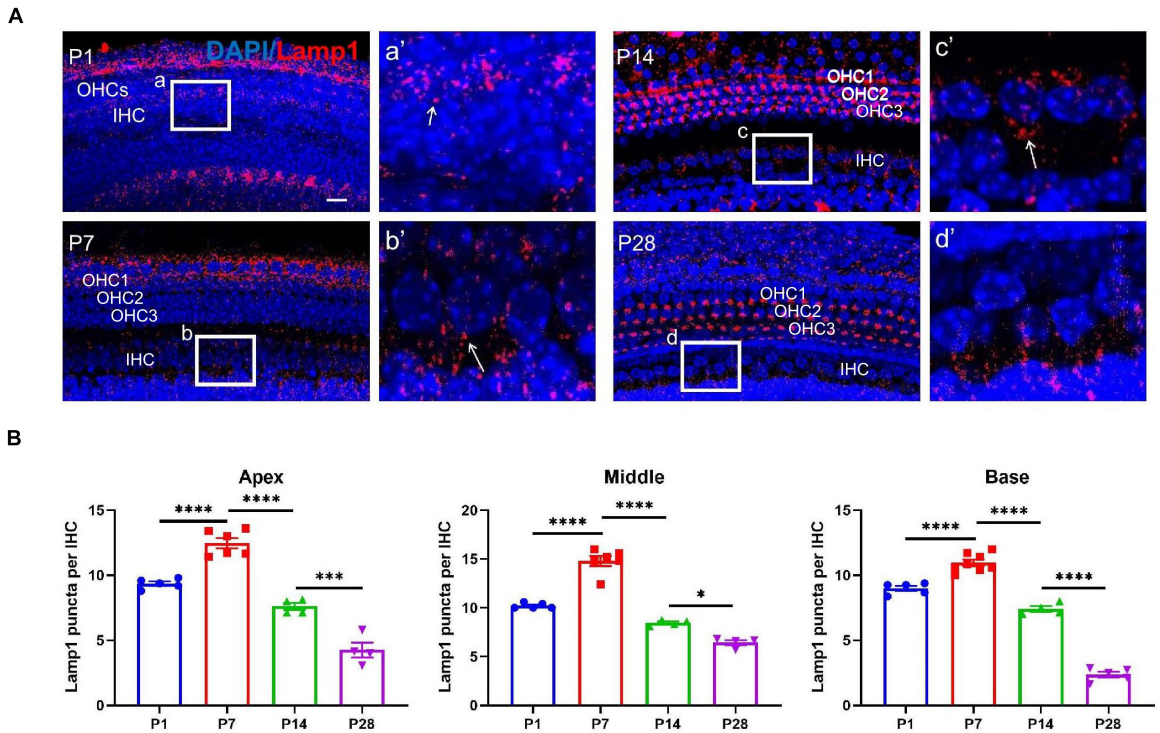

FIGURE 5 | LAMP1 detection in the ribbon synapses regions. **(A)** LAMP1 was identified using anti-LAMP1 (red, indicated), and white frames at P1 **(a)**, P7 **(b)**, P14 **(c),** and P28 **(d)** indicate the regions of ribbon synapses; **(a′–d′)** are enlarged images of panels **(a–d)**, respectively; white arrows indicate LAMP1-stained positive spots. Scale bar = 5 μm. **(B)** Quantitative analysis of the number of positive puncta on P1, P7, P14, and P28. Correspondingly, the highest number of LAMP1 puncta appeared at P7, and a remarkable loss of LAMP1 puncta was found at P14 and P28 across frequencies (apex, middle and base) (*$p < 0.05$; ***$p < 0.001$; ****$p < 0.0001$). LAMP1, lysosomal-associated membrane protein1.

Changes in the Number of Auditory Nerve Fibers in the Developing Cochlea

To further investigate whether the postsynaptic auditory nerve fibers undergo corresponding changes in synaptic alterations, we detected alterations in the auditory nerve fibers. Auditory nerve fibers were traced using anti-NF200, and we observed a massive number of auditory nerve fibers at both P1 and P7; the number of auditory nerve fibers decreased significantly at P14 and P28 (**Figure 7**), suggesting that postsynaptic auditory nerve fibers also undergo remarkable pruning in developing cochlea.

Inhibiting Autophagy Activity in the Developing Cochlea Hinders Synaptic Pruning and Impairs Hearing Function

In this study, we used 3-methyladenine (3-MA), an inhibitor of autophagy flux (Rubinsztein et al., 2007; Aburto et al., 2012; Liu et al., 2021), to investigate whether inhibiting autophagy activities in the developing cochlea significantly affects ribbon synaptic pruning. Here, 3-MA administration was applied at P7 and suspended at P14; interestingly, we found that LC3B-stained spots in IHCs nearly vanished compared with in the controls (**Figures 8A,E**). Next, we detected changes inCtBP2-positive spots; correspondingly, the number of CtBP2-positive spots in the 3-MA-treated group increased remarkably compared with in the normal controls (**Figures 8B,F**). Furthermore, we explored whether the inhibition of autophagy activities in the developing cochlea can impair hearing function. We estimated the ABR threshold and changes in the amplitude of ABR wave I and found a significantly enhanced ABR threshold, as well as a reduced amplitude of ABR wave I, suggesting that inhibiting autophagy activities in the developing cochlea impairs hearing function (**Figures 8C,D**).

DISCUSSION

Our findings showed that there may be a dramatic loss in the number of cochlear ribbon synapses during auditory development and maturation. Moreover, there is similar pruning of postsynaptic auditory nerve fibers during ribbon synaptic development and hearing onset. Finally, our findings demonstrated that robust autophagic activities in the early stage of auditory development regulate synaptic refinement and pruning of auditory nerve fibers.

The transformation of ribbon synapses during development is required for correct acoustic formation (Raphael and Altschuler, 2003). Thus, the ribbon synapses in the cochlea should undergo dramatic changes before the onset of hearing to meet the

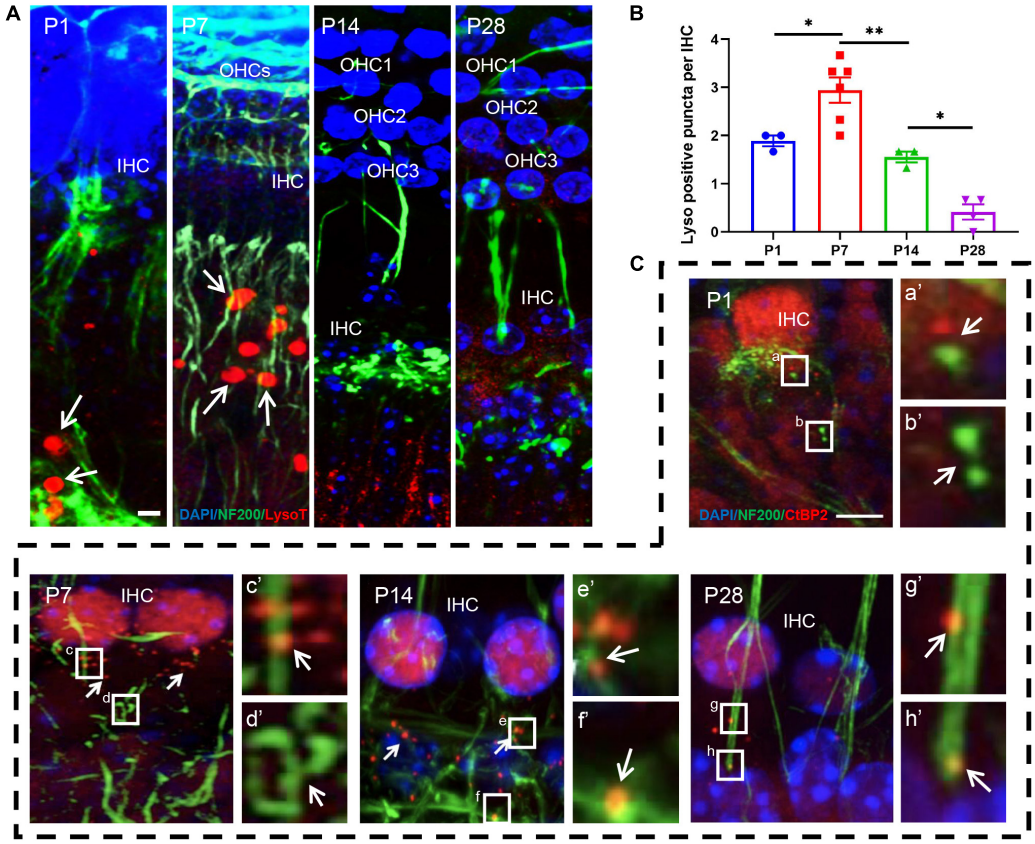

FIGURE 6 | LysoTracker Red detection and examination of co-localization between ribbon synapses and auditory nerve fibers. **(A)** The signals of LysoTracker Red (red signals in round shape) were clearly observed at P1 and P7 (white arrows indicated); auditory nerve fibers were identified using anti-NF200 (green, corded). Signals for LysoTracker Red almost disappeared at P14 and P28. Scale bar = 5 μm. **(B)** Quantitative analysis of LysoTracker Red signals. The largest number of signals was found at P7, and a significant loss of LysoTracker Red signals was observed at P14 and P28 (*$p < 0.05$; **$p < 0.01$). **(C)** Poor co-localization between CtBP2-positive puncta and NF200-stained spots at P1: white frames **(a,b)** and enlarged images [**(a′,b′)** white arrows indicated] with the red and green signals clearly separated. A significantly improved co-localization level between red and green signals can be found at P7, P14 and P28; see c and d (P7), e and f (P14), g and h (P28), as well as their enlarged images [**(c′–h′)** respectively]. NF200, neurofilament 200.

requirement of auditory development (Huang et al., 2007; Kros, 2007; Johnson et al., 2009; Roux et al., 2009). Our studies revealed the timeline of ribbon synapses during development and maturation, as well as the possible mechanism of synaptic elimination and neural pruning. In consistent with quantitative analysis of the synaptic number, the analysis of the size or shape of synaptic spot is also an indicator of synaptic plasticity. A previous study reported that ribbon synapse puncta are T-shaped or table-shaped at P1 (Vollrath and Spiwoks-Becker, 1996). Our results were partially different from those of a previous study because we found that the size of CtBP2 puncta in postnatal mice is larger than that of mature mice. Huang reported that CtBP2-positive puncta increased significantly in the first week of postnatal life (Huang et al., 2012), consistent with the data observed in this study. In our study, the maximum number of pre-synaptic CtBP2-positive puncta appeared at P7. Sending reported that the population of ribbon synapses is dynamic, and the synaptic structure gradually matures overtime (Sendin et al., 2007). Our data revealed consistent evidence that immature ribbon synapses with no function are excessively formed during the early stages of development. However, the mechanisms underlying the quantitative changes in ribbon synapses during synaptic development have remained unclear (Sobkowicz et al., 1982; Friedman et al., 2000; Roux et al., 2009). In this study, we proposed novel findings that changes in the number of ribbon synapses are driven by synaptic elimination and axon pruning, which may be attributed to lysosome-mediated autophagy flux that activates the onset of hearing.

During development, massive contacts between IHCs and SGNs are eliminated because the afferent fibers are refined or retracted, leading to a significant reduction in synapses (Sobkowicz et al., 1982; Huang et al., 2012). In this study, we found that the synaptic puncta increased robustly in both IHCs and outer hair cells at P7; this fluctuating timeline for the quantification and distribution of ribbon synapses is consistent with the previous report (Liberman and Liberman, 2016). During the development of the cochlea, the populations of type II SGNs

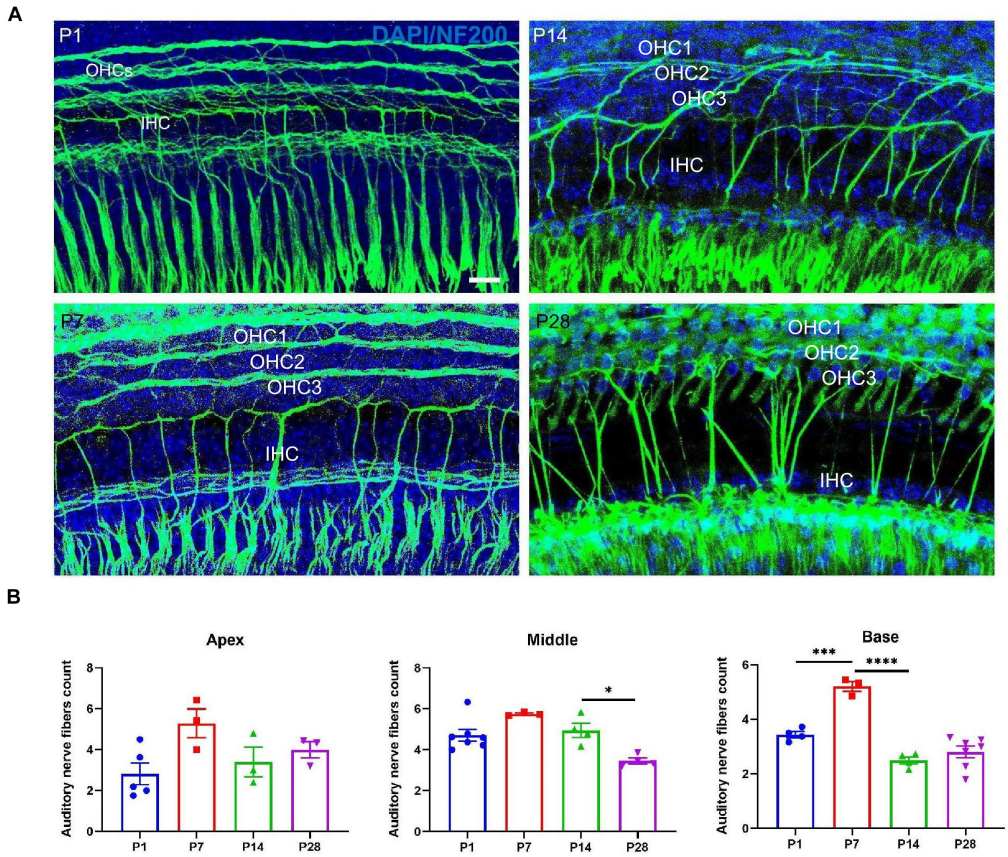

FIGURE 7 | Examination of the number of auditory nerve fibers. **(A)** Auditory nerve fibers were traced using anti-NF200 (green), and a massive number of auditory nerve fibers were seen at P1 and P7; a reduced number of auditory nerve fibers appeared at P14 and P28. Scale bar = 5 μm. **(B)** Compared with P1 and P7, quantitative analysis showed a significant loss of auditory nerve fibers at P14 and P28 in the middle and basal turns (*$p < 0.05$) and no significant difference at the apical turn ($p > 0.05$), suggesting that postsynaptic auditory nerve fibers also undergo significant pruning in the developing cochlea (***$p < 0.001$; ****$p < 0.0001$). NF200, neurofilament 200.

obviously decrease because of the apoptosis of the neurons (Barclay et al., 2011).

In mice, hearing onset occurs around P12-14, with a significant decrease in pre- and post-synaptic puncta during this period. Before hearing onset, there is a large number of round- or ovular-shaped immature cochlear ribbon synapses; further, they are tethered with a few vesicles (Wong et al., 2014). After the onset of hearing, the ribbon synapses begin to mature, the ribbon shape is elliptical or rod-like, and each ribbon is associated with a single afferent fiber. Such a structure may be essential for the release of neuron transmitters (Nicol and Walmsley, 2002; Yang et al., 2010). An additional experiment demonstrated that maturation of the ribbon synapse is also mediated by thyroid hormones, indicating that many factors are involved in the process of synaptic elimination (Rüsch et al., 1998; Sendin et al., 2007). First, our data show a new mechanism underlying ribbon synaptic elimination and axon pruning in the cochlea through the robust cellular activity of lysosome-mediated autophagy.

In this study, several markers identifying autophagy activity were used to estimate the level of autophagy in the developing cochlea. Among these markers, LC3B is the most widely used indicator of autophagic activity (Barth et al., 2010; He et al., 2017). In addition, LAMP1 and LysoTracker were also used to detect autophagy flux because these two markers can trace lysosome-mediated autophagy (Aburto et al., 2012; Yuan et al., 2015). Application of the three markers can provide convincing evidence of autophagy activity, and in our study, all three markers traced similar autophagy flux in the developing cochlea, which strongly illustrates the refinement of ribbon synapses and the pruning of postsynaptic neurofilaments during cochlear development. Furthermore, treatment with 3-MA, an inhibitor of autophagic flux (Rubinsztein et al., 2007; Aburto et al., 2012), caused a significant increase in the number of ribbon synapses, demonstrating that this synaptic effect is mediated *via* autophagy in the cochlea. In this study, we found a significant reduction of auditory neural fibers at P14&28 in response to the synaptic loss, we hypothesis that it could be due to the decreased number of synaptic signals, so that postsynaptic auditory nerve fibers are unable to find sufficient targets to built up synaptic contacts. Previous study has proposed that the level of autophagic activity in the cochlea of maturated mice decreases significantly and

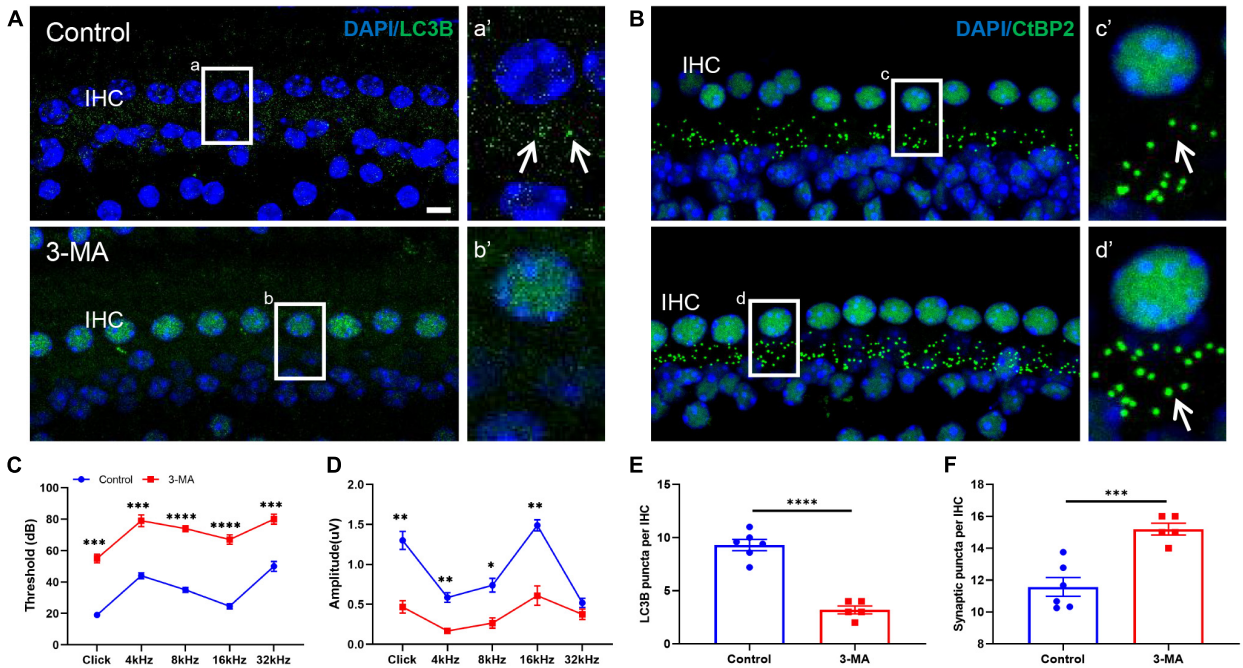

FIGURE 8 | Inhibiting autophagic activity in the developing cochlea increased the number of ribbon synapses but impaired hearing function. **(A,a,b)** and their respective enlarged images **(a′,b′)** show that 3-MA administration can cause a significant loss of LC3B-positive puncta compared with the controls. **(B)** Normal CtBP2 puncta (green) can be seen in the control group; the white frame indicates **(c)**; **(c′)** is the enlarged image of panel **(c)**. 3-MA administration caused an increased number of CtBP2 puncta; the white frame indicates **(d)**, panel **(d′)** is the enlarged image of panel **(d)**. **(C)** ABR thresholds were significantly increased across frequencies in the 3-MA-administrated group compared with controls (***$p < 0.001$; ****$p < 0.0001$). **(D)** Compared with the controls, a significant reduction in ABR wave I amplitude appeared in the 3-MA group at click, 4, 8, 16, and 32 kHz (*$p < 0.05$; **$p < 0.01$). **(E)** A significant reduction in LC3B-positive puncta can be seen in the 3-MA group compared with the controls (****$p < 0.0001$). **(F)** A significant enhancement in the number of ribbon synaptic spots can be seen in the 3-MA group compared with controls (***$p < 0.001$). 3-MA, 3-methyladenine; ABR, auditory brainstem response.

is nearly undetectable (Xiong et al., 2020a), in this study, we have found consistent results (data not shown), suggesting that autophagy is a critical regulator in ribbon synapse maturation in developing cochlea.

Our study found a relatively stable number of ribbon synapses at P28. The stability of ribbon synapses could indicate a strengthening of the synapses to meet the increasing need for sound coding; the data is consistent with previous reports (Shi et al., 2015; Yu et al., 2015). However, there is a lack of functional evidence in this study; for example, although we estimated the hearing function of the mice, we did not detect functional alterations in the level of IHCs corresponding to the activity of lysosome-mediated autophagy. With the utilization of combined approaches, including high-resolution optical imaging, electrophysiological recording, and patch-clamp electrophysiology, more detailed information on the mechanisms will be revealed in the future.

DATA AVAILABILITY STATEMENT

The original contributions presented in the study are included in the article/supplementary material, further inquiries can be directed to the corresponding author/s.

ETHICS STATEMENT

The animal study was reviewed and approved by Animal Ethics Committee of Capital Medical University.

AUTHOR CONTRIBUTIONS

KL contributed to the design of the study, analyzed and interpreted the result. SG and ZT contributed to the design of the study. RG, YX, WX, WW, YQ, and ZD conducted the experiments. RG, YX, WX, SG, and KL analyzed the generated data. RG, YX, and KL wrote the manuscript. All authors reviewed and approved the final version of the manuscript.

FUNDING

This work was supported by the National Natural Science Foundation of China (82071037, 81770997, and 81830030); Xiaogan Natural Science Program Project (XGKJ2021010036); and The Joint Funding Project of Beijing Natural Science Foundation and Beijing Education Committee (KZ201810025040).

REFERENCES

Aburto, M., Sánchez-Calderón, H., Hurlé, J., Varela-Nieto, I., and Magariños, M. (2012). Early otic development depends on autophagy for apoptotic cell clearance and neural differentiation. *Cell Death Dis.* 3:e394. doi: 10.1038/cddis.2012.132

Ban, B., Jun, M., Ryu, H., Jang, D., Ahmad, S., and Lee, J. (2013). Autophagy negatively regulates early axon growth in cortical neurons. *Mol. Cell. Biol.* 33, 3907–3919. doi: 10.1128/mcb.00627-13

Barclay, M., Ryan, A., and Housley, G. (2011). Type I vs type II spiral ganglion neurons exhibit differential survival and neuritogenesis during cochlear development. *Neural Dev.* 6:33. doi: 10.1186/1749-8104-6-33

Barth, S., Glick, D., and Macleod, K. (2010). Autophagy: assays and artifacts. *J. Pathol.* 221, 117–124. doi: 10.1002/path.2694

Beurg, M., Michalski, N., Safieddine, S., Bouleau, Y., Schneggenburger, R., Chapman, E., et al. (2010). Control of exocytosis by synaptotagmins and otoferlin in auditory hair cells. *J. Neurosci.* 30, 13281–13290. doi: 10.1523/jneurosci.2528-10.2010

Beutner, D., and Moser, T. (2001). The presynaptic function of mouse cochlear inner hair cells during development of hearing. *J. Neurosci.* 21, 4593–4599. doi: 10.1523/jneurosci.21-13-04593.2001

Chen, J., Sun, Y., Wang, P., Long, D., Li, W., Li, L., et al. (2013). Induction of autophagy by TOCP in differentiated human neuroblastoma cells lead to degradation of cytoskeletal components and inhibition of neurite outgrowth. *Toxicology* 310, 92–97. doi: 10.1016/j.tox.2013.05.012

Ding, Y., Meng, W., Kong, W., He, Z., and Chai, R. (2020). The role of foxG1 in the inner ear. *Front. Cell Dev. Biol.* 8:614954. doi: 10.3389/fcell.2020.614954

Ehret, G. (1985). Behavioural studies on auditory development in mammals in relation to higher nervous system functioning. *Acta Otolaryngol. Suppl.* 421, 31–40. doi: 10.3109/00016488509121754

Friedman, H., Bresler, T., Garner, C., and Ziv, N. (2000). Assembly of new individual excitatory synapses: time course and temporal order of synaptic molecule recruitment. *Neuron* 27, 57–69. doi: 10.1016/s0896-6273(00)00009-x

Fu, X., Wan, P., Li, P., Wang, J., Guo, S., Zhang, Y., et al. (2021). Mechanism and prevention of ototoxicity induced by aminoglycosides. *Front. Cell. Neurosci.* 15:692762. doi: 10.3389/fncel.2021.692762

Fuchs, P., Glowatzki, E., and Moser, T. (2003). The afferent synapse of cochlear hair cells. *Curr. Opin. Neurobiol.* 13, 452–458. doi: 10.1016/s0959-4388(03)00098-9

Guo, L., Cao, W., Niu, Y., He, S., Chai, R., and Yang, J. (2021). Autophagy regulates the survival of hair cells and spiral ganglion neurons in cases of noise, ototoxic drug, and age-induced sensorineural hearing loss. *Front. Cell. Neurosci.* 15:760422. doi: 10.3389/fncel.2021.760422

He, Z., Fang, Q., Li, H., Shao, B., Zhang, Y., Zhang, Y., et al. (2019). The role of FOXG1 in the postnatal development and survival of mouse cochlear hair cells. *Neuropharmacology* 144, 43–57. doi: 10.1016/j.neuropharm.2018.10.021

He, Z., Guo, L., Shu, Y., Fang, Q., Zhou, H., Liu, Y., et al. (2017). Autophagy protects auditory hair cells against neomycin-induced damage. *Autophagy* 13, 1884–1904. doi: 10.1080/15548627.2017.1359449

He, Z., Li, M., Fang, Q., Liao, F., Zou, S., Wu, X., et al. (2021). FOXG1 promotes aging inner ear hair cell survival through activation of the autophagy pathway. *Autophagy* 17, 4341–4362. doi: 10.1080/15548627.2021.1916194

He, Z., Zou, S., Li, M., Liao, F., Wu, X., Sun, H., et al. (2020). The nuclear transcription factor FoxG1 affects the sensitivity of mimetic aging hair cells to inflammation by regulating autophagy pathways. *Redox Biol.* 28:101364. doi: 10.1016/j.redox.2019.101364

Huang, L., Barclay, M., Lee, K., Peter, S., Housley, G., Thorne, P., et al. (2012). Synaptic profiles during neurite extension, refinement and retraction in the developing cochlea. *Neural Dev.* 7:38. doi: 10.1186/1749-8104-7-38

Huang, L., Thorne, P., Housley, G., and Montgomery, J. (2007). Spatiotemporal definition of neurite outgrowth, refinement and retraction in the developing mouse cochlea. *Development* 134, 2925–2933. doi: 10.1242/dev.001925

Jean, P., Lopez de la Morena, D., Michanski, S., Jaime Tobón, L., Chakrabarti, R., Picher, M., et al. (2018). The synaptic ribbon is critical for sound encoding at high rates and with temporal precision. *eLife* 7:e29275. doi: 10.7554/eLife.29275

Johnson, S., Franz, C., Knipper, M., and Marcotti, W. (2009). Functional maturation of the exocytotic machinery at gerbil hair cell ribbon synapses. *J. Physiol.* 587, 1715–1726. doi: 10.1113/jphysiol.2009.168542

Johnson, S., Marcotti, W., and Kros, C. (2005). Increase in efficiency and reduction in Ca2+ dependence of exocytosis during development of mouse inner hair cells. *J. Physiol.* 563, 177–191. doi: 10.1113/jphysiol.2004.074740

Kros, C. (2007). How to build an inner hair cell: challenges for regeneration. *Hear. Res.* 227, 3–10. doi: 10.1016/j.heares.2006.12.005

Liberman, L., and Liberman, M. (2016). Postnatal maturation of auditory-nerve heterogeneity, as seen in spatial gradients of synapse morphology in the inner hair cell area. *Hear. Res.* 339, 12–22. doi: 10.1016/j.heares.2016.06.002

Liu, K., Li, S., and Jiang, X. (2009). Quantitative analysis of the ribbon synapse number of cochlear inner hair cells in C57BL/6J mice using the three-dimensional modeling method. *Sci. China C Life Sci.* 52, 807–812. doi: 10.1007/s11427-009-0116-2

Liu, W., Xu, L., Wang, X., Zhang, D., Sun, G., Wang, M., et al. (2021). PRDX1 activates autophagy via the PTEN-AKT signaling pathway to protect against cisplatin-induced spiral ganglion neuron damage. *Autophagy* 17, 4159–4181. doi: 10.1080/15548627.2021.1905466

Liu, W., Xu, X., Fan, Z., Sun, G., Han, Y., Zhang, D., et al. (2019). Wnt signaling activates tp53-induced glycolysis and apoptosis regulator and protects against cisplatin-induced spiral ganglion neuron damage in the mouse cochlea. *Antioxid. Redox Signal.* 30, 1389–1410. doi: 10.1089/ars.2017.7288

Moser, T., and Beutner, D. (2000). Kinetics of exocytosis and endocytosis at the cochlear inner hair cell afferent synapse of the mouse. *Proc. Natl. Acad. Sci. U.S.A.* 97, 883–888. doi: 10.1073/pnas.97.2.883

Nicol, M., and Walmsley, B. (2002). Ultrastructural basis of synaptic transmission between endbulbs of held and bushy cells in the rat cochlear nucleus. *J. Physiol.* 539, 713–723. doi: 10.1113/jphysiol.2001.012972

Qi, Y., Yu, S., Du, Z., Qu, T., He, L., Xiong, W., et al. (2019). Long-term conductive auditory deprivation during early development causes irreversible hearing impairment and cochlear synaptic disruption. *Neuroscience* 406, 345–355. doi: 10.1016/j.neuroscience.2019.01.065

Raphael, Y., and Altschuler, R. (2003). Structure and innervation of the cochlea. *Brain Res. Bull.* 60, 397–422. doi: 10.1016/s0361-9230(03)00047-9

Roux, I., Hosie, S., Johnson, S., Bahloul, A., Cayet, N., Nouaille, S., et al. (2009). Myosin VI is required for the proper maturation and function of inner hair cell ribbon synapses. *Hum. Mol. Genet.* 18, 4615–4628. doi: 10.1093/hmg/ddp429

Rowland, A., Richmond, J., Olsen, J., Hall, D., and Bamber, B. (2006). Presynaptic terminals independently regulate synaptic clustering and autophagy of GABAA receptors in *Caenorhabditis elegans*. *J. Neurosci.* 26, 1711–1720. doi: 10.1523/jneurosci.2279-05.2006

Rubinsztein, D., Gestwicki, J., Murphy, L., and Klionsky, D. (2007). Potential therapeutic applications of autophagy. *Nat. Rev.Drug Discov.* 6, 304–312. doi: 10.1038/nrd2272

Rüsch, A., Erway, L., Oliver, D., Vennström, B., and Forrest, D. (1998). Thyroid hormone receptor beta-dependent expression of a potassium conductance in inner hair cells at the onset of hearing. *Proc. Natl. Acad. Sci. U.S.A.* 95, 15758–15762. doi: 10.1073/pnas.95.26.15758

Safieddine, S., El-Amraoui, A., and Petit, C. (2012). The auditory hair cell ribbon synapse: from assembly to function. *Annu. Rev. Neurosci.* 35, 509–528. doi: 10.1146/annurev-neuro-061010-113705

Sendin, G., Bulankina, A., Riedel, D., and Moser, T. (2007). Maturation of ribbon synapses in hair cells is driven by thyroid hormone. *J. Neurosci.* 27, 3163–3173. doi: 10.1523/jneurosci.3974-06.2007

Shen, W., and Ganetzky, B. (2009). Autophagy promotes synapse development in *Drosophila*. *J. Cell Biol.* 187, 71–79. doi: 10.1083/jcb.200907109

Shi, L., Liu, K., Wang, H., Zhang, Y., Hong, Z., Wang, M., et al. (2015). Noise induced reversible changes of cochlear ribbon synapses contribute to temporary hearing loss in mice. *Acta Otolaryngol.* 135, 1093–1102. doi: 10.3109/00016489.2015.1061699

Sobkowicz, H., Rose, J., Scott, G., and Slapnick, S. (1982). Ribbon synapses in the developing intact and cultured organ of Corti in the mouse. *J. Neurosci.* 2, 942–957. doi: 10.1523/jneurosci.02-07-00942.1982

Song, J., Misgeld, T., Kang, H., Knecht, S., Lu, J., Cao, Y., et al. (2008). Lysosomal activity associated with developmental axon pruning. *J. Neurosci.* 28, 8993–9001. doi: 10.1523/jneurosci.0720-08.2008

Vollrath, L., and Spiwoks-Becker, I. (1996). Plasticity of retinal ribbon synapses. *Microsc. Res. Tech.* 35, 472–487. doi: 10.1002/(SICI)1097-0029(19961215)35:6<472::AID-JEMT6>3.0.CO;2-K

Wang, Q., and Green, S. (2011). Functional role of neurotrophin-3 in synapse regeneration by spiral ganglion neurons on inner hair cells after excitotoxic trauma *in vitro*. *J. Neurosci.* 31, 7938–7949. doi: 10.1523/jneurosci.1434-10.2011

Wei, H., Chen, Z., Hu, Y., Cao, W., Ma, X., Zhang, C., et al. (2021). Topographically conductive butterfly wing substrates for directed spiral ganglion neuron growth. *Small* 17:e2102062. doi: 10.1002/smll.202102062

Wichmann, C., and Moser, T. (2015). Relating structure and function of inner hair cell ribbon synapses. *Cell Tissue Res.* 361, 95–114. doi: 10.1007/s00441-014-2102-7

Wong, A., Rutherford, M., Gabrielaitis, M., Pangrsic, T., Göttfert, F., Frank, T., et al. (2014). Developmental refinement of hair cell synapses tightens the coupling of Ca2+ influx to exocytosis. *EMBO J.* 33, 247–264. doi: 10.1002/embj.201387110

Xiong, W., Wei, W., Qi, Y., Du, Z., Qu, T., Liu, K., et al. (2020a). Autophagy is required for remodeling in postnatal developing ribbon synapses of cochlear inner hair cells. *Neuroscience* 431, 1–16. doi: 10.1016/j.neuroscience.2020.01.032

Xiong, W., Yu, S., Liu, K., and Gong, S. (2020b). Loss of cochlear ribbon synapses in the early stage of aging causes initial hearing impairment. *Am. J. Transl. Res.* 12, 7354–7366.

Yang, Y., Fedchyshyn, M., Grande, G., Aitoubah, J., Tsang, C., Xie, H., et al. (2010). Septins regulate developmental switching from microdomain to nanodomain coupling of Ca(2+) influx to neurotransmitter release at a central synapse. *Neuron* 67, 100–115. doi: 10.1016/j.neuron.2010.06.003

Yu, F., Hao, S., Yang, B., Zhao, Y., Zhang, R., Zhang, W., et al. (2015). Insulin resistance due to dietary iron overload disrupts inner hair cell ribbon synapse plasticity in male mice. *Neurosci. Lett.* 597, 183–188. doi: 10.1016/j.neulet.2015.04.049

Yuan, H., Wang, X., Hill, K., Chen, J., Lemasters, J., Yang, S., et al. (2015). Autophagy attenuates noise-induced hearing loss by reducing oxidative stress. *Antioxid. Redox Signal.* 22, 1308–1324. doi: 10.1089/ars.2014.6004

Zhou, H., Qian, X., Xu, N., Zhang, S., Zhu, G., Zhang, Y., et al. (2020). Disruption of Atg7-dependent autophagy causes electromotility disturbances, outer hair cell loss, and deafness in mice. *Cell Death Dis.* 11:913. doi: 10.1038/s41419-020-03110-8

Conflict of Interest: The authors declare that the research was conducted in the absence of any commercial or financial relationships that could be construed as a potential conflict of interest.

Publisher's Note: All claims expressed in this article are solely those of the authors and do not necessarily represent those of their affiliated organizations, or those of the publisher, the editors and the reviewers. Any product that may be evaluated in this article, or claim that may be made by its manufacturer, is not guaranteed or endorsed by the publisher.

frontiers in Molecular Neuroscience

ORIGINAL RESEARCH
published: 07 March 2022
doi: 10.3389/fnmol.2021.808553

F-Actin Dysplasia Involved in Organ of Corti Deformity in *Gjb2* Knockdown Mouse Model

Xiao-zhou Liu[1†], Yuan Jin[1†], Sen Chen[1], Kai Xu[2], Le Xie[1], Yue Qiu[1], Xiao-hui Wang[1], Yu Sun[1,3] and Wei-jia Kong[1,3]**

[1]*Department of Otorhinolaryngology, Union Hospital, Tongji Medical College, Huazhong University of Science and Technology, Wuhan, China,* [2]*Department of Otolaryngology, Head and Neck Surgery, The Second Affiliated Hospital of Nanchang University, Nanchang, China,* [3]*Institute of Otorhinolaryngology, Tongji Medical College, Huazhong University of Science and Technology, Wuhan, China*

Mutations in the *GJB2* gene encoding connexin26 (Cx26) protein are one of the most common causes of hereditary deafness. Previous studies have found that different Cx26-null mouse models have severe hearing loss and deformity of the organ of Corti (OC) as well as a reduction in microtubules in pillar cells (PCs). To explore the underlying mechanism of OC deformity caused by Cx26 downregulation further, we established Cx26 knockdown (KD) mouse models at postnatal days (P)0 and P8. The actin filaments contained in the pillar cells of mice in the P0 KD group were reduced by 54.85% and vinculin was increased by 22%, while the outer hair cells (OHCs) showed normal F-actin content. In the P8 KD group, PCs and OHCs of mice also showed almost normal F-actin content. The G-actin/F-actin ratio increased by 38% in the P0 KD group. No significant change was found in the mRNA or protein expression level of G-actin or the cadherin–catenin core complex in the P0 KD group at P6. Moreover, immunofluorescence showed that the intensity of LRRK2 was reduced by 97% in the P0 KD group at P6. Our results indicate that Cx26 is involved in the maturation of the cytoskeleton during the development of the OC at the early postnatal stage. The polymerization of G-actin into F-actin is prevented in Cx26 KD mice.

Keywords: connexin26, GJB2, hearing loss, cochlear development, f-actin

OPEN ACCESS

Edited by:
Daniele Dell'Orco,
University of Verona, Italy

Reviewed by:
Manuel Aureliano,
University of Algarve, Portugal
Yongyi Yuan,
PLA General Hospital, China

****Correspondence:***
Yu Sun
sunyu@hust.edu.cn
Wei-jia Kong
entwjkong@hust.edu.cn

[†]These authors have contributed equally to this work

Specialty section:
This article was submitted to Molecular Signalling and Pathways, a section of the journal Frontiers in Molecular Neuroscience

Received: *03 November 2021*
Accepted: *13 December 2021*
Published: *07 March 2022*

Citation:
Liu X-z, Jin Y, Chen S, Xu K, Xie L, Qiu Y, Wang X-h, Sun Y and Kong W-j (2022) F-Actin Dysplasia Involved in the Organ of Corti Deformity in Gjb2 Knockdown Mouse Model. Front. Mol. Neurosci. 14:808553. doi: 10.3389/fnmol.2021.808553

INTRODUCTION

Hearing loss is the most common congenital sensory disorder (Chan and Chang, 2014). Approximately one–two out of every 1,000 newborns have hearing loss (Sun et al., 2009). The genes encoding connexins are the most common genetic causes of congenital hereditary deafness (Martínez et al., 2009). Six connexins form a hemichannel, and two hemichannels from a pair of adjacent cells form a gap junction (Harris, 2001). Gap junctions are channels for material exchange and communication between cells, which allow ions, microRNAs, second messengers, and small molecules ≤1.5 kDa to pass through (Zhu et al., 2015). In the inner ear of mammals, connexin26 (Cx26) encoded by the *GJB2* gene is one of the most widely-distributed gap junction proteins (Ahmad et al., 2003). Mutations in the *GJB2* gene are the most common cause of human autosomal hereditary hearing loss. However, the mechanism is still not completely clear.

Mutations in *GJB2* cause variable levels of congenital hearing loss (Rabionet et al., 2000). Due to the difficulty in obtaining human pathological specimens, the mechanism of *GJB2* gene mutation-induced deafness is mainly studied using the *GJB2* gene knock-down mouse model (Qu et al., 2012; Chang et al., 2015; Chen et al., 2018a; Xie et al., 2019). We and others have found the failure of the tunnel of Corti (TC) to open and the disappearance of Nuel's space (Ns) in *Gjb2* KD mice (Chen et al., 2018b). Abnormal development of the cytoskeleton in PCs seems to be the main reason for the deformity of OC (Chen et al., 2018b). Actin filaments and microtubules jointly form a cytoskeletal network. Previous research has shown that the stereocilia structure of hair cellis formed from actin filaments which are composed of a mixture of β-actin and γ-actin, and mutations in the gene encoding actin can cause hereditary deafness (Patrinostro et al., 2018). However, few researchers have focused on the actin filaments of the inner ear supporting cells.

Mice with Cx26 KD before P4 suffer from severely impaired hearing, with deformity of the OC and reduction of microtubules in the pillar cells (Wang et al., 2009). In addition, Deiter's cells (DCs) are unable to develop into finger-like structures (Chen et al., 2018b). However, the mice with knockdown of Cx26 after P6 show normal hearing and the OC displays normal architecture. Therefore developmental abnormality of OC might be a better explanation for the hearing loss caused by Cx26 KD at the early postnatal stage. To explore the underlying mechanism of OC deformity caused by Cx26 downregulation further, we established mice that knockdown Cx26 at P0 and P8. We analyzed the composition of actin filaments such as β-actin and γ-actin, main ingredients of the cadherin–catenin core complex and molecules that are involved in the regulatory mechanism of microfilament assembly in Cx26 KD mice. We found a decrease in F-actin with an increase of vinculin and a reduction of LRRK2 in P0 knockdown mice. Abnormal development of microfilaments may be involved in the mechanism of deafness caused by Cx26 KD. In addition, reduction of LRRK2 may be the cause of the reduction of F-actin in the P0 KD group.

MATERIALS AND METHODS

Mouse Models

Cx26loxP/loxP mice and Rosa26CreER mice were provided by Prof. Xi Lin at Emory University. Tamoxifen-inducible Cx26loxP/loxP; Rosa26CreER mice were generated by crossbreeding of the Cx26loxP/loxP mice with Rosa26CreER mice. Mouse genotyping was performed by PCR amplification of tail genomic DNA. The methods of breeding and genotyping the mice are detailed in our previous article (Chen et al., 2018b). The genotyping primers were as follows:

Cx26 (F): 5′-ACAGAAATGTGTTGGTGATGG-3′,

Cx26 (R): 5′-CTTTCCAATGCTGGTGGAGTG-3′,

Rosa26Cre (F): 5′-AGCTAAACATGC TTCATCGTCG GTC-3′,

Rosa26Cre (R): 5′-TATC CAGGTTACGGATATAGTTCA TG-3′,

In this experiment, to observe the expression pattern of Cx26, a smaller dose of TMX (total dose 1.5 mg/10 g per day for 2 days) was administered to Cx26loxP/loxP; Rosa26CreER mice at P0/P1(P0 KD Group) and P8/P9 (P8 KD Group), and cochlear Cx26 was partly and randomly knocked out in different types of cells of this group (the randomly Cx26-null group).

All mice were raised in a sterile constant temperature environment at the specific-pathogen-free Experimental Animal Centre of Huazhong University of Science and Technology. All experimental work passed the ethical review of the animal experiments and was conducted in accordance with the policies of the Committee on Animal Research of Tongji Medical College, Huazhong University of Science and Technology.

Auditory Brainstem Response

Auditory brainstem response (ABR) was examined at P20. Mice were treated with combined anesthesia by intraperitoneal injection with ketamine (120 mg/kg) and chlorpromazine (20 mg/kg). Anaesthetised mice were then placed on an electric blanket to maintain body temperature at 37–38°C. Thresholds evoked by tone bursts of 8, 16, 24, 32, and 40 kHz were generated and responses were recorded using a Tucker-Davis Technologies system (RZ6, Tucker-Davis Tech., Alachua, FL, USA). If any mice suffered from severe hearing loss, the ABR test in the intensity range of 50–90 dB SPL was used. The lowest sound level that could be recognized was considered to be the auditory threshold.

Transmission Electron Microscopy (TEM)

This process has been described in detail in previous studies (Chen et al., 2018b). After the animals were euthanized, a hole was excavated using tweezers at the apex cochleae and then the cochleae were soaked in a mixture of 2% paraformaldehyde and 2.5% glutaraldehyde in 0.1 M phosphate-buffered saline (PBS). The cochleae were decalcified for 48 h in 10% disodium EDTA (pH 7.2). Next, the sample was soaked in 1% osmium tetroxide. After dehydration, the sample was embedded in resin and sectioned, and the ultrathin sections were stained with uranyl acetate and lead citrate. Electron microscopy examination (FEI Tecnai G2 20 TWIN; Hillsboro, OR, USA) was used to observe the ultrathin sections. The OC was magnified ×420 and images were captured for examination.

Western Blot

After the animals were euthanized, the membranous labyrinths of the cochleae were dissected carefully in ice-cold 1% PBS. Two membranous labyrinthine tissues from each mouse's left and right cochleae were combined to generate one sample. During the dissection, the tube containing the tissue was placed on ice. For cochlear explants, each of two basement membranes was considered to constitute a sample. Membranous labyrinths and cochlear explants were lysed with cold RIPA lysis buffer containing 1% PMSF. A BCA protein quantification kit (Beyotime Biotechnology, Jiangsu, China; P0010) was used to measure the protein concentration. Equal amounts of protein (5 μg) were separated by gel electrophoresis on a 12% sodium dodecyl sulfate (SDS) polyacrylamide gel, then electroblotted onto a polyvinylidene difluoride (PVDF) membrane. Proteins were then detected using the following antibodies: anti-GAPDH rabbit monoclonal antibody (ANT324; Antgene, Biotechnology Company Ltd, Wuhan, China); anti-β-actin rabbit polyclonal

antibody (ANT322, Antgene); anti-gamma-actin rabbit polyclonal antibody (11227-1-AP; Proteintech, Rosemont, IL, USA); anti-Cx26 rabbit polyclonal antibody (71-0500; Invitrogen, Carlsbad, CA, USA); anti-H3 histone rabbit antibody (A2348; ABclonal, Woburn, MA, USA); anti-α-catenin rabbit antibody (A19004, ABclonal); anti-LRRK2 rabbit polyclonal antibody (A17253, ABclonal); anti-RHOA rabbit antibody (A17253, ABclonal); anti-Arp2 rabbit antibody (A5734, ABclonal); anti-Arp3 rabbit antibody (A1046, ABclonal); anti-Vinculin rabbit antibody (A14193, ABclonal); anti-β-catenin rabbit antibody (YT0676, Immunoway, Plano, TX, USA); anti-p120-ctn rabbit antibody (12180-1-AP, Proteintech); anti-α-catenin rabbit antibody (YT0676, Immunoway); the dilution ratio of all solutions containing primary antibodies was 1:1,000. Briefly, GAPDH and histone H3 were used as the reference proteins in line with the manufacturer's instructions. A SuperSignal West Dura chemiluminescent substrate kit was used to detect the complexes according to the manufacturer's instructions. The western blots were semi-quantified using Image J (NIH, Bethesda, MD, USA) to measure the intensities of the bands.

RNA Preparation and Real-Time Quantitative Polymerase Chain Reaction (RT-qPCR)

The procedure used for RT-qPCR was as described in a previous article (Xu et al., 2021). RT-qPCR was performed to determine the transcriptional expression level of the following genes: *Gjb2*, *Acta1*, *Acta2*, *Actb*, *Actg1*, *Actg2*, *Actc1*, *Cdh1* (E-cadherin), *Ctnna1* (α-catenin), *Ctnnb1* (β-catenin), and *Ctnnd1* (p120-ctn). After the animals were euthanized, the membranous labyrinths of the cochleae were dissected carefully on ice. The membranous labyrinthine tissues from each mouse's left and right cochleae were used to generate one sample. There were six biological replicates for each experimental condition. Total RNA was extracted from the collected tissues using an RNAprep Pure Tissue Kit (Tiangen Biotech Co. Ltd., Beijing, China) and was reverse transcribed using a PrimeScript RT Reagent Kit with gDNA eraser (Takara Bio Inc., Shiga, Japan). Real-time PCR was performed in a LightCycler 480 instrument (Roche, Basel, Switzerland). Analysis of relative gene expression data between sample groups was performed according to the standard 2−ΔΔCP method. The following primers were used for RT-qPCR:

Gjb2 (F): 5′- CTCGGGGGTGTCAACAAACA-3′,
Gjb2 (R): 5′- CACGAGGATCATGATGCGGA-3′,
Acta1 (F): 5′- GAGCGTGGCTATTCCTTCGT-3′,
Acta1 (R): 5′- GAAACGCTCATTGCCGATGG-3′,
Acta2 (F): 5′- GTACCACCATGTACCCAGGC-3′,
Acta2 (R): 5′- GCTGGAAGGTAGACAGCGAA-3′,
Actg2 (F): 5′-ACAGAAATGTGTTGGTGATGG-3′,
Actg2 (R): 5′- TCTTCTGGTGCTACTCGAAGC-3′,
Actg1 (F): 5′- GAGCAAGAAATGGCTACTGCTG-3′,
Actg1 (R): 5′- AGCAATGCCTGGGTACATGG-3′,
Actb (F): 5′- GCGGGCGACGATGCT-3′,
Actb (R): 5′- GCCACAGGATTCCATACCCA-3′,
Actc1 (F): 5′- AAACTGTGTTACGTCGCCCT-3′,
Actc1 (R): 5′- GGGCCTGCCTCATCATACTC-3′,
Gapdh (F): 5′- GAAGGTCGGTGTGAACGGAT-3′,
Gapdh (R): 5′- CTCGCTCCTGGAAGATGGTG-3′,
Ctnnb1 (F): 5′- ATGGAGCCGGACAGAAAAGC-3′,
Ctnnb1 (R): 5′- TGGGAGGTGTCAACATCTTCTT-3′,
Ctnna1 (F): 5′- GTCCACGCAGGCAACATAAAC-3′,
Ctnna1 (R): 5′- CTGTGTAACAAGAGGCTCCAAC -3′,
Ctnnd1 (F): 5′- GTGGAAACCTACACCGAGGAG -3′,
Ctnnd1 (R): 5′-CTTTCCAATGCTGGTGGAGTG-3′,
Cdh1 (F): 5′-AACCCAAGCACGTATCAGGG-3′,
Cdh1 (R): 5′-ACTGCTGGTCAGGATCGTTG-3′,

Immunofluorescence Staining

After the animals were euthanized, the cochleae were carefully dissected from the temporal bones and fixed in 4% paraformaldehyde in 0.01 M PBS at room temperature for 2 h. The apical basement membranes were dissected in 0.01 M PBS. The tissues were incubated in a blocking solution (10% donkey serum with 0.1% Triton X-100) for 1 h at room temperature, and then placed in antibody solution (diluted in 1% BSA in PBST) and incubated overnight at 4°C. The next day, the tissue was placed on a shaker at room temperature for 1 h, then washed four times with 0.01 M PBS for 10 min each time. Samples were then incubated for 2 h at room temperature in 0.01 M PBS containing the secondary antibody. After repeating the washing step, DAPI (4',6-diamidino-2-phenylindole dihydrochloride) and phalloidin were dripped onto the tissue before covering with a coverslip and incubating for 2 h in the dark at room temperature. The following antibodies and reagents were used for immunofluorescence staining in this study: anti-Cx26 mouse polyclonal antibody (1:300, 131800, Invitrogen), LRRK2 (1:200, A0859, ABclonal), Alexa Fluor 647 donkey anti-rabbit IgG (1:200, ANT032S, Antgene), or Alexa Fluor 568 goat anti-Mouse IgG (1:200, RS3508, Immunoway). DAPI (C1005; Beyotime Biotechnology) and phalloidin (40736ES75; Yeasen, Shanghai, China) were used for nuclear and F-actin staining, respectively. Images were obtained with a laser scanning confocal microscope (Nikon, Tokyo, Japan).

G-Actin/F-Actin Ratio Measurement

A G-Actin/F-actin *in vivo* Assay Biochem Kit (Cytoskeleton Inc., Denver, CO, USA; BK037) was used to evaluate the G-Actin/F-actin ratio of the cochlea. G-actin and F-actin proteins were separated according to the instructions. In brief, the membranous labyrinths of the cochleae were dissected in 0.01 M PBS. Tissues were frozen in liquid nitrogen and ground into a powder. LAS2 buffer (1 ml per 0.1 g of tissue) was added to the sample, then F-actin Enhancing Solution was added to the sample at a volume ratio of 1:100. The tissue was lysed in the mixed solution for 10 min at 37°C, then the lysate was placed in a centrifuge and centrifuged at 2,000 rpm for 5 min to remove impurities after lysis. The supernatants were then pipetted into clearly-labeled ultracentrifuge tubes, and centrifuged at 100,000× *g*, 37°C for 1 h. The supernatant, which contained G-actin, was separated and the F-actin depolymerization buffer was added to the precipitate. The sample was placed on ice for 1 h,

inverting the sample every 15 min, to obtain the G-actin solution produced by the depolymerization of F-actin. Finally, 5× SDS sample buffer was added to each tube, and western blotting was used to evaluate the G-actin/F-actin ratio.

Data Analysis

All data are presented as means ± SE and plotted using GraphPad Prism (Version 8.0.1, GraphPad Software Inc., La Jolla, CA, USA). Student's t-tests or correlation analyses were performed in SPSS software (Version 19, IBM SPSS Statistics, IBM Corp., Armonk, NY, USA), and $p < 0.05$ was considered to be statistically significant.

RESULTS

Hearing Loss and Deformity of the Organ of Corti Were Observed in Mice Only When *Gjb2* Was Knockdown at the Early Postnatal Stage

The hearing of mice gradually matures and stabilizes at P16–P18. During the development of the OC, the height of the OC increases and opens with the formation of the TC (Chen et al., 2014). In order to observe the effects of Cx26 knowdown at different stages on the hearing and the morphology of the OC in mice, auditory brainstem response (ABR) measurements and morphological observations were performed on P20 mice injected with tamoxifen (TMX) at P0 and P8. Consistent with previous reports, mice in the P0 KD group ($n = 6$) showed severe hearing loss at the frequency of detection. The ABR thresholds evoked by click stimulations in the P0 KD group ($n = 6$) remained above 90 dB sound pressure level (SPL) and thresholds evoked by tone-bursts across a range of frequencies (4 K, 8 K, 16 K, 32 K, 40 K) were up to at least 85 dB SPL (**Figures 1A,B,E**). Meanwhile, the ABR thresholds evoked by click stimulations in the P8 KD group ($n = 6$) were almost 15 ± 3.43 dB SPL (**Figures 1C,D**), and thresholds evoked by tone-bursts across a range of frequencies (4 K, 8 K, 16 K, 32 K, 40 K) were 33 ± 3.72, 19 ± 1.86, 19 ± 4.48, 32 ± 5.33, and 41 ± 4.78 dB SPL (**Figure 1F**). This shows that there was no significant difference in hearing between the Cx26 P8 KD group and the control group. Deformity of the OC was observed only in the P0 KD group by electron microscopy (**Figures 2A–D**).

F-Actin Decreased by 54.85% in PCs of the P0 KD Group

Actin filaments, also known as F-actin, constitute an important part of the cytoskeleton. The actin cytoskeleton within a cell is necessary for the maintenance of cell shape, cell motility, and intracellular transport. A mixture of β-actin and γ-actin filaments formed stereocilia of hair cells and previously we have reported that the formation of the OC might be in association with the cytoskeleton in pillar cells (Dominguez and Holmes, 2011). The classic research method is to label the microfilament skeleton with fluorescently-labeled phalloidin (Prentki et al., 1979). No Cx26 expression was detected in inner pillar cells (IPCs) or outer pillar cells (OPCs) either in the P0 KD group or the P8 KD group (**Figures 3A–D**). The fluorescence intensity of phalloidin-labeled F-actin in the P0 KD group was reduced by 54.85% at P7 compared with the control group in both OPCs and IPCs (**Figures 3E,F,N**). In contrast, the P8 KD group showed no significant difference in the fluorescence intensity of phalloidin-labeled actin filaments at P15 (**Figures 3G,H,P**). However, no significant difference in F-actin staining of hair cells was observed between the P0 KD group and the P8 KD group (**Figures 3I–M,O**).

The Ratio of G-Actin/F-Actin Increased in the P0 KD Group

F-actin is formed by polymerization of G-actin (Rottner et al., 2017). In order to perform these functions, the F-actin network must assemble and depolymerize at the right time and place. To verify whether the assembly process of F-actin is disturbed, we analyzed the G-actin/F-actin ratio in the P0 KD group. Compared with the control group, the ratio of G-actin/F-actin increased by 38% in the P0 KD group (**Figures 5A,B**). This result suggests that there may be interference in the process of assembly of G-actin into F-actin or depolymerization of F-actin into G-actin caused by Cx26 KD at the early postnatal stage.

No Change Was Found in the mRNA or Protein Expression Level of G-Actin

The actin family includes α-actin, β-actin, and γ-actin (Dominguez and Holmes, 2011). In non-muscle tissues, F-actin is mainly composed of γ-actin and β-actin, which are encoded by *ACTG* and *ACTB* genes (Pollard and Cooper, 2009). In order to detect the effect of Cx26 KD on the transcription level of the gene encoding G-actin, we used Quantitative Real-time PCR (QPCR) to analyze the mRNA expression level of *Actg1*, *Actg2*, *Actb*, *Acta1*, *Acta2*, and *Actc1* in the P0 KD group at P7. Compared with the control group, there was no significant difference in the mRNA levels of *Actg1*, *Actg2*, *Acta1*, *Acta2*, or *Actb* (**Figures 4A–E**). However, we detected the mRNA transcript of Actc1 in only a few specimens. We speculate that actc1 might be expressed in spiral ganglion instead of the OC and samples may be accidentally contaminated with other tissues during anatomical sampling. Similarly, we measured the protein expression level of G-actin with H3 and Gpadh as internal reference proteins. The result showed that there were no significant differences between the protein expression levels of β-actin and γ-actin (**Figures 5D–I**).

No Changes Were Found in the mRNA and Protein Expression Levels of the Cadherin–Catenin Core Complex

The actin cytoskeleton is linked to the cadherin complex on the cell membrane (**Figure 4J**; Gloushankova et al., 2017). E-cadherin directly interacts with its two cytoplasmic binding partners p120ctn and β-catenin, and β-catenin interacts with α-catenin. Meanwhile, α-catenin interacts directly with F-actin, thereby linking E-cadherin to the junctional actin (Brieher and Yap, 2013). To investigate whether Cx26 KD affects the cadherin–catenin core complex, we analyzed

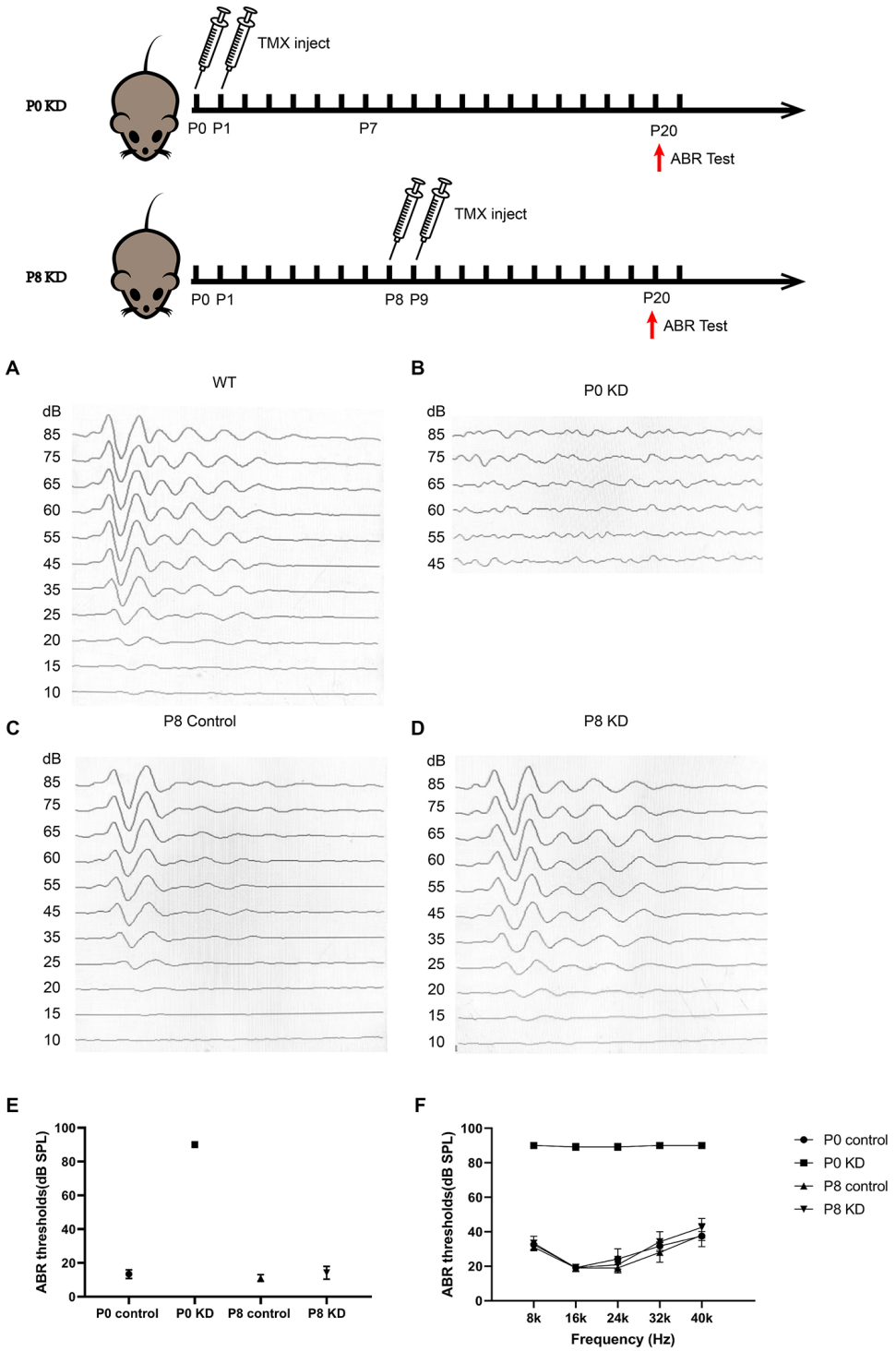

FIGURE 1 | Mice that Cx26 were knockdown at P0 have severely impaired hearing. Auditory thresholds (n = 6 in each group) evoked by click **(A–E)** or tone-bursts **(F)** were measured in the P0 control, P0 KD, P8 control, and P8 KD groups. All ABR tests were performed at P20.

mRNA and protein expression levels of the components of the cadherin complex such as E-cadherin, p120ctn, α-catenin, and β-catenin in the P0 KD group at P7. The QPCR results showed that, compared with the control group, there were no significant differences in the mRNA expression level of E-cadherin, α-catenin, β-catenin, or p120-catenin (**Figures 4A–E**). Western blot results show that in comparison with the corresponding control groups,

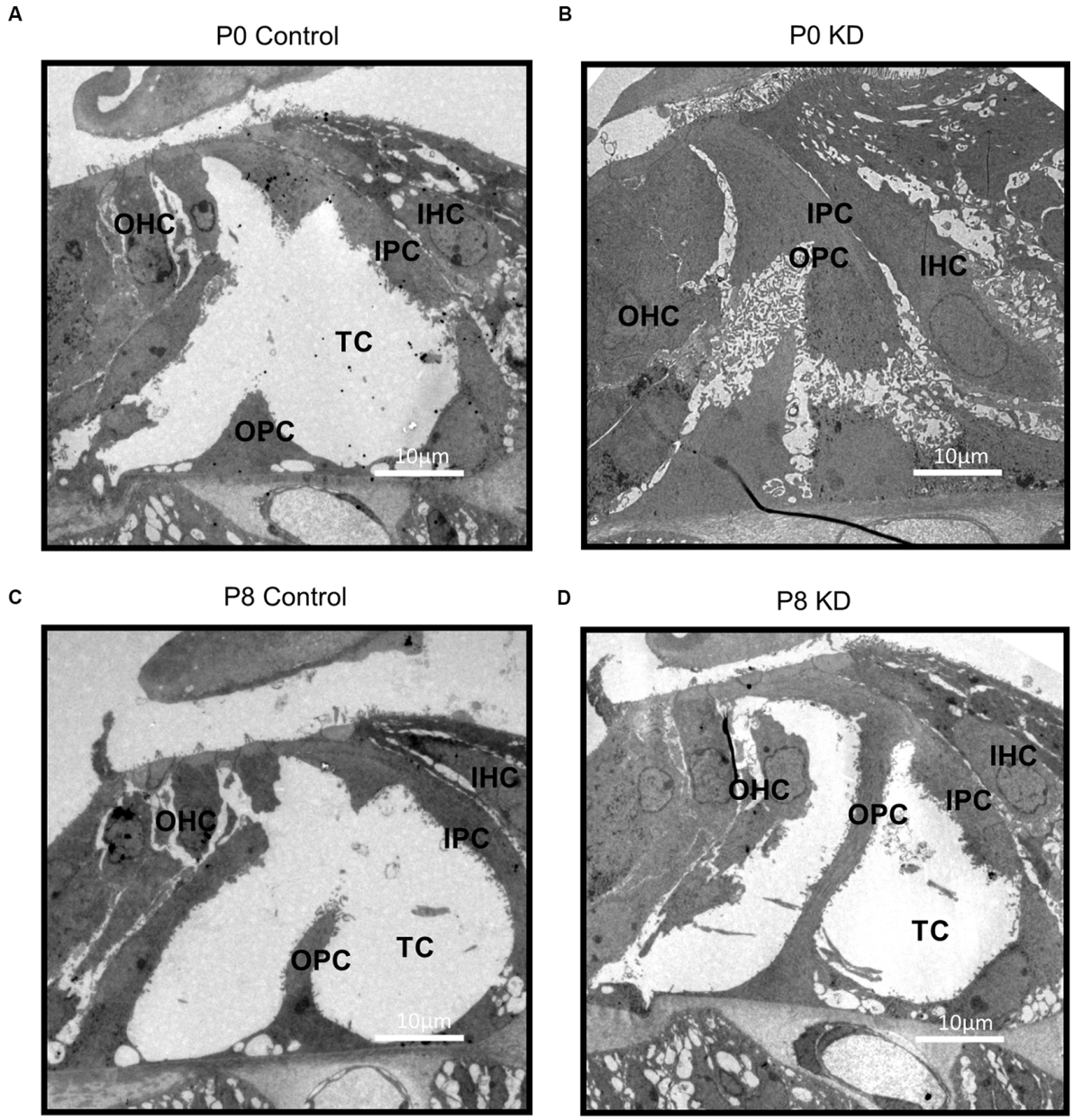

FIGURE 2 | Deformity of OC was only observed in P0 KD Group. A full view of the OC sections obtained from the P0 control **(A)**, P0 KD groups **(B)**, P8 control **(C)**, and P8 KD **(D)**. Scale bar: ∼10 μm **(A–D)**. DC, Deiter's cells; IHC, inner hair cells; OHC, outer hair cells; IPC, inner pillar cells; OPC, outer pillar cells; TC, tunnel of Corti; NS, Nuel's space.

Cx26 is significantly downregulated (**Figures 5C,D**), while there is no significant difference in the protein expression level of E-cadherin, p120-cadherin, α-catenin or β-catenin (**Figures 6A–G**).

Vinculin Increased in PCs of the P0 KD Group

Cytoskeleton assembly is regulated in a complex manner within the cell. There are many actin-binding proteins which play important roles in maintaining actin cytoskeleton stability. Vinculin enables mechanical coupling between the actin cytoskeleton and the extracellular matrix (Kelley et al., 2020). Changes in the expression level of vinculin have been found to reshape actin filaments or regulate their assembly (Kelley et al., 2020). In order to investigate the mechanism of action of Cx26 KD on actin filaments, we analyzed the protein expression levels of vinculin, Arp2, Arp3, and RHOA. Compared with the control group, there were no significant differences in the protein expression levels of Arp2, Arp3, or RHOA (**Figures 7A–F**). However, compared with the control group,

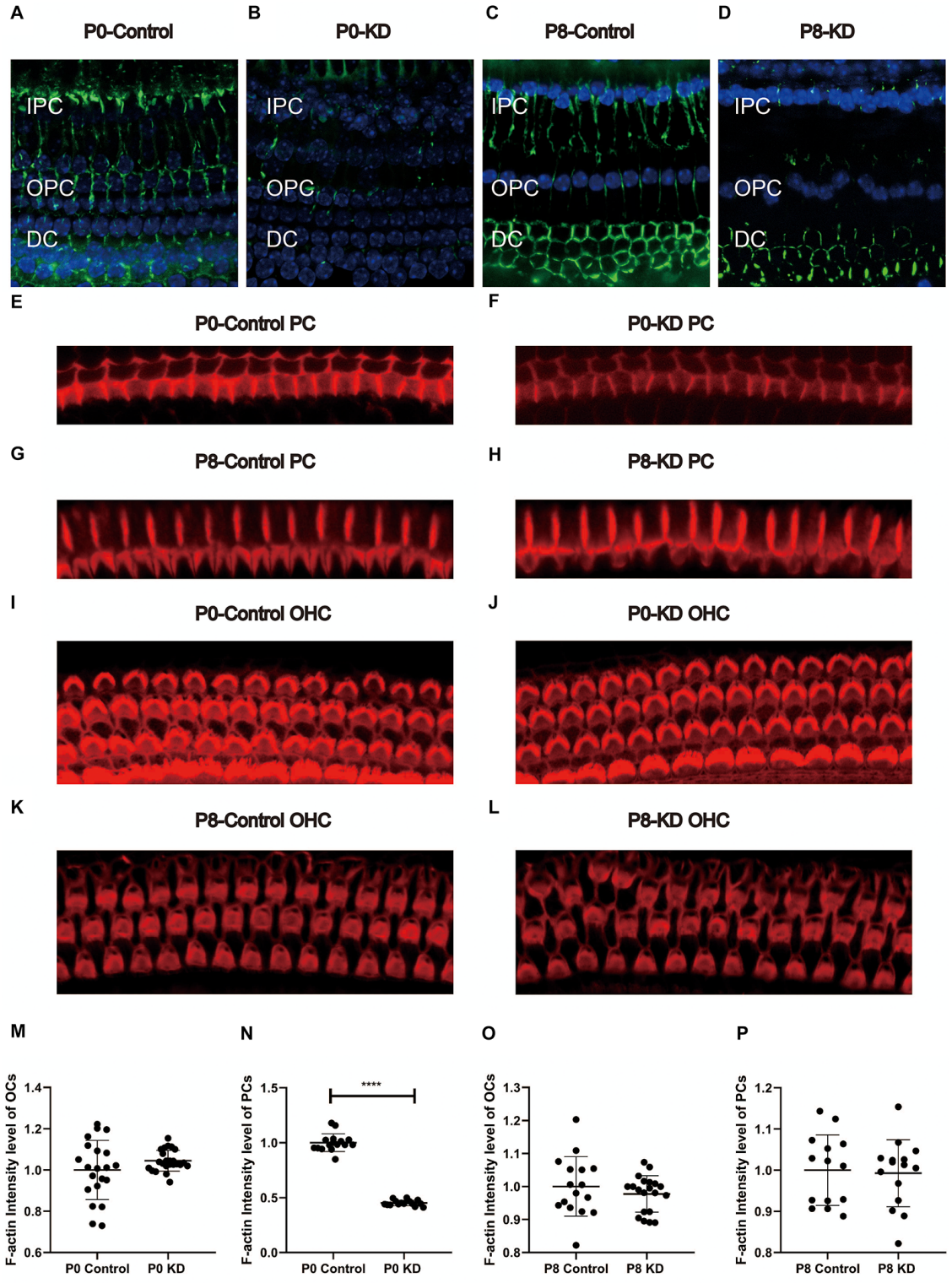

FIGURE 3 | Immunofluorescence staining of Cx26 and F-actin at p6 in P0 KD and p8 KD group. Immunofluorescence staining of Cx26 of support cell in P0 control **(A)**, P0 KD groups **(B)**, P8 control **(C)**, and P8 KD **(D)**. Staining of microfilaments labeled at the top of the pillar cells with phalloidin in P0 control **(E)**, P0 KD groups **(F)**, P8 control **(G)**, and P8 KD **(H)**. Staining of microfilaments labeled at outer hair cells with phalloidin in P0 control **(I)**, P0 KD groups **(J)**, P8 control **(K)**, and P8 KD **(L)**. Statistics of F-actin fluorescence intensity of PCs or OCs (**M**–**P**; $n = 3$ in each group). All the staining were performed 7 days after injection of TMX. Scale bar: ∼10 μm **(A–L)**. IPC, inner pillar cells; OPC, outer pillar cells; DC, Deiter's cells. ****Significantly different from the control group ($P < 0.0001$).

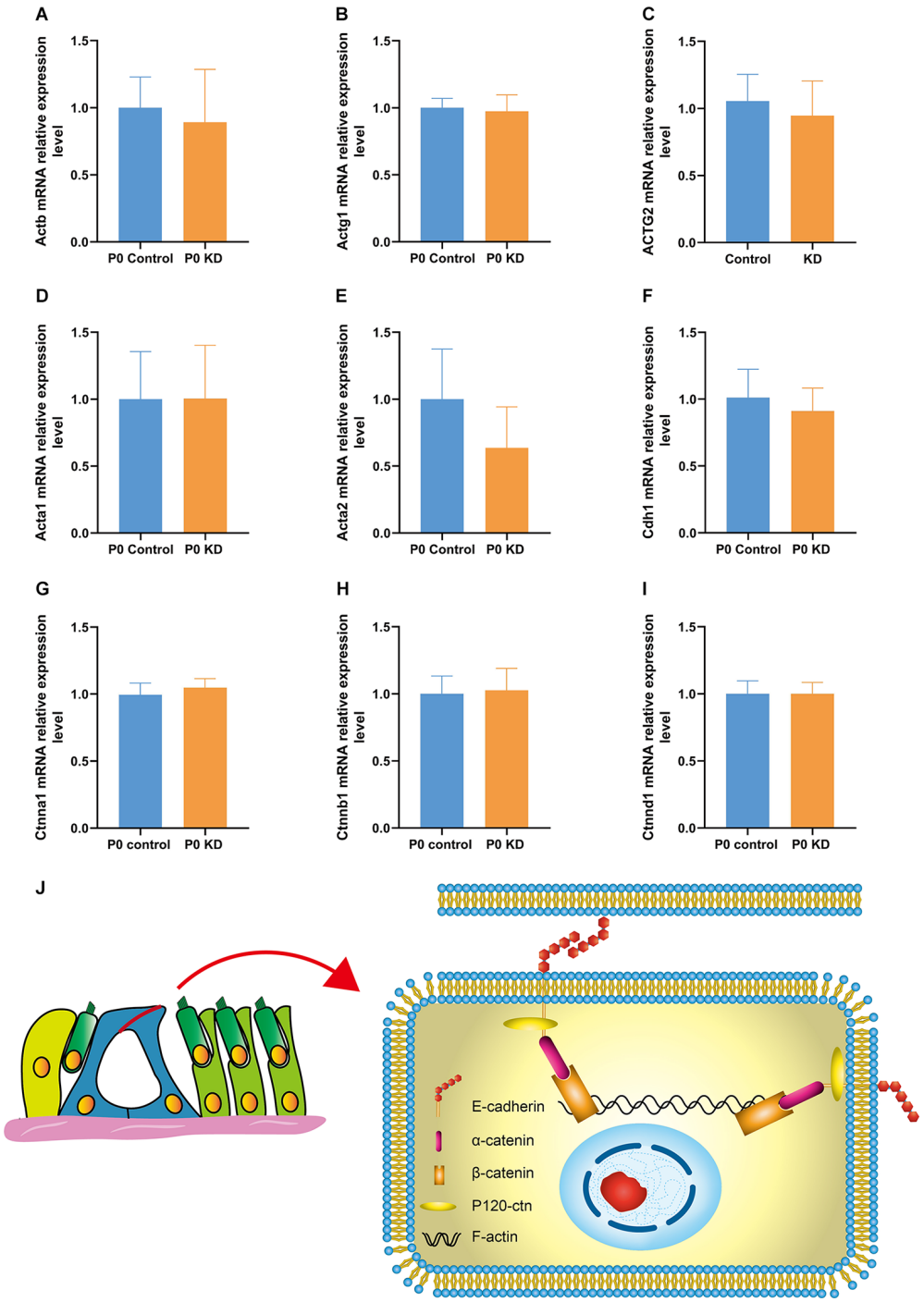

FIGURE 4 | mRNA expression relative expression level of G-actin and the cadherin–catenin core complex in P0 KD group. mRNA expression level in P0 control and P0 KD groups **(A–I)**. The differences between the P0 KD group and the P0 control group were not significant ($P > 0.05$). Adhesive protein complexes at adherens junctions between IPCs and OPCs **(J)**.

the content of vinculin in the P0 KD group increased by 22% (**Figure 7A**). This suggests that vinculin may be involved in the development of actin filaments in the OC caused by Cx26 KD.

LRRK Decreased in PCs of the P0 KD Group

Previous studies have reported that LRRK2 regulates the microfilament cytoskeleton, and its loss causes a decrease

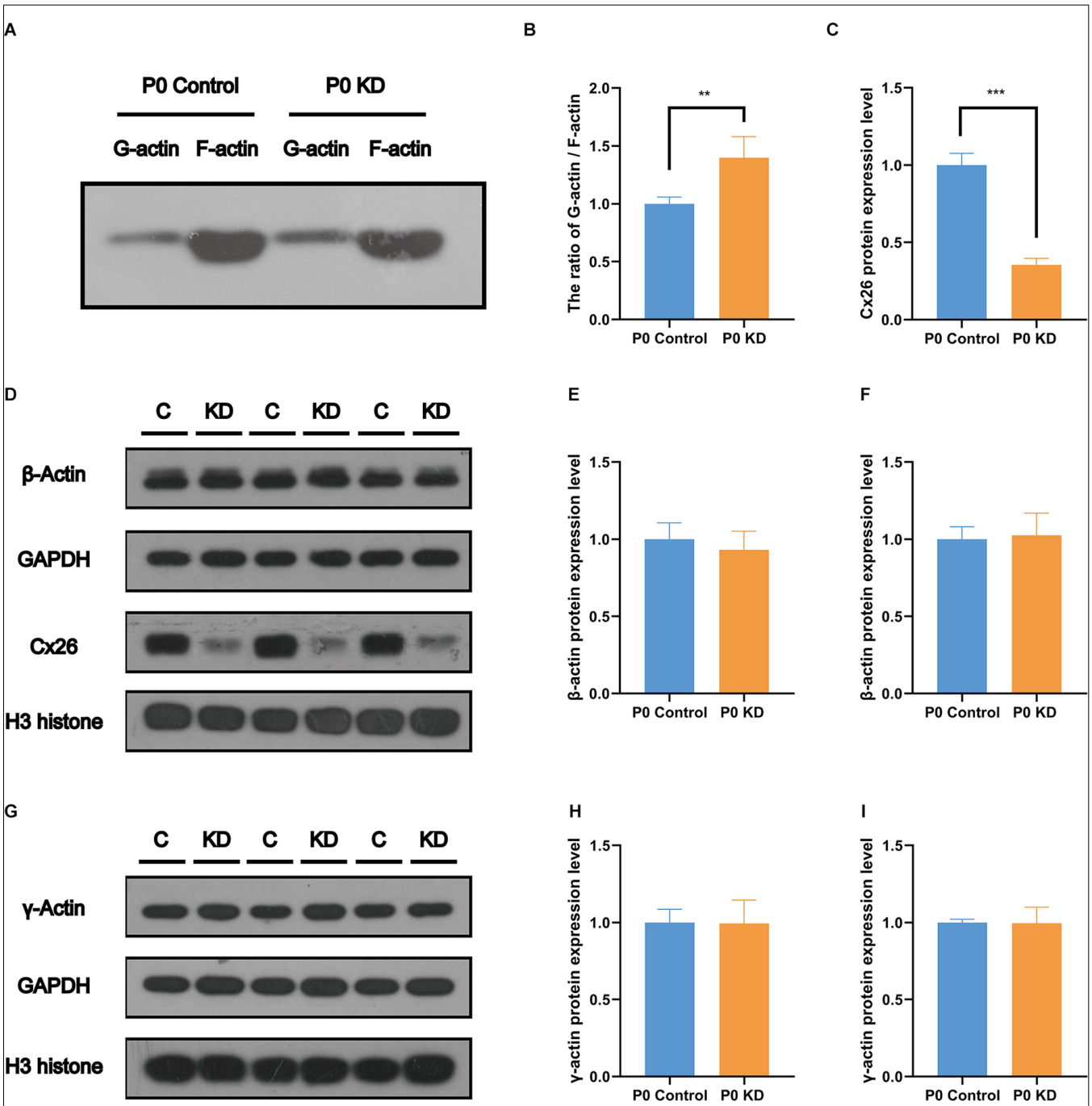

FIGURE 5 | No change was found in the protein expression level of G-actin. Protein expression level of Cx26, β-actin **(A)**, and γ-actin **(E)** in P0 control and P0 KD groups. β-actin and γ-actin protein expression level in cochlear of Cx26 KD mouse models. The ratio of G-actin/F-actin in P0 control and P0 KD group **(B)** respectively. Western blotting F-actin and G-actin in Western blot results of protein expression level of Cx26, β-actin **(D)** and γ-actin **(G)** in P0 control and P0 KD groups. Camparison of relative Cx26 **(C)**, β-actin **(E,H)**, and γ-actin **(F,I)** protein expression in P0 control and P0 KD groups. GAPDH **(C,E,H)** and H3 **(F,I)** was used as the control, respectively. The differences of β-actin and γ-actin expression level between the P0 KD and the P0 control group were not significant ($P > 0.05$). ***Significant difference from the control group ($P < 0.001$). **Significant difference from the control group ($P < 0.01$).

in the F-actin content in neuronal filopodia (Caesar et al., 2015; Yan et al., 2020). One of the mechanisms by which LRRK2 regulates the actin cytoskeleton is its interaction with the small GTPases CDC42 and Rac1, both of which are key factors for regulating actin filaments. In order to investigate the mechanism underlying the effect of Cx26 KD on actin filaments, we analyzed the protein expression level of LRRK2. Compared with the control group, the fluorescence

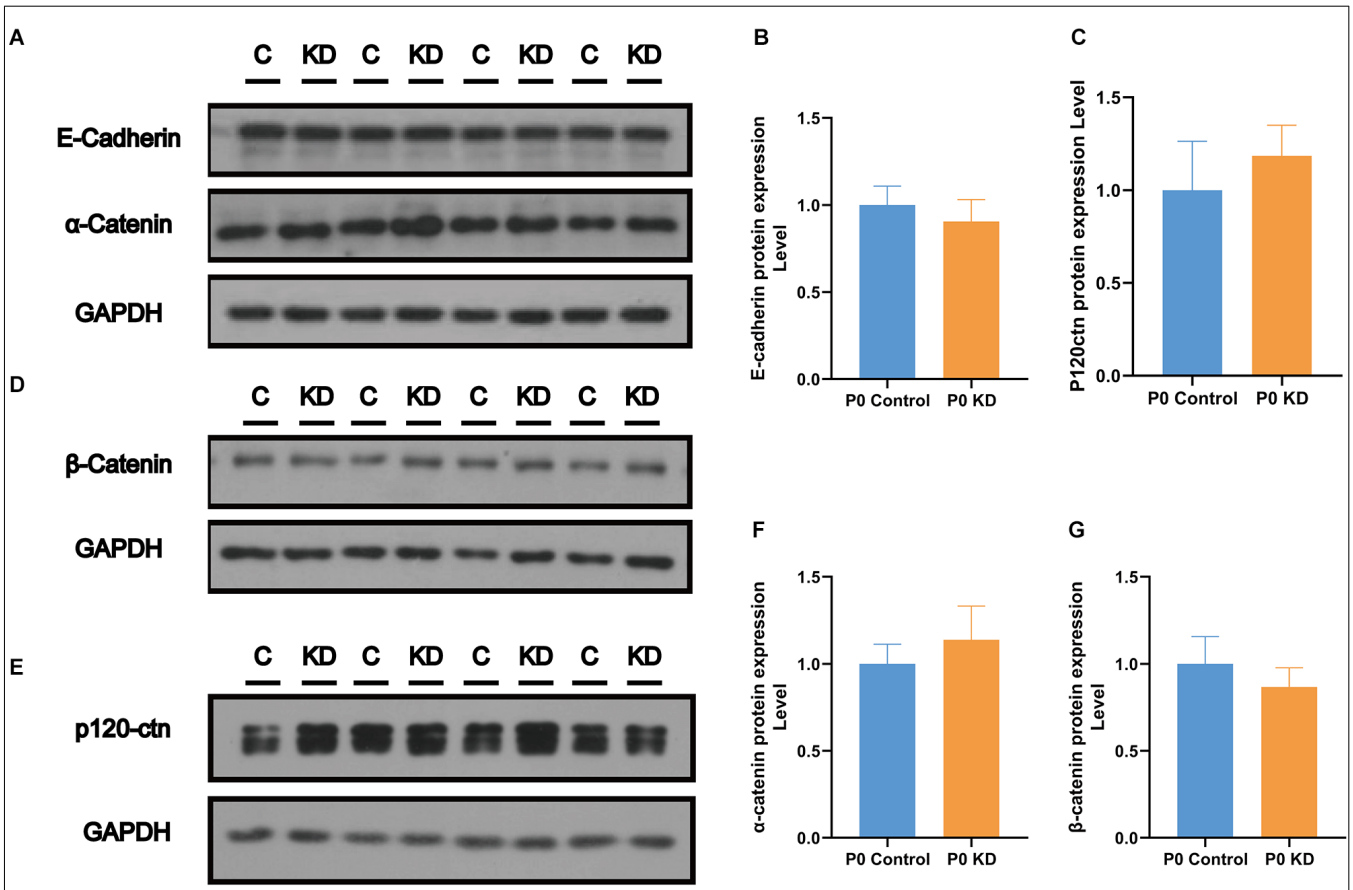

FIGURE 6 | No change was found in the protein expression level of the cadherin–catenin core complex. Protein expression level of E-cadherin, α-catenin **(A)**, β-catenin **(D)**, and p120-ctn **(E)** in P0 control and P0 KD groups. Comparison of relative E-cadherin **(B)**, p120ctn **(C)**, α-catenin **(F)**, and β-catenin **(G)** protein expression in P0 control and P0 KD groups. GAPDH was used as the control.

intensity of LRRK2 in the P0 KD group was reduced by 97%. This suggests that LRRK2 may be involved in the abnormal development of actin filaments in the OC caused by Cx26 KD.

DISCUSSION

Deformity of the OC May Be an Important Reason for Congenital *Gjb2*-Related Hearing Loss

In previous studies, it was found that several strains of transgenic mouse models with reduced cochlear Cx26 suffered from serious hearing loss, accompanied by cochlear developmental disorders, loss of hair cells, decreased intracochlear potential, and the reduction of active cochlear amplification (Griffith et al., 2006; Zhao and Yu, 2006; Kibschull et al., 2008). Pathological phenomena of abnormal development, such as failure of the TC to open and disappearance of Nuel's space have also been observed in some human cases (Wang et al., 2009). Circulatory disturbance of potassium ions was considered to be the main mechanism of deafness in Cx26-null mice. These studies and our previous study have shown that knockdown *Gjb2* in the early stage can cause severe hearing loss (**Figures 1A,B**) in mice and abnormal morphology of the OC (**Figures 2A,B**), while loss of Cx26 in late inner ear development (P8) does not cause deformity of the OC (**Figures 2C,D**) or hearing loss (**Figures 1A,B**; Chen et al., 2018b). Therefore, deformity of the OC may be a particularly important reason for congenital *Gjb2*-related hearing loss.

Cytoskeleton Development Disorder Due to *Gjb2* KD Contributes to OC Deformity

IPCs and OPCs together build the structure and shape of the TC. Our previous study suggested that deletion of the *Gjb2* gene in the early postnatal period causes microtubule abnormalities, which may be one of the mechanisms underlying the OC deformity of *Gjb2*-related hearing loss (Chen et al., 2018b). Actin filaments also play an important role in a variety of important life activities such as cell growth, deformation, and migration. In this experiment, we observed a significant decrease in the F-actin content of PCs and DCs in the P0 KD group at P6, while there was no significant difference in F-actin in the P8 KD

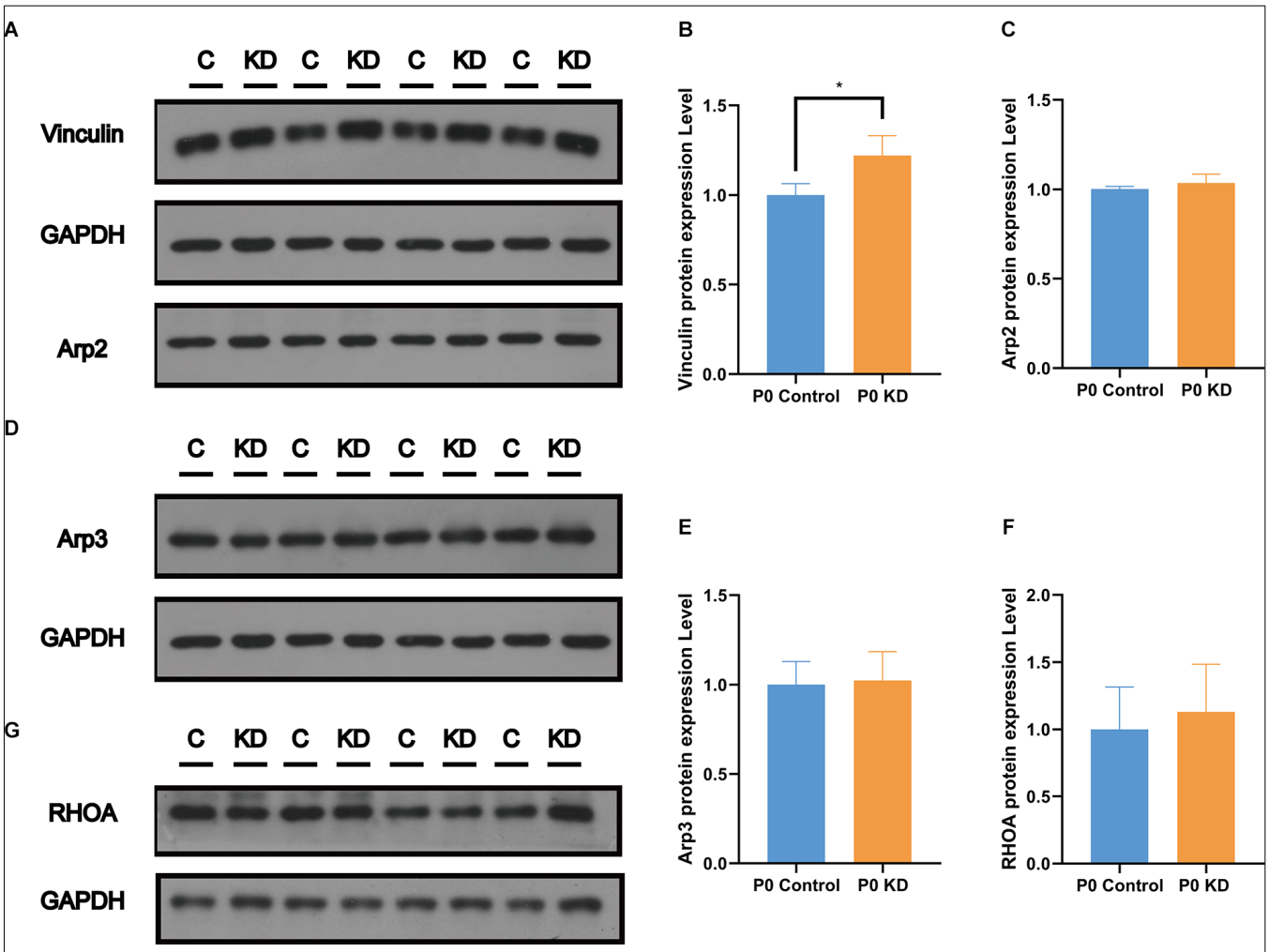

FIGURE 7 | Significant increase of Vinculin was observed in the P0 KD group at P6. Protein expression level of Vinculin, Arp2 **(A)**, Arp3 **(D)**, and RHOA **(G)** in P0 control and P0 KD groups. Comparison of Vinculin **(B)**, Arp2 **(C)**, Arp3 **(E)**, and RHOA **(F)** by western blot in P0 control and P0 KD groups. The differences of Arp2, Arp3, and RHOA expression level between the P0 KD and the P0 control group were not significant ($P > 0.05$). *Significantly different from the control group ($P < 0.05$).

group (**Figures 3E–H,N,P**, **Figure 8**). We tested the ratio of G-actin/F-actin, and the results showed that the ratio of G-actin/F-actin increased by 38% in the P0 KD group (**Figure 5A**). These results suggest that knockdown Cx26 in the early postnatal period will also cause abnormal development of actin filaments. The disordered cytoskeleton of PCs (both microtubule and microfilament) was essential for OC molding. Since OHCs do not express Cx26, Cx26 KD that occurs in PCs may not affect the actin cytoskeleton of hair cells.

Reduction of LRRK2 Due to *Gjb2* KD May Be the Reason for Cytoskeleton Development Disorder

In order to identify the cause of the disordered microfilament network, we analyzed the mRNA and protein levels of G-actin (**Figures 4A–E**, **5D–I**) and actin-binding proteins (**Figures 4F–I**, **6**, **7**, **8**) in the P0 KD group. The results showed that neither the mRNA level nor the protein level of β-actin and γ-actin has changed. In addition, the protein levels of the components of the cadherin complex connected to the microfilament network on the cell membrane, such as E-cadherin, α-catenin, β-catenin, and p120-catenin, were not changed (Griffith et al., 2006). Furthermore, we tried to detect some molecules that regulate F-actin network assembly. Our research showed that the Arp2/3 complex played an important role in F-actin assembly and nucleation (**Figures 7A–F**; Tang and Brieher, 2012). However, there were no significant changes in the protein level of Arp2 or Arp3.

We observed that vinculin increased by 22% in the P0 KD group. Vinculin is a cytoplasmic actin-binding protein, which directly binds to actin, stimulating actin polymerization and recruiting actin remodeling proteins (Bays and DeMali, 2017).

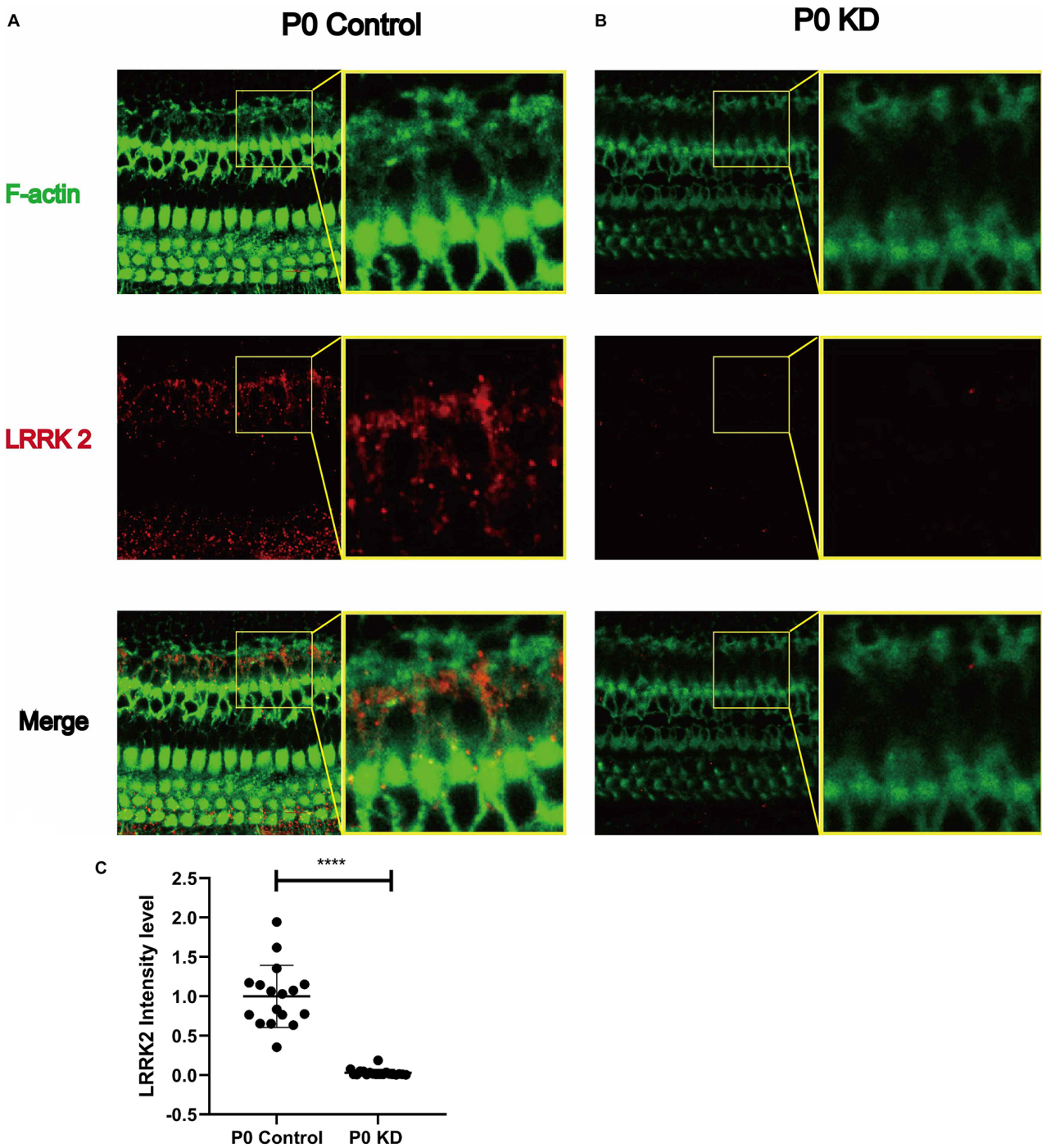

FIGURE 8 | Significant reduction of LRRK2 was observed in the P0 KD group at P6. Immunofluorescence staining of LRRK2 in P0 control **(A)**, P0 KD groups **(B)**. Comparison of LRRK2 intensity between P0 KD group and P0 Control group **(C)**. ****Significantly different from the control group ($P < 0.0001$).

Vinculin binds actin filaments to grow focal adhesions and regulates actin dynamics, and studies have shown that the tail domain of vinculin inhibits the extension of the F-actin barbed ends (Le Clainche et al., 2010). Vinculin stimulates the formation of new F-actin bundles in cells (Kovacs et al., 2011). Thus the increase of vinculin may be the cells' response to abnormal skeletal development, to compensate by increasing the generation of new actin filaments.

We observed that LRRK2 in the P0 KD group was reduced by 97% (**Figure 8**). In previous studies of Parkinson's disease, LRRK2 was found to be associated with changes in the cytoskeleton (Russo et al., 2014;

Harvey and Outeiro, 2019). Under the stoichiometric conditions tested *in vitro*, Lrrk2 decreased the number of polymerized actin filaments, thus affecting the G-actin/F-actin ratio in favor of the monomer. Depletion of Lrrk2 in NIH3T3 cells leads to significant morphological alterations, which suggests that the cytoskeleton of NIH3T3 cells is affected (Meixner et al., 2011). In another study, up-regulation of LRRK2 caused by VIP was found to significantly reduce the F-/G-actin ratio (Niu et al., 2012). Thus the reduction of LRRK2 due to *Gjb2* KD may be the underlying reason for the cytoskeleton development disorder. A large part of LRRK2 research has involved the study of its interactions with small GTPases. The Rho-family of small GTPases is known as the master regulators of the actin cytoskeleton (Yan et al., 2020). The majority of previous studies were focused on RhoA, Rac1, and Cdc42. LRRK2 has been shown to bind RAC1, which increases the interaction of rac1 and p21-activated kinase and enhances rac1 activity, resulting in the regulation of actin cytoskeleton dynamics.

We observed reduced numbers of actin filaments in the malformed OC in Cx26 KD mice. We believe that the disordered development of the cytoskeleton composed of actin filaments and microtubules is the major reason for deformity of the OC.

DATA AVAILABILITY STATEMENT

The original contributions presented in the study are included in the article, further inquiries can be directed to the corresponding author/s.

ETHICS STATEMENT

The animal study was reviewed and approved by Committee on Animal Research of Tongji Medical College, Huazhong University of Science and Technology.

AUTHOR CONTRIBUTIONS

YS and W-jK conceived and designed the study, reviewed and edited the manuscript. X-zL, YJ, SC, KX, LX, YQ, and X-hW performed the experiments. X-zL and YJ wrote the manuscript. All authors contributed to the article and approved the submitted version.

FUNDING

This work was financially supported by the National Natural Science Foundation of China (No. 81771003, No. 81873700, and No. 82071508).

ACKNOWLEDGMENTS

We are grateful to the Center for Instrumental Analysis and Metrology, Institute of Virology, Chinese Academy of Science for our Electron Microscopy (EM), and thanks to An-Na Du, Ding Gao for their help with EM experiments.

REFERENCES

Ahmad, S., Chen, S., Sun, J., and Lin, X. (2003). Connexins 26 and 30 are co-assembled to form gap junctions in the cochlea of mice. *Biochem. Biophys. Res. Commun.* 307, 362–368. doi: 10.1016/s0006-291x(03)01166-5

Bays, J. L., and DeMali, K. A. (2017). Vinculin in cell-cell and cell-matrix adhesions. *Cell. Mol. Life Sci.* 74, 2999–3009. doi: 10.1007/s00018-017-2511-3

Brieher, W. M., and Yap, A. S. (2013). Cadherin junctions and their cytoskeleton(s). *Curr. Opin. Cell Biol.* 25, 39–46. doi: 10.1016/j.ceb.2012.10.010

Caesar, M., Felk, S., Aasly, J. O., and Gillardon, F. (2015). Changes in actin dynamics and F-actin structure both in synaptoneurosomes of LRRK2(R1441G) mutant mice and in primary human fibroblasts of LRRK2(G2019S) mutation carriers. *Neuroscience* 284, 311–324. doi: 10.1016/j.neuroscience.2014.09.070

Chan, D. K., and Chang, K. W. (2014). GJB2-associated hearing loss: systematic review of worldwide prevalence, genotype and auditory phenotype. *Laryngoscope* 124, E34–E53. doi: 10.1002/lary.24332

Chang, Q., Tang, W., Kim, Y., and Lin, X. (2015). Timed conditional null of connexin26 in mice reveals temporary requirements of connexin26 in key cochlear developmental events before the onset of hearing. *Neurobiol. Dis.* 73, 418–427. doi: 10.1016/j.nbd.2014.09.005

Chen, S., Sun, Y., Lin, X., and Kong, W. (2014). Down regulated connexin26 at different postnatal stage displayed different types of cellular degeneration and formation of organ of Corti. *Biochem. Biophys. Res. Commun.* 445, 71–77. doi: 10.1016/j.bbrc.2014.01.154

Chen, S., Xu, K., Xie, L., Cao, H. Y., Wu, X., Du, A. N., et al. (2018a). The spatial distribution pattern of Connexin26 expression in supporting cells and its role in outer hair cell survival. *Cell Death Dis.* 9:1180. doi: 10.1038/s41419-018-1238-x

Chen, S., Xie, L., Xu, K., Cao, H. Y., Wu, X., Xu, X. X., et al. (2018b). Developmental abnormalities in supporting cell phalangeal processes and cytoskeleton in the Gjb2 knockdown mouse model. *Dis. Model Mech.* 11:dmm033019. doi: 10.1242/dmm.033019

Dominguez, R., and Holmes, K. C. (2011). Actin structure and function. *Ann. Rev. Biophys.* 40, 169–186. doi: 10.1146/annurev-biophys-042910-155359

Gloushankova, N. A., Rubtsova, S. N., and Zhitnyak, I. Y. (2017). Cadherin-mediated cell-cell interactions in normal and cancer cells. *Tissue Barriers* 5:e1356900. doi: 10.1080/21688370.2017.1356900

Griffith, A. J., Yang, Y., Pryor, S. P., Park, H. J., Jabs, E. W., Nadol, J. B., et al. (2006). Cochleosaccular dysplasia associated with a connexin 26 mutation in keratitis-ichthyosis-deafness syndrome. *Laryngoscope* 116, 1404–1408. doi: 10.1097/01.mlg.0000224549.75161.ca

Harris, A. L. (2001). Emerging issues of connexin channels: biophysics fills the gap. *Q. Rev. Biophys.* 34, 325–472. doi: 10.1017/s0033583501003705

Harvey, K., and Outeiro, T. F. (2019). The role of LRRK2 in cell signalling. *Biochem. Soc. Trans.* 47, 197–207. doi: 10.1042/BST20180464

Kelley, C. F., Litschel, T., Schumacher, S., Dedden, D., Schwille, P., and Mizuno, N. (2020). Phosphoinositides regulate force-independent interactions between talin, vinculin and actin. *eLife* 9:e56110. doi: 10.7554/eLife.56110

Kibschull, M., Gellhaus, A., and Winterhager, E. (2008). Analogous and unique functions of connexins in mouse and human placental development. *Placenta* 29, 848–854. doi: 10.1016/j.placenta.2008.07.013

Kovacs, E. M., Verma, S., Ali, R. G., Ratheesh, A., Hamilton, N. A., Akhmanova, A., et al. (2011). N-WASP regulates the epithelial junctional actin cytoskeleton through a non-canonical post-nucleation pathway. *Nat. Cell Biol.* 13, 934–943. doi: 10.1038/ncb2290

Le Clainche, C., Dwivedi, S. P., Didry, D., and Carlier, M. F. (2010). Vinculin is a dually regulated actin filament barbed end-capping and side-binding protein. *J. Biol. Chem.* 285, 23420–23432. doi: 10.1074/jbc.M110.102830

Martínez, A. D., Acuña, R., Figueroa, V., Maripillan, J., and Nicholson, B. (2009). Gap-junction channels dysfunction in deafness and hearing loss. *Antioxid. Redox Signal.* 11, 309–322. doi: 10.1089/ars.2008.2138

Meixner, A., Boldt, K., Van Troys, M., Askenazi, M., Gloeckner, C. J., Bauer, M., et al. (2011). A QUICK screen for Lrrk2 interaction partners--leucine-rich repeat kinase 2 is involved in actin cytoskeleton dynamics. *Mol. Cell. Proteomics* 10:M110.001172. doi: 10.1074/mcp.M110.001172

Niu, J., Yu, M., Wang, C., and Xu, Z. (2012). Leucine-rich repeat kinase 2 disturbs mitochondrial dynamics *via* Dynamin-like protein. *J. Neurochem.* 122, 650–658. doi: 10.1111/j.1471-4159.2012.07809.x

Patrinostro, X., Roy, P., Lindsay, A., Chamberlain, C. M., Sundby, L. J., Starker, C. G., et al. (2018). Essential nucleotide- and protein-dependent functions of Actb/β-actin. *Proceed. Natl. Acad. Sci. U S A* 115, 7973–7978. doi: 10.1073/pnas.1807895115

Pollard, T. D., and Cooper, J. A. (2009). Actin, a central player in cell shape and movement. *Science* 326, 1208–1212. doi: 10.1126/science.1175862

Prentki, M., Chaponnier, C., Jeanrenaud, B., and Gabbiani, G. (1979). Actin microfilaments, cell shape and secretory processes in isolated rat hepatocytes. Effect of phalloidin and cytochalasin D. *J. Cell Biol.* 81, 592–607. doi: 10.1083/jcb.81.3.592

Qu, Y., Tang, W., Zhou, B., Ahmad, S., Chang, Q., Li, X., et al. (2012). Early developmental expression of connexin26 in the cochlea contributes to its dominate functional role in the cochlear gap junctions. *Biochem. Biophys. Res. Commun.* 417, 245–250. doi: 10.1016/j.bbrc.2011.11.093

Rabionet, R., Zelante, L., López-Bigas, N., D'Agruma, L., Melchionda, S., Restagno, G., et al. (2000). Molecular basis of childhood deafness resulting from mutations in the GJB2 (connexin 26) gene. *Hum. Genet.* 106, 40–44. doi: 10.1007/s004390051007

Rottner, K., Faix, J., Bogdan, S., Linder, S., and Kerkhoff, E. (2017). Actin assembly mechanisms at a glance. *J. Cell Sci.* 130, 3427–3435. doi: 10.1242/jcs.206433

Russo, I., Bubacco, L., and Greggio, E. (2014). LRRK2 and neuroinflammation: partners in crime in Parkinson's disease? *J. Neuroinflammation* 11:52. doi: 10.1186/1742-2094-11-52

Sun, Y., Tang, W., Chang, Q., Wang, Y., Kong, W., and Lin, X. (2009). Connexin30 null and conditional connexin26 null mice display distinct pattern and time course of cellular degeneration in the cochlea. *J. Comp. Neurol.* 516, 569–579. doi: 10.1002/cne.22117

Tang, V. W., and Brieher, W. M. (2012). α-Actinin-4/FSGS1 is required for Arp2/3-dependent actin assembly at the adherens junction. *J. Cell Biol.* 196, 115–130. doi: 10.1083/jcb.201103116

Wang, Y., Chang, Q., Tang, W., Sun, Y., Zhou, B., Li, H., et al. (2009). Targeted connexin26 ablation arrests postnatal development of the organ of Corti. *Biochem. Biophys. Res. Commun.* 385, 33–37. doi: 10.1016/j.bbrc.2009.05.023

Xie, L., Chen, S., Xu, K., Cao, H. Y., Du, A. N., Bai, X., et al. (2019). Reduced postnatal expression of cochlear Connexin26 induces hearing loss and affects the developmental status of pillar cells in a dose-dependent manner. *Neurochem. Int.* 128, 196–205. doi: 10.1016/j.neuint.2019.04.012

Xu, K., Chen, S., Xie, L., Qiu, Y., Bai, X., Liu, X-Z., et al. (2021). Local macrophage-related immune response is involved in cochlear epithelial damage in distinct Gjb2-related hereditary deafness models. *Front. Cell Dev. Biol.* 8:597769. doi: 10.103389/fcell.2020.597769

Yan, X., Li, M., Luo, Z., Zhao, Y., Zhang, H., and Chen, L. (2020). VIP induces changes in the F-/G-actin ratio of schlemm's canal endothelium *via* LRRK2 transcriptional regulation. *Invest. Ophthalmol. Vis. Sci.* 61:45. doi: 10.1167/iovs.61.6.45

Zhao, H. B., and Yu, N. (2006). Distinct and gradient distributions of connexin26 and connexin30 in the cochlear sensory epithelium of guinea pigs. *J. Comp. Neurol.* 499, 506–518. doi: 10.1002/cne.21113

Zhu, Y., Zong, L., Mei, L., and Zhao, H. B. (2015). Connexin26 gap junction mediates miRNA intercellular genetic communication in the cochlea and is required for inner ear development. *Sci. Rep.* 5:15647. doi: 10.1038/srep15647

Conflict of Interest: The authors declare that the research was conducted in the absence of any commercial or financial relationships that could be construed as a potential conflict of interest.

Publisher's Note: All claims expressed in this article are solely those of the authors and do not necessarily represent those of their affiliated organizations, or those of the publisher, the editors and the reviewers. Any product that may be evaluated in this article, or claim that may be made by its manufacturer, is not guaranteed or endorsed by the publisher.

frontiers in Molecular Neuroscience

ORIGINAL RESEARCH
published: 16 March 2022
doi: 10.3389/fnmol.2022.832813

Pseudo-Temporal Analysis of Single-Cell RNA Sequencing Reveals *Trans*-Differentiation Potential of Greater Epithelial Ridge Cells Into Hair Cells During Postnatal Development of Cochlea in Rats

Jianyong Chen[1,2,3†], Dekun Gao[1,2,3†], Junmin Chen[1,2,3†], Shule Hou[1,2,3], Baihui He[1,2,3], Yue Li[1,2,3], Shuna Li[1,2,3], Fan Zhang[1,2,3], Xiayu Sun[1,2,3], Yulian Jin[1,2,3], Lianhua Sun[1,2,3*] and Jun Yang[1,2,3*]*

[1] Department of Otorhinolaryngology-Head and Neck Surgery, Xinhua Hospital, Shanghai Jiao Tong University School of Medicine, Shanghai, China, [2] Institute of Ear Science, School of Medicine, Shanghai Jiao Tong University, Shanghai, China, [3] Shanghai Key Laboratory of Otolaryngology and Translational Medicine, Shanghai, China

The hair cells of the cochlea play a decisive role in the process of hearing damage and recovery, yet knowledge of their regeneration process is still limited. Greater epithelial ridge (GER) cells, a type of cell present during cochlear development that has the characteristics of a precursor sensory cell, disappear at the time of maturation of hearing development. Its development and evolution remain mysterious for many years. Here, we performed single-cell RNA sequencing to profile the gene expression landscapes of rats' cochlear basal membrane from P1, P7, and P14 and identified eight major subtypes of GER cells. Furthermore, single-cell trajectory analysis for GER cells and hair cells indicated that among the different subtypes of GER, four subtypes had transient cell proliferation after birth and could transdifferentiate into inner and outer hair cells, and two of them mainly transdifferentiated into inner hair cells. The other two subtypes eventually transdifferentiate into outer hair cells. Our study lays the groundwork for elucidating the mechanisms of the key regulatory genes and signaling pathways in the *trans*-differentiation of GER cell subtypes into hair cells and provides potential clues to understand hair cell regeneration.

Keywords: sc-RNA sequencing, pseudo-temporal analysis, cochlear basal membrane, greater epithelial ridge cells, hair cells

OPEN ACCESS

Edited by:
Yu Sun,
Huazhong University of Science and Technology, China

Reviewed by:
Shan Sun,
Fudan University, China
Jie Tang,
Southern Medical University, China

***Correspondence:**
Yulian Jin
jinyulian8548@xinhuamed.com.cn
Lianhua Sun
sunlianhua@xinhuamed.com.cn
Jun Yang
yangjun@xinhuamed.com.cn

† These authors have contributed equally to this work

Specialty section:
This article was submitted to Molecular Signalling and Pathways, a section of the journal Frontiers in Molecular Neuroscience

Received: *10 December 2021*
Accepted: *08 February 2022*
Published: *16 March 2022*

Citation:
Chen J, Gao D, Chen J, Hou S, He B, Li Y, Li S, Zhang F, Sun X, Jin Y, Sun L and Yang J (2022) Pseudo-Temporal Analysis of Single-Cell RNA Sequencing Reveals Trans-Differentiation Potential of Greater Epithelial Ridge Cells Into Hair Cells During Postnatal Development of Cochlea in Rats. Front. Mol. Neurosci. 15:832813. doi: 10.3389/fnmol.2022.832813

INTRODUCTION

In the mammalian auditory system, irreversible damage to cochlear hair cells can be caused by noise stimulation, aging, ototoxic drugs, infections, hereditary susceptibility, and autoimmune diseases, resulting in permanent sensorineural deafness (Wagner and Shin, 2019). Studies have shown that in lower vertebrates, hair cells can regenerate after damage (Cruz et al., 1987), but hair cell regeneration has not been achieved in the mature mammalian cochlea (Brigande and Heller, 2009). The damage and loss of cochlear hair cells are still an important cause of mammalian auditory injury.

The Corti's organ is composed of a certain number of sensory hair cells and supporting cells arranged in a highly ordered manner into a precise chimeric structure (Lim, 1986). The hair cells are located on the basal membrane of the Corti's organ and are closely connected to the non-sensory epithelial cells, which are the main components of the auditory pathway. Hair cells are divided into inner and outer hair cells. Supporting cells are composed of several different types, including inner and outer pillar cells, Deiters cells, Hensen cells, Claudius cells, inner phalangeal cells, and inner border cells. The heads of the inner and outer pillar cells are articulated, and the bases are separated to form a triangular spiral tunnel. Inside the tunnel, there is a single row of inner hair cells on the inner phalangeal cells inside the inner pillar cells. Between the inner phalangeal cells and the inner hair cell is the inner border cell, and its inner side is the inner sulcus. The bottom cell of the inner sulcus has a single layer of cubic epithelium, which is the inner sulcus cell, which comes from the greater epithelial ridge (GER) (Lim and Anniko, 1985).

Histological studies revealed that progenitor cells of the rodent cochlear epithelium develop from the auditory vesicles at embryonic day (E) 11.5, and subsequently proliferate and expand into medial GER and lateral lesser epithelial ridge (LER). From about E15 to birth, GER and LER gradually differentiate into hair cells and supporting cells of the primitive Corti's organ (Driver and Kelley, 2020). Zheng and Gao (2000) transfected a math1-expressing plasmid into the cochlea of newborn rats and found that myosin VIIa (a specific marker of hair cells) and peanut agglutinin-labeled hair cells were produced in the GER region. The origin of these ectopic hair cells is thought to be columnar epithelial cells located in GER.

Greater epithelial ridge normally exists in the late embryonic and early postnatal stages and is located around the inner hair cells, which is one of the signs of immature cochlear morphology (Hinojosa, 1977). After birth, the cell structure rearranges, the number of cells decreases, and the cells degenerate and disappear to become internal sulcus cells around 10–12 days, and eventually form the inner sulcus, at which point the auditory development of cochlea is mature (Kelley, 2007; Dayaratne et al., 2014). The emergence of ectopic hair cells is a surprising discovery since the precursor cells of hair cells were previously thought to originate from the sensory epithelium, but the columnar epithelial cells in GER are located outside of the sensory epithelium, so the researchers considered that GER cells were likely to be the precursor cell pool for hair cell regeneration in the cochlea (Zine et al., 2001). At the same time, a study using adenoviral vectors to transfect genes into the cochlea of mature guinea pigs showed that immature hair cells were generated in the area where GER was located and connected to auditory neurons, further demonstrating that GER was probably a precursor cell for cochlear hair cells (Kawamoto et al., 2003). In addition, organoid developmental regeneration studies showed that different types of non-sensory epithelial cells had the potential for organoid regeneration and development and that organoids derived from GER cells contained cells positive for hair cell markers, suggesting that GER cells had the characteristics of precursor sensory cells after mitosis (Kubota et al., 2021).

Single-cell transcriptome sequencing technology has shown that there are different cell subtypes within the GER region, and different cell subtypes have heterogeneity of gene expression and diversity of biological functions (Kolla et al., 2020; Chen et al., 2021). At present, which GER subtype may transform into inner hair cells and which GER subtype may transform into outer hair cells has not been reported in the literature. In this study, we investigated the differentiation trajectories of different subtypes of GER by single-cell trajectory analysis. The results showed that among the different subtypes of GER, four subtypes had transient cell proliferation after birth and could transdifferentiate into inner and outer hair cells, and two of them mainly transdifferentiated into inner hair cells. The other two subtypes eventually transdifferentiate into outer hair cells. In this study, we revealed the key regulatory genes and signaling pathways in the *trans*-differentiation of GER cell subtypes into hair cells, providing new ideas for the study of the influencing factors and mechanisms of hair cell differentiation and regeneration.

MATERIALS AND METHODS

Tissue Preparation

Female and/or male Sprague–Dawley (SD) rats were selected for this study, which was purchased from Shanghai SIPPR-BK Laboratory Animal Co. In this study, The P1 means the first postnatal day, the P7 day refers to the seventh day after birth, and P14 is the fourteenth postnatal day. Forty SD rats were randomly selected for each period. The animal experiments were performed following the ethical requirements approved by the Animal Care and Use Committee of Shanghai Jiao Tong University School of Medicine. To obtain fresh cochlear basal membrane tissue, the approved guillotine method was used. Cochlear basal membrane tissue was isolated from the temporal bone using a microdissection technique in cold RNase-free Hank's Balanced Salt Solution (HBSS), and the ear capsule was carefully transferred to a tray containing 0.01 M cold phosphate-buffered sodium saline (PBS, pH 7.35, GIBCO, Invitrogen Inc., Carlsbad, CA, United States). The spiral ganglia, spiral ligaments, and vascular striae were carefully separated from the cochlear basal membrane, and the isolated cochlear basal membrane was washed twice with PBS without potassium and magnesium.

Preparation of Single-Cell Suspensions

Cochlear basal membrane tissues were removed *ex vivo* and placed in pre-chilled sterile PBS (calcium-free and magnesium-free) solution, then washed and cut into 0.5 mm^2 pieces. The tissue was dissociated into single cells using a dissociation solution (0.35% collagenase IV5, 2 mg/ml papain, 120 units/ml DNase I) in a 37°C water bath, and digestion was terminated with PBS containing 10% fetal bovine serum. The acquired cell suspension was filtered through a 70–30 um filter and centrifuged for 5 min (4°C, 300 g). The cell precipitate was resuspended in 100 ul of PBS (0.04% BSA) and 1 ml of erythrocyte lysis buffer (MACS 130-094-183) was added and the remaining erythrocytes were lysed by incubation at room temperature for 10 min. After centrifugation again, the precipitate is suspended in 100 μl of Dead Cell Removal Microbeads (MACS 130-090-101) and the dead cells are removed using the Miltenyi®

Dead Cell Removal Kit (MACS 130-090-101). The cells were suspended in PBS (0.04% BSA) after repeated centrifugation and resuspension twice.

Cell viability was checked by trypan blue assay to ensure it was above 85%, single-cell suspensions were counted using a hematocrit plate and the concentration was adjusted to 700–1200 cells/μl.

Chromium 10× Genomics Library and Sequencing

Single-cell suspensions were loaded into 10× Chromium according to kit instructions to capture 5000 single cells, followed by cDNA amplification and library construction according to standard procedures. Sequencing was performed using an Illumina NovaSeq 6000 sequencing system (paired-end multiplex run, 150 bp) by LC-Bio Technology Co. Ltd. (Hangzhou, China) with a minimum depth of 20,000 reads per cell.

Bioinformatics Analysis of scRNA-Seq Data

Illumina bcl2fastq software was used to demultiplex and convert sequencing results to FASTQ data format. Sample demultiplexing, barcode processing and single-cell 3′ gene counting by using the Cell Ranger pipeline[1] and sc-RNA-seq data were aligned to Rattus norvegicus reference genome (Source: Rattus norvegicus UCSC; version: rn6), Single-cells were processed using 10× Genomics Chromium Single Cell 3′ Solution was used to process the captured single cell (Baslan et al., 2012; Shapiro et al., 2013; Huang et al., 2018). The Cell Ranger output was loaded into Seurat (version 3.1.1) to be used for dimensional reduction, clustering, and analysis of scRNA-sequencing data. A total of 34,927 cells, in the end, passed quality control: all genes expressed in less than 1 cell were removed, the number of genes expressed per cell >500 as low and <5000 as high cut-off, UMI counts <500, and the percentage of mitochondria-DNA-derived genes expressed was <25%. The percent of mitochondrial-DNA-derived gene-expression <25%.

Identification of the Major Cell Types and Their Subtypes

We used Seurat software to reduce the dimensionality of all 34,927 cells to visualize them and projected them into two dimensions using the t-SNE method (Satija et al., 2015), with the following steps briefly described: (1) Calculation of gene expression values using the LogNormalize method in Seurat software; (2) Dimensionality reduction of data was performed by using PCA (Principal component analysis) based on the first 2000 highest variable genes. Within all the PCs, the top 10 PCs were used to do clustering and t-SNE analysis; (3) To find clusters, the Seurat Find Clusters function is used to divide all cells into different cell populations with a resolution of 0.8, and clustering results were visualized by using t-distributed Stochastic Neighbor Embedding (tSNE); (4) Marker genes for each cluster were identified with the Wilcoxon rank-sum test with default parameters *via* the FindAllMarkers function in Seurat.

Trajectory and Pseudotime Analysis

CellTrails and Monocle 2[2] (Trapnell et al., 2014) software were used to perform trajectory and pseudotime analysis. We first identified genes that changed over time using a previous study (Yee, 2004) and then performed a likelihood ratio test analysis of differential genes using the differential gene test function to identify significant genes with FDR less than 0.05. Finally, the genes were clustered into groups using the pam function in the cluster R package, and cell sorting and trajectory construction were performed on these genes in an unsupervised manner.

Trajectory Gene Dynamics and Differential Gene Expression

To identify genes whose expression is significantly altered during cochlear development, we took advantage of the fit Dynamic function in CellTrails. We extracted the developmental trajectory of each cluster from the branching trajectory map and calculated the association of gene expression using the R mgcv package.[3] The derived gene sets were then further characterized by the AnimalTFDB 3.0 database containing 1,636 transcription factors (Hu et al., 2019). Finally, dynamic differences in expression between genes were determined using the contrastTrailExpr function. The root means square deviation (RMSD) was used to estimate the difference between trail expressions.

Cell State Identification

The CellTrails package[4] uses spectral embedding and hierarchical clustering methods to identify the state of cell clusters (Ellwanger et al., 2018) and to infer the topology of developmental trajectories. The approach first identifies the most obvious variable genes using the method of M3Drop[5] and then identifies scRNA-Seq datasets using the Michaelis–Menten model (Andrews and Hemberg, 2019). M3Drop identifies differentially expressed genes at 5% FDR and clusters were visualized in a force-based layout, based on log ratios of high-weight paths between clusters. According to the principle of FDR less than 1%, the Wilcoxon rank-sum test was used to identify differentially expressed genes or marker genes among cell clusters.

Pathway Enrichment Analysis

Gene Ontology (GO) enrichment analysis was performed using the GO package (Brionne et al., 2019) and Kyoto Encyclopedia of Genes and Genomes (KEGG) pathway enrichment analysis was performed using Ingenuity Pathway Analysis (IPA)

[1]https://support.10xgenomics.com/single-cell-gene-expression/software/pipelines/latest/what-is-cell-ranger, version 3.1.0.

[2]http://cole-trapnell-lab.github.io/monocle-release/docs/, version 2.8.0.

[3]https://doi.org/10.1201/9781315370279

[4]https://doi.org/10.18129/B9.bioc.CellTrails, v1.4.0.

[5]https://doi.org/10.18129/B9.bioc.M3Drop, v1.12.0.

(Krämer et al., 2014) to examine enrichment in clusters processes. Both analyses allow us to determine which GO terms and/or metabolic pathways are significantly enriched during development. Adjusted p-values < 0.05 were considered statistically significantly different.

Cell-Cell Communication Analysis

To investigate the potential interactions between different cell subpopulations in GER cells, inner and outer hair cells, CellPhoneDB was used for communication analysis (Dou et al., 2021). First, pairwise comparisons were performed between the cell clusters included in the analysis. The cluster labels of all cells were first randomized 1000 times to determine the average receptor and ligand expression levels for each interacting cell cluster. A null distribution for each receptor-ligand pair was generated. The probability of cell-type specificity of the corresponding receptor-ligand complex was obtained by calculating the proportion of the mean higher than the actual mean to derive a P-value. Finally, biologically relevant interactions are derived.

Fluorescence *in situ* Hybridization to Verify Gene Expression Changes

The localization of gene expression and dynamic changes at postnatal day 1 (P1), day 7 (P7), and day 14 (P1) were verified by Paraffin-DIG (digoxigenin)-TSA (Tyramine Signal Amplification)-ISH protocol. Cochlear basal membranes of P1, P7, and P14 SD rats of both sexes were collected and fixed in 4% paraformaldehyde overnight. The Cochleae tissues were then dehydrated with graded alcohol, paraffinized, embedded, and sectioned at a 10-μm thickness on a cryostat. The hybridization protocol was performed according to the manufacturer's recommendations. After RNA ISH, sections were washed with 2 × SSC for 10 min at 37°C, twice with 1 × SSC for 5 min, and then with 0.5 × SSC for 10 min at room temperature. If more non-specific hybrids appear, formamide can be added for washing. Blocking solution (rabbit serum) was added to the section and incubated at room temperature for 30 min, and then remove the blocking solution and add anti-digoxigenin-labeled peroxidase. The sections were incubated at 37 °C for 40 min and then washed with PBS four times for 5 min each. Nuclei were counterstained with DAPI for 15 s at room temperature. After that, a Nikon Eclipse CI upright fluorescence microscope was used to obtain all fluorescent images.

Statistical Analysis

All statistical analyses of the cochlear cells data described in this paper were performed using Prism version 7.0 (GraphPad Software) and calculated according to the relative abundances. Experimental data are presented as the mean ± SEM. Comparisons were made by one-way analyses of variance or students' unpaired two-tailed t-tests and unpaired Wilcoxon rank-sum test among three different stages. P values were calculated using a two-tailed Student's t-test, and P values < 0.05 were considered statistically significant differences.

RESULTS

scRNA-Seq Identifies Eight Greater Epithelial Ridge Cell Clusters According to the Cells Number Dynamic Change and Gene Expression for Significant Marker Genes During Postnatal Auditory Development in Rats

Single-cell RNA sequencing technology was used to perform transcriptome analysis of rat cochlear basal membrane at three critical periods (P1, P7, and P14), and cells with the same gene expression pattern were clustered together according to the cellular gene expression pattern (**Figure 1A**). After sequencing analysis, we constructed cell profiles and identified 27 cell clusters in the three periods (**Figure 1B**). We can see that the number of cells in some clusters decreased significantly or even disappeared at day P14, some clusters were present in increased numbers at day P7 and then decreased significantly and disappeared further by day P14, and some clusters showed no significant changes. The gene expression heat map shows the top three expressed genes for each different cell cluster (**Figure 1C** and **Supplementary Table 1**).

Greater epithelial ridge cells, also referred to as Kölliker's organ (KO) (Dou et al., 2021) are temporary structures during the development of cochlear hearing, during which there is programmed apoptosis and autophagy, and they eventually degenerate and disappear after the cochlear hearing has matured (Hou et al., 2019, 2020). From the dynamic change analysis of cell numbers, four-cell clusters, 0, 3, 4, and 6, showed a gradual decrease in cell numbers from P1 to P14 and disappeared on P14, and we tentatively considered four cell clusters 0, 3, 4, and 6 as different subtypes of GER cells (Chen et al., 2021), which is consistent with Kolla's study (Kolla et al., 2020). In addition, we also found that clusters 2, 7, 9, and 12 showed an increase in the number of cells from P1 to P7, while degenerated and disappeared at P14 days (**Figure 2** and **Supplementary Table 1**).

We further selected the characteristic genes Otor, Dbi, Emcn, Ccn3, Col9a1, Gpc3, Col2a1, Igfbp4, Serpinf1, and Mme in these eight cell clusters, and analyzed the expression patterns of these genes (**Figure 3**). It can be seen from the gene expression pattern map that the Otor gene was highly expressed on clusters 0, 2, 4, 6, and 12, with a higher expression on clusters 0, 4, and 12. Dbi, Slc1a3, and Ccn3 genes were consistently expressed on clusters 0, 3, 4, and 6; Gpc3 was highly expressed on clusters 3, 7, and 9, and Col2a1 had similar expression characteristics on clusters 0, 2, 9, and 12. The Igfbp40 gene was present in clusters 2, 9, and 12, while the Serpinf1 gene had similar expression characteristics in clusters 0, 2, 7, 9, and 12 (**Figure 4**).

Based on the expression levels of genes in different clusters and the spatial regional distribution of gene expression on the t-SEN map, we found that clusters 0, 2, 3, 4, 6, 7, 9, and 12 have similar expression characteristics, among which clusters 4 and 6, clusters

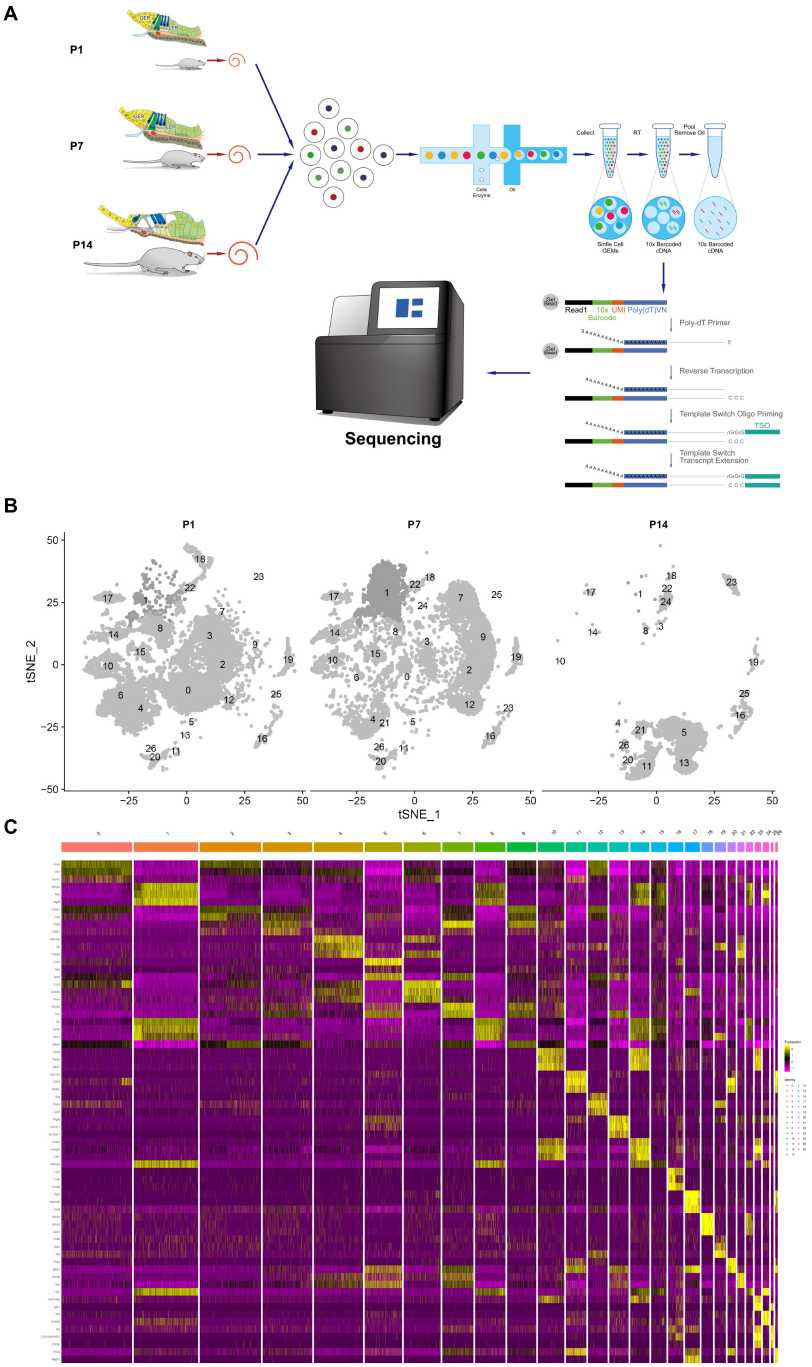

FIGURE 1 | Global expression profiling of cochlear duct cells by scRNA-Seq and cell clusters identification from P1, P7, and P14. **(A)** Cross-section diagrams of the cochlear canals, and the scheme of cochlear duct preparation, single-cell isolation, and Chromium 10× Genomics library and scRNA-seq at P1, P7, and P14. **(B)** t-SNE plots of cochlear cell clusters at P1 (left), P7 (middle), and P14 (right) based on the origins (number) are shown. **(C)** Heat map for cochlear duct cell clusters. The top three differentials expressed (DE) genes for the 27 identified clusters are shown. Cellular identity for each cluster is indicated by a color bar at the top of the heat map. The color ranges from blue to bright yellow indicates low to high gene expression levels, respectively.

0, 3, and 12, and clusters 2, 7, and 9 were more similar in spatial distribution and gene expression patterns. Through the dynamic changes, gene expression patterns, and spatial distribution of the above cell clusters, we believe that clusters 2, 7, 9, and 12 may be other subclusters of GER cells, and these subsets may have the ability to differentiate or transdifferentiate into other cells based on their proliferative properties from P1 to P 7 (**Figure 2**).

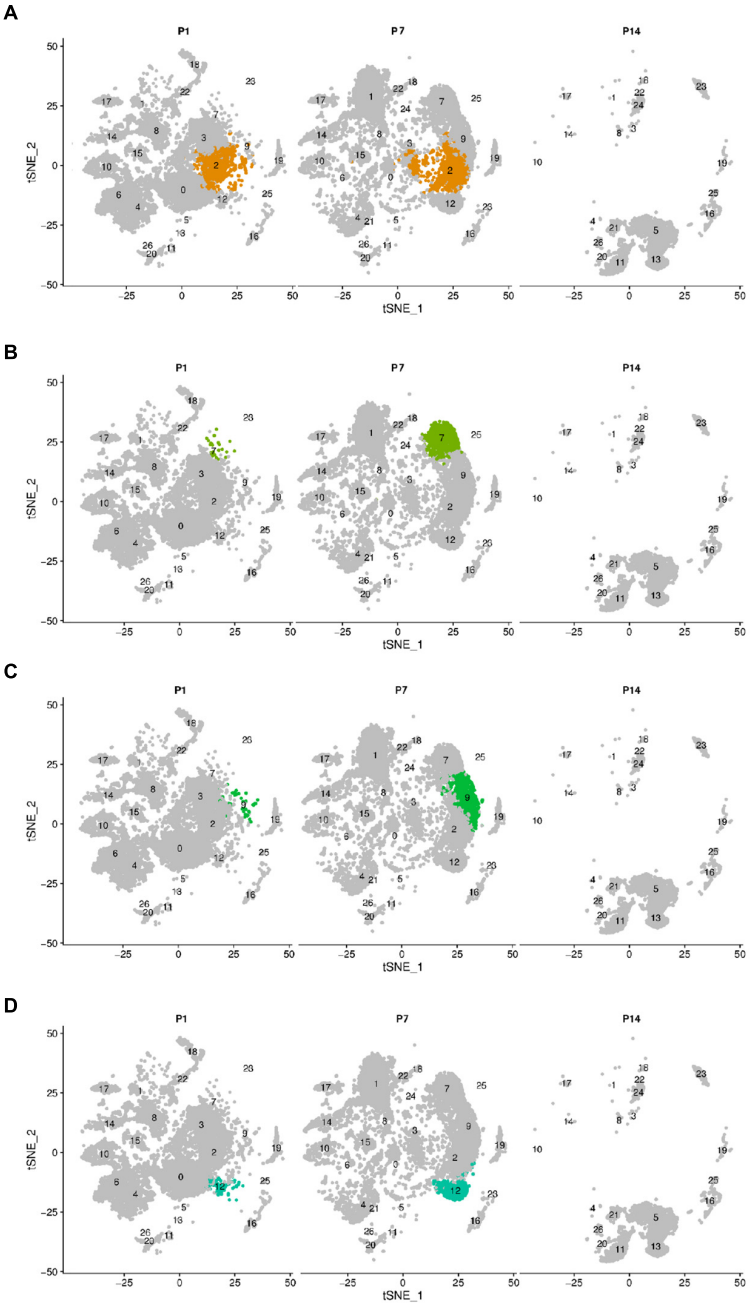

FIGURE 2 | The change of cell number of the above different cell clusters in three different periods of P1, P7, and P14. Cells were clustered using a graph-based shared nearest-neighbor clustering approach plotted by a tSNE plot. **(A)** tSNE plot of Cluster 2. **(B)** tSNE plot of Cluster 7. **(C)** tSNE plot of Cluster 9. **(D)** tSNE plot of Cluster 12. Clusters 2, 7, 9, and 12 showed an increase in the number of cells from P1 to P7, while degenerated and disappeared at P14 days.

scRNA-Seq Identifies Three Inner Hair Cell Subtypes

As seen from the t-SEN plot, cluster 11 was closely linked to clusters 20 and 26 in terms of spatial structure and was significantly increased at P14 as with clusters 5, 13, and 21 (**Figure 5A**). Analysis of gene expression in these cell clusters revealed that clusters 11, 20, and 26 had very similar gene expression consistency with significant differences from Cluster 5, Cluster 13, and Cluster 21 (**Figure 5B**). In addition, the spatial distribution of t-SEN shows a segmentation but close spatial location, suggesting a close functional association between these cell clusters.

The violin plot further analyzed the expression of Coch, Gjb2, Gjb6, Cemip, Cldn5, Slc2a1, Atp2a3, Plvap genes in cluster 11 and compared the results with those of clusters 20, 26, 5, 13,

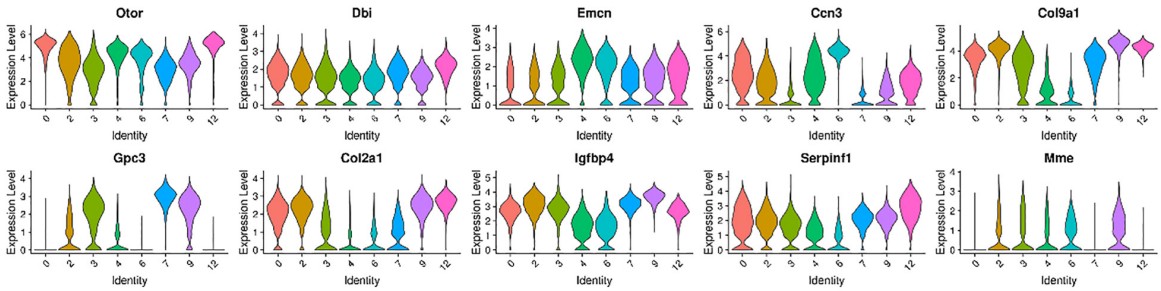

FIGURE 3 | Violin plots showing select genes that are deferentially expressed in the GER cluster 0, 3, 4, and 6 with the number of cells decreased from P1 to P14, and GER cluster 2, 7, 9, and 12 with the number of cells increased from P1 to P7 and degenerated and disappeared at P14 days. The Y-axis, log-normalized transcript counts. These eight clusters had similar expression characteristics.

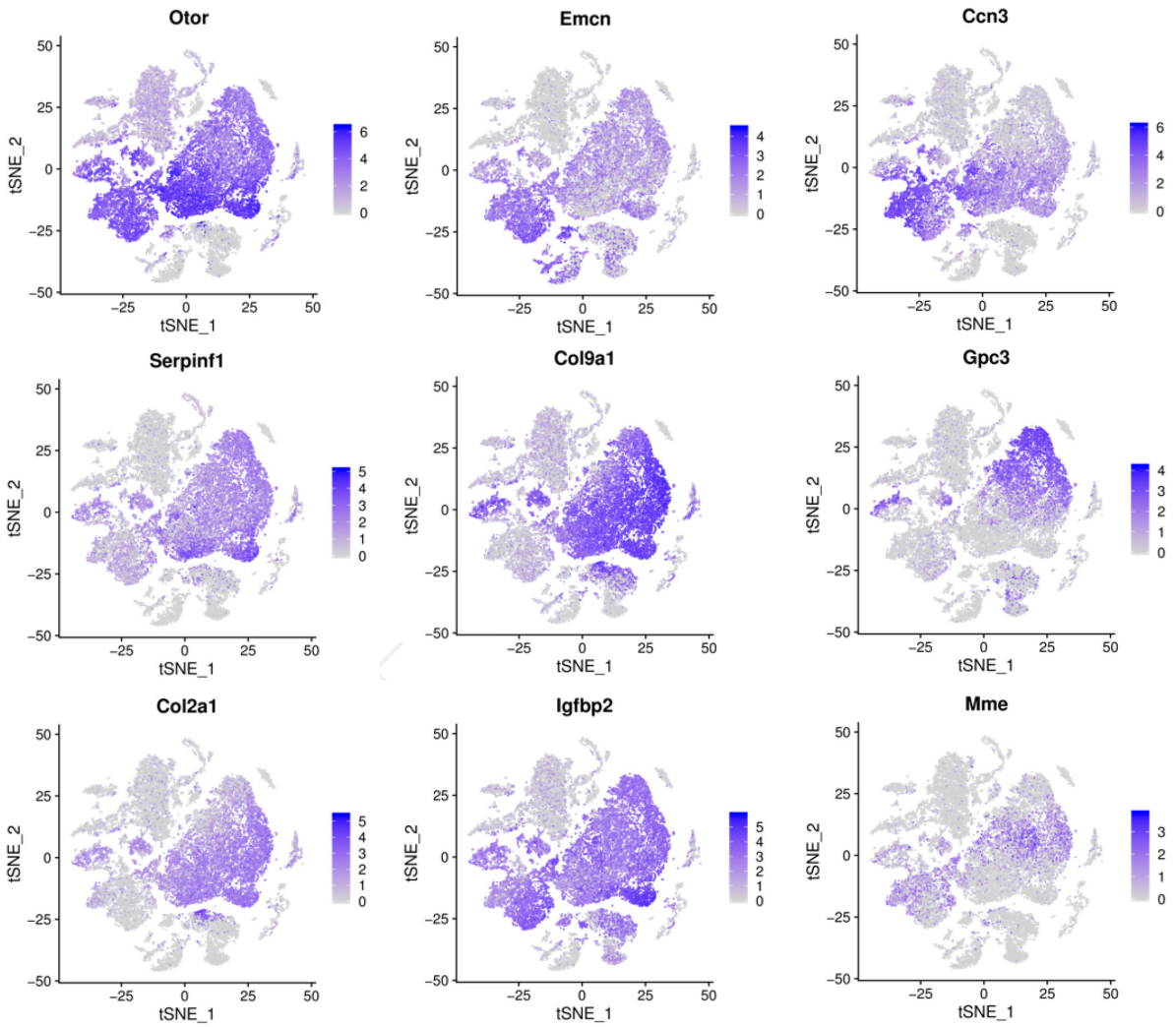

FIGURE 4 | Cells landscape of cochlea duct revealed by scRNA-seq analysis, which was performed on single-cell suspensions pooled from P1, P7, and P14. All samples were analyzed using canonical correlation analysis with the Seurat R package. Cells were clustered using a graph-based shared nearest-neighbor clustering approach plotted by tSNE plot. Feature Plots showing transcript accumulation for specific cell marker genes in individual cells of clusters 0, 2, 3, 4, 6, 7, 9, 12. Color intensity indicates the relative transcript level for the indicated gene in each cell.

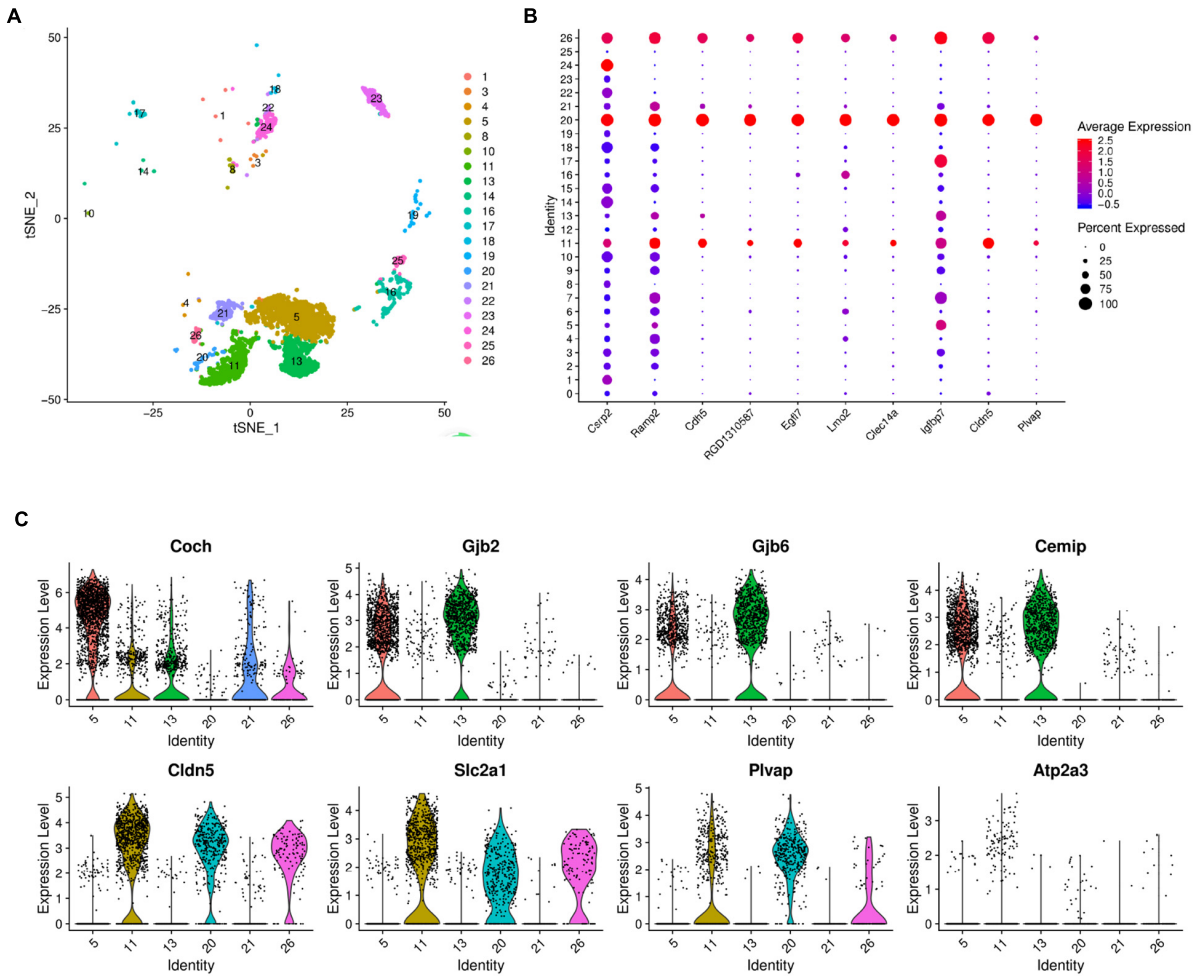

FIGURE 5 | Gene expression in inner cell clusters. **(A)** The t-SEN plots of clusters 11, 20, and 26 were closely linked to clusters 5, 13, and 21 in terms of spatial structure. **(B)** Dot plots representing gene expression levels of different cell clusters. Each dot was sized to represent the proportion of cells of each type expressing the marker gene and colored to represent the mean expression of each marker gene across all cell clusters. **(C)** Violin plots showing select genes that are deferentially expressed in the clusters of 11, 20, 26, and clusters 5, 13, and 21. Y-axis, log-normalized transcript counts.

and 21. The plot shows that clusters 11, 20, and 26 have similar gene expressions, while clusters 5, 13, and 21 have distinct gene expression characteristics of the supporting cells (**Figure 5C**).

Three support cell-specific genes, Coch, Gjb2, and Gjb6, are significantly high-expressed in clusters 5 and 13, and Gjb2 and Gjb6 genes encode gap junction proteins (Connexin, Cx) 26 and 30, which constitute the major isoforms of gap junction channel coupling between cochlear support cells (Rabionet et al., 2000; Meşe et al., 2007). Support cells are coupled to each other *via* Cx26 and/or Cx30 gap junction channels or hemichannels, forming a network of support cells that transmit ions, signals, and nutrient molecules and constitute the microenvironment of nearby or surrounding hair cells (Johnson et al., 2017; Mammano, 2019). Both impaired differentiation of supporting cells and impaired substance or signaling between supporting cells can cause impaired auditory development leading to congenital or acquired deafness, as has been demonstrated in transgenic mouse models of deafness (del Castillo et al., 2002). Cochlear hair cell regeneration studies have further confirmed that regenerating hair cells cannot obtain functional maturity without the provision of an appropriate and stable microenvironment by supporting cells, suggesting that these three clusters may play a major regulatory role in the development of cochlear hearing as non-sensory supporting cells (Roccio et al., 2020). In addition, the violin plot showed that Cldn5, Slc2a1, Plvap, Atp2a3 were more highly expressed on clusters 11, 20, and 26. Previous transcriptome studies on mice have shown that Atp2a3, Cabp2, and Shtn1 are specific marker genes for inner hair cells (Pirvola et al., 1995; Liu et al., 2014; Wiwatpanit et al., 2018), and our study found consistent high expression of the Atp2a3 gene specifically on clusters 11, 20, and 26 (**Figure 5C**), which was consistent with Kolla's study according to the results of single-cell RNA Sequencing (Kolla et al., 2020). Therefore, we tentatively considered the above three clusters as different subtypes of inner hair cells.

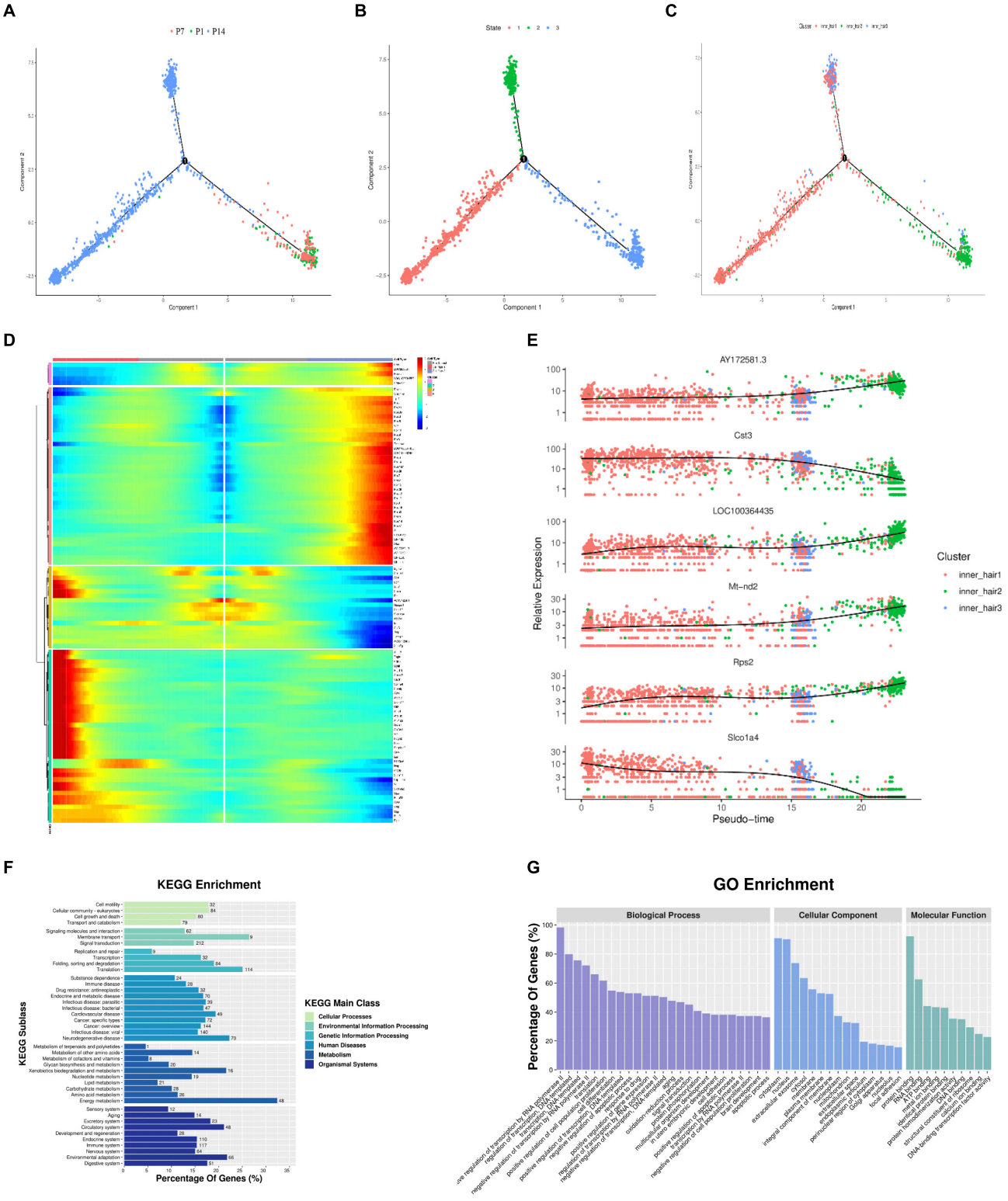

FIGURE 6 | Pseudotime trajectory of the inner hair cell. **(A–C)** Monocle analyses show the development of inner hair cells at different cell developmental periods **(A)**, developmental states **(B)**, and branches of development **(C)**. **(D)** Heatmap of DEGs in different blocks along the pseudotime trajectory. The Red color represents an abundant expression of genes. **(E)** Dynamic gene expression with pseudotime trajectory. **(F)** GO enrichment analysis of genes in cells through fate 1 and fate 2. **(G)** Functional enrichment analyses with KEGG performed with the enriched genes in cells through fate 1 and fate 2.

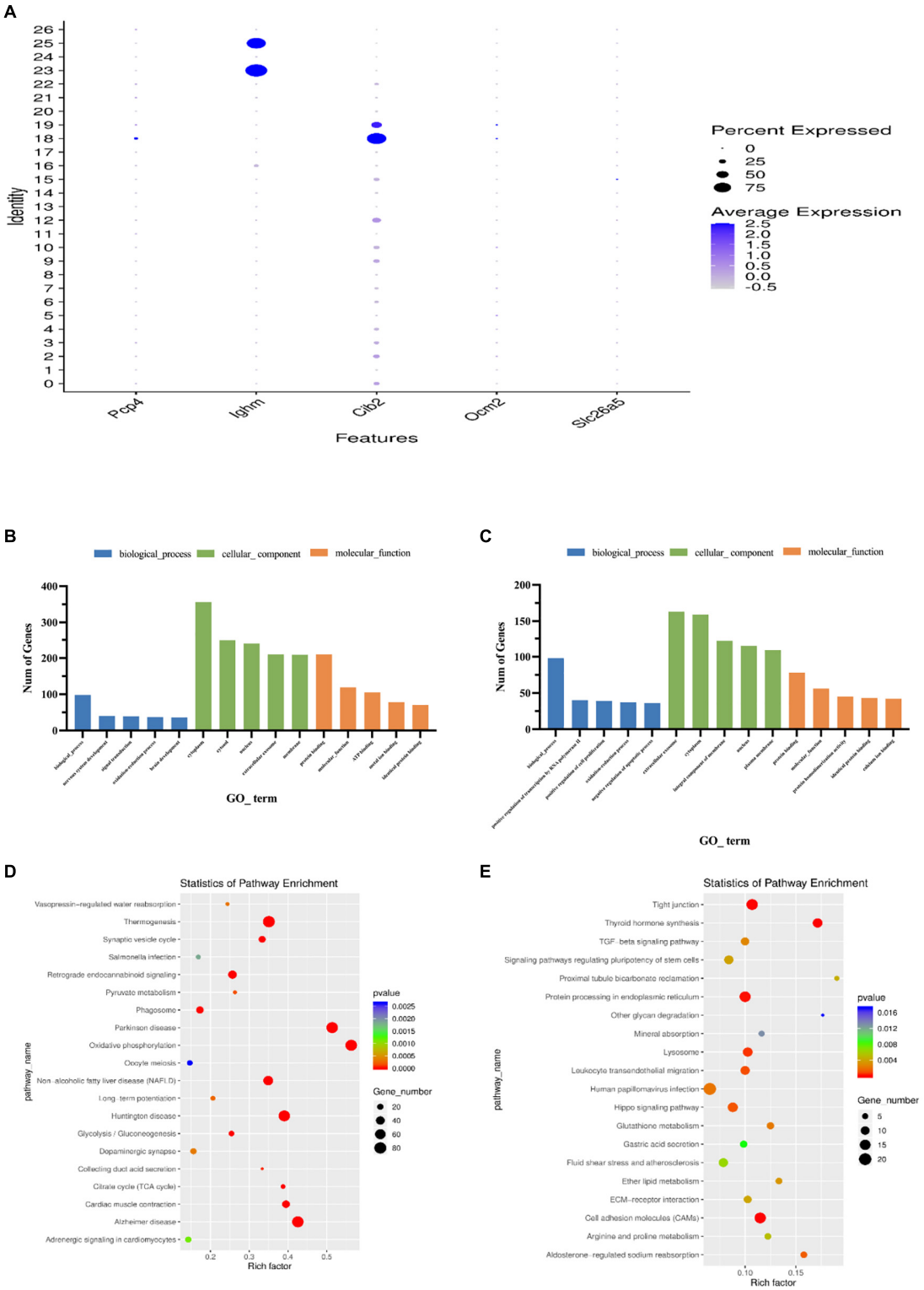

FIGURE 7 | Features of outer hair cell subtypes. **(A)** Accumulation of marker gene transcripts by cluster. This dot plot indicates the level of marker gene expression (dot intensity) and the fraction of cells in each cluster expressing a given marker gene (dot size). **(B)** GO enrichment analysis of genes for cluster 18. **(C)** GO enrichment analysis of genes for cluster 19. **(D)** Functional enrichment analyses using KEGG pathways for cluster 18. **(E)** Functional enrichment analyses using KEGG pathways for cluster 19. The x-axis is the item of go function, the ordinate represents the enriched genes by each item, and the cycle size indicates the significance and corresponding significance values displayed as log10 (*P*-value).

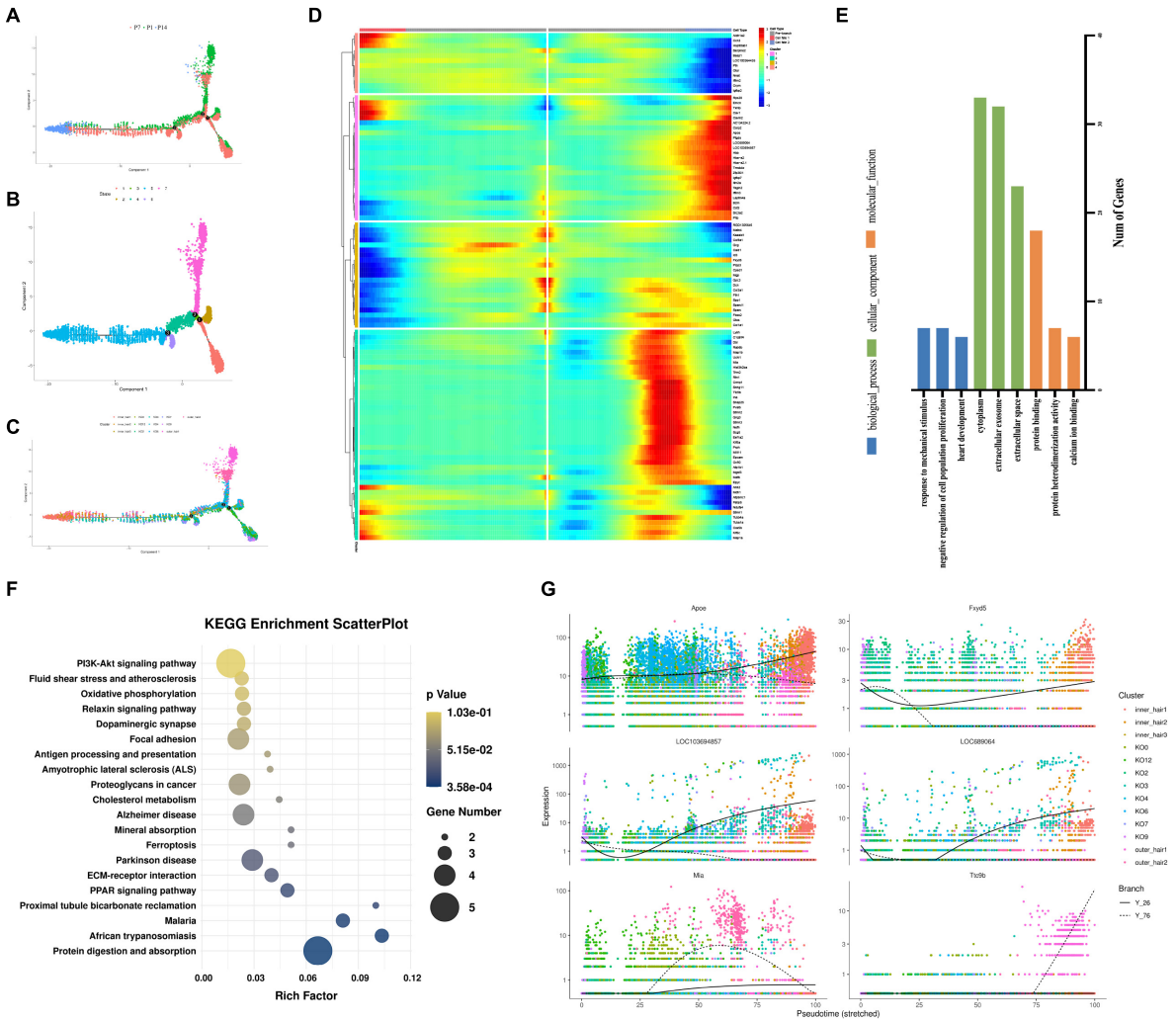

FIGURE 8 | Developmental trajectories of KO cells and inner and outer hair cells. **(A–C)** Monocle analyses show the development of KO cells and inner and outer hair cells. **(D)** Heatmap of different blocks of DEGs along the pseudotime trajectory. **(E)** GO enrichment analysis of genes in Fate 1 and Fate 2 cell fate transitions for KO cells and inner and outer hair cells. **(F)** Functional enrichment analyses using KEGG pathways in Fate1 and Fate 2 cell fate transitions. **(G)** Dynamic gene expression with pseudotime trajectory.

Inner Hair Cell Trajectory Development

The developmental trajectories of the three different subtypes of inner hair cells were analyzed, and the results showed the existence of three different cell developmental periods, developmental states, and a branch of development (**Figures 6A,B**). The cells started to develop from state 1 and transformed into state 2 and state 3 by the first branch.

The main cells in state 1 are cluster 20, with a small number of clusters 11 and 26.

By the time of the first branch, cluster 20 gradually degenerated, and clusters 11 and 26 gradually increased, with cluster 11 increasing more markedly, suggesting that cluster 11 is the main inner hair cell subtype in the maturing cochlear hearing (**Figure 6C**). As seen from the genetic heat map of cell fate transitions, the genes that were highly expressed during the transition toward Fate1 were mainly Acta2, Tagln, Rgs5, Col4a1, Dcn, GSn. The genes that were highly expressed during the transition toward Fate2 were mainly LOC100364435, Rpsa, Rpl17, Rack1, Otir, Actg1 (**Figure 6D**).

Throughout the cell developmental trajectory, we found AY172581.3, Cst3, LOC100364435, Mt-nd2, Rps2, Slco1a4 were the major regulatory genes, with the expression of Cst3 and Slco1a4 downregulated and the expression of AY172581.3, LOC100364435, Mt-nd2, Rps2 upregulated (**Figure 6E**). GO function and KEGG signaling pathway analysis of the genes enriched in Fate1 and Fate 2 cell fate transitions showed that genes were mainly enriched in positive regulative of transcription by RNA polymerase-II of Biological process, the cytoplasm of cellular components, and Protein binding in molecular function of GO functional analysis (**Figure 6F** and **Supplementary Table 2**), and KEGG signaling pathway analysis showed genes mainly

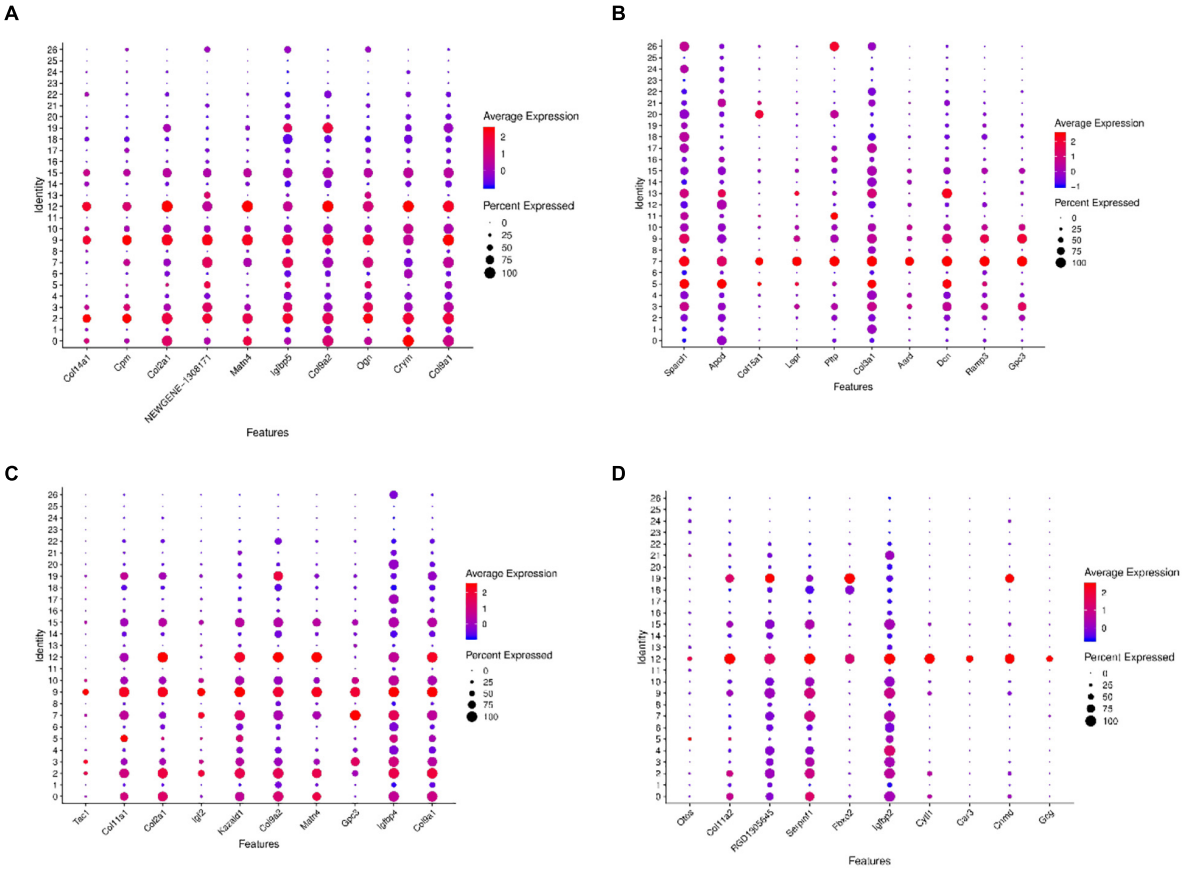

FIGURE 9 | Dot plots representing expression levels of the KO2, KO7, KO9, and KO12 clusters. All samples were analyzed using dot plot analysis with the Seurat R package. Expression levels of the top ten genes on cluster 2 **(A)**, cluster 7 **(B)**, cluster 9 **(C)**, cluster 12 **(D)** are shown. Each dot was sized to represent the proportion of cells of each type expressing the marker gene and colored to represent the mean expression of each marker gene across all cells.

enriched in the Ribosome signaling pathway (**Figure 6G** and **Supplementary Table 3**).

scRNA-Seq Identifies Two Outer Hair Cell Subtypes

Single-cell sequencing results showed that Cib2 was found to be significantly differentially expressed in clusters 18 and 19, with cluster 18 being more highly expressed (**Figure 7A**). The Cib2 protein is responsible for maintaining Ca^{2+} homeostasis in cells and interacting with integrins-transmembrane receptors essential for cell adhesion, migration, and activation of signaling pathways, and is widely expressed in various human and animal tissues, mainly in skeletal muscle, nervous tissue, inner ear, and retina (Jacoszek et al., 2017). Now, Cib2 has been added to the extensive list of genes associated with hearing, loss, and previous studies have been shown that Cib2 is a specific gene expressed on outer hair cells (Riazuddin et al., 2012; Burns et al., 2015). Single-cell transcriptome sequencing based on P7-day mice by Kolla et al. (2020) also showed that Cib2 was highly and nearly specific expressed in outer hair cells clusters (White et al., 2006). In this study, gene expression analysis revealed that Cib2 was significantly higher and specifically expressed on both clusters 18 and 19, which were tentatively considered as two different subtypes of outer hair cells. GO functional analysis showed that both clusters 18 and 19 are enriched in the biological process. In terms of cellular components, cluster 18 is mainly enriched in the cytoplasm, and cluster 19 is mainly enriched in the Extracellular exosome. Both clusters are enriched in Protein binding in molecular function (**Figures 7B,C** and **Supplementary Tables 4, 5**). KEGG signaling pathway analysis revealed that Cluster18 was mainly enriched in the Thermogenesis signaling pathway, while Cluster19 was mainly enriched in the Tight junction and Cell adhesion molecules signaling pathways (**Figures 7D,E** and **Supplementary Tables 6, 7**).

Developmental Trajectory Analysis Showed Four Greater Epithelial Ridge Cell Subtypes Had the Potential to Transdifferentiate Into Inner and Outer Hair Cells

Although cochlear hair cell regeneration does not occur in adult mammals, the neonatal mouse cochlea inner the

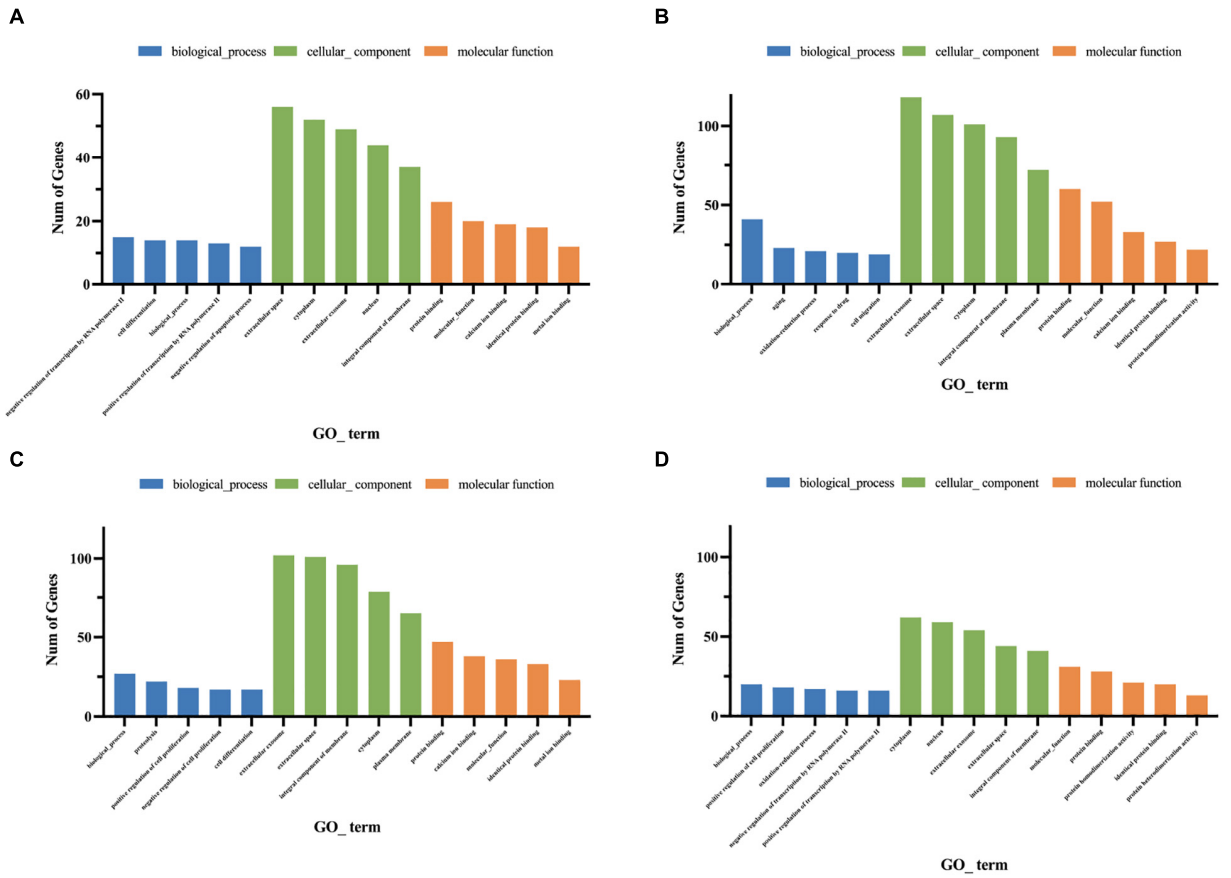

FIGURE 10 | Gene ontology enrichment analysis of genes for cluster 2 **(A)**, cluster 7 **(B)**, cluster 9 **(C)**, cluster 12 **(D)**. The Go functions include molecular functions, cellular components, and biological processes. The x-axis is the item of go function, and the ordinate represents the enriched genes by each item.

first two neonatal weeks shows limited and organoid-generating regenerative potential (Oshima et al., 2007). To determine whether GER (KO) cells may have the potential to transdifferentiate into inner and outer hair cells, we further performed the cell development perspective by single-cell RNA sequencing trajectory analysis and found it interesting that the main cell clusters at the beginning of cell development were KO2, KO7, KO9, and KO12, which were firstly increased in the number of cells from P1 to P7, while degenerated and disappeared at P14 days. At the second branch, part of the cells developed toward outer hair cells (**Figures 8A–C**) and part toward inner hair cells (**Figures 8A–C**). As seen from the genetic heat map of the cell fate transition, the genes that are highly expressed when the cells are transitioning toward fate 1 are mainly Aldh1a2, Ccn3, Ank2, Stmn1, Map1a, Kif5c. The genes that are highly expressed when the cells are transitioning toward fate 2 are mainly Rps28, Apoe, Ac134224.2, Ptgds, Cst3, Igfbp7, Hbb, Hba-a2, Tagln2, Tmsb4x, Crsp2 (**Figure 8D**). Go function and KEGG signaling pathway analysis of the genes enriched in Fate1 and Fate 2 cell fate transitions showed that genes were mainly enriched in negative regulation of cell population proliferation of biological process, and cytoplasm in a cellular component, and Protein binding in molecular function (**Figure 8E**), and KEGG signaling pathway analysis showed genes mainly enriched in the PI3K-AKT signaling pathway (**Figure 8F**). In the whole process of cell development, Apoe, Fxyd5, LOC103694857, LOC689064, Mia, Itc9b are the main regulatory genes and are upregulated (**Figure 8G**).

Gene Ontology Function and Kyoto Encyclopedia of Genes and Genomes Pathway Analysis the Four *Trans*-Differentiations Potential Greater Epithelial Ridge Cell Clusters

Further gene expression analysis of the above four clusters with *trans*-differentiation potential revealed that they all have similar gene expression patterns. Relatively specific highly expressed genes were Crym, Col9a2, Col2a1, Col9a1 in cluster 2 (**Figure 9A**), Lepr, Ramp3, Gpc3 in cluster 7 (**Figure 9B**), Igfbp4, Gpc3 in cluster 9 (**Figure 9C**), and Cytl1, Cnmd, Serpinf1, and Col11a2 in cluster 12 (**Figure 9D**).

Gene ontology functional analysis showed that all four cell clusters were enriched in Protein binding in terms of molecular function, cluster 2 was mainly enriched in Extracellular space (**Figure 10A** and **Supplementary Table 8**), clusters 7 and 9 were

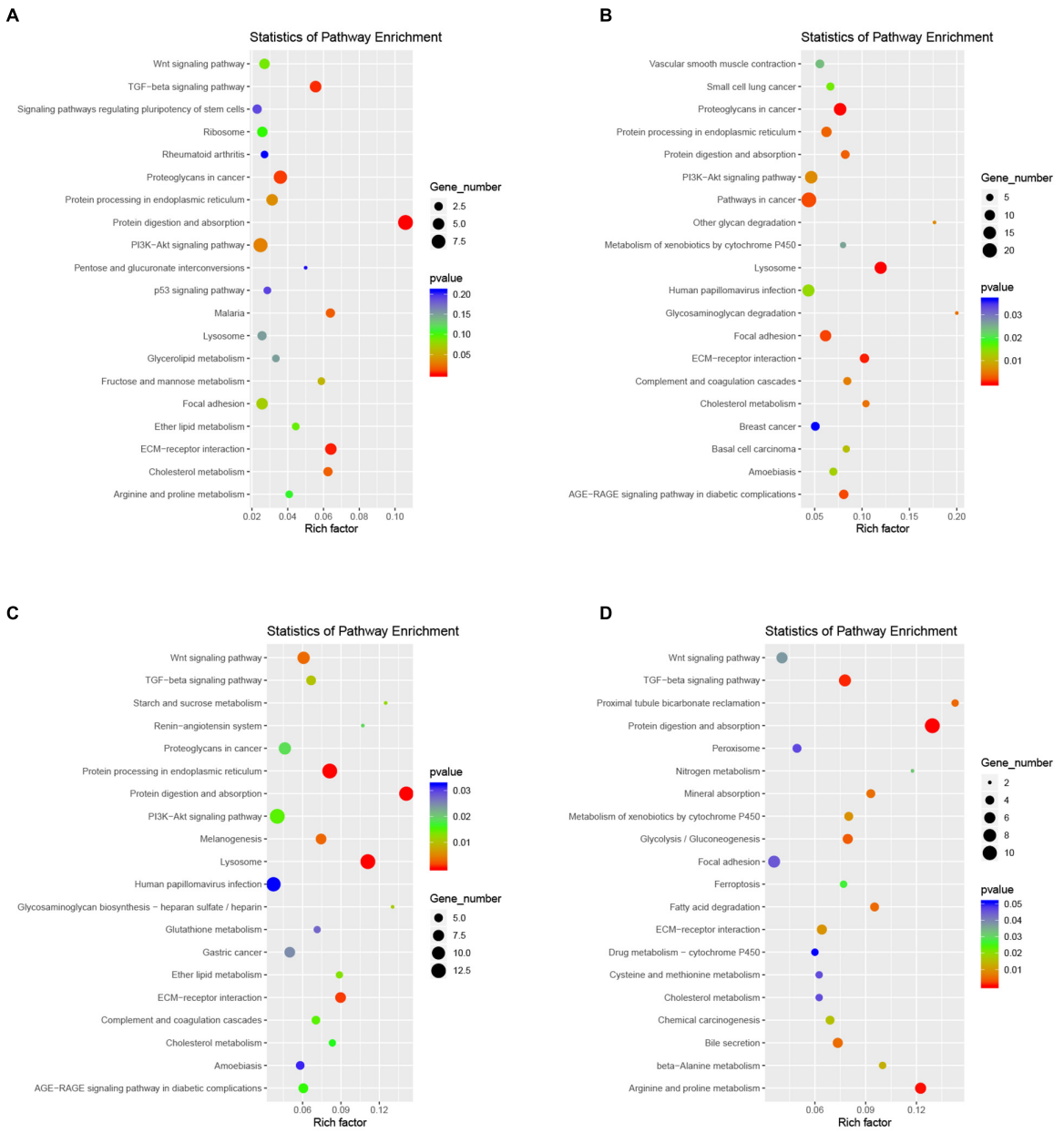

FIGURE 11 | Functional enrichment analyses using KEGG pathways for cluster 2 **(A)**, cluster 7 **(B)**, cluster 9 **(C)**, cluster 12 **(D)**. The cycle size indicates the corresponding significance values displayed as log10 (*P*-value). The much bigger the triangle size, the much more genes enriched in this pathway.

mainly enriched in Extracellular exosome (**Figures 10B,C** and **Supplementary Tables 9, 10**), and cluster12 was mainly enriched in Cytoplasm (**Figure 10D** and **Supplementary Table 11**). Cluster 2 is mainly enriched in the Negative regulation of transcription by RNA polymerase II (**Figure 10A**), while the other three cell groups are mainly enriched in the biological process (**Figures 10B–D**). KEGG signaling pathway analysis revealed the following enriched signaling pathways: Cluster 2 (**Figure 11A**) and cluster 12 (**Figure 11D**) were mainly in Protein digestion and absorption; Cluster 7 was mainly in the pathway in cancer (**Figure 11B**); Cluster 9 was in Protein digestion and absorption, in addition to two signaling pathways, Protein processing endoplasmic reticulum and Lysosome (**Figure 11C**).

Complex Cell-Cell Communication Networks Exist in Greater Epithelial Ridge (Kölliker's Organ) Cells and Cochlear Inner and Outer Hair Cells

To systematically assess the associated complex cellular responses, we attempted to map ligand-receptor interactions with our scRNA-seq data to better understand cellular behaviors

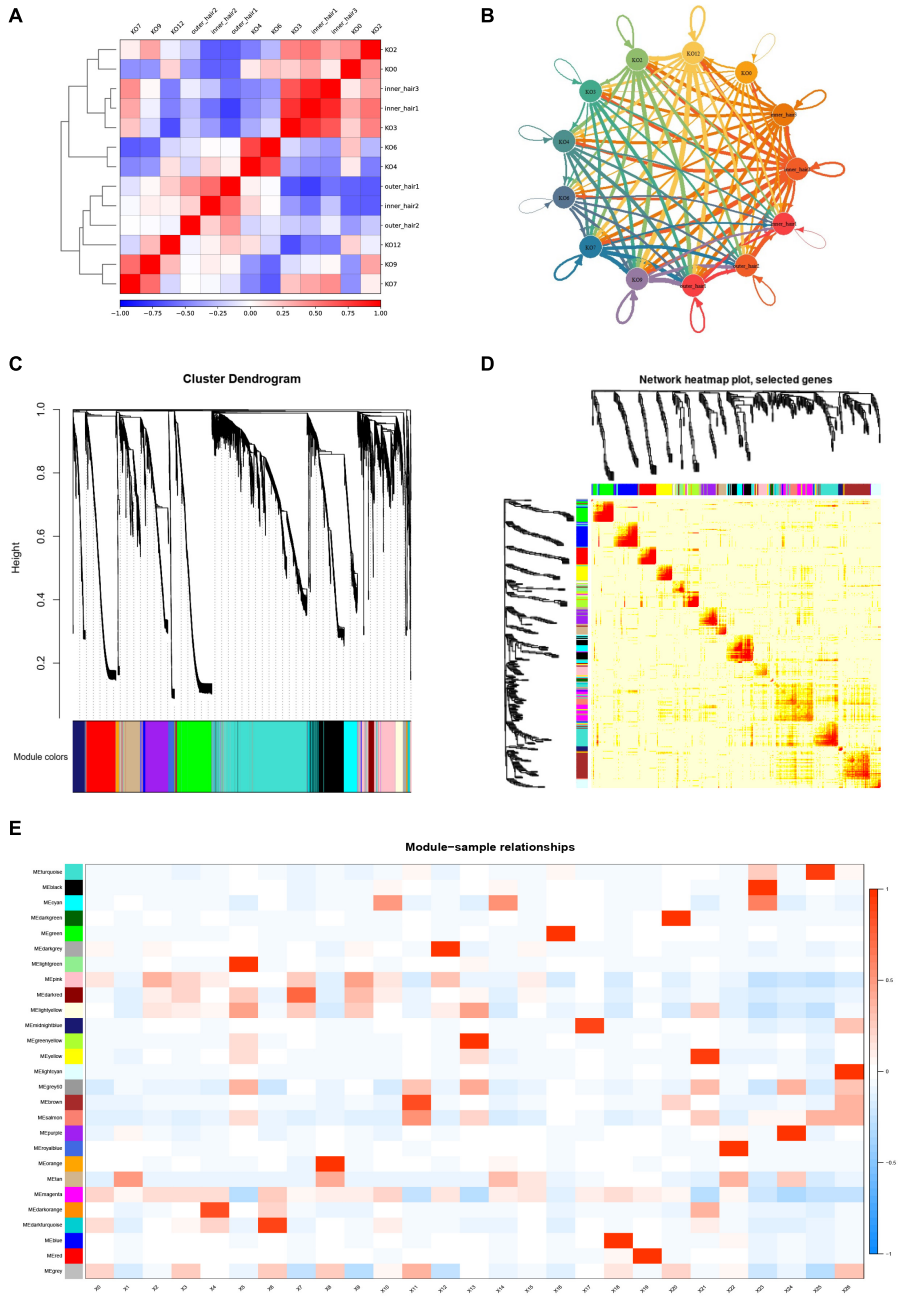

FIGURE 12 | Cell-cell communication networks and WGCNA analysis of KO cell clusters and hair cell clusters. **(A)** Heatmap in KOs and hair cells. The red color indicates a significant interaction. **(B)** Capacity for intercellular communication among KOs and hair cells. Each line color indicates the ligands expressed by the cell population represented in the same color (labeled). The lines connected to cell types expressed the cognate receptors. The line thickness was proportional to the number of ligands when cognate receptors were present in the recipient cell type. **(C)** The dendrogram of gene modules built by WGCNA. **(D)** Network heatmap plot. The module corresponds to branches. The bright red color of nodes represented stronger the genetic correlation of this module. **(E)** Module-trait relationship between different gene modules. The number in each cell represents the degree of correlation, and red means positive correlation at this stage; blue means negative correlation at this stage. Different colors represent the diverse specific gene modules detected by WGCNA.

and responses to neighboring cells in the cochlear basal membrane. We considered the expression levels of ligands and receptors within GER cell clusters and the inner and outer hair cell clusters and predicted molecular interactions between cell populations *via* specific protein complexes. We then generated a potential intercellular communication network among all cells in the GER cell clusters and hair cell clusters separately. Broadcast ligands for which cognate receptors were detected and manifested broad communication between GER cell and the inner and outer hair cell (**Figures 12A,B** and **Supplementary Figures 1–13**).

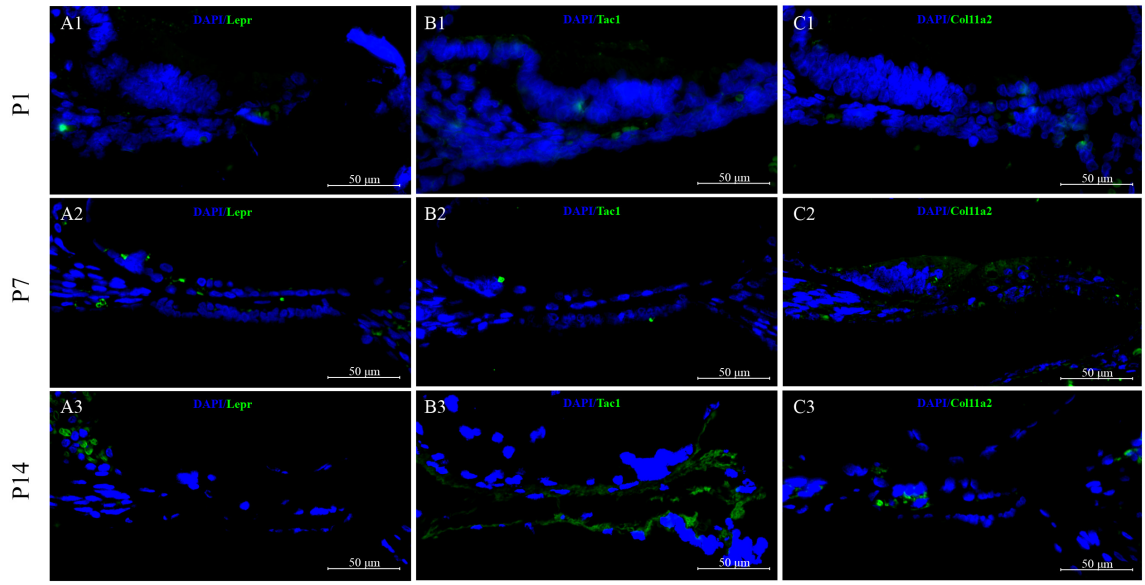

FIGURE 13 | Validation of high expression gene of GER cell clusters at P1, P7, and P14. Lepr was low expressed in the GER region at P1 **(A1)**, and upregulated expression in GER and inner hair cell region at P7 **(A2)**, but the expression was significantly reduced and almost disappeared at P14 **(A3)**. Tac1and Col11a2 were low expressed at P1 **(B1,C1)** but showed a significantly upregulated expression in GER at P7 **(B2,C2)**. While during the P14 period, Tac1and Col11a2 were nearly disappeared in the GER region and were centrally expressed in the hair cell region **(B3,C3)**.

The WGCNA method was further used to analyze the gene association patterns between different subtypes of GER cells and the inner and outer hair cells of the cochlea (**Figures 12C,D**). We found that the blue module was the most significant and associated with the GV phase, while the yellow module was the most significant and associated with the MI phase and the magenta module was the most significant and associated with the MII phase (**Figure 12E**).

Fluorescence *in situ* Hybridization Shows the Presence of Dynamic Gene Expression Changes in the Cochlear Basal Membrane

To validate the cell-type-specific genes, we used fluorescence *in situ* hybridization (FISH) to localize transcripts in cross-sections from P1 to P14 cochlear basal membrane (**Figure 13**). Three genes with high expression on clusters 7, 9, and 12 based on scRNA-seq results were selected for FISH: Lepr, Tac1, and Col11a2. The FISH results showed that Lepr was low expressed in the GER region at P1 (**Figure 13A1**), and sign up the regulated expression in GER and inner hair cell region at P7 (**Figure 13A2**), but almost disappeared in GER and inner hair cell region at P14 (**Figure 13A3**). While we found Tac1 and Col11a2 genes showed patterns of expression that were consistent with the single-cell results. From the FISH results, it could be seen that Tac1and Col11a2 were low expressed to the whole cochlear basal membrane at P1 (**Figures 13B1,C1**), and up the regulated expression in GER at P7 (**Figures 13B2,C2**). While at P14, Tac1, and Col11a2 were nearly disappeared in the GER region and were centrally expressed in the hair cell region (**Figures 13B3,C3**).

DISCUSSION

Greater epithelial ridge is a cluster of columnar cells located on the medial side of the cochlear hair cells, which is temporarily present during the development of the cochlea and is one of the signs of immaturity (Hinojosa, 1977). During the development of hearing, the GER gradually degenerates from the basal turn to the apex turn. After the cochlea matures and hearing appears, the GER degenerates and is replaced by cells from the internal sulcus (Lim and Anniko, 1985). Single-cell sequencing studies by Kolla et al. (2020) identified four distinct GER (KO) cell subtypes (KO1, KO2, KO3, and KO4) in the cochlear GER of P1-day CD1 female mice. These four cell subtypes have massive highly expressed genes, including high expression of Dcn, Ddost, Pdia6, Rcn3, Sdf2l1 in KO1 cell; high expression of Cpxm2, Ctgf, Fkbp9, Kazald1, Tectb in KO2 cell; Cst3, Gjb6, Net1, Tectb, Tsen15 in KO3 cell; high expression of Calb1, Crabp1, Epyc, Itm2a, Stmn2 in KO4 cell. The study defined the cell subtypes with high expression of Calb1 gene in the medial region of GER as the medial region of GER cell subtype based on the expression of Calb1 and Fabp7 and the outer region of GER. The other three subtypes in the outer region of GER with high expression of Fabp7 gene were further defined as L.KO1, L.KO2, and L.KO3 cells, respectively. Kolla et al. (2020) showed that these four cell subtypes are highly similar in terms of gene expression patterns and metabolic functions, but at the same time they are heterogeneous, and it is tentatively considered that these four cell subtypes are different subtypes of GER cells.

Considering that the cochlear auditory development of P7 rats is not fully mature, it is still in a process of orderly differentiation and gradual developmental maturation (Tritsch et al., 2007;

Tritsch and Bergles, 2010). Based on our previous study (Chen et al., 2021), we further selected the P14 time point jointly with the three key periods of P1, P7 for a single-cell transcriptomic study, and we found that the four previously identified subtypes of GER cell populations 0, 3, 4, and 6 gradually decreased from P1 to P14, and disappeared by P14 days (**Figure 1B**). However, it is interesting and noteworthy that we found four cell clusters (clusters 2, 7, 9, and 12) with similar spatial distribution and gene expression (**Figures 2**, **3**). These four cell clusters gradually increased in the number of cells from P1 to P7, but gradually decreased in number from P7 to P14 days, and disappeared by P14 days, which seems to be consistent with the outcome of the disappearance of GER cells. In terms of gene expression patterns, these four cell clusters are highly expressed in Col2a1, Col9a1, Col9a2, and Col11a2, which are the major gene members of the Col family, and mutations in these genes are associated with hearing loss (Richards et al., 2013; Hofrichter et al., 2019; Kjellström et al., 2021).

In addition, based on the KEGG signaling pathway showed that these clusters are mainly enriched in the Protein digestion and absorption signaling pathway, which was previously shown to regulate intracellular Ca^{2+} concentration and dynamic homeostasis, inducing cellular processes such as cell migration proliferation, and differentiation. GER supports the spontaneous cellular release of adenosine triphosphate (ATP), which acts as a paracrine receptor on the P2X purinergic receptors of neighboring IHCs to produce phospholipase C (PLC)-dependent inositol triphosphate (IP3), the release of Ca^{2+} from the intracellular calcium pool, and the release of the neurotransmitter glutamate from IHCs, which activates type I spiral neurons (SGNs) to generate action potentials, thereby mimicking the mechanical-electrical signal transduction effect triggered by sound waves transmitted through the external ear canal, allowing IHCs spontaneously increase the frequency of action potential delivery and promote the functional maturation of IHCs (Tritsch et al., 2007; Majumder et al., 2010; Rodriguez et al., 2012; Mammano, 2013). We consider that these four cell clusters may be other subtypes of GER cells and regulate the balance of Ca^{2+} through the mechanisms described above, which in turn induce and promote the maturation or possible *trans*-differentiation of cochlear hair cells into inner and outer hair cells.

Adult mammalian cochlear hair cells have no regenerative capacity, but neonatal mouse cochlear hair cells show a limited and transient regenerative potential, and studies have shown that this regenerative potential is largely attributable to the non-sensory cells in the neonatal mouse cochlea (Shou et al., 2003; Woods et al., 2004; Gubbels et al., 2008). The mitotic division of neonatal murine cochlear non-sensory cells is normally quiescent, and the regenerative capacity of these cells is further activated during early apoptosis of hair cells due to various factors (Shi et al., 2013; Bramhall et al., 2014; Cox et al., 2014; Hu et al., 2016). GER cells are a transient population of newborn cells with the ability to regenerate and transform with some cell subtypes located within the GER region that retain the characteristics of precursor sensory cells (Zheng and Gao, 2000; Kelly and Chen, 2007; Driver et al., 2008). GER cells maintain a high degree of morphological consistency, and Kolla et al. (2020) found the existence of two types of precursor sensory cells (pro-sensory cells) expressing Cdkn1b and Sox2 marker genes based on single-cell sequencing technology in E14 and E16-day mouse cochlea, which are located in the medial precursor sensory cell population (MPsCs) and lateral precursor sensory cell population (LPsCs) of GER structures, respectively, while the results of single-cell trajectory analysis showed that MPsCs cells have a clear ability to convert to IPhCs or IHCs. LPsCs cells may convert to DCs or OHCs, without clear divergence (Kolla et al., 2020). In addition, Kubota et al. (2021) similarly confirmed that GER cells have a great potential for organoid formation and classified GER cells into three large subtypes S2, S3, and S4 cell subtypes based on single-cell sequencing results. The researchers similarly found in P2 day mice that GER cell subtypes located in the lateral and medial regions could regenerate into hair cells and supporting cells. GER cells cultured at higher densities in the presence of EFI_CVPM [small molecules (CHIR99021, valproic acid, 2-phospho-L-ascorbic acid, and TGFß receptor inhibitor 616452)] were found to be the most efficient cochlear organoid-forming cell population (McLean et al., 2017), with the most lateral GER cell population expressing Lgr5 positivity and the more medially located GER cell population expressing Lgr5 negativity, both having the ability to generate cochlear organoids. Previous studies on the development of other organoids have shown that activation of the WNT signaling pathway can induce high Lgr5 expression and further promote the developmental process (Chai et al., 2011, 2012; Shi et al., 2012, 2013). Therefore, Lgr5 expression in GER cells is not an indicator of stem cells or proliferative potential. The present single-cell transcriptome results also showed that the above-mentioned cell subtypes with proliferative capacity located in the outer part of GER, but its Lgr5 gene expression is not significant, which also suggests that cochlear development is different from other tissues and organs development.

In the present study, our single-cell transcriptomics-based study showed a significant increase in the number of cell clusters 2, 7, 9, and 12 at P7, with more significant increases in cell clusters 7 and 9, only to disappear further at P14. In general, GER cells gradually degenerate and disappear, while other types of supporting cells gradually increase and eventually replace GER cells as the main supporting cells in the cochlea. We consider that clusters 2, 7, 9, and 12 may be subtypes of GER cells with regenerative differentiation potential, which have similar gene expression patterns and biological characteristics, with cluster 7 and cluster 9 being more similar and cluster 2 and cluster 12 being closer. In a rough classification, they can be divided into two large subtypes, but in terms of some specific gene expression, such as Tac1 which is more abundantly expressed on cluster 9, they can be finely divided into four subtypes. To further explore whether these four clusters with proliferative capacity have the potential to transdifferentiate into inner and outer hair cells, we further constructed the developmental trajectory and fate transduction using single-cell pseudo-temporal analysis. The single-cell developmental trajectory shows that the major cell subtypes at the beginning of cell development are clusters 2, 7, 9, and 12 (see **Figures 8A–C**). As the cells develop further, the four-cell clusters mentioned above gradually develop in two different

trajectory directions, with one part developing toward the outer hair cells and the other part shifting toward the inner hair cells. The cell developmental trajectory analysis suggested that these four cell subtypes have the potential to transdifferentiate into outer and inner hair cells, among which cluster 2 and cluster 12 may have the potential to transdifferentiate into outer hair cells (see **Figure 8C**), while cluster 7 and cluster 9 may only have the potential to transdifferentiate into inner hair cells (see **Figure 8C**). Since the present study was mainly based on raw letter data, further experimental confirmation is still needed for subsequent studies.

Although studies have shown that GER cells have the potential for organoid regeneration and development, do they have the potential to transdifferentiate into hair cells? Kubota et al. (2021)'s study found that large organoids derived from GER cells contained cells positive for hair cell markers, suggesting that GER cells have the characteristics of precursor sensory cells after mitosis. In addition, it was also found that GER cells can also generate hair cell-like cells after Atoh1 expression (Woods et al., 2004). These findings and the evidence provided by our study suggest that GER cells are a distinct population of cochlear cells characterized by a response to various reprogramming strategies, including phenotypic transformation (*via* Atoh1 expression) and proliferation/de-differentiation, culminating in degeneration and disappearance after maturation of cochlear hearing development.

In conclusion, our study lays the groundwork for elucidating the mechanisms of the key regulatory genes and signaling pathways in the *trans*-differentiation of GER cell subtypes into hair cells and provides potential clues to understand hair cell regeneration and further study of hair cell regeneration. Also, our study reveals the key molecular mechanisms of large epithelial crest supporting cells in promoting cochlear hearing development, which is very important to further elucidate the development of the peripheral auditory system.

DATA AVAILABILITY STATEMENT

The datasets presented in this study can be found in online repositories. The names of the repository/repositories and accession number(s) can be found below: https://www.ncbi.nlm.nih.gov/geo/query/acc.cgi?acc=GSE195702.

ETHICS STATEMENT

The animal study was reviewed and approved by The Institutional Animal Care and Use Committee of the Shanghai Jiao Tong University School of Medicine.

AUTHOR CONTRIBUTIONS

JiC, LS, and JY designed this study. JiC and JuC took the cochlear tissue. SH, BH, YL, SL, FZ, and XS assisted with data acquisition, analysis, and processing. JiC and DG analyzed and interpreted the data and drafted the manuscript. JY, YJ, and LS revised the manuscript. All authors contributed to the article and approved the submitted version.

FUNDING

This study was funded by the National Natural Science Foundation of China (81873698).

ACKNOWLEDGMENTS

We are grateful to the National Natural Science Foundation for supporting this study, and to LC Sciences for their support and guidance.

SUPPLEMENTARY MATERIAL

The Supplementary Material for this article can be found online at: https://www.frontiersin.org/articles/10.3389/fnmol.2022.832813/full#supplementary-material

REFERENCES

Andrews, T. S., and Hemberg, M. (2019). M3Drop: dropout-based feature selection for scRNASeq. *Bioinformatics* 35, 2865–2867. doi: 10.1093/bioinformatics/bty1044

Baslan, T., Kendall, J., Rodgers, L., Cox, H., Riggs, M., Stepansky, A., et al. (2012). Genome-wide copy number analysis of single cells. *Nat. Protoc.* 7, 1024–1041. doi: 10.1038/nprot.2012.039

Bramhall, N. F., Shi, F., Arnold, K., Hochedlinger, K., and Edge, A. S. (2014). Lgr5-positive supporting cells generate new hair cells in the postnatal cochlea. *Stem Cell Rep.* 2, 311–322. doi: 10.1016/j.stemcr.2014.01.008

Brigande, J. V., and Heller, S. (2009). Quo vadis, hair cell regeneration? *Nat. Neurosci.* 12, 679–685. doi: 10.1038/nn.2311

Brionne, A., Juanchich, A., and Hennequet-Antier, C. (2019). ViSEAGO: a Bioconductor package for clustering biological functions using Gene Ontology and semantic similarity. *BioData Min.* 12:16. doi: 10.1186/s13040-019-0204-1

Burns, J. C., Kelly, M. C., Hoa, M., Morell, R. J., and Kelley, M. W. (2015). Single-cell RNA-Seq resolves cellular complexity in sensory organs from the neonatal inner ear. *Nat. Commun.* 6:8557. doi: 10.1038/ncomms9557

Chai, R., Kuo, B., Wang, T., Liaw, E. J., Xia, A., Jan, T. A., et al. (2012). Wnt signaling induces proliferation of sensory precursors in the postnatal mouse cochlea. *Proc. Natl. Acad. Sci. U.S.A.* 109, 8167–8172. doi: 10.1073/pnas.1202774109

Chai, R., Xia, A., Wang, T., Jan, T. A., Hayashi, T., Bermingham-Mcdonogh, O., et al. (2011). Dynamic expression of Lgr5, a Wnt target gene, in the developing and mature mouse cochlea. *J. Assoc. Res. Otolaryngol.* 12, 455–469. doi: 10.1007/s10162-011-0267-2

Chen, J., Gao, D., Chen, J., Hou, S., He, B., Li, Y., et al. (2021). Single-cell RNA sequencing analysis reveals greater epithelial ridge cells degeneration during postnatal development of cochlea in rats. *Front. Cell Dev. Biol.* 9:719491. doi: 10.3389/fcell.2021.719491

Cox, B. C., Chai, R., Lenoir, A., Liu, Z., Zhang, L., Nguyen, D. H., et al. (2014). Spontaneous hair cell regeneration in the neonatal mouse cochlea in vivo. *Development* 141, 816–829. doi: 10.1242/dev.103036

Cruz, R. M., Lambert, P. R., and Rubel, E. W. (1987). Light microscopic evidence of hair cell regeneration after gentamicin toxicity in chick cochlea. *Arch. Otolaryngol. Head Neck Surg.* 113, 1058–1062. doi: 10.1001/archotol.1987.01860100036017

Dayaratne, M. W., Vlajkovic, S. M., Lipski, J., and Thorne, P. R. (2014). Kölliker's organ and the development of spontaneous activity in the auditory system: implications for hearing dysfunction. *Biomed. Res. Int.* 2014:367939. doi: 10.1155/2014/367939

del Castillo, I., Villamar, M., Moreno-Pelayo, M. A., Del Castillo, F. J., Alvarez, A., Tellería, D., et al. (2002). A deletion involving the connexin 30 gene in nonsyndromic hearing impairment. *N. Engl. J. Med.* 346, 243–249. doi: 10.1056/NEJMoa012052

Dou, S., Wang, Q., Qi, X., Zhang, B., Jiang, H., Chen, S., et al. (2021). Molecular identity of human limbal heterogeneity involved in corneal homeostasis and privilege. *Ocul. Surf.* 21, 206–220. doi: 10.1016/j.jtos.2021.04.010

Driver, E. C., and Kelley, M. W. (2020). Development of the cochlea. *Development* 147:dev162263. doi: 10.1242/dev.162263

Driver, E. C., Pryor, S. P., Hill, P., Turner, J., Rüther, U., Biesecker, L. G., et al. (2008). Hedgehog signaling regulates sensory cell formation and auditory function in mice and humans. *J. Neurosci.* 28, 7350–7358. doi: 10.1523/jneurosci.0312-08.2008

Ellwanger, D. C., Scheibinger, M., Dumont, R. A., Barr-Gillespie, P. G., and Heller, S. (2018). Transcriptional dynamics of hair-bundle morphogenesis revealed with celltrails. *Cell Rep.* 23, 2901–2914.e2913. doi: 10.1016/j.celrep.2018.05.002

Gubbels, S. P., Woessner, D. W., Mitchell, J. C., Ricci, A. J., and Brigande, J. V. (2008). Functional auditory hair cells produced in the mammalian cochlea by in utero gene transfer. *Nature* 455, 537–541. doi: 10.1038/nature07265

Hinojosa, R. (1977). A note on development of Corti's organ. *Acta Otolaryngol.* 84, 238–251. doi: 10.3109/00016487709123963

Hofrichter, M. A. H., Doll, J., Habibi, H., Enayati, S., Vahidi Mehrjardi, M. Y., Müller, T., et al. (2019). Exome-wide copy number variation analysis identifies a COL9A1 in frame deletion that is associated with hearing loss. *Eur. J. Med. Genet.* 62:103724. doi: 10.1016/j.ejmg.2019.103724

Hou, S., Chen, J., and Yang, J. (2019). Autophagy precedes apoptosis during degeneration of the Kölliker's organ in the development of rat cochlea. *Eur. J. Histochem.* 63:3025. doi: 10.4081/ejh.2019.3025

Hou, S., Chen, P., Chen, J., Chen, J., Sun, L., Chen, J., et al. (2020). Distinct expression patterns of apoptosis and autophagy-associated proteins and genes during postnatal development of spiral ganglion neurons in rat. *Neural Plast.* 2020:9387560. doi: 10.1155/2020/9387560

Hu, H., Miao, Y. R., Jia, L. H., Yu, Q. Y., Zhang, Q., and Guo, A. Y. (2019). AnimalTFDB 3.0: a comprehensive resource for annotation and prediction of animal transcription factors. *Nucleic Acids Res.* 47, D33–D38. doi: 10.1093/nar/gky822

Hu, L., Lu, J., Chiang, H., Wu, H., Edge, A. S., and Shi, F. (2016). Diphtheria toxin-induced cell death triggers wnt-dependent hair cell regeneration in neonatal mice. *J. Neurosci.* 36, 9479–9489. doi: 10.1523/jneurosci.2447-15.2016

Huang, X. T., Li, X., Qin, P. Z., Zhu, Y., Xu, S. N., and Chen, J. P. (2018). Technical advances in single-cell RNA sequencing and applications in normal and malignant hematopoiesis. *Front. Oncol.* 8:582. doi: 10.3389/fonc.2018.00582

Jacoszek, A., Pollak, A., Płoski, R., and Ołdak, M. (2017). Advances in genetic hearing loss: CIB2 gene. *Eur. Arch. Otorhinolaryngol.* 274, 1791–1795. doi: 10.1007/s00405-016-4330-9

Johnson, S. L., Ceriani, F., Houston, O., Polishchuk, R., Polishchuk, E., Crispino, G., et al. (2017). Connexin-mediated signaling in nonsensory cells is crucial for the development of sensory inner hair cells in the mouse cochlea. *J. Neurosci.* 37, 258–268. doi: 10.1523/jneurosci.2251-16.2016

Kawamoto, K., Ishimoto, S., Minoda, R., Brough, D. E., and Raphael, Y. (2003). Math1 gene transfer generates new cochlear hair cells in mature guinea pigs in vivo. *J. Neurosci.* 23, 4395–4400. doi: 10.1523/jneurosci.23-11-04395.2003

Kelley, M. W. (2007). Cellular commitment and differentiation in the organ of Corti. *Int. J. Dev. Biol.* 51, 571–583. doi: 10.1387/ijdb.072388mk

Kelly, M., and Chen, P. (2007). Shaping the mammalian auditory sensory organ by the planar cell polarity pathway. *Int. J. Dev. Biol.* 51, 535–547. doi: 10.1387/ijdb.072344mk

Kjellström, U., Martell, S., Brobeck, C., and Andréasson, S. (2021). Autosomal recessive Stickler syndrome associated with homozygous mutations in the COL9A2 gene. *Ophthalmic Genet.* 42, 161–169. doi: 10.1080/13816810.2020.1861309

Kolla, L., Kelly, M. C., Mann, Z. F., Anaya-Rocha, A., Ellis, K., Lemons, A., et al. (2020). Characterization of the development of the mouse cochlear epithelium at the single cell level. *Nat. Commun.* 11:2389. doi: 10.1038/s41467-020-16113-y

Krämer, A., Green, J., Pollard, J. Jr., and Tugendreich, S. (2014). Causal analysis approaches in Ingenuity pathway analysis. *Bioinformatics* 30, 523–530. doi: 10.1093/bioinformatics/btt703

Kubota, M., Scheibinger, M., Jan, T. A., and Heller, S. (2021). Greater epithelial ridge cells are the principal organoid-forming progenitors of the mouse cochlea. *Cell Rep.* 34:108646. doi: 10.1016/j.celrep.2020.108646

Lim, D. J. (1986). Functional structure of the organ of Corti: a review. *Hear Res.* 22, 117–146. doi: 10.1016/0378-5955(86)90089-4

Lim, D. J., and Anniko, M. (1985). Developmental morphology of the mouse inner ear. A scanning electron microscopic observation. *Acta Otolaryngol. Suppl.* 422, 1–69.

Liu, H., Pecka, J. L., Zhang, Q., Soukup, G. A., Beisel, K. W., and He, D. Z. (2014). Characterization of transcriptomes of cochlear inner and outer hair cells. *J. Neurosci.* 34, 11085–11095. doi: 10.1523/jneurosci.1690-14.2014

Majumder, P., Crispino, G., Rodriguez, L., Ciubotaru, C. D., Anselmi, F., Piazza, V., et al. (2010). ATP-mediated cell-cell signaling in the organ of Corti: the role of connexin channels. *Purinergic Signal.* 6, 167–187. doi: 10.1007/s11302-010-9192-9

Mammano, F. (2013). ATP-dependent intercellular Ca2+ signaling in the developing cochlea: facts, fantasies and perspectives. *Semin. Cell Dev. Biol.* 24, 31–39. doi: 10.1016/j.semcdb.2012.09.004

Mammano, F. (2019). Inner ear connexin channels: roles in development and maintenance of cochlear function. *Cold Spring Harb. Perspect. Med.* 9:a033233. doi: 10.1101/cshperspect.a033233

McLean, W. J., Yin, X., Lu, L., Lenz, D. R., Mclean, D., Langer, R., et al. (2017). Clonal expansion of Lgr5-positive cells from mammalian cochlea and high-purity generation of sensory hair cells. *Cell Rep.* 18, 1917–1929. doi: 10.1016/j.celrep.2017.01.066

Meşe, G., Richard, G., and White, T. W. (2007). Gap junctions: basic structure and function. *J. Invest. Dermatol.* 127, 2516–2524. doi: 10.1038/sj.jid.5700770

Oshima, K., Grimm, C. M., Corrales, C. E., Senn, P., Martinez Monedero, R., Géléoc, G. S., et al. (2007). Differential distribution of stem cells in the auditory and vestibular organs of the inner ear. *J. Assoc. Res. Otolaryngol.* 8, 18–31. doi: 10.1007/s10162-006-0058-3

Pirvola, U., Cao, Y., Oellig, C., Suoqiang, Z., Pettersson, R. F., and Ylikoski, J. (1995). The site of action of neuronal acidic fibroblast growth factor is the organ of Corti of the rat cochlea. *Proc. Natl. Acad. Sci. U.S.A.* 92, 9269–9273. doi: 10.1073/pnas.92.20.9269

Rabionet, R., Gasparini, P., and Estivill, X. (2000). Molecular genetics of hearing impairment due to mutations in gap junction genes encoding beta connexins. *Hum. Mutat.* 16, 190–202. doi: 10.1002/1098-1004(200009)16:3<190::AID-HUMU2>3.0.CO;2-I

Riazuddin, S., Belyantseva, I. A., Giese, A. P., Lee, K., Indzhykulian, A. A., Nandamuri, S. P., et al. (2012). Alterations of the CIB2 calcium- and integrin-binding protein cause Usher syndrome type 1J and nonsyndromic deafness DFNB48. *Nat. Genet.* 44, 1265–1271. doi: 10.1038/ng.2426

Richards, A. J., Fincham, G. S., Mcninch, A., Hill, D., Poulson, A. V., Castle, B., et al. (2013). Alternative splicing modifies the effect of mutations in COL11A1 and results in recessive type 2 Stickler syndrome with profound hearing loss. *J. Med. Genet.* 50, 765–771. doi: 10.1136/jmedgenet-2012-101499

Roccio, M., Senn, P., and Heller, S. (2020). Novel insights into inner ear development and regeneration for targeted hearing loss therapies. *Hear Res.* 397:107859. doi: 10.1016/j.heares.2019.107859

Rodriguez, L., Simeonato, E., Scimemi, P., Anselmi, F., Calì, B., Crispino, G., et al. (2012). Reduced phosphatidylinositol 4,5-bisphosphate synthesis impairs inner ear Ca2+ signaling and high-frequency hearing acquisition. *Proc. Natl. Acad. Sci. U.S.A.* 109, 14013–14018. doi: 10.1073/pnas.1211869109

Satija, R., Farrell, J. A., Gennert, D., Schier, A. F., and Regev, A. (2015). Spatial reconstruction of single-cell gene expression data. *Nat. Biotechnol.* 33, 495–502. doi: 10.1038/nbt.3192

Shapiro, E., Biezuner, T., and Linnarsson, S. (2013). Single-cell sequencing-based technologies will revolutionize whole-organism science. *Nat. Rev. Genet.* 14, 618–630. doi: 10.1038/nrg3542

Shi, F., Hu, L., and Edge, A. S. (2013). Generation of hair cells in neonatal mice by β-catenin overexpression in Lgr5-positive cochlear progenitors. *Proc. Natl. Acad. Sci. U.S.A.* 110, 13851–13856. doi: 10.1073/pnas.1219952110

Shi, F., Kempfle, J. S., and Edge, A. S. (2012). Wnt-responsive Lgr5-expressing stem cells are hair cell progenitors in the cochlea. *J. Neurosci.* 32, 9639–9648. doi: 10.1523/jneurosci.1064-12.2012

Shou, J., Zheng, J. L., and Gao, W. Q. (2003). Robust generation of new hair cells in the mature mammalian inner ear by adenoviral expression of Hath1. *Mol. Cell Neurosci.* 23, 169–179. doi: 10.1016/s1044-7431(03)00066-6

Trapnell, C., Cacchiarelli, D., Grimsby, J., Pokharel, P., Li, S., Morse, M., et al. (2014). The dynamics and regulators of cell fate decisions are revealed by pseudotemporal ordering of single cells. *Nat. Biotechnol.* 32, 381–386. doi: 10.1038/nbt.2859

Tritsch, N. X., and Bergles, D. E. (2010). Developmental regulation of spontaneous activity in the Mammalian cochlea. *J. Neurosci.* 30, 1539–1550. doi: 10.1523/jneurosci.3875-09.2010

Tritsch, N. X., Yi, E., Gale, J. E., Glowatzki, E., and Bergles, D. E. (2007). The origin of spontaneous activity in the developing auditory system. *Nature* 450, 50–55. doi: 10.1038/nature06233

Wagner, E. L., and Shin, J. B. (2019). Mechanisms of hair cell damage and repair. *Trends Neurosci.* 42, 414–424. doi: 10.1016/j.tins.2019.03.006

White, P. M., Doetzlhofer, A., Lee, Y. S., Groves, A. K., and Segil, N. (2006). Mammalian cochlear supporting cells can divide and trans-differentiate into hair cells. *Nature* 441, 984–987. doi: 10.1038/nature04849

Wiwatpanit, T., Lorenzen, S. M., Cantú, J. A., Foo, C. Z., Hogan, A. K., Márquez, F., et al. (2018). Trans-differentiation of outer hair cells into inner hair cells in the absence of INSM1. *Nature* 563, 691–695. doi: 10.1038/s41586-018-0570-8

Woods, C., Montcouquiol, M., and Kelley, M. W. (2004). Math1 regulates development of the sensory epithelium in the mammalian cochlea. *Nat. Neurosci.* 7, 1310–1318. doi: 10.1038/nn1349

Yee, T. W. (2004). Quantile regression via vector generalized additive models. *Stat. Med.* 23, 2295–2315. doi: 10.1002/sim.1822

Zheng, J. L., and Gao, W. Q. (2000). Overexpression of Math1 induces robust production of extra hair cells in postnatal rat inner ears. *Nat. Neurosci.* 3, 580–586. doi: 10.1038/75753

Zine, A., Aubert, A., Qiu, J., Therianos, S., Guillemot, F., Kageyama, R., et al. (2001). Hes1 and Hes5 activities are required for the normal development of the hair cells in the mammalian inner ear. *J. Neurosci.* 21, 4712–4720. doi: 10.1523/jneurosci.21-13-04712.2001

Conflict of Interest: The authors declare that the research was conducted in the absence of any commercial or financial relationships that could be construed as a potential conflict of interest.

Publisher's Note: All claims expressed in this article are solely those of the authors and do not necessarily represent those of their affiliated organizations, or those of the publisher, the editors and the reviewers. Any product that may be evaluated in this article, or claim that may be made by its manufacturer, is not guaranteed or endorsed by the publisher.

frontiers in Molecular Neuroscience

REVIEW
published: 24 March 2022
doi: 10.3389/fnmol.2022.854635

Regeneration of Hair Cells in the Human Vestibular System

*Yikang Huang[1,2], Huanyu Mao[1,2] and Yan Chen[1,2]**

[1] State Key Laboratory of Medical Neurobiology, Department of Otorhinolaryngology, Eye and ENT Hospital, MOE Frontiers Center for Brain Science, ENT Institute, Fudan University, Shanghai, China, [2] NHC Key Laboratory of Hearing Medicine, Fudan University, Shanghai, China

The vestibular system is a critical part of the human balance system, malfunction of this system will lead to balance disorders, such as vertigo. Mammalian vestibular hair cells, the mechanical receptors for vestibular function, are sensitive to ototoxic drugs and virus infection, and have a limited restorative capacity after damage. Considering that no artificial device can be used to replace vestibular hair cells, promoting vestibular hair cell regeneration is an ideal way for vestibular function recovery. In this manuscript, the development of human vestibular hair cells during the whole embryonic stage and the latest research on human vestibular hair cell regeneration is summarized. The limitations of current studies are emphasized and future directions are discussed.

Keywords: human, vestibule, hair cell, development, regeneration

OPEN ACCESS

Edited by:
Yu Sun,
Huazhong University of Science and Technology, China

Reviewed by:
Zuhong He,
Wuhan University, China
Renjie Chai,
Southeast University, China

***Correspondence:**
Yan Chen
chenyan0528@fudan.edu.cn

Specialty section:
This article was submitted to Molecular Signalling and Pathways, a section of the journal Frontiers in Molecular Neuroscience

Received: *14 January 2022*
Accepted: *14 February 2022*
Published: *24 March 2022*

Citation:
Huang Y, Mao H and Chen Y (2022) Regeneration of Hair Cells in the Human Vestibular System. Front. Mol. Neurosci. 15:854635. doi: 10.3389/fnmol.2022.854635

INTRODUCTION

Vestibular sensory epithelia are composed of hair cells (HCs) and supporting cells (SCs). HCs of the vestibular sensory epithelia, which are surrounded by supporting cells, convert mechanical signals, such as head movement or tilt, into electrical signals (Gao et al., 2019; Liu et al., 2019; Qi et al., 2019, 2020; Tan et al., 2019). These signals are then transmitted by afferent fibers to the vestibular nuclei that send out fibers projected to the corresponding neural structures to control eye movement, posture, and balance (Cullen, 2012; Guo et al., 2019, 2020, 2021b,c; Hu et al., 2021; Wei et al., 2021).

Hair cells are easily injured by ototoxic drugs (Li et al., 2018; Zhang et al., 2019; Zhong et al., 2020; Fu et al., 2021b), aging (Cheng et al., 2019; Guo et al., 2021a; He et al., 2021), genetic factors (Qian et al., 2020; Cheng et al., 2021; Fu et al., 2021a; Lv et al., 2021; Zhang S. et al., 2021) and infections (Han et al., 2020; He et al., 2020; Zhang Y. et al., 2021). The loss of human vestibular HCs is closely related to balance dysfunction (Tsuji et al., 2000; Ishiyama et al., 2015). It has been stated that the annual incidence of vertigo is about 11% (Corrales and Bhattacharyya, 2016), and the lifetime prevalence of moderate to severe vertigo and dizziness is about 30% (Strupp et al., 2020). However, our current understanding of the development and generation of vestibular HCs is mainly derived from rodent models. Here, we review the current information on the development of human vestibular epithelia, as well as the latest progress made in restoring human vestibular HCs upon damage.

Abbreviations: AAV, adeno-associated virus; AD, adenovirus; Anxa4, annexin A4; Atoh1, atonal homolog 1; BDNF, brain-derived neurotrophic factor; bHLH, basic helix-loop-helix; caspase-3, cysteine aspartate-specific protease-3; CMV, cytomegalovirus; E, embryonic day; EGF, epidermal growth factor; FGF, fibroblast growth factor; GATA3: GATA binding protein 3; GW, gestational week; HATH1, human homolog of Atoh1; HC, hair cell; hESCs, human embryonic stem cells; IDPN: 3,3′-iminodiproprionitrile; IGF-1, insulin-like growth factor-1; IGF-2, insulin-like growth factor-1; LGR5: leucine-rich repeat-containing G protein-coupled receptor 5; MAPK, mitogen-activated protein kinase; Mapt, microtubule associated protein; mTOR, mammalian target of rapamycin; Ocm, oncomodulin; PI-3K, activation of phosphatidylinositol-3 kinase; PKC, protein kinase C; RA, retinoic acid; rhGGF2, recombinant human glial growth factor 2; SC, supporting cell; SOX2: SRY (sex-determining region Y)-box 2; Spp1, secreted phosphoprotein 1; TGF-α, transforming growth factor alpha.

STRUCTURE OF HUMAN VESTIBULAR SENSORY EPITHELIA

The human vestibular sensory epithelia, like that of other mammals, are composed of three crista ampullaris perpendicular to each other for sensing rotational motion of the head, and the utricular and saccular maculae, which detect linear acceleration (Angelaki and Cullen, 2008). In the mature state, the average surface areas of human cristae, utricular maculae and saccular maculae are around 0.9, 3.6, and 2.2 mm^2, respectively (Watanuki and Schuknecht, 1976).

Hair cells are vestibular receptors located on sensory epithelia and surrounded by supporting cells. According to the different afferent synaptic terminals, human vestibular HCs can be further classified into two types: Type I HCs innervated by flask-shaped calyces and Type II HCs innervated by boutons (Wersall, 1956). There are several other morphological and functional differences between the two types which have been widely discussed in rodents (Rüsch et al., 1998), and the characteristics of these two types of HCs are similar in the human vestibule (Oghalai et al., 1998; Lim et al., 2014).

The human vestibular sensory epithelia can be divided into central and peripheral regions according to different characteristics. In the cristae, the central regions account for 46% of the total surface area. Type I HCs account for 70% of the central region HCs, while type II HCs account for 50% of the peripheral region HCs in the human cristae (Rosenhall, 1972a). In the utricular maculae, the central striola region accounts for about 8.6% of the surface area. The proportion of type I HCs in the striola region is higher and type II HCs show a high density in the peripheral region. The HC distribution in saccule maculae is similar to that of the utricle maculae (Rosenhall, 1972b).

Interestingly, the polarity of the hair bundle, which is determined by the position of kinocilia of HCs, varies between the human utricular and saccular maculae. The orientation of the utricular kinocilia is directed from the periphery toward the striola, while the kinocilia orientation is opposite in the saccule. Moreover, the striolar region of the utricular maculae is crescent, while the saccular maculae are "S" shaped (Rosenhall, 1972b).

Both the vestibular hair cell distribution and cilia polarity of humans are similar to those of mice. However, the number and differentiation time of vestibular HCs are significantly different between the two species, as will be discussed below.

DEVELOPMENT OF HUMAN VESTIBULAR EPITHELIA

Morphological Development of Human Vestibular Organs

Anatomical studies have shown many details of human vestibular development (**Figure 1**). The formation of the otic placode is regarded as the first sign of inner ear development, which is the result of the ectoderm's inner layer thickening at gestational week (GW) 3 (O'Rahilly, 1963). The otic placode then invaginates to form the otic cup that in turn pinches off the surrounding ectoderm and converts into the otic vesicle, composed of a dorsal (vestibular) and a ventral (cochlear) pouch, at the rhombomere 5 level by GW 4 (Streeter, 1906). From GW 4–5, the dorsal pouch expands into a triangular-shaped region forming the base of the three semicircular canals. The development of human anterior and posterior semicircular canals starts at embryonic days 41–43 with the depression of vestibular pouch wall, while the development of lateral semicircular canals begins a little later at embryonic days 44–46 (Yasuda et al., 2007). All semicircular canals are discernible at embryonic day (E) 47–E48 (Toyoda et al., 2015). Meanwhile, the atrium, which is the primordium of the utricle and saccule, can be observed in the ventral part of the vestibular pouch. Subsequently, a horizontal cleft that separates the atrium into an upper and lower compartment appears and the utricle and saccule are clearly detectable at E49–E51 (Streeter, 1906; Yasuda et al., 2007). By the end of the 5th month of the embryo, the bony labyrinth has been formed and the vestibular system is intact in morphology (Jeffery and Spoor, 2004), after which there is only a modest increase in the distance between the semicircular canals (Johnson Chacko et al., 2019).

Maturation of the human vestibular sensory epithelia includes lengthening of the cristae and thinning of the maculae. The length of cristae increases rapidly from GW 8–9 but slows down and changes in shape during GW 9–12. The anterior crista undergoes a second rapid growth during GW 12–14, reaching approximately 55% of adult size (Dechesne and Sans, 1985). The reduction of utricular epithelial thickness can be divided into two stages: GW 7–8 and GW 11–13, during which the number of supporting cell layers decreases significantly, while the thickness remains unchanged during GW 8–12. Finally, the supporting cell nuclei tend to be arranged in a single layer and the hair cell nuclei migrate to the cell base (Dechesne and Sans, 1985).

The morphogenesis of vestibular organs in humans is similar to that in rodents, but the human vestibular organs have been distinct in the early embryonic stage (by the end of GW 7, **Figure 1**; Streeter, 1906), while the mouse counterparts do not attain its mature shape until the late embryonic stage. The vestibular organs of mice become distinguishable on E15 and the membranous labyrinth morphology approaches maturity as late as E17 (Morsli et al., 1998).

Differentiation of Vestibular Hair Cells

Cilia

Differentiation of human vestibular sensory epithelium does not occur until GW 7. The differentiation level of vestibular HCs is usually judged by their cilia, stereocilia and kinocilia.

Crista stereocilia are detectable at GW 8, during which time cristae are covered by short hair bundles with the putative kinocilia, the latter are longer than stereocilia in most cases and located at the edge of the bundle. Subsequently, there is a lengthening of cristae stereocilia, which leads to the longer and more mature hair bundles at GW10–11. From GW 12–14, the length of the hair bundles increases significantly, and the number of growing hair bundles decreased (Dechesne and Sans, 1985).

In the case of the utricle, the hair bundles observed at GW 10 are very short, and some kinocilia are shorter than the adjacent

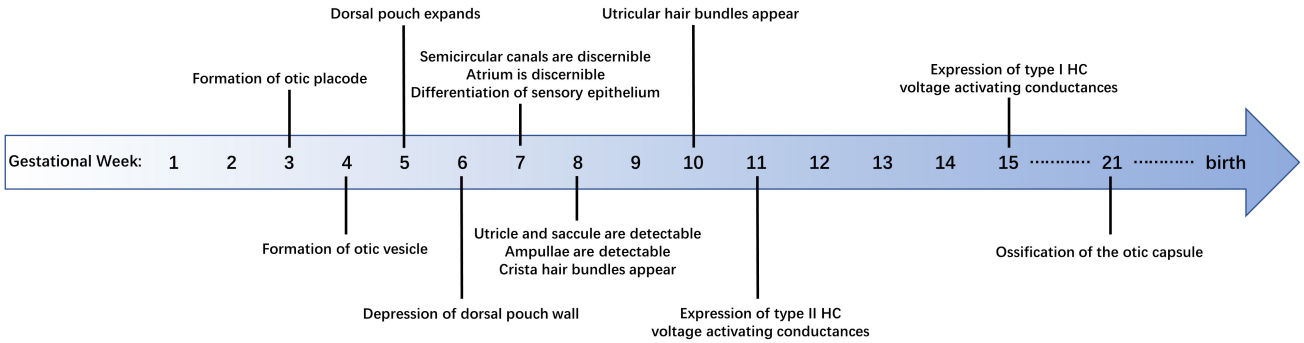

FIGURE 1 | Summary of developmental milestones in the development of human vestibular sensory epithelia.

stereocilia. At GW 12, some hair bundles in the protruding utricle are close to maturity, while some are still growing. At GW 14, the hair bundles are morphologically mature and the number of newborn bundles decreases, while the microvilli are still abundant (Rosenhall and Engström, 1974; Dechesne and Sans, 1985), which indicates the HCs have not been fully developed so far.

From GW 14–18, hair bundles of HCs further mature in both human utricle and cristae. Stereocilia of the HCs in GW 18 fetus seem to be thicker than those in the GW 14 fetus. However, the number and diameter of stereocilia do not change significantly after GW 14, with about 80–100 stereocilia per HC (Rosenhall and Engström, 1974; Hoshino, 1982).

Molecular Marker

The differentiation of mammalian HCs is accompanied by the expression of cell-specific molecular markers, such as MyosinVIIa and Sox2. In the human vestibule, MyosinVIIa and Sox2 staining can be observed as early as GW 9. Moreover, the expression of MyosinVIIa is restricted to the vestibular HCs, while Sox2 is expressed in the supporting cells and a few of the HCs (Chacko et al., 2020).

In order to distinguish different cell types, recent work on mouse utricles has identified specific molecular markers for Type II HCs (Calretinin, Anxa4, and Mapt) and Type I HCs (Spp1 and Ocm) (McInturff et al., 2018). However, it remains to be investigated whether these vestibular hair cell markers are applicable to human specimens.

Electrophysiology

Evidences in electrophysiology demonstrate the functional similarities between human and rodent HCs. Whole-cell conductances of human vestibular HCs from GW 11–14 fetus are similar to those of mature type II HCs from rodents. The peak outward conductances obtained from human type II HCs increase from GW 15–18. Moreover, the rodent type I HC specific low-voltage activated K+ conductance, which is called $G_{K,\ L}$, can also be detected in GW 15 human cristae, although relatively small (Lim et al., 2014). The similarities were further confirmed by the voltage-dependent currents that are expressed in vestibular HCs of both adult humans and rodents (Oghalai et al., 1998). However, so far there are few studies on the electrophysiological differences of vestibular HCs between humans and other mammals.

Hair Cell Number

There are no reports about the accurate time point at which the progenitors of human vestibular sensory epithelium begin to differentiate into hair cells since the spatio-temporal expression patterns of atonal homolog 1 (ATOH1), which is critical to HC formation, has not been investigated in the human vestibule so far. The distinct high expression of the HC marker, MyosinVIIa, is first observed in the crista as early as GW 9, indicating that some vestibular HCs have been formed at GW 9 (Johnson Chacko et al., 2020). But how these immature hair cells differentiate into type I and type II vestibular hair cells is not clear.

There is no significant difference in the number of cristae HCs between adults and the 4th–6th month fetuses: an average of 7,800 HCs per cristae at GW 16–23 and 7,500 HCs per cristae after birth (Rosenhall, 1972a). Another study observed an average of 8,005 HCs (type I 4,119 and type II 3,886) per lateral cristae of adults aged 26–67 years (Lopez et al., 2005).

It is reported that the number of HCs in the utricular and saccular maculae is about 2–4 times that in the cristae (Watanuki and Schuknecht, 1976). This study divided the specimens by age into the embryonic group (GW 14–23) and the postnatal group (<40 years old), and the average number of HCs was comparable between the two groups. As for the utricle, the average number is 33,100 (2,300 in the central area), with 32,900 HCs in the embryonic group and 33,200 in the postnatal group. The average number of saccular maculae HCs is 18,800 (1,600 in the central area), with 19,100 in the embryonic group and 18,400 in the postnatal group. Another study about utricles shows that the average number of utricular HCs at GW 16 is about 36,000, not significantly different from that at the age of 15, but significantly higher than the 13,000 at GW 10–12 (Severinsen et al., 2010).

Overall, the time point of HC differentiation is remarkably earlier in humans than that in rodents. As mentioned above, the number of human vestibular HCs reaches the adult level no later than the 5th month of gestation. In contrast,

over half the mouse HC population is formed after birth (Burns et al., 2012).

Factors Related to the Development of Human Vestibular Sensory Epithelia

Several reviews have summarized the relevant regulatory factors in hair cell development in animal models. In general, mammalian hair cell development involves the emergence of Sox2-labeled pro-sensory areas, the expression of transcription factor Atoh1, the regulation of cell cycle by factors such as $p27^{Kip1}$, and the manipulation by signaling pathways such as Notch, Fgf, Wnt, Shh, and Bmp (Wu and Kelley, 2012; Atkinson et al., 2015; Whitfield, 2015). However, there haven't been many studies on the regulation of human hair cell development so far.

Proliferation and apoptosis are essential processes during human inner ear development. It is demonstrated by Ki-67 staining that the percentages of proliferating cells in the utricle and semicircular canal are 43 and 38%, respectively, at GW 6, but decrease to 24 and 30% at GW 9. However, the trend of Bcl-2 expression in the vestibular epithelium is opposite to that of Ki67 during GW 7–10. Moreover, cysteine aspartate-specific protease-3 (caspase-3) and insulin-like growth factor-1 (IGF-1) are also expressed during vestibular epithelial development (Tafra et al., 2014). These results suggest that factors related to proliferation and apoptosis may contribute to the morphogenesis and differentiation of vestibular sensory epithelia.

Brain-derived neurotrophic factor (BDNF) is a neurotrophic protein. Previous studies have shown that BDNF plays an important role in vestibular nerve development in animals (Fritzsch et al., 1997). In the human vestibule, BDNF is firstly expressed in the entire utricular sensory epithelium, but its expression decreases from GW 9–12 and is restricted in the extrastriola at GW 12. In adult human utricles, BDNF is only present in the apical part of HCs. The expression of p75NTR in vestibular organs and TrkB and C in nerve fibers increase with development, suggesting an essential role of neurotrophic receptors in the survival of vestibular neurons during early embryonic stages (Johnson Chacko et al., 2017).

Another study reported the expression of several key transcription factors during human inner ear development. For the vestibular sensory epithelia, LGR5 expression increased from GW 8–12 and was broad in the apical poles of the vestibular HCs. Another transcription factor, GATA3, was expressed in the striola of the utricular and saccular maculae at GW 11. Expression for SOX2 was primarily restricted to the utricular supporting cells at GW 9, suggesting its function in regulating the differentiation of supporting cells (Johnson Chacko et al., 2020). These results indicate that the active transcription factors during the development of the mammalian inner ear may also play a critical role in the development of human vestibular sensory epithelia. However, the spatio-temporal expression patterns of other genes essential for hair cell formation, such as Math1, Six1, Gfi1, and Pou4f3, are not explored in the human vestibule up to now.

In general, research on vestibules of human embryos is quite limited and the previous work mainly focused on the expression of specific molecules. Further experiments are required for demonstrating the similarities and differences of vestibular hair cell development between human and animal models, and the underlying mechanisms as well.

REGENERATION OF HUMAN VESTIBULAR HAIR CELLS

Discovery of Hair Cells Regeneration in the Mammalian Vestibular Epithelium

Considering that no artificial device can be used to replace vestibular function, recovery from vestibular dysfunction mainly depends on the compensation of central vestibular function, which can hardly lead to a full recovery. Promoting vestibular HC regeneration is an ideal way for vestibular function recovery.

Many studies have shown differences in the regeneration ability of vestibular sensory epithelium between different species. Non-mammalian vertebrates such as birds are able to produce HCs throughout their lives (Balak et al., 1990; Roberson et al., 1992; Weisleder and Rubel, 1992). In contrast, the restoration of vestibular HCs is relatively limited in mammals (Forge et al., 1993; Wang et al., 2015; Wu et al., 2016; You et al., 2018; Zhang et al., 2020), which can be realized through two processes, namely, mitosis or trans-differentiation (Rubel et al., 1995).

Loss of vestibular HCs, whether induced by aminoglycoside antibiotics (Kawamoto et al., 2009), IDPN (Zeng et al., 2020) or other injury methods (Golub et al., 2012; González-Garrido et al., 2021), significantly enhances spontaneous regenerative proliferation. However, compared to the complete recovery of vestibular function in most non-mammalian vertebrates (Jones and Nelson, 1992; Carey et al., 1996), both the number and the function of the newborn HCs are limited in the mammalian vestibular epithelium (Forge et al., 1993; Kawamoto et al., 2009; Golub et al., 2012; Zeng et al., 2020; González-Garrido et al., 2021). As a result, techniques to boost the regeneration of mammalian vestibular HCs are needed.

Manipulation of Vestibular Hair Cell Regeneration in Mammals

Considering the important role of growth factors in the development of the mammalian inner ear, many studies want to reveal whether they could also initiate the generation of vestibular HCs. Through *in vitro* culture, transforming growth factor alpha (TGF-α) is first found to be capable of restoring HCs in adult mouse vestibular organs after injury (Lambert, 1994). Subsequently, epidermal growth factor (EGF) (Yamashita and Oesterle, 1995), fibroblast growth factor (FGF) family members, IGF-1 and IGF-2 (Zheng et al., 1997) are demonstrated to trigger the proliferation of rat vestibular epithelial cells together with TGF-α. Recombinant human glial growth factor 2 (rhGGF2) and insulin are also capable of evoking great cell proliferation in the utricular epithelium of neonatal rats (Gu et al., 2007). Compared to TGF-α alone, simultaneous infusion of TGF-α and insulin into the rat inner ear shows combined effects in producing HCs (Kuntz and Oesterle, 1998a,b). Furthermore,

combined utilization of TGF-α, IGF-1, and retinoic acid (RA) and BDNF performs well in restoring type I vestibular HCs *in vivo* and suggests application value (Kopke et al., 2001).

Regulation of intracellular signals is another method of promoting regeneration. Activation of phosphatidylinositol-3 kinase (PI-3K), mammalian target of rapamycin (mTOR), protein kinase C (PKC), mitogen-activated protein kinase (MAPK) and increased intracellular calcium enhance the proliferation of cells in murine vestibular epithelia. All of these signals are closely associated with the S-phase entry (Montcouquiol and Corwin, 2001).

The basic helix-loop-helix (bHLH) transcription factor, atonal homolog 1 or Atoh1, is critical for the differentiation of HCs (Bermingham et al., 1999). Atoh1 overexpression activates the HC differentiation in murine vestibular epithelia both *in vitro* (Zheng and Gao, 2000; Huang et al., 2009; Qian et al., 2021) and *in vivo* (Staecker et al., 2007; Schlecker et al., 2011; Gao et al., 2016; Sayyid et al., 2019), which can be enhanced by injury (Staecker et al., 2007; Schlecker et al., 2011; Sayyid et al., 2019; Hicks et al., 2020; Qian et al., 2021) and depressed by aging (Gao et al., 2016). On the other hand, Atoh1 deletion inhibits the spontaneous returning of HCs significantly (Hicks et al., 2020).

Disrupting the lateral inhibition established by Notch signaling is another classic strategy for producing new HCs. After adding DAPT and TAPI-1, two inhibitors of the Notch signaling pathway, to the explanted utricles of adult mice, enhanced hair cell regeneration was observed, especially in the striolar/juxtastriolar region (Lin et al., 2011). DAPT treatment also leads to extensive HC generation in cristae explants of adult mice (Slowik and Bermingham-McDonogh, 2013). Moreover, downregulation of the Notch target gene Hes5 through siRNA can also induce the trans-differentiation of supporting cells and boost hair cell regeneration in the damaged mouse utricles (Jung et al., 2013).

Apart from the traditional means mentioned above, recent studies have revealed some new targets for regulating HC regeneration. Several studies connected the ability of supporting cells to reenter the cell cycle during murine utricular development or after injury to nuclear Yap signaling (Gnedeva et al., 2017, 2020; Kastan et al., 2021). Collado et al. (2011) found the accumulation of E-Cadherin as an inhibitor for trans-differentiation of supporting cells. Knockdown of Foxg1 in supporting cells was revealed to be another viable method of enhancing HC regeneration in the neonatal mouse utricle (Zhang et al., 2020). In order to achieve better regenerative effects, attempts have been made to simultaneously promote supporting cells proliferation and hair cell differentiation through a combined regulation of multiple signaling pathways, such as Wnt and Notch (Wu et al., 2016).

Although vestibular hair cell regeneration in mammals still faces many hurdles, the good news is that murine vestibular function, under certain modulations, has been partially restored after injury (Kopke et al., 2001; Staecker et al., 2007; Schlecker et al., 2011). However, whether the regeneration phenomenon can also be discovered in humans and whether it can be regulated in the same manner as in rodents are questions that must be addressed for the clinical application of regenerative techniques.

Regenerative Potential of Human Vestibular Hair Cells

Studies on the regenerative potential of human vestibular HCs started almost at the same time as that of other mammals. Through *in vitro* experiments, Warchol et al. (1993) found proliferating supporting cells after neomycin injury in the human utricle. After 25 days of culture, some labeled nuclei in the lumenal stratum that was normally occupied by the nuclei of HCs appeared, which suggested the restoration of HCs (Warchol et al., 1993). In another study, 22 patients with Meniere's disease were tested on their vestibular function 1–2 years after gentamicin treatment. The horizontal semicircular canal afferent nerve restored its excitability to warm and cold water in 38% of them, which was regarded as functional evidence for HC regeneration (De Waele et al., 2002). However, the evidence here is insufficient, in which the study could not confirm the direct cause of the functional recovery, since vestibular inhibition and central compensation could also lead to functional restoration. The morphological evidence came in 2015. Immature hair bundles were observed in human vestibular specimens harvested from elderly patients (Taylor et al., 2015). Given that no evidence of the hair bundle restoration has been detected on surviving "bald" HCs, there is likely to be spontaneous HC regeneration occurring in human utricles.

Another approach to investigate the stemness of vestibular sensory epithelial cells is to extract progenitors or stem cells from the human inner ear. It was first realized by Chen et al. (2009) who extracted stem cells capable of differentiating into HCs from the fetal cochlea in 2009. Since then, attempts have been made in vestibular organs. Hu et al. (2012) isolated sensory epithelial cells from postoperative human utricular specimens and cultured them *in vitro*. The proliferated cells expressed genes in pre-sensory cells or stem cells such as SOX2 and $P27^{KIP1}$ and showed characteristics of mesenchymal cells when cultured on 2D substrates (Hu et al., 2012). A recent study demonstrated that the human vestibular epithelial cells have a strong sphere-forming ability through *in vitro* culture. Furthermore, the clonal spheres were able to produce cells expressing markers of HCs and displayed differentiation ability (Senn et al., 2020). The existence of multipotent progenitor cells in the adult human vestibule indicates the capability of sensory epithelial cells to re-enter the cell cycle and provides a promising source for neonatal HCs.

In conclusion, the regenerative potential of human vestibular HCs has been revealed from different aspects, reflecting the similarities between human and rodent vestibules. Therefore, the theoretical basis for the regulation of human hair cell regeneration following the example of other mammals has been established.

Application of Gene Therapy in Human Vestibular Sensory Epithelia

As is mentioned above, overexpression of Atoh1 serves as a classic approach to triggering regeneration of vestibular HCs in rodents. In 2003, Shou et al. (2003) upregulated HATH1 (a human homolog of Atoh1) in cultured adult rat utricular maculae through local adenoviral treatment and robust production of

new HCs was observed in normal and gentamicin-injured utricles as a result of supporting cell conversion, implying the conserved function of the atonal homologs during the revolution. Moreover, considering the similarity between human and murine homologs of atonal in giving rise to HCs, overexpressing HATH1 may be a promising target for gene therapy in human balance organs.

Choosing a suitable transduction vector is essential for inner ear gene therapy. Adenovirus has been demonstrated to efficiently transfect both HCs and supporting cells, thus becoming a competitive candidate. In 2007, Kesser et al. (2007) developed a multi-gene deletion and replication-free adenovirus vector (AD2) to test its transfection efficacy in human tissues, which drove the expression of the green fluorescent protein GFP gene (AD2-GFP) by cytomegalovirus (CMV) promoter. Results indicated that both supporting cells and HCs were transfected and the transfection rate was higher in supporting cells and varied with viral titer and transfection time. Furthermore, the adenovirus vector also performed well when GFP and wild-type potassium channel gene KCNQ4 were transfected simultaneously into the human inner ear, with 17.3% hair cell transfection rate for GFP and 10% for KCNQ4 (Kesser et al., 2007). Adeno-associated virus (AAV) is another promising vector that has enabled efficient gene transfer to several organs. Recently, an AAV variant (AAV-ie) has been designed for inner ear gene delivery. It was shown that AAV-ie infected about 93% of SCs and 76% of HCs in human utricle. In addition, the saccular macula and cristae could be transduced as well (Tan et al., 2019).

Based on the maturity of the transduction vector, Taylor et al. (2018) made the first attempt to generate HCs in human utricle. Taylor et al. (2018) collected utricles from patients undergoing excision of vestibular schwannoma and HCs were ablated through gentamicin. Ad2-GFP-Atoh1 was used here to transfect utricular maculae and supporting cells were efficiently transduced. Compared with the control group, transfection successfully increased the HC number in the maculae. Moreover, Notch signaling pathway inhibitor TAPI-1 also induced regeneration in human utricles, while the newborn HCs were fewer than those in the Atoh1 transfection group. Finally, no synergistic effect of the two treatments was observed, implying Atoh1 overexpression as a more effective solution. This study creates a precedent for gene therapy targeting the human inner ear.

FUTURE PERSPECTIVES

Although gene therapy targeting human vestibular epithelium has triggered HC regeneration successfully, many problems remain to be addressed before more mature and functional HCs can be generated. Considering the similarities between vestibular and auditory sensory epithelium, recent studies on the cochlea may offer some inspiration.

Atoh1-induced HC regeneration still has some limitations in both mouse and human vestibules. First, the number of hair cells could not be fully restored after injury. Second, nearly all the new hair cells converted from supporting cells were Sox2 + type II hair cells, the lack of new type I hair cells is not conducive to vestibular rehabilitation. Moreover, the regenerated hair cells were immature, as demonstrated by immature cilia (Schlecker et al., 2011; Taylor et al., 2018; Sayyid et al., 2019; Qian et al., 2021). Recent studies report some progresses in cochlear hair cell regeneration by manipulating multiple signaling pathways or transcriptional factors (Walters et al., 2017; Lee et al., 2020; Menendez et al., 2020; Chen et al., 2021; Sun et al., 2021). In order to improve both the quality and quantity of new vestibular hair cells, regulating multiple factors which can promote the maturation and subtype differentiation of vestibular hair cells may be an important strategy. In addition, it might be beneficial to combine epigenetic regulatory factors with Atoh1 overexpression to promote hair cell regeneration in the human vestibule.

Generating organoids provides ideal models for screening drug candidates for the treatment of inner ear diseases. Recent studies have succeeded in producing otic organoids from human pluripotent stem cells. Some of them shared many characteristics with human vestibular epithelia (Koehler et al., 2017; Jeong et al., 2018; van der Valk et al., 2021). In the future, exploring the regulatory mechanisms underlying hair cell formation using organoids and the latest techniques, such as single-cell and single-nuclear sequencing, may help to identify regulatory pathways and key factors which play important roles in the maturation and subtype differentiation of vestibular hair cells. Progresses in this area will contribute to the study of hair cell regeneration in human vestibule and balance function reconstruction.

Chen et al. (2012) transplanted otic neuroprogenitors derived from human embryonic stem cells (hESCs) into ouabain-treated gerbils (an auditory neuropathy model) through the round window, and restoration of auditory evoked response was observed. The protocol of transplanting progenitor cells discussed here offers another promising strategy for generating functional HCs in the human vestibule.

Trans-differentiation of Lgr5+ or Plp1+ supporting cells is traditionally regarded as the main source of postnatal hair cell generation in utricles (Wang et al., 2015, 2019). However, the latest studies suggested transitional epithelial cells (TECs) located at the border between sensory and non-sensory regions to be another reliable source of HCs (Huang et al., 2009; Burns et al., 2015; Gao et al., 2016; Jan et al., 2021; Qian et al., 2021). How to achieve effective trans-differentiation from TECs into supporting cells or HCs could be another future direction.

AUTHOR CONTRIBUTIONS

YH, YC, and HM wrote and revised the manuscript. All authors contributed to the article and approved the submitted version.

FUNDING

This work was supported by the National Natural Science Foundation of China (No. 82071049).

REFERENCES

Angelaki, D. E., and Cullen, K. E. (2008). Vestibular system: the many facets of a multimodal sense. *Annu. Rev. Neurosci.* 31, 125–150. doi: 10.1146/annurev.neuro.31.060407.125555

Atkinson, P. J., Huarcaya Najarro, E., Sayyid, Z. N., and Cheng, A. G. (2015). Sensory hair cell development and regeneration: similarities and differences. *Development* 142, 1561–1571. doi: 10.1242/dev.114926

Balak, K. J., Corwin, J. T., and Jones, J. E. (1990). Regenerated hair cells can originate from supporting cell progeny: evidence from phototoxicity and laser ablation experiments in the lateral line system. *J. Neurosci.* 10, 2502–2512. doi: 10.1523/jneurosci.10-08-02502.1990

Bermingham, N. A., Hassan, B. A., Price, S. D., Vollrath, M. A., Ben-Arie, N., Eatock, R. A., et al. (1999). Math1: an essential gene for the generation of inner ear hair cells. *Science* 284, 1837–1841. doi: 10.1126/science.284.5421.1837

Burns, J. C., Kelly, M. C., Hoa, M., Morell, R. J., and Kelley, M. W. (2015). Single-cell RNA-Seq resolves cellular complexity in sensory organs from the neonatal inner ear. *Nat. Commun.* 6:8557. doi: 10.1038/ncomms9557

Burns, J. C., On, D., Baker, W., Collado, M. S., and Corwin, J. T. (2012). Over half the hair cells in the mouse utricle first appear after birth, with significant numbers originating from early postnatal mitotic production in peripheral and striolar growth zones. *J. Assoc. Res. Otolaryngol.* 13, 609–627. doi: 10.1007/s10162-012-0337-0

Carey, J. P., Fuchs, A. F., and Rubel, E. W. (1996). Hair cell regeneration and recovery of the vestibuloocular reflex in the avian vestibular system. *J. Neurophysiol.* 76, 3301–3312. doi: 10.1152/jn.1996.76.5.3301

Chacko, L. J., Sergi, C., Eberharter, T., Dudas, J., Rask-Andersen, H., Hoermann, R., et al. (2020). Early appearance of key transcription factors influence the spatiotemporal development of the human inner ear. *Cell Tissue Res.* 379, 459–471.

Chen, W., Johnson, S. L., Marcotti, W., Andrews, P. W., Moore, H. D., and Rivolta, M. N. (2009). Human fetal auditory stem cells can be expanded in vitro and differentiate into functional auditory neurons and hair cell-like cells. *Stem Cells* 27, 1196–1204. doi: 10.1002/stem.62

Chen, W., Jongkamonwiwat, N., Abbas, L., Eshtan, S. J., Johnson, S. L., Kuhn, S., et al. (2012). Restoration of auditory evoked responses by human ES-cell-derived otic progenitors. *Nature* 490, 278–282. doi: 10.1038/nature11415

Chen, Y., Gu, Y., Li, Y., Li, G. L., Chai, R., Li, W., et al. (2021). Generation of mature and functional hair cells by co-expression of Gfi1, Pou4f3, and Atoh1 in the postnatal mouse cochlea. *Cell Rep.* 35:109016. doi: 10.1016/j.celrep.2021.109016

Cheng, C., Hou, Y., Zhang, Z., Wang, Y., Lu, L., Zhang, L., et al. (2021). Disruption of the autism-related gene Pak1 causes stereocilia disorganization, hair cell loss, and deafness in mice. *J. Genet. Genomics* 48, 324–332. doi: 10.1016/j.jgg.2021.03.010

Cheng, C., Wang, Y., Guo, L., Lu, X., Zhu, W., Muhammad, W., et al. (2019). Age-related transcriptome changes in Sox2+ supporting cells in the mouse cochlea. *Stem Cell Res. Ther.* 10:365. doi: 10.1186/s13287-019-1437-0

Collado, M. S., Thiede, B. R., Baker, W., Askew, C., Igbani, L. M., and Corwin, J. T. (2011). The postnatal accumulation of junctional E-cadherin is inversely correlated with the capacity for supporting cells to convert directly into sensory hair cells in mammalian balance organs. *J. Neurosci.* 31, 11855–11866. doi: 10.1523/jneurosci.2525-11.2011

Corrales, C. E., and Bhattacharyya, N. (2016). Dizziness and death: an imbalance in mortality. *Laryngoscope* 126, 2134–2136. doi: 10.1002/lary.25902

Cullen, K. E. (2012). The vestibular system: multimodal integration and encoding of self-motion for motor control. *Trends Neurosci.* 35, 185–196. doi: 10.1016/j.tins.2011.12.001

De Waele, C., Meguenni, R., Freyss, G., Zamith, F., Bellalimat, N., Vidal, P. P., et al. (2002). Intratympanic gentamicin injections for Meniere disease: vestibular hair cell impairment and regeneration. *Neurology* 59, 1442–1444. doi: 10.1212/wnl.59.9.1442

Dechesne, C. J., and Sans, A. (1985). Development of vestibular receptor surfaces in human fetuses. *Am. J. Otolaryngol.* 6, 378–387. doi: 10.1016/s0196-0709(85)80016-8

Forge, A., Li, L., Corwin, J. T., and Nevill, G. (1993). Ultrastructural evidence for hair cell regeneration in the mammalian inner ear. *Science* 259, 1616–1619. doi: 10.1126/science.8456284

Fritzsch, B., Silos-Santiago, I., Bianchi, L. M., and Fariñas, I. (1997). The role of neurotrophic factors in regulating the development of inner ear innervation. *Trends Neurosci.* 20, 159–164. doi: 10.1016/s0166-2236(96)01007-7

Fu, X., Wan, P., Li, P., Wang, J., Guo, S., Zhang, Y., et al. (2021b). Mechanism and Prevention of Ototoxicity Induced by Aminoglycosides. *Front. Cell. Neurosci.* 15:692762. doi: 10.3389/fncel.2021.692762

Fu, X., An, Y., Wang, H., Li, P., Lin, J., Yuan, J., et al. (2021a). Deficiency of Klc2 Induces Low-Frequency Sensorineural Hearing Loss in C57BL/6 J Mice and Human. *Mol. Neurobiol.* 58, 4376–4391. doi: 10.1007/s12035-021-02422-w

Gao, S., Cheng, C., Wang, M., Jiang, P., Zhang, L., Wang, Y., et al. (2019). Blebbistatin Inhibits Neomycin-Induced Apoptosis in Hair Cell-Like HEI-OC-1 Cells and in Cochlear Hair Cells. *Front. Cell. Neurosci.* 13:590. doi: 10.3389/fncel.2019.00590

Gao, Z., Kelly, M. C., Yu, D., Wu, H., Lin, X., Chi, F. L., et al. (2016). Spatial and Age-Dependent Hair Cell Generation in the Postnatal Mammalian Utricle. *Mol. Neurobiol.* 53, 1601–1612. doi: 10.1007/s12035-015-9119-0

Gnedeva, K., Jacobo, A., Salvi, J. D., Petelski, A. A., and Hudspeth, A. J. (2017). Elastic force restricts growth of the murine utricle. *Elife* 6:e25681. doi: 10.7554/eLife.25681

Gnedeva, K., Wang, X., McGovern, M. M., Barton, M., Tao, L., Trecek, T., et al. (2020). Organ of Corti size is governed by Yap/Tead-mediated progenitor self-renewal. *Proc. Natl. Acad. Sci. U. S. A.* 117, 13552–13561. doi: 10.1073/pnas.2000175117

Golub, J. S., Tong, L., Ngyuen, T. B., Hume, C. R., Palmiter, R. D., Rubel, E. W., et al. (2012). Hair cell replacement in adult mouse utricles after targeted ablation of hair cells with diphtheria toxin. *J. Neurosci.* 32, 15093–15105. doi: 10.1523/jneurosci.1709-12.2012

González-Garrido, A., Pujol, R., López-Ramírez, O., Finkbeiner, C., Eatock, R. A., and Stone, J. S. (2021). The Differentiation Status of Hair Cells That Regenerate Naturally in the Vestibular Inner Ear of the Adult Mouse. *J. Neurosci.* 41, 7779–7796. doi: 10.1523/jneurosci.3127-20.2021

Gu, R., Montcouquiol, M., Marchionni, M., and Corwin, J. T. (2007). Proliferative responses to growth factors decline rapidly during postnatal maturation of mammalian hair cell epithelia. *Eur. J. Neurosci.* 25, 1363–1372. doi: 10.1111/j.1460-9568.2007.05414.x

Guo, R., Li, J., Chen, C., Xiao, M., Liao, M., Hu, Y., et al. (2021b). Biomimetic 3D bacterial cellulose-graphene foam hybrid scaffold regulates neural stem cell proliferation and differentiation. *Colloids Surf. B Biointerfaces* 200:111590. doi: 10.1016/j.colsurfb.2021.111590

Guo, R., Liao, M., Ma, X., Hu, Y., Qian, X., Xiao, M., et al. (2021c). Cochlear implant-based electric-acoustic stimulation modulates neural stem cell-derived neural regeneration. *J. Mater. Chem. B* 9, 7793–7804. doi: 10.1039/d1tb01029h

Guo, L., Cao, W., Niu, Y., He, S., Chai, R., and Yang, J. (2021a). Autophagy Regulates the Survival of Hair Cells and Spiral Ganglion Neurons in Cases of Noise, Ototoxic Drug, and Age-Induced Sensorineural Hearing Loss. *Front. Cell. Neurosci.* 15:760422. doi: 10.3389/fncel.2021.760422

Guo, R., Ma, X., Liao, M., Liu, Y., Hu, Y., Qian, X., et al. (2019). Development and Application of Cochlear Implant-Based Electric-Acoustic Stimulation of Spiral Ganglion Neurons. *ACS Biomater. Sci. Eng.* 5, 6735–6741. doi: 10.1021/acsbiomaterials.9b01265

Guo, R., Xiao, M., Zhao, W., Zhou, S., Hu, Y., Liao, M., et al. (2020). 2D Ti(3)C(2)T(x)MXene couples electrical stimulation to promote proliferation and neural differentiation of neural stem cells. *Acta Biomater.* 139, 105–117. doi: 10.1016/j.actbio.2020.12.035

Han, S., Xu, Y., Sun, J., Liu, Y., Zhao, Y., Tao, W., et al. (2020). Isolation and analysis of extracellular vesicles in a Morpho butterfly wing-integrated microvortex biochip. *Biosens. Bioelectron.* 154:112073. doi: 10.1016/j.bios.2020.112073

He, Z. H., Li, M., Fang, Q. J., Liao, F. L., Zou, S. Y., Wu, X., et al. (2021). FOXG1 promotes aging inner ear hair cell survival through activation of the autophagy pathway. *Autophagy* 17, 4341–4362. doi: 10.1080/15548627.2021.1916194

He, Z. H., Zou, S. Y., Li, M., Liao, F. L., Wu, X., Sun, H. Y., et al. (2020). The nuclear transcription factor FoxG1 affects the sensitivity of mimetic aging hair cells to inflammation by regulating autophagy pathways. *Redox Biol.* 28:101364. doi: 10.1016/j.redox.2019.101364

Hicks, K. L., Wisner, S. R., Cox, B. C., and Stone, J. S. (2020). Atoh1 is required in supporting cells for regeneration of vestibular hair cells in adult mice. *Hear. Res.* 385:107838. doi: 10.1016/j.heares.2019.107838

Hoshino, T. (1982). Scanning electron microscopic observation of the foetal labyrinthine vestibule. *Acta Otolaryngol.* 93, 349–354. doi: 10.3109/00016488209130892

Hu, Y., Li, D., Wei, H., Zhou, S., Chen, W., Yan, X., et al. (2021). Neurite Extension and Orientation of Spiral Ganglion Neurons Can Be Directed by Superparamagnetic Iron Oxide Nanoparticles in a Magnetic Field. *Int. J. Nanomedicine* 16, 4515–4526. doi: 10.2147/ijn.S313673

Hu, Z., Luo, X., Zhang, L., Lu, F., Dong, F., Monsell, E., et al. (2012). Generation of human inner ear prosensory-like cells *via* epithelial-to-mesenchymal transition. *Regen. Med.* 7, 663–673. doi: 10.2217/rme.12.53

Huang, Y., Chi, F., Han, Z., Yang, J., Gao, W., and Li, Y. (2009). New ectopic vestibular hair cell-like cells induced by Math1 gene transfer in postnatal rats. *Brain Res.* 1276, 31–38. doi: 10.1016/j.brainres.2009.04.036

Ishiyama, G., Lopez, I. A., Sepahdari, A. R., and Ishiyama, A. (2015). Meniere's disease: histopathology, cytochemistry, and imaging. *Ann. N. Y. Acad. Sci.* 1343, 49–57. doi: 10.1111/nyas.12699

Jan, T. A., Eltawil, Y., Ling, A. H., Chen, L., Ellwanger, D. C., Heller, S., et al. (2021). Spatiotemporal dynamics of inner ear sensory and non-sensory cells revealed by single-cell transcriptomics. *Cell Rep.* 36:109358. doi: 10.1016/j.celrep.2021.109358

Jeffery, N., and Spoor, F. (2004). Prenatal growth and development of the modern human labyrinth. *J. Anat.* 204, 71–92. doi: 10.1111/j.1469-7580.2004.00250.x

Jeong, M., O'Reilly, M., Kirkwood, N. K., Al-Aama, J., Lako, M., Kros, C. J., et al. (2018). Generating inner ear organoids containing putative cochlear hair cells from human pluripotent stem cells. *Cell Death Dis.* 9:922. doi: 10.1038/s41419-018-0967-1

Johnson Chacko, L., Blumer, M. J. F., Pechriggl, E., Rask-Andersen, H., Dietl, W., Haim, A., et al. (2017). Role of BDNF and neurotrophic receptors in human inner ear development. *Cell Tissue Res.* 370, 347–363. doi: 10.1007/s00441-017-2686-9

Johnson Chacko, L., Sergi, C., Eberharter, T., Dudas, J., Rask-Andersen, H., Hoermann, R., et al. (2020). Early appearance of key transcription factors influence the spatiotemporal development of the human inner ear. *Cell Tissue Res.* 379, 459–471. doi: 10.1007/s00441-019-03115-6

Johnson Chacko, L., Wertjanz, D., Sergi, C., Dudas, J., Fischer, N., Eberharter, T., et al. (2019). Growth and cellular patterning during fetal human inner ear development studied by a correlative imaging approach. *BMC Dev. Biol.* 19:11. doi: 10.1186/s12861-019-0191-y

Jones, T. A., and Nelson, R. C. (1992). Recovery of vestibular function following hair cell destruction by streptomycin. *Hear. Res.* 62, 181–186. doi: 10.1016/0378-5955(92)90184-o

Jung, J. Y., Avenarius, M. R., Adamsky, S., Alpert, E., Feinstein, E., and Raphael, Y. (2013). siRNA targeting Hes5 augments hair cell regeneration in aminoglycoside-damaged mouse utricle. *Mol. Ther.* 21, 834–841. doi: 10.1038/mt.2013.18

Kastan, N., Gnedeva, K., Alisch, T., Petelski, A. A., Huggins, D. J., Chiaravalli, J., et al. (2021). Small-molecule inhibition of Lats kinases may promote Yap-dependent proliferation in postmitotic mammalian tissues. *Nat. Commun.* 12:3100. doi: 10.1038/s41467-021-23395-3

Kawamoto, K., Izumikawa, M., Beyer, L. A., Atkin, G. M., and Raphael, Y. (2009). Spontaneous hair cell regeneration in the mouse utricle following gentamicin ototoxicity. *Hear. Res.* 247, 17–26. doi: 10.1016/j.heares.2008.08.010

Kesser, B. W., Hashisaki, G. T., Fletcher, K., Eppard, H., and Holt, J. R. (2007). An in vitro model system to study gene therapy in the human inner ear. *Gene Ther.* 14, 1121–1131. doi: 10.1038/sj.gt.3302980

Koehler, K. R., Nie, J., Longworth-Mills, E., Liu, X. P., Lee, J., Holt, J. R., et al. (2017). Generation of inner ear organoids containing functional hair cells from human pluripotent stem cells. *Nat. Biotechnol.* 35, 583–589. doi: 10.1038/nbt.3840

Kopke, R. D., Jackson, R. L., Li, G., Rasmussen, M. D., Hoffer, M. E., Frenz, D. A., et al. (2001). Growth factor treatment enhances vestibular hair cell renewal and results in improved vestibular function. *Proc. Natl. Acad. Sci. U. S. A.* 98, 5886–5891. doi: 10.1073/pnas.101120898

Kuntz, A. L., and Oesterle, E. C. (1998a). Transforming growth factor-alpha with insulin induces proliferation in rat utricular extrasensory epithelia. *Otolaryngol. Head Neck Surg.* 118, 816–824. doi: 10.1016/s0194-5998(98)70275-x

Kuntz, A. L., and Oesterle, E. C. (1998b). Transforming growth factor alpha with insulin stimulates cell proliferation in vivo in adult rat vestibular sensory epithelium. *J. Comp. Neurol.* 399, 413–423. doi: 10.1002/(sici)1096-9861(19980928)399:3<413::aid-cne9>3.0.co;2-3

Lambert, P. R. (1994). Inner ear hair cell regeneration in a mammal: identification of a triggering factor. *Laryngoscope* 104, 701–718. doi: 10.1288/00005537-199406000-00010

Lee, S., Song, J. J., Beyer, L. A., Swiderski, D. L., Prieskorn, D. M., Acar, M., et al. (2020). Combinatorial Atoh1 and Gfi1 induction enhances hair cell regeneration in the adult cochlea. *Sci. Rep.* 10:21397. doi: 10.1038/s41598-020-78167-8

Li, A., You, D., Li, W., Cui, Y., He, Y., Li, W., et al. (2018). Novel compounds protect auditory hair cells against gentamycin-induced apoptosis by maintaining the expression level of H3K4me2. *Drug Deliv.* 25, 1033–1043. doi: 10.1080/10717544.2018.1461277

Lim, R., Drury, H. R., Camp, A. J., Tadros, M. A., Callister, R. J., and Brichta, A. M. (2014). Preliminary characterization of voltage-activated whole-cell currents in developing human vestibular hair cells and calyx afferent terminals. *J. Assoc. Res. Otolaryngol.* 15, 755–766. doi: 10.1007/s10162-014-0471-y

Lin, V., Golub, J. S., Nguyen, T. B., Hume, C. R., Oesterle, E. C., and Stone, J. S. (2011). Inhibition of Notch activity promotes nonmitotic regeneration of hair cells in the adult mouse utricles. *J. Neurosci.* 31, 15329–15339. doi: 10.1523/jneurosci.2057-11.2011

Liu, Y., Qi, J., Chen, X., Tang, M., Chu, C., Zhu, W., et al. (2019). Critical role of spectrin in hearing development and deafness. *Sci. Adv.* 5:eaav7803. doi: 10.1126/sciadv.aav7803

Lopez, I., Ishiyama, G., Tang, Y., Tokita, J., Baloh, R. W., and Ishiyama, A. (2005). Regional estimates of hair cells and supporting cells in the human crista ampullaris. *J. Neurosci. Res.* 82, 421–431. doi: 10.1002/jnr.20652

Lv, J., Fu, X., Li, Y., Hong, G., Li, P., Lin, J., et al. (2021). Deletion of Kcnj16 in Mice Does Not Alter Auditory Function. *Front. Cell. Dev. Biol.* 9:630361. doi: 10.3389/fcell.2021.630361

McInturff, S., Burns, J. C., and Kelley, M. W. (2018). Characterization of spatial and temporal development of Type I and Type II hair cells in the mouse utricle using new cell-type-specific markers. *Biol. Open* 7:bio038083. doi: 10.1242/bio.038083

Menendez, L., Trecek, T., Gopalakrishnan, S., Tao, L., Markowitz, A. L., Yu, H. V., et al. (2020). Generation of inner ear hair cells by direct lineage conversion of primary somatic cells. *Elife* 9:e55249. doi: 10.7554/eLife.55249

Montcouquiol, M., and Corwin, J. T. (2001). Intracellular signals that control cell proliferation in mammalian balance epithelia: key roles for phosphatidylinositol-3 kinase, mammalian target of rapamycin, and S6 kinases in preference to calcium, protein kinase C, and mitogen-activated protein kinase. *J. Neurosci.* 21, 570–580. doi: 10.1523/jneurosci.21-02-00570.2001

Morsli, H., Choo, D., Ryan, A., Johnson, R., and Wu, D. K. (1998). Development of the mouse inner ear and origin of its sensory organs. *J. Neurosci.* 18, 3327–3335. doi: 10.1523/jneurosci.18-09-03327.1998

Oghalai, J. S., Holt, J. R., Nakagawa, T., Jung, T. M., Coker, N. J., Jenkins, H. A., et al. (1998). Ionic currents and electromotility in inner ear hair cells from humans. *J. Neurophysiol.* 79, 2235–2239. doi: 10.1152/jn.1998.79.4.2235

O'Rahilly, R. (1963). The early development of the otic vesicle in staged human embryos. *J. Embryol. Exp. Morphol.* 11, 741–755. doi: 10.1242/dev.11.4.741

Qi, J., Liu, Y., Chu, C., Chen, X., Zhu, W., Shu, Y., et al. (2019). A cytoskeleton structure revealed by super-resolution fluorescence imaging in inner ear hair cells. *Cell Discov.* 5:12. doi: 10.1038/s41421-018-0076-4

Qi, J., Zhang, L., Tan, F., Liu, Y., Chu, C., Zhu, W., et al. (2020). Espin distribution as revealed by super-resolution microscopy of stereocilia. *Am. J. Transl. Res.* 12, 130–141.

Qian, F., Wang, X., Yin, Z., Xie, G., Yuan, H., Liu, D., et al. (2020). The slc4a2b gene is required for hair cell development in zebrafish. *Aging* 12, 18804–18821. doi: 10.18632/aging.103840

Qian, X., Ma, R., Wang, X., Xu, X., Yang, J., Chi, F., et al. (2021). Simultaneous gentamicin-mediated damage and Atoh1 overexpression promotes hair cell regeneration in the neonatal mouse utricle. *Exp. Cell Res.* 398:112395. doi: 10.1016/j.yexcr.2020.112395

Roberson, D. F., Weisleder, P., Bohrer, P. S., and Rubel, E. W. (1992). Ongoing production of sensory cells in the vestibular epithelium of the chick. *Hear. Res.* 57, 166–174. doi: 10.1016/0378-5955(92)90149-h

Rosenhall, U. (1972a). Mapping of the cristae ampullares in man. *Ann. Otol. Rhinol. Laryngol.* 81, 882–889. doi: 10.1177/000348947208100622

Rosenhall, U. (1972b). Vestibular macular mapping in man. *Ann. Otol. Rhinol. Laryngol.* 81, 339–351. doi: 10.1177/000348947208100305

Rosenhall, U., and Engström, B. (1974). Surface Structures of the Human Vestibular Sensory Regions. *Acta Otolaryngol.* 77, 3–18. doi: 10.1080/16512251.1974.11675749

Rubel, E. W., Dew, L. A., and Roberson, D. W. (1995). Mammalian vestibular hair cell regeneration. *Science* 267, 701–707. doi: 10.1126/science.7839150

Rüsch, A., Lysakowski, A., and Eatock, R. A. (1998). Postnatal development of type I and type II hair cells in the mouse utricle: acquisition of voltage-gated conductances and differentiated morphology. *J. Neurosci.* 18, 7487–7501. doi: 10.1523/jneurosci.18-18-07487.1998

Sayyid, Z. N., Wang, T., Chen, L., Jones, S. M., and Cheng, A. G. (2019). Atoh1 Directs Regeneration and Functional Recovery of the Mature Mouse Vestibular System. *Cell Rep.* 28, 312–324.e4. doi: 10.1016/j.celrep.2019.06.028

Schlecker, C., Praetorius, M., Brough, D. E., Presler, R. G. Jr., Hsu, C., Plinkert, P. K., et al. (2011). Selective atonal gene delivery improves balance function in a mouse model of vestibular disease. *Gene Ther.* 18, 884–890. doi: 10.1038/gt.2011.33

Senn, P., Mina, A., Volkenstein, S., Kranebitter, V., Oshima, K., and Heller, S. (2020). Progenitor Cells from the Adult Human Inner Ear. *Anat. Rec.* 303, 461–470. doi: 10.1002/ar.24228

Severinsen, S. A., Sørensen, M. S., Kirkegaard, M., and Nyengaard, J. R. (2010). Stereological estimation of total cell numbers in the young human utricular macula. *Acta Otolaryngol.* 130, 773–779. doi: 10.3109/00016480903397694

Shou, J., Zheng, J. L., and Gao, W. Q. (2003). Robust generation of new hair cells in the mature mammalian inner ear by adenoviral expression of Hath1. *Mol. Cell. Neurosci.* 23, 169–179. doi: 10.1016/s1044-7431(03)00066-6

Slowik, A. D., and Bermingham-McDonogh, O. (2013). Hair cell generation by notch inhibition in the adult mammalian cristae. *J. Assoc. Res. Otolaryngol.* 14, 813–828. doi: 10.1007/s10162-013-0414-z

Staecker, H., Praetorius, M., Baker, K., and Brough, D. E. (2007). Vestibular hair cell regeneration and restoration of balance function induced by math1 gene transfer. *Otol. Neurotol.* 28, 223–231. doi: 10.1097/MAO.0b013e31802b3225

Streeter, G. L. (1906). On the development of the membranous labyrinth and the acoustic and facial nerves in the human embryo. *Am. J. Anat.* 6, 139–165. doi: 10.1002/aja.1000060103

Strupp, M., Dlugaiczyk, J., Ertl-Wagner, B. B., Rujescu, D., Westhofen, M., and Dieterich, M. (2020). Vestibular Disorders. *Dtsch. Arztebl. Int.* 117, 300–310. doi: 10.3238/arztebl.2020.0300

Sun, S., Li, S., Luo, Z., Ren, M., He, S., Wang, G., et al. (2021). Dual expression of Atoh1 and Ikzf2 promotes transformation of adult cochlear supporting cells into outer hair cells. *Elife* 10:e66547. doi: 10.7554/eLife.66547

Tafra, R., Brakus, S. M., Vukojevic, K., Kablar, B., Colovic, Z., and Saraga-Babic, M. (2014). Interplay of proliferation and proapoptotic and antiapoptotic factors is revealed in the early human inner ear development. *Otol. Neurotol.* 35, 695–703. doi: 10.1097/mao.0000000000000210

Tan, F., Chu, C., Qi, J., Li, W., You, D., Li, K., et al. (2019). AAV-ie enables safe and efficient gene transfer to inner ear cells. *Nat. Commun.* 10:3733. doi: 10.1038/s41467-019-11687-8

Taylor, R. R., Filia, A., Paredes, U., Asai, Y., Holt, J. R., Lovett, M., et al. (2018). Regenerating hair cells in vestibular sensory epithelia from humans. *Elife* 7:e34817. doi: 10.7554/eLife.34817

Taylor, R. R., Jagger, D. J., Saeed, S. R., Axon, P., Donnelly, N., Tysome, J., et al. (2015). Characterizing human vestibular sensory epithelia for experimental studies: new hair bundles on old tissue and implications for therapeutic interventions in ageing. *Neurobiol. Aging* 36, 2068–2084. doi: 10.1016/j.neurobiolaging.2015.02.013

Toyoda, S., Shiraki, N., Yamada, S., Uwabe, C., Imai, H., Matsuda, T., et al. (2015). Morphogenesis of the inner ear at different stages of normal human development. *Anat. Rec.* 298, 2081–2090. doi: 10.1002/ar.23268

Tsuji, K., Velázquez-Villaseñor, L., Rauch, S. D., Glynn, R. J., Wall, C. III, and Merchant, S. N. (2000). Temporal bone studies of the human peripheral vestibular system. Meniere's disease. *Ann. Otol. Rhinol. Laryngol. Suppl.* 181, 26–31. doi: 10.1177/00034894001090s505

van der Valk, W. H., Steinhart, M. R., Zhang, J., and Koehler, K. R. (2021). Building inner ears: recent advances and future challenges for in vitro organoid systems. *Cell Death Differ.* 28, 24–34. doi: 10.1038/s41418-020-00678-8

Walters, B. J., Coak, E., Dearman, J., Bailey, G., Yamashita, T., Kuo, B., et al. (2017). In Vivo Interplay between p27(Kip1), GATA3, ATOH1, and POU4F3 Converts Non-sensory Cells to Hair Cells in Adult Mice. *Cell Rep.* 19, 307–320. doi: 10.1016/j.celrep.2017.03.044

Wang, T., Chai, R., Kim, G. S., Pham, N., Jansson, L., Nguyen, D. H., et al. (2015). Lgr5+ cells regenerate hair cells *via* proliferation and direct transdifferentiation in damaged neonatal mouse utricle. *Nat. Commun.* 6:6613. doi: 10.1038/ncomms7613

Wang, T., Niwa, M., Sayyid, Z. N., Hosseini, D. K., Pham, N., Jones, S. M., et al. (2019). Uncoordinated maturation of developing and regenerating postnatal mammalian vestibular hair cells. *PLoS Biol.* 17:e3000326. doi: 10.1371/journal.pbio.3000326

Warchol, M. E., Lambert, P. R., Goldstein, B. J., Forge, A., and Corwin, J. T. (1993). Regenerative proliferation in inner ear sensory epithelia from adult guinea pigs and humans. *Science* 259, 1619–1622. doi: 10.1126/science.8456285

Watanuki, K., and Schuknecht, H. F. (1976). A morphological study of human vestibular sensory epithelia. *Arch. Otolaryngol.* 102, 853–858.

Wei, H., Chen, Z., Hu, Y., Cao, W., Ma, X., Zhang, C., et al. (2021). Topographically Conductive Butterfly Wing Substrates for Directed Spiral Ganglion Neuron Growth. *Small* 17:e2102062. doi: 10.1002/smll.202102062

Weisleder, P., and Rubel, E. W. (1992). Hair cell regeneration in the avian vestibular epithelium. *Exp. Neurol.* 115, 2–6. doi: 10.1016/0014-4886(92)90211-8

Wersall, J. (1956). Studies on the structure and innervation of the sensory epithelium of the cristae ampulares in the guinea pig; a light and electron microscopic investigation. *Acta Otolaryngol. Suppl.* 126, 1–85.

Whitfield, T. T. (2015). Development of the inner ear. *Curr. Opin. Genet. Dev.* 32, 112–118. doi: 10.1016/j.gde.2015.02.006

Wu, D. K., and Kelley, M. W. (2012). Molecular mechanisms of inner ear development. *Cold Spring Harb. Perspect. Biol.* 4:a008409. doi: 10.1101/cshperspect.a008409

Wu, J., Li, W., Lin, C., Chen, Y., Cheng, C., Sun, S., et al. (2016). Co-regulation of the Notch and Wnt signaling pathways promotes supporting cell proliferation and hair cell regeneration in mouse utricles. *Sci. Rep.* 6:29418. doi: 10.1038/srep29418

Yamashita, H., and Oesterle, E. C. (1995). Induction of cell proliferation in mammalian inner-ear sensory epithelia by transforming growth factor alpha and epidermal growth factor. *Proc. Natl. Acad. Sci. U. S. A.* 92, 3152–3155. doi: 10.1073/pnas.92.8.3152

Yasuda, M., Yamada, S., Uwabe, C., Shiota, K., and Yasuda, Y. (2007). Three-dimensional analysis of inner ear development in human embryos. *Anat. Sci. Int.* 82, 156–163. doi: 10.1111/j.1447-073X.2007.00176.x

You, D., Guo, L., Li, W., Sun, S., Chen, Y., Chai, R., et al. (2018). Characterization of Wnt and Notch-Responsive Lgr5+ Hair Cell Progenitors in the Striolar Region of the Neonatal Mouse Utricle. *Front. Mol. Neurosci.* 11:137. doi: 10.3389/fnmol.2018.00137

Zeng, S., Ni, W., Jiang, H., You, D., Wang, J., Lu, X., et al. (2020). Toxic Effects of 3,3′-Iminodipropionitrile on Vestibular System in Adult C57BL/6J Mice In Vivo. *Neural Plast.* 2020:1823454. doi: 10.1155/2020/1823454

Zhang, S., Dong, Y., Qiang, R., Zhang, Y., Zhang, X., Chen, Y., et al. (2021). Characterization of Strip1 Expression in Mouse Cochlear Hair Cells. *Front. Genet.* 12:625867. doi: 10.3389/fgene.2021.625867

Zhang, Y., Li, W., He, Z., Wang, Y., Shao, B., Cheng, C., et al. (2019). Pre-treatment With Fasudil Prevents Neomycin-Induced Hair Cell Damage by Reducing the Accumulation of Reactive Oxygen Species. *Front. Mol. Neurosci.* 12:264. doi: 10.3389/fnmol.2019.00264

Zhang, Y., Li, Y., Fu, X., Wang, P., Wang, Q., Meng, W., et al. (2021). The Detrimental and Beneficial Functions of Macrophages After Cochlear Injury. *Front. Cell. Dev. Biol.* 9:631904. doi: 10.3389/fcell.2021.631904

Zhang, Y., Zhang, S., Zhang, Z., Dong, Y., Ma, X., Qiang, R., et al. (2020). Knockdown of Foxg1 in Sox9+ supporting cells increases the trans-differentiation of supporting cells into hair cells in the neonatal mouse utricle. *Aging* 12, 19834–19851. doi: 10.18632/aging.104009

Zheng, J. L., and Gao, W. Q. (2000). Overexpression of Math1 induces robust production of extra hair cells in postnatal rat inner ears. *Nat. Neurosci.* 3, 580–586. doi: 10.1038/75753

Zheng, J. L., Helbig, C., and Gao, W. Q. (1997). Induction of cell proliferation by fibroblast and insulin-like growth factors in pure rat inner ear epithelial cell cultures. *J. Neurosci.* 17, 216–226. doi: 10.1523/jneurosci.17-01-00216.1997

Zhong, Z., Fu, X., Li, H., Chen, J., Wang, M., Gao, S., et al. (2020). Citicoline Protects Auditory Hair Cells Against Neomycin-Induced Damage. *Front. Cell. Dev. Biol.* 8:712. doi: 10.3389/fcell.2020.00712

Conflict of Interest: The authors declare that the research was conducted in the absence of any commercial or financial relationships that could be construed as a potential conflict of interest.

Advantages of publishing in Frontiers

OPEN ACCESS
Articles are free to read for greatest visibility and readership

FAST PUBLICATION
Around 90 days from submission to decision

HIGH QUALITY PEER-REVIEW
Rigorous, collaborative, and constructive peer-review

TRANSPARENT PEER-REVIEW
Editors and reviewers acknowledged by name on published articles

Frontiers
Avenue du Tribunal-Fédéral 34
1005 Lausanne | Switzerland

Visit us: www.frontiersin.org
Contact us: frontiersin.org/about/contact

REPRODUCIBILITY OF RESEARCH
Support open data and methods to enhance research reproducibility

DIGITAL PUBLISHING
Articles designed for optimal readership across devices

FOLLOW US
@frontiersin

IMPACT METRICS
Advanced article metrics track visibility across digital media

EXTENSIVE PROMOTION
Marketing and promotion of impactful research

LOOP RESEARCH NETWORK
Our network increases your article's readership